Electrocardiology 2013

Proceedings

of the 40th International Congress on Electrocardiology

Glasgow, August 7th – 10th , 2013

Editors

Julie Kennedy Peter Macfarlane

ELECTROCARDIOLOGY 2013

ISBN 978-80-969-672-8-5

Proceedings of the

40th International Congress on Electrocardiology

ELECTROCARDIOLOGY

Glasgow, Scotland.
7th-10th August, 2013

2013

Editors:

Julie Kennedy

Peter W. Macfarlane

University of Glasgow

ELECTROCARDIOLOGY 2013

Proceedings of the 40th International Congress on Electrocardiology

Editors: Julie Kennedy, Peter W. Macfarlane
Publisher: Institute of Measurement Science
Slovak Academy of Sciences
Dúbravská cesta 9, 841 04 Bratislava
Slovakia

ISBN 978-80-969-672-8-5

Printed in Slovakia
by VEDA, Publishing House of the Slovak Academy of Sciences

Preface

The 40th International Congress on Electrocardiology (ICE2013) was held in the University of Glasgow, Scotland, from August 7th-10th, 2013, under the auspices of the Institute of Cardiovascular and Medical Sciences. This was a very successful meeting attended by over 200 individuals, including accompanying persons. Plenary talks were given by world leading specialists Professors Michel Haissaguerre, Yoram Rudy and Hein Wellens and approximately 150 papers and posters were presented during the meeting.

Delegates were invited to submit manuscripts for publication in the Proceedings or for consideration as an article to be published in the Journal of Electrocardiology. In this book can be found 39 papers, while a further 6 manuscripts appeared in the Journal of Electrocardiology in the March/April issue 2014. The contents of these Proceedings indicate the wide range of topics usually presented at the International Congress on Electrocardiology.

It is interesting to note that the 5th International Congress on Electrocardiology was held in Glasgow in 1978 and the Proceedings at that time were published under the title of Progress in Electrocardiology. Thirty five years later, progress can only be regarded as being exceptional in this area. Automated ECG interpretation is a basic technique used in most large hospitals world wide, a solution to the inverse problem has led to commercial products for assistance with ablation of accessory pathways or of arrhythmogenic foci and for location of infarcted myocardium, while much has been learned about cardiac electrophysiology, to list only a few areas of development.

A pre ICE2013 workshop on so called early repolarization was held and many manuscripts relating to this topic were published in the Journal of Electrocardiology in the September/October issue 2013. Sincere thanks are due to Dr. Galen Wagner, the Editor of the Journal, for all the work he expended in stimulating and editing papers for this issue of the Journal. It is hoped that a consensus paper arising from the workshop will be published in the near future.

In summary, therefore, the effective proceedings of ICE2013 can be found in two issues of the Journal of Electrocardiology as well as this book. Whether or not this is the optimum approach remains a matter for continued discussion but the important point is that the International Society of Electrocardiology should continue to flourish in the years to come.

The Organising Committee would like to take this opportunity to thank all of those who were involved in creating such a successful international conference. Locally, there were many staff and spouses who helped during the meeting, namely in alphabetical order, Pamela Armstrong, Elaine Clark, Brian Devine, Louise Inglis, Julie Kennedy, Shahid Latif, Irene Macfarlane, David and Kathryn McLaren, and Mark and Jean Watts to whom sincere thanks are offered. The Organising Committee would also like to thank the staff of the University of Glasgow Conference and Visitor Services Office for all their assistance before and during the conference.

Finally, with respect to this book, sincere thanks are due to Julie Kennedy for undertaking the lengthy task of carefully editing all the papers with a contribution from the undersigned. The

Organising Committee would also like to thank Pamela Armstrong for help with the final preparation of the book and indeed for very significant administrative assistance in organising the conference. Sincere thanks are also due to Dr. Milan Tysler for his assistance in arranging the publication of the book through the Veda Publishing House in Bratislava.

Our only regret is the length of time taken to produce the Proceedings due to initial delays in knowing which papers would be included and then a surfeit of tasks requiring to be accomplished – not only related to this book!

Hopefully, those who attended the meeting in Glasgow will have happy memories of both the scientific and social aspects of the Congress.

Peter W. Macfarlane
On behalf of the Local Organising Committee (LOC)

LOC Colin Berry
Derek Connelly
Peter Macfarlane
Rachel Myles
Andrew Rankin
Godfrey Smith
Tony Workman

The 40th International Congress on Electrocardiology was organised under the auspices of the International Society of Electrocardiology.

INTERNATIONAL SOCIETY OF ELECTROCARDIOLOGY

President:

C. Pastore, *Brazil*.

President-elect:

W. Zareba, *USA*.

Past President:

M. Hiraoka, *Japan*.

Secretary:

L. Bacharova, *Slovakia*.

Treasurer:

P. W. Macfarlane, *UK*.

Council:

A. Baranchuk, *Canada*.
L. De Ambroggi, *Italy*.
P. Dorostkar, *USA*.
B. Gorenek, *Turkey*.
T. Ikeda, *Japan*.
G. Kozmann, *Hungary*.
J. Liebman, *USA*.
R. S. MacLeod, *USA*.
P. Platanov, *Sweden*..
M. Potse, *The Netherlands*.
A. Ribeiro, *Brazil*.
M. Roschevsky, *Russia*.
M. Sobieszczanska, *Poland*.
M. Tysler, *Slovakia*.
A. Van Ooosterom, *The Netherlands*.
G. Wagner, *USA*.

CONTENTS

1. Conduction Abnormalities

CLINICAL CHARACTERISTICS OF J WAVES (EARLY REPOLARIZATION) IN PATIENTS WITH IDIOPATHIC VENTRICULAR FIBRILLATION

[1]M. Hiraoka, [2]Y Sekiguchi, [3]M. Takagi, [1]Y Yokoyama, [4]N. Aihara,[2]K. Aonuma, and the Japan Idiopathic Ventricular Fibrillation Study Investigators

[1]Tokyo Medical and Dental University, Tokyo, Japan
[2]University of Tsukuba, Tsukuba, Ibaraki, Japan
[3]Osaka City University, Osaka, Japan
[4]Senri Chuo Hospital, Senri, Osaka, Japan
Email: m-hiraoka0401@ivory.plala.or.jp

Abstract. *This paper assesses the clinical features and ECG findings in patients with idiopathic ventricular fibrillation recruited from the Japan Idiopathic Ventricular Fibrillation (IVF) Study registry. Patients with the Brugada Syndrome were excluded. A second part of the study reviewed the prevalence and prognostic value of a J wave and ST segment morphology in patients with the Brugada Syndrome. Sixty four patients had IVF. Only 24 (38%) had an early repolarization pattern. Slurring was present in 10, notching in 8 and both in 6. There were 3 (12%) of 460 patients with Brugada Syndrome who displayed a J wave/early repolarization pattern in the inferior and/or lateral leads. Multivariate analysis showed that syncope, J waves in the inferior or lateral leads as well as horizontal ST segments after a J wave were significant predictors for cardiac events.*

Keywords: J wave, Early Repolarization, Idiopathic Ventricular Fibrillation, Brugada Syndrome

1. Introduction

The J wave or early repolarization (ER) pattern in the electrocardiogram (ECG) is considered to be a marker for a high risk of idiopathic ventricular fibrillation (IVF) in patients [1-3]. While an ER pattern seems to be quite prevalent in IVF patients, there are a number of IVF patients without the ER pattern. Clinical features and ECG characteristics of IVF patients with and without ER have not been comparatively explored. The aim of the first part of this study was to characterize the clinical features and ECG presentation in patients with IVF excluding Brugada Syndrome (BrS).

The prevalence and prognostic value of the J wave and ST-segment morphology after the J wave in patients with BrS have been discussed [4-6]. The second part of the study explored these problems in our cohort of patients with BrS.

2. Methods

Subjects were collected from patients with IVF and BrS enrolled in the Japan Idiopathic Ventricular Fibrillation Study (J-IVFS) registry. J-IVFS was a multi-center study of IVF including BrS in Japan which had been enrolling cases from February 2002 [7]. The criteria for enrollment were (1) type 1 ECG for BrS, (2) at least one episode of documented VF for IVF, and (3) exclusion of major structural abnormality of the heart.

3. Results

I. IVF with and without J wave/ER

Sixty four patients met the enrollment criteria for IVF. Patients having BrS defined by the presence of a raised J point and ST-segment elevation in leads V1~V3 (type 1 ECG), or a positive response to the pilsicainide provocation test were excluded from this part of the study. There were 24 (38%) of 64 patients with ER, while the rest of the 40 cases (62%) had no ER pattern. ER was present in inferior leads in 11 cases (44%), both inferior and lateral leads in 8 cases (33%), and lateral leads alone in 5 cases (21%). As to the type of ER, the slurred type was most prevalent, occurring in 10 cases (44%), notched type in 8 cases (33%), and both slurred and notched types in 6 cases (25%).

The clinical characteristics showed a male predominance in the ER(+) group, but no gender predominance was apparent in the ER(-) group. Other parameters such as age of symptom onset, multiple experiences of syncope, family history of sudden cardiac death, history of AF, exercise induced ventricular arrhythmias, inducible VF by electrophysiological study (EPS) and positive late potential in the signal averaged ECG were not different when the two groups were compared.

ECG parameters showed an abnormal axis deviation of QRS and/or bundle branch block in 9 cases in the ER(-) group, but none in the ER(+) group. Differences between other parameters were not evident between the two groups. The ER(-) group was divided into cardiac conduction (CD)(+) and CD(-) group. Therefore, 64 IVF cases were divided into 3 groups, ER(+), ER(-)/CD(+), and ER(-)/CD(-) group. The electrocardiographic features of the 3 groups showed prolonged P-R interval and QRS duration in the ER (-)/CD (+) group compared to those in the other two groups. There were no differences in other ECG parameters among the three groups [8].

II. Prevalence and prognostic value of J wave/ER in BrS.

The prevalence of the J wave in the infero-lateral leads was examined with our cohort of patients with BrS. There were 53 patients (12%) out of 460 BrS displaying J wave/ER in the inferior and/or lateral leads. When we divided them into VF, Syncope and Asymptomatic groups, the VF group had a higher incidence of J wave (17%) than the other two but there was no statistically significant difference. The follow-up study for cardiac events in patients with BrS demonstrated that the VF group had a worse prognosis than other two groups. Multivariate analyses revealed symptoms (VF and/or syncope), QRS duration in V2 > 90msec, J wave both in inferior and lateral leads, and horizontal ST-segment elevation after the J wave were significant predictors for cardiac events. When we evaluated predictive values in patients excluding the VF group, namely in the Syncope and Asymptomatic groups, the same parameters were shown to have significant predictive values [9].

4. Discussion

Among the 64 cases of IVF excluding cases of BrS, there were 24 patients (38%) with J wave/ER, most of whom were male, of which the results found were in agreement with the previous reports [1-3]. The rest of the 62% did not show a J wave and there was no gender predominance in the ER(-) group. In the ER(-) group, 9 cases showed ventricular conduction disturbance (CD) with abnormal axis deviation and/or bundle branch block, revealing

prolongation of PR interval and QRS duration. Therefore, the ER(-)/CD(+) group appeared to represent a distinct clinical entity.

BrS patients showing J wave/ER in infero-lateral leads accounted for 53 of 460 cases or 12%, which was not high and was comparable with other reports [4- 6]. There were no differences in the incidences of J wave in the infero-lateral leads among the VF, Syncope and Asymptomatic groups. The presence of a J wave in inferior or lateral leads was shown to have predictive value for cardiac events [6]. Our results indicated that the presence of a J wave in either inferior or lateral leads was not predictive for cardiac events but its presence both in inferior and lateral leads showed predictive value. Furthermore, we showed for the first time, tha horizontal ST elevation following the J wave has a predictive value. The presence of a J wave in the inferior and lateral leads and horizontal ST-segment morphology after a J wave may be related to a highly arrhythmogenic substrate in patients with BrS.

References

[1] Haissaguerre M, Derval N, Sacher F, et al. Sudden cardiac arrest associated with early repolarization. *New England Journal of Medicine*, 2008; 358: 20: 16-2023.

[2] Rosso R, Kogan E, Belhassen B, et al. J-point elevation in survivors of primary ventricular fibrillation and matched control subjects: Incidence and clinical significance. *Journal of American College of Cardiology*, 2008; 52: 1231-1238.

[3] Nam GB, Kim YH, Antzelevitch C: Augmentation of J waves andelectrical storms in patients with early repolarization. *New England Journal of Medicine*, 2008; 358: 2078-2079.

[4] Letsas KP, Sache r F, Probst V, et al. Prevalence of early repolarization pattern in inferolateral leads in patients with Brugada syndrome. *Heart Rhythm*, 2008; 5: 1685-1689.

[5] Sarkozy A, Chierchia GB, Paparella G, et al. Inferior and lateral electrocardiographic repolarization abnormalities in Brugada syndrome. *Circulation Arrhythmia Electrophysiology*, 2009; 2: 154-161.

[6] Kamakura S, Ohe T, Nakazawa K, et al. Long-term prognosis of probands with Brugada-pattern ST-elevation in leads V1-V3. *Circulation Arrhythmia Electrophysiology*, 2009; 2: 495-503.

[7] Takagi M, Yokoyama Y, Aonuma K, Aihara N, Hiraoka M. Clinical characteristics and risk stratification in symptomatic and asymptomatic patients with Brugada syndrome: multicenter study in Japan. *Journal of Cardiovascular Electrophysiology*, 2007; 18: 1244-1251.

[8] Sekiguchi Y, Aonuma K, Takagi M, Aihara N, Yokoyama Y, Hiraoka M. New Clinical and Electrocardiographic Classification in Patients with Idiopathic Ventricular Fibrillation. *Journal of Cardiovascular Electrophysiology*, 2013; 24: 902-908.

[9] Takagi M, Aonuma K, Sekiguchi Y, Yokoyama Y, Aihara N, Hiraoka M, The Japan Idiopathic Ventricular Fibrillation Study Investigators. The prognostic value of early repolarization (J wave) and ST-segment morphology after J wave in Brugada syndrome: Multicenter study. *Heart Rhythm*, 2013; 10: 533-539.

BRUGADA PHENOCOPY – MORE QUESTIONS THAN ANSWERS

A. Baranchuk, D.D. Anselm

Division of Cardiology, Electrophysiology and Pacing, Queen's University,
Kingston General Hospital, Kingston, Canada
Email: barancha@kgh.kari.net

Abstract. *Brugada Phenocopies (BrP) continue to emerge as clinical entities that are distinct from true congenital Brugada Syndrome (BrS). BrP are characterized by type 1 and type 2 Brugada electrocardiogram (ECG) patterns in leads V1-V3; however, BrP are elicited by various underlying associated conditions. In this study, we review the progress made to-date regarding BrP, discuss areas of ongoing controversy, and identify opportunities for further investigation.*

Keywords: Brugada Syndrome, Brugada Phenocopy, Genetics, Ion Channels

1. Introduction

Brugada Syndrome (BrS) is an inherited cardiac channelopathy characterized by type 1 and type 2 ECG patterns in leads V1-V3 which predispose individuals to malignant ventricular arrhythmias and sudden cardiac death (Fig. 1, Panel A) [1]. Brugada Phenocopies (BrP), however, are clinical entities that have ECG patterns that are identical to true congenital BrS but are elicited by various factors such as electrolyte disturbances, mechanical compression, poor ECG filters, and myocardial ischemia (Fig. 1, Panel B) [2]. The term *Brugada Phenocopy* was introduced to describe a Brugada ECG pattern in the context of propofol infusion syndrome [3]. The term *Phenocopy* was chosen because it was previously used to describe an environmental condition that imitates one produced by a gene; therefore, it served as a reasonable and succinct description for all acquired Brugada-like ECG manifestations [4]. In this paper, we review the progress made to-date regarding BrP, discuss areas of ongoing controversy, and identify opportunities for further investigation.

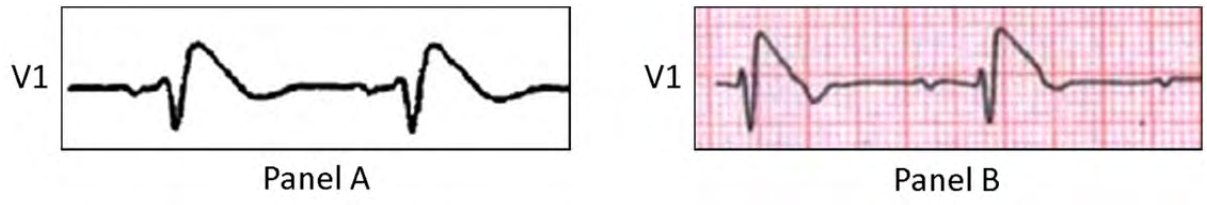

Fig. 1. Comparison of true congenital Brugada Syndrome and Brugada Phenocopy. Classical congenital type 1 "coved" Brugada ECG pattern (Panel A) [1]. Brugada Phenocopy in a patient presenting with an acute inferior ST-segment elevation myocardial infarction with right ventricular involvement (Panel B) [5]. Lead V1 is identical to the type 1 Brugada ECG pattern. Reproduced with permission [1, 5].

2. Methods

Based on our previous literature review [2], we performed an updated search on Ovid MEDLINE(R) and Ovid OLDMEDLINE(R) (January 2011 to September Week 1, 2013), EMBASE (January 2011 to 2013 Week 37), and PubMed (January 2011 to September Week 1, 2013). On all the databases, the MeSH heading "Brugada Syndrome" search results were combined with keyword search results for: Brugada-like, mimicking Brugada, induced Brugada syndrome, Brugada type, Brugada sign, Brugada-pattern, and Acquired Brugada.

In addition, we included the search term “Brugada Phenocopy” on all databases. We also included published papers from non-indexed journals for proven BrP. The inclusion and exclusion criteria were previously described [2].

3. Results

Thirty-one case reports meeting inclusion criteria were subdivided into various categories such as metabolic conditions, mechanical compression and myocardial ischemia in the original literature review [2]. Since that time, an additional 15 papers were published as complete case reports [5-19] and three abstracts [20-22] for proven or suspected BrP. In addition, 5 papers have been published further discussing the etiology, pathophysiology and conceptual evolution of the BrP [23-27]. This has lead to the current BrP etiological categories (Table 1) and diagnostic criteria (Table 2).

Table 1 Brugada Phenocopy Etiological Categories

Etiological Category
i. Metabolic Conditions
ii. Mechanical Compression
iii. Ischemia & Pulmonary Embolism
iv. Myocardial & Pericardial Disease
v. ECG Modulation
vi. Miscellaneous

Reproduced with permission [26].

4. Discussion

The diagnostic distinction between BrP and true congenital BrS focuses on a few key features. The first is that patients with BrP have a reversible underlying condition such as adrenal insufficiency, hypokalemia, or myocardial ischemia which elicits the Brugada ECG pattern. Once this underlying condition resolves, there is normalization of the ECG. Secondly, patients with BrP have a low clinical pretest probability of true BrS as opposed to a high pretest probability in patients with true BrS. The third feature is that patients with BrP have a negative provocative challenge with a sodium channel blocker, while those with true BrS have a positive provocative challenge (Table 2). Additionally, while patients with high-risk true congenital BrS are candidates for ICD implantation, the clinical implications of patients with BrP remain unknown. Therefore, the only BrP treatment recommendations at this time would be to focus on resolution of the underlying condition as further intervention has not yet been investigated or validated.

Table 2 Clarification of Brugada ECG Pattern, Brugada Phenocopy, and True Congenital Brugada Syndrome

Brugada ECG Pattern
i. The ECG pattern has a type 1 or type 2 Brugada morphology as currently defined by Bayés de Luna et al [1]
Diagnostic Criteria for Brugada Phenocopy [2,5,12,25]
i. The ECG pattern has a type 1 or type 2 Brugada morphology
ii. The patient has an underlying condition that is identifiable
iii. The ECG pattern resolves after resolution of the underlying condition
iv. There is a low clinical pretest probability of true Brugada Syndrome determined by lack of symptoms, medical history, and family history
v. Negative provocative testing with sodium channel blockers such as ajmaline, flecainide, or procainamide
vi. Provocative testing not mandatory if surgical RVOT manipulation has occurred within the last 96 hours
vii. The results of genetic testing are negative (desirable but not mandatory because the SCN5A mutation is identified in only 20% to 30% of probands affected by true Brugada Syndrome)
Features that suggest true congenital Brugada Syndrome
i. The ECG pattern has a type 1 or type 2 Brugada morphology
ii. There is a high clinical pretest probability of true congenital Brugada Syndrome determined by presence of symptoms, medical history, and family history
iii. Positive provocative testing with sodium channel blockers such as ajmaline, flecainide, or procainamide. This indicates sodium channel dysfunction consistent with true Brugada Syndrome
iv. The results of genetic testing are positive (desirable but not mandatory because the SCN5A mutation is identified in only 20% to 30% of probands affected by true Brugada Syndrome)

ECG indicates electrocardiogram; RVOT, right ventricular outflow tract; and SCN5A; sodium channel voltage-gated type V alpha subunit.

Brugada Phenocopy – Genetics

The inclusion of genetic testing regarding BrP continues to be an area of discussion and will undoubtedly evolve. We have not included genetics as a mandatory diagnostic criterion since only 20-30% of probands with true congenital BrS have positive genetic tests [28-30]. Therefore, the vast majority of patients with BrS will have negative genetic testing at this time. Additionally, even within families known to carry genetic mutations consistent with

BrS, there is a poor correlation between genetic testing, ECG manifestations, and clinical outcomes [28]. Furthermore, the presence of genetic mutations in true congenital BrS has been shown to be a poor predictor of arrhythmic events [31] and is not a cost effective method of risk stratification in unselected patients diagnosed with BrS [30]. Therefore, mandatory diagnostic genetic testing in the context of BrP would likely be of poor yield at this time.

We also acknowledge that not all patients with exposure to various underlying conditions such as hypokalemia, hyperkalemia, adrenal insufficiency or myocardial ischemia will develop a Brugada ECG pattern. This suggests a possible genetic predisposition for these ECG phenomena. However, looking into the same genes that are associated with true congenital BrS may not be of diagnostic yield.

Brugada Phenocopy - Pathophysiology

Interestingly, there must be a fundamental pathophysiological difference in sodium channel function when comparing BrP and BrS patients who are exposed to the similar environmental stimulus. For example, Postema et al [32] reported a case of true congenital BrS in the context of hyperkalemia and acidosis. This patient underwent as *positive* provocative challenge with ajmaline and *negative* SCN5A genetic testing. Interestingly, Recasens et al [13, 23, 34] reported a similar case, however consistent with BrP, where the patient presented with hyperkalemia, hyponatremia, and acidosis with *negative* flecainide provocative challenge. Given the negative sodium channel provocative test, one may suspect alternative underlying mechanisms with various genetic, structural, and environmental interactions yet to be elucidated [33].

Brugada Phenocopy – Clinical Reproducibility

The chronological emergence of new ECG phenomena should include: (i) phenomenological observation; (ii) speculation on pathophysiological mechanisms; (iii) clinical reproducibility; and (iv) experimental model validation.

In the context of BrP, we are at the forefront of this emerging concept. There have been multiple observations of Brugada ECG manifestations in the absence of true congenital BrS [5-22]. Initially, various terms such as Brugada-like patterns, acquired Brugada syndrome, and Brugada mimicking ECGs were used to describe these cases. Using prior and emerging cases, we have consolidated the terminology and created a definition (Table 2), an etiological classification (Table 1), and a systematic diagnostic approach to study these cases [2, 5, 12, 25, 26].

Speculations on the pathophysiological mechanisms of BrP were published elsewhere [2, 10, 12, 19, 25, 26, 27] and finally, clinical reproducibility was demonstrated in the context of recurrent severe hypokalemia [19]. Briefly, a young patient with diarrhea was admitted to hospital due to severe hypokalemia (K 1.5 mmol/L) with acidosis. The ECG depicted a typical type 1 Brugada ECG pattern. Upon resolution of the metabolic disorder, the ECG returned to normal. A flecainide test did not induce a Brugada type 1 pattern. Before diarrhea completely resolved, the patient presented with a second episode of hypokalemia (K 2.6 mmol/L) without acidosis. The ECG again depicted a typical type 1 Brugada ECG pattern which resolved after correction of the metabolic abnormality. This case confirms clinical reproducibility, which as suggested above, is the third step in the validation model of new ECG phenomenon.

Beyond Clinical Reproducibility – More Questions than Answers

The key to completely understanding the mechanisms behind BrP is to reproduce these phenomena under strictly controlled environmental conditions [34-36]. The development of experimental validation models will help us determine whether BrP are transient alterations of the sodium channels that are not reproducible with a sodium channel blocking test, or alternatively, a malfunction of other ion channels. Similarly, a model that induces genetic modifications to reproduce the conditions of true BrS and exposing this model to the well described conditions of BrP would help us to understand whether they are entities that belong to the same spectrum or completely different entities. In that sense, the model that found genetic alterations in patients with acquired Long QT [37] should serve as inspiration to develop the BrP experimental model.

In order to learn about the natural history of BrP, we are developing an international online database at www.brugadaphenocopy.com which will allow for longitudinal follow-up. We encourage all investigators that are currently reporting on these cases to use the term *Brugada Phenocopy* in order to facilitate literature searches and to help establish this emerging concept [38, 39].

References

[1] Bayés de Luna A, Brugada J, Baranchuk A, et al. Current electrocardiographic criteria for diagnosis of Brugada pattern: a consensus report. *J Electrocardiol*, 2012; 45: 433.

[2] Baranchuk A, Nguyen T, Ryu MH, et al. Brugada phenocopy: new terminology and proposed classification. *Ann Noninvasive Electrocardiol*, 2012; 17:299.

[3] Pérez Riera AR, Uchida AH, Schapachnik E, Dubner S, Filho CF, Ferreira C. Propofol infusion syndrome and Brugada syndrome electrocardiographic phenocopy. *Cardiol J*, 2010; 17:130.

[4] Arce M, Riera ARP, Femenia F, Baranchuk A. Brugada electrocardiographic phenocopy in a patient with chronic Chagasic cardiomyopathy. *Cardiol J*, 2010; 17:525.

[5] Anselm DD, Barbosa-Barros R, de Sousa Belém L, Nogueira de Macedo R, Pérez-Riera AR, Baranchuk A. Brugada Phenocopy induced by acute inferior ST-segment elevation myocardial infarction with right ventricular involvement. *Inn Card Rhythm Manag*, 2013; 4: 1092.

[6] Nguyen T, Smythe J, Baranchuk A. Rhabdomyoma of the interventricular septum presenting as a Brugada phenocopy. *Cardiol Young*, 2011; 21: 591.

[7] Nakashima D, Yokoyama R, Tsukuda K, Utsu N, Miyakoshi K. A case showed Brugada-like electrocardiogram by a stent implantation. *Medical Journal of Minami Osaka Hospital*, 2011; 58: 43.

[8] Alvarez PA, Vázquez Blanco M, Lerman J. Brugada type 1 electrocardiographic pattern induced by severe hyponatremia. *Cardiology*, 2011; 118: 97.

[9] Chinushi M, Ohno Y, Sanada A, Aizawa Y. Brugada-type ST-segment elevation influenced by postesophageal reconstruction. *J Cardiovasc Electrophysiol*, 2011; 22: 1292.

[10] Wang JG, McIntyre WF, Kong W, Baranchuk A. Electrocution-induced Brugada phenocopy. *Int J Cardiol*, 2012; 160: e35.

[11] García-Niebla J, Serra-Autonell G, Bayés de Luna A. Brugada syndrome electrocardiographic pattern as a result of improper application of a high pass filter. *Am J Cardiol*, 2012; 110: 318.

[12] Anselm DD, Pérez-Riera AR, Femenía F, Baranchuk A. Brugada Phenocopy in a patient with surgically repaired Pentalogy of Fallot. *Revista Iberoamericana de Arritmologia*, 2012; 3: 20.
[13] Recasens L, Meroño O, Ribas N. Hyperkalemia mimicking a pattern of Brugada syndrome. *Rev Esp Cardiol*, 2013; 66: 309.
[14] Gazzoni GF, Borges AP, Bergoli LC, Soares JL, Kalil C, Bartholomay E. Brugada-like electrocardiographic changes induced by hypokalemia. *Arq Bras Cardiol*, 2013; 100: e35.
[15] Wynne J, Littmann L. Brugada electrocardiogram associated with pulmonary embolism. *Int J Cardiol*, 2013; 162: e32.
[16] Liu R, Chang Q. Hyperkalemia-induced Brugada pattern with electrical alternans. *Ann Noninvasive Electrocardiol*, 2013; 95.
[17] Reingardienė D, Vilčinskaitė J, Bilskienė D. Brugada-like electrocardiographic patterns induced by hyperkalemia. *Medicina* 2013; 49: 148.
[18] Awad SFM, Barbosa-Barros R, de Sousa Belem L, et al. Brugada Phenocopy in a patient with Pectus Excavatum: Systematic review of the ECG manifestations associated with Pectus Excavatum. *Ann Noninvasive Electrocardiol*, 2013 (in press). (2013 Sep;18(5):415-20. doi: 10.1111/anec.12082.)
[19] Genaro NR, Anselm DD, Cervino N, et al. Brugada Phenocopy clinical reproducibility demonstrated by recurrent hypokalemia. *Ann Noninvasive Electrocardiol*, 2013 (in press). (2013 Oct 23. doi: 10.1111/anec.12101. [Epub ahead of print])
[20] Khaire SS, Nagarajarao H, Quin EM, Borganelli SM, Marshall RC. Electrocardiographic brugada pattern induced by quetiapine overdose. *J Investig Med*, 2012; 60: 322.
[21] Khan A, Nash P. Brugada type ECG: Unmasked by a pheochromocytoma. *Eur Heart J*, 2012; 33:1120.
[22] Ertem AG, Dotan M, Kilic H, Yeter E. Brugada like electrocardiography pattern induced by adrenal crisis. *Int J Cardiol*, 2013; 163 Suppl: S204.
[23] Anselm DD, Baranchuk A. Brugada Phenocopy Emerging as a New Concept. *Rev Esp Cardiol*, 2013 ;66: 755.
[24] Recasens L, Meroño O, Bazan V, Ribas N. Brugada Phenocopy Emerging as a New Concept. Response. *Rev Esp Cardiol*, 2013; 66: 756.
[25] Anselm DD, Baranchuk A. Brugada Phenocopy: redefinition and updated classification. *Am J Cardiol*, 2013; 111: 453.
[26] Anselm DD, Baranchuk A. Brugada Phenocopy in the context of pulmonary embolism. *Int J Cardiol*, 2013; 168: 560.
[27] Anselm DD, Rodriguez Genaro N, Baranchuk A. Possible Brugada Phenocopy induced by hypokalemia in a patient with congenital hypokalemic periodic paralysis. *Arq Bras Cardiol*, 2013 (in press). (http://www.arquivosonline.com.br/2014/english/10201/pdf/i10201015.pdf letter to the editor)
[28] Probst V, Wilde AA, Barc J, et al. SCN5A mutations and the role of genetic background in the pathophysiology of Brugada syndrome. *Circ Cardiovasc Genet*, 2009; 2: 552.
[29] Priori SG, Gasparini M, Napolitano C, et al. Risk stratification in Brugada syndrome: results of the PRELUDE (PRogrammed Electrical stimUlation preDictive valuE) registry. *J Am Coll Cardiol*, 2012; 59: 37.
[30] Bai R, Napolitano C, Bloise R, Monteforte N, Priori SG. Yield of genetic screening in inherited cardiac channelopathies: how to prioritize access to genetic testing. *Circ Arrhythm Electrophysiol*, 2009; 2: 6.

[31] Probst V, Veltmann C, Eckardt L, et al. Long-term prognosis of patients diagnosed with Brugada syndrome: Results from the FINGER Brugada Syndrome Registry. *Circulation*, 2010; 121: 635.
[32] Postema PG, Vlaar AP, DeVries JH, Tan HL. Familial Brugada syndrome uncovered by hyperkalaemic diabetic ketoacidosis. *Europace*, 2011; 13: 1509.
[33] Hoogendijk MG, Opthof T, Postema PG, Wilde AA, de Bakker JM, Coronel R. The Brugada ECG pattern: a marker of channelopathy, structural heart disease, or neither? Toward a unifying mechanism of the Brugada syndrome. *Circ Arrhythm Electrophysiol*, 2010; 3: 283.
[34] Wilde AA, Postema PG, Di Diego JM, et al. The pathophysiological mechanism underlying Brugada syndrome: depolarization versus repolarization. *J Mol Cell Cardiol*, 2010; 49: 543.
[35] Yan GX, Antzelevitch C. Cellular basis for the Brugada syndrome and other mechanisms of arrhythmogenesis associated with ST-segment elevation. *Circulation*, 1999; 100: 1660.
[36] Di Diego JM, Cordeiro JM, Goodrow RJ, et al. Ionic and cellular basis for the predominance of the Brugada syndrome phenotype in males. *Circulation*, 2002; 106: 2004.
[37] Mahida S, Hogarth AJ, Cowan C, Tayebjee MH, Graham LN, Pepper CB. Genetics of congenital and drug-induced long QT syndromes: current evidence and future research perspectives. *J Interv Card Electrophysiol*, 2013; 37: 9.
[38] Postema PG, Wilde AA. Do J waves constitute a syndrome? *J Electrocardiol*, 2013; 46: 461.
[39] Peters S. Early repolarization pattern in patients with provocable Brugada phenocopy: A marker of additional arrhythmogenic cardiomyopathy? *Int J Cardiol*, 2013. doi: 10.1016/j.ijcard.2013.07.089. [Epub ahead of print].(2013 Oct 12;168(5):4928-9. doi: 10.1016/j.ijcard.2013.07.089. Epub 2013 Jul 25.)

VCG PATTERNS FOR DIFFERENTIAL DIAGNOSIS IN RIGHT END-CONDUCTION DELAY, EARLY REPOLARIZATION AND BRUGADA SYNDROME

C.A. Pastore, N. Samesima, E. Kaiser, H.G Pereira Filho

Heart Institute (InCor) – Hospital das Clínicas da Faculdade de Medicina da USP, São Paulo, Brazil
Email: ecg_pastore@incor.usp.br

Abstract. *Electrocardiographic (ECG) and vectorcardiographic (VCG) events occurring almost concomitantly during electrical activation of the heart may present similar electrocardiographic aspects such as the QRS loop right end-conduction delay (RECD), early repolarization (ER) phenomenon in anterior leads, and J-point elevation in leads V1-V3 in Brugada syndrome (BrS) which can confuse the correct diagnosis,. To analyse the three planes of VCG to establish differential aspects that could identify these entities, ECGs/VCGs of patients with BS (n = 20), ER (n = 15) and RECD (n = 10) were analysed, and specific characteristics were compared. ECG characteristics were typical for these abnormalities, but with difficulties in differentiating right end-conduction delay from ER notch/delay or J point elevation in BrS. In the horizontal plane, VCG loops showed slowing at the end of ventricular electrical activation in all cases, followed by a very precise/small gap between the end of QRS and beginning of T-wave loops, in all BrS and ER cases. This gap was not evidenced in RECD (0/10). The QRS loop in RECD was always located in the right posterior quadrant (10/10). In BrS, this location was 100% in the right anterior quadrant, while in ER it was 100% in left posterior quadrant. Also, with respect to ER and BrS cases, a "break" in the QRS loop, very much resembling a "nose", was seen immediately before the beginning of the T-wave loop in BrS (18/18). In ER, however, there was the clear presence of a "fishhook" shape at the end of the QRS loop in 100% cases. In conclusion,ECG tracings where aspects of Brugada Syndrome, ER and RECD occur in association with one another or with other variations, pose a challenge to the reader's ability to make an accurate differential interpretation. Vectorcardiography can enable better observation of the corresponding ECG alterations and help to distinguish them, thus preventing the need for inadequate and excessive diagnostic tests.*

Keywords: Differential Diagnosis, Right End-Conduction Delay, Early Repolarization, Brugada Syndrome

1. Introduction

The vagaries of electrical activation of the heart produce waves on the electrocardiogram that characterize classic phenomena which are familiar to us; however, they may also yield similar ECG aspects for situations which have distinct etiologies. Alterations of the J point (consisting of the final portion of the QRS complex and the beginning of the ST-segment) have been thoroughly described in a number of pathologies [1, 3]. However, the underlying mechanisms of such alterations can have an autonomic origin or be the result of dysfunctional ion channels, or even reflect disturbances in the electrical conduction of impulses [2]. The careful observation of electrocardiographic patterns, and knowledge gained by contributions that vectorcardiographic loops may offer, enable us to distinguish, with qualified accuracy, many reasons that can lead to a J point alteration. This can be done through a regional analysis of electro-verctorcardiographic alterations, e.g., those which occur in the epicardial region of the right ventricle in the Brugada syndrome (BrS), seen in leads V1, V2 and V3;

alterations caused by the early repolarization (ER) phenomenon, most commonly present in the anterior wall of the left ventricle, observed in leads V3, V4 and V5; or even those of the end-conduction delay of the right ventricle (RECD), with its diffuse pattern that can be detected in leads D1, aVR, V1, V5 and V6.

Therefore, the comparative electro-vectorcardiographic study of such alterations can aid in the differential diagnosis of the pathologies described above, and may create new ECG-VCG criteria that may thoroughly define the underlying etiology of these conditions.

2. Methods

We analysed ECG/VCG tracings of 1) 20 patients with Brugada syndrome (BrS) types I/II; 2) 15 patients with Early Repolarization (ER) patterns: presence of a notching or a delay at the final portion of the QRS complex, a J point elevation, with or without ST-segment elevation; and 3) 10 patients with Right End-Conduction Delay (RECD). Specific characteristics of those tracings were compared, as QRS duration, onset and offset of QRS loop, J point and ST segment localization in the three planes (frontal, horizontal and sagittal).

3. Results

The usual ECG aspects were obtained for these abnormalities. However, some difficulties have arisen as to the differentiation of a right end-conduction delay from the typical early repolarization notching/delay, or from the J point elevation in BrS. In the horizontal plane, VCG loops in all BrS and ER cases showed a slowing at the end of the ventricular electrical activation, followed by a very neat gap between the end of the QRS complex and the beginning of the T-wave loops. This gap was not evidenced in RECD (0/10). The QRS loop in RECD was always located in the right posterior quadrant (10/10). In BrS this location was 100% in the right anterior quadrant, while in ER it was 100% in the left posterior quadrant.

Also, by comparing ER and BrS tracings, we noticed that a "break" in the QRS loop, very much resembling a "nose", was seen immediately before the beginning of the T-wave loop in BrS (18/18). In ER, however, there was the clear presence of a "fishhook" shape at the end of the QRS loop, in 100% of the cases.

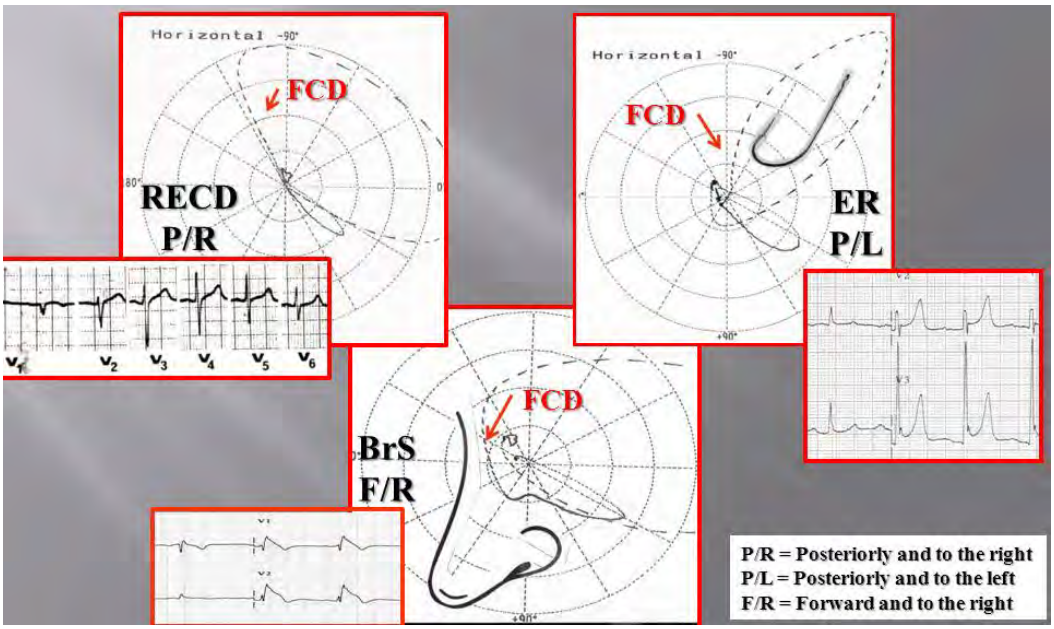

Fig. 1. Differential ECG/VCG aspects of the final conduction delay (FCD) in cases of (clockwise) Right End-Conduction Delay (RECD), Early Repolarization (ER) and Brugada Syndrome (BrS).

4. Discussion

The difficulties in identifying electrocardiographic alterations in situations where different cardiac electrical phenomena overlap have been known for a long time [1]. Therefore, when there is the need for differential diagnosis, all the tools at hand must be employed to explain the electrical nuances of ventricular activation.

As we made further investigations into the electrical phenomena of the J point syndromes, we were stimulated to study the vectorcardiographic loops, which enable us to have a spatial visualization of those uncharacteristic and intermittent manifestations. This discussion intends to show the importance of describing the various manifestations of the different types of early repolarization, and also some of the similar characteristics they share with the Brugada syndrome. The many similarities of ER and BrS include the genetic inheritance of patterns, they occur predominantly in the male gender and in healthy young individuals, the variability of appearance they show on the ECG, and their response to a drug challenge (autonomic modulation).

The differences we can find among these patterns are clinically significant. Although they may have a benign expression, they may also include electrical situations in which there is a high risk of severe arrhythmias and even sudden cardiac death.

From the electro-vectorcardiographic viewpoint, we were able to define neatly distinct patterns in those two syndromes (ER and Brugada), which can allow us to precisely differentiate between those two phenomena. (See Fig. 1)

As we thoroughly studied the final conduction delay (FCD) aspects, which were present in both syndromes, we could see that they shared many similar aspects. Therefore, we compared ECG and VCG tracings of patients with either early repolarization or Brugada syndrome, with those of patients with a final conduction delay, in order to demonstrate the significance of FCDs in characterizing the different patterns; in addition, we observed whether FCDs were capable of altering the ECG/VCG aspects of the syndromes we were studying.

Pérez-Riera et al., in 2012, [4] have already compared and described the Brugada patterns with those of incomplete and complete right bundle-branch block. Our findings attempted to establish a relationship with the alterations occurring at the final portion of the QRS complexes and VCG loops (J point, ST-segment and T-wave), particularly in the precordial leads V1, V2 and V3, to understand the presence of gaps in the two syndromes we were studying (Fig. 1). Such findings, which in general can be explained by electrical gradients or ion channel dysfunctions, can define distinct types of behaviour of ventricular repolarization that may or may not be the grounds for severe arrhythmias (dispersion of repolarization).

The localization of the alterations as defined by the vectorcardiogram could distinguish the events described above, and could enable us to have a clearer observation of the related electrocardiographic modifications.

An accurate definition of the syndromes as described above can make it easier, and may even contribute, to the election of a therapeutic approach, when necessary, thus preventing the performance of inadequate and excessive diagnostic tests.

5. Conclusions

- Analysis of the differential ECG patterns can be better noticed after performing a vectorial interpretation of the activation.
- The classic ECG aspects of Brugada Syndrome, ER and RECD are well known, however, when they occur associated to one another or with other variations, many diagnostic difficulties may arise.
- Localization of the alterations as defined by the Vectorcardiogram can distinguish the events above described, and can enable easier observation of the related electrocardiographic modifications.
- A proper definition of the above described syndromes can make it easier, and also may contribute, to the choice of the necessary therapeutic approach, thus preventing the performance of inadequate and excessive diagnostic tests.

References

[1] Osborn JJ. Experimental hypothermia: respiratory and blood pH changes in relation to cardiac function. *Am J Physiol*, 1953; 175:389.

[2] Gussak I, Antzelevitch C. Early repolarization syndrome: clinical characteristics and possible cellular and ionic mechanisms. *J Electrocardiol*, 2000; 33: 299.

[3] Haissaguerre M, Derval N, Sacher F, et al. Sudden cardiac arrest associated with early repolarization. *N Engl J Med* 2008; 358: 2016.

[4] Pérez-Riera AR, Ferreira Filho C, Abreu LC, Ferreira C, Yanowitz FG, Femenia F, et al. Do patients with electrocardiographic Brugada type 1 pattern have associated right bundle branch block? A comparative vectorcardiographic study. *Europace* 2012; 14: 889–897.

FUSION OF BIVENTRICULAR INCOMPLETE BUNDLE BRANCH BLOCK IN HEALTHY YOUNG ADULTS AND IN PATIENTS WITH MODERATE PULMONARY HYPERTENSION. FRAGMENTED DEPOLARIZATION – A NEW REAL ECG ENTITY.

[1]L. Regős, [2]A. Simon, [3]B. Garai, [4]I. Berényi, [5]Z. Antalóczy

[1]Újpesti Health Nonprofit Kft, Budapest, Hungary
[2]Szt. Imre Hospital Cardiology, Budapest. Hungary
[3]Károlyi Sándor Hospital, Budapest, Hungary
[4]Balatonfüred Heart Hospital, Balatonfüred, Hungary
[5]Postgraduate Medical School, Budapest, Hungary
Email: regos44@gmail.com

Abstract. *Interpretation and decomposition of fragmented depolarization may result in new ECG attributes, even in healthy patients. Searching for their components, we aimed to produce new groups making use of well-documented incomplete ventricular conduction disturbances, and demonstrating their attributes simultaneously. As a result of this, first analyzing then synthesizing procedure, displaying the different incomplete right ventricular and incomplete left ventricular blocks simultaneously, we present the narrow-QRS-characterized benign version of the arborization block as a new ECG entity.*

Keywords: Biventricular Incomplete Blocks, Fragmented Depolarization, Competition of Vector Components, Arborization Block-like Forms.

1. Introduction

If we make a comparison between the electrical occurrences of the heart and a human head, the shape or outline of the latter may correspond to the electrical vectors produced by the heart. Turning the head, showing the characteristic profile, it may be interpreted as a diagnosis based on the ECG signals in the frontal plane leads as the resultant vectors of the atrium and the ventricle are displayed dominantly in the frontal plane. Henceforth we concentrate on the incomplete conduction disturbances in the frontal plane.

Within the QRS complex, the vector components either compete with each other or can appear at the same time. The two best examples which modify the shape of the original electrocardiogram (ECG), are ventricular preexcitation (Fig. 1A) and complete left bundle branch block (Fig. 1B).

In contrast, the rS complex of left anterior (antero-superior) hemiblock (LAH) and the Q wave of postero-inferior myocardial infarction (PI MI) can be observed simultaneously, forming a W complex in the inferior leads.

When studying the ECG waveform and interpreting the depolarization vectors in detail, it is not always advantageous to use the conventional ECG (QRS) nomenclature. On the other hand, if we use the numerical values of the sampled vectors, taken every 5 or 10 msec, we can lose the amplitude maxima of waves and depart from the graphical representation used by clinicians.

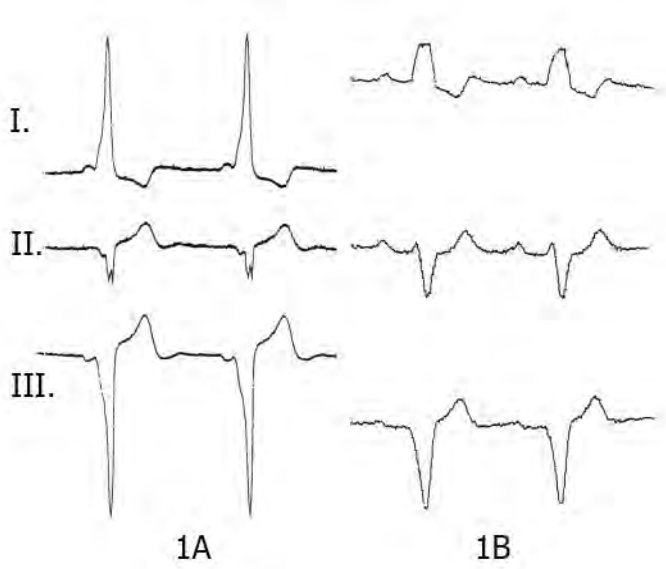

Fig. 1. Abnormal, left ventricular epi-endocardial transmural activation changes of the normal ECG characters. Partial (delta wave) in ventricular pre-excitation (1A), and whole depolarization in left bundle branch block (1B).

2. Methods

Cases were selected from 2,500 patients over a period of six months from an outpatients' department which received 20 persons per day. Fifty nine patients were selected on the basis of incomplete conduction disturbances of which 36 were female and 23 male with an average age of 22.6 years. 60 % of the chosen patients were healthy sportsmen/sportswomen aged between 16-20 years. Using echocardiographic measurements, we found moderately elevated, symptom free idiopathic pulmonary hypertension in 25 out of all of the patients. The arterial mid-pressure was below 28 mmHg. [1] The chosen ECG deviations were grouped on the basis of incomplete right ventricular conduction disturbance, i.e. incomplete right bundle branch block (IRBBB): 1: type SI-SII-SIIII (n=20); 2: SI-QIII (n=18); 3: both SI-SII-SIII and SI-QIII patterns (n=8), (see Fig. 2A, 2B, 2C) [2].

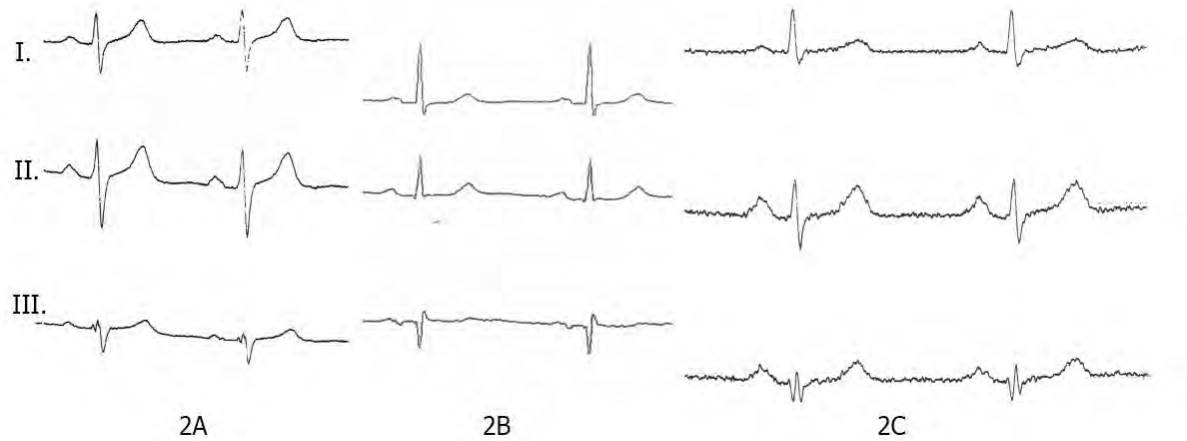

Fig. 2. Incomplete right bundle branch blocks. 2A: SI-SII-SIII 2B: SI-QIII 2C: SI-SII-SIII and SI-QIII, both patterns.

The presence or absence of IRBBB signals in lead V1 was also recorded in each group, but is not shown here.

In addition, two further patterns were formed. Both are characterized by a depolarization inhomogeneity. 4: IRBBB+LAH (n=16): biventricular incomplete blocks and arborization block-like types (Fig. 3A). 5: from the unhealthy group: IRBBB+PI MI (Fig 3B, 3C).

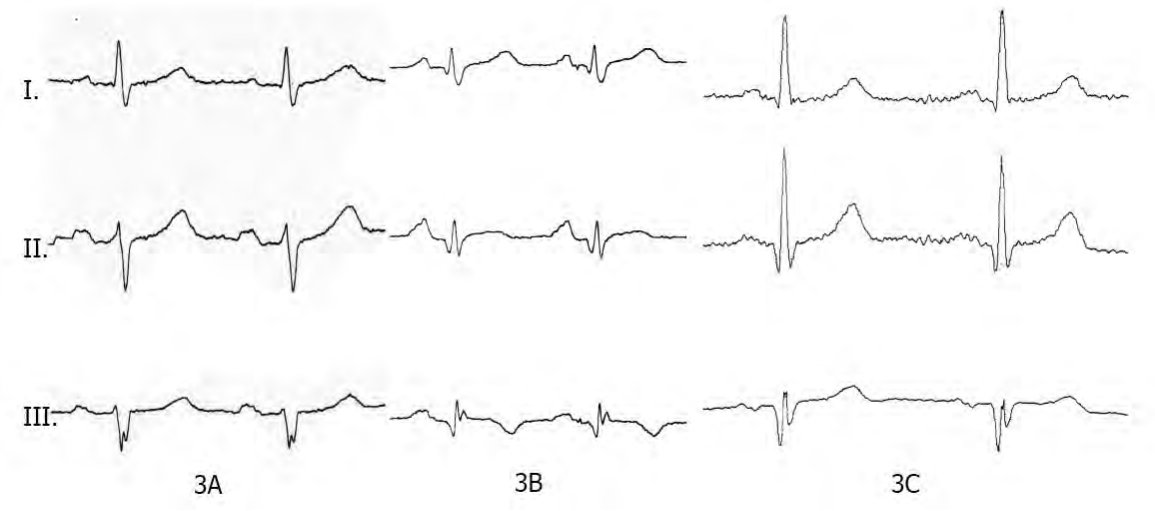

Fig. 3. Left and right ventricular incomplete bundle branch blocks: SI-SII-SIII and left anterior hemiblock (3A). Postero-inferior myocardial infarction and right incomplete conduction disturbances, SI-QIII (3B), QI-SIII (3C).

3. Results

IRBBB morphologies, also well documented in the ECG literature, are found in groups 1 and 2. Their ECG characteristics (i.e. the names of their identifying waveforms), are displayed mainly in the frontal plane (Fig 2.). In group 3 (8 patients) the simultaneous appearance of SI-QIII and SI-SII-SIII patterns are demonstrated (Fig. 2C). In this group it can be seen that the typical ECG characteristics are different from each other. In lead I, fusion of the S waves can be seen in some cases resulting in a jagged waveform. In lead III the Q and S waves are displayed independently, separated in time on the ECG (Fig. 2C).

Group 4 illustrates that any of the IRBBB morphologies can be accompanied by a left ventricular incomplete conduction disturbance, in most cases also LAH. The LAH + complete RBBB morphology, as a clinical entity, is known as Lenegre's disease [34]. In cases of LAH+IRBBB fusion, two versions are prevalent: a) LAH+SI-QIII, where a W complex appears in lead III; and b) LAH+SI-SII-SIII, where a W complex can be seen in lead III (Fig. 3A). It does not occur only in young and healthy persons (mainly in sportsmen/sportswomen) but is also as a symptom of ischemic heart disease.

In group 5, a pattern similar to the latter electrical fusion can be seen. To establish sub-groups for the conduction disturbances of the right ventricle, in the first step an up-to-now accepted standpoint should be rejected, namely that the Tawara branch is homogenous. In our opinion, IRBBB can evolve not only on an ischemic basis but also in case of mild burdening of the ventricles, at their weak points. The cases shown confirm this theory [2]. In this group the pattern of IRBBB + postero-inferior infarction can be observed. In the first case, SI-QIII IRBBB morphology is attached to the known combination of inferior infarction (Fig. 3B). This results in an unusual fragmentation of depolarization. In the second case, the postero-inferior infarction is decisive, too, which is now accompanied by QI-SIII IRBBB. This is also characterized by the W morphology in lead III. (Fig. 3C).

Although in the Figures there are no such groups, theoretically it is necessary to demonstrate the existence of more cases in which the simultaneous occurrence of QI-SIII+SI-SII-SIII or QI-SIII+SI-QIII combined with LAH are displayed.

Finally, we demonstrated some unusual wave fragmentations (Fig.4.)

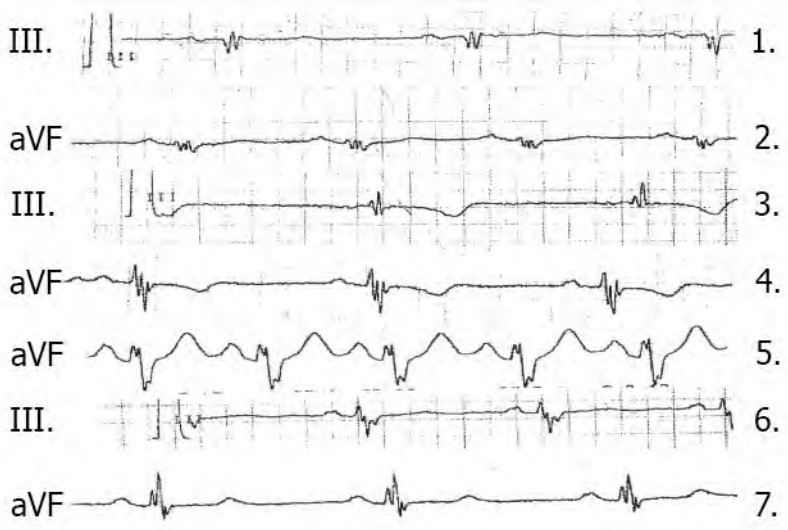

Fig. 4. Leads: III, or aVF. Unusual wave fragmentations in the leads. The depolarization morphology cannot be characterized by the classic Q, R, and S names. Curve 5. shows MW morphology and P enlargement too, the P pulmonale-like wave is an intermittent right atrial internodal block.

4. Discussion

In young people, ECG deviations are often observed in the absence of any underlying pathology. The best known is the respiratory arrhythmia. Incomplete conduction disturbances are often manifested among the ventricular bundle branch blocks,. In cases of their combination, attached to incomplete conduction disturbances of the left ventricle, a fragmentation, i.e. breaking into many components of the QRS are seen. This bizarre pattern often cannot be explained in clinical practice. There are few definitions in the literature on the arborization block, which in the case of serious cardiac disease (necroses, cardiomyopathy), causes enlarged depolarization (QRS>140 msec) leading to grave depolarization inhomogeneity, which can be the root cause of life-threatening rhythm disturbances [5], [6]. Conduction block in the Purkinje system, namely arborization block, causes QRS complexes to be distorted and markedly prolonged. Another feature is low voltage. In case of the simultaneous occurrence of right ventricular incomplete conduction disturbances (group 3.), combined with LAH, (group 4.) similar patterns can be seen even at narrow QRS and regular amplitudes, frequently without causing any clinical danger (Fig. 4.). They can be caused by excessive intensive training by young sportspeople, transitionally increasing values of pulmonary circulation pressure and the resulting pressure-burden of the right ventricle, mild damage of the Purkinje-myocardium junction. By interpreting and breaking down these fragmented depolarization waves, we can exclude the defects of serious myocardial defects and the significant activation delays in the heart muscle. As a result, we describe an ECG entity unknown until now, the fragmented but narrow QRS, which is neither combined with significant depolarization inhomogeneity, nor with life-threatening rhythm disturbances. In group 5, two patients are described who had suffered from postero-inferior myocardial infarction. Their heart muscles are damaged. In the case of the first patient, the fragmentation of the depolarization is explained by the components of both incomplete conduction

disturbances (2 different types of IRBBB). With the second patient, the origin of the QRS pattern change is the rarer IRBBB combined with left ventricular necrosis, the QI-SIII. It is important to note that the QRS width of neither of the patients is less than 120 msec.

5. Conclusion

We tried to analyse phenomena in unusual and seemingly unclassifiable ECG deviations. By making a correct diagnosis, the opinion concerning the patient's life-chances, the medical treatment (prescribing ß-blockers or not) may change fundamentally. ECG patterns manifesting themselves simultaneously and not as fusion, constitute, in our opinion, a new chapter of cardiology open to further investigation.

References

[1] Galiè, N, Torbicki, A, Barst, R, Dartevelle, P, Haworth, S, Higenbottam, T, Olschewski, H: Guidelines on diagnosis and treatment of pulmonary arterial hypertension. The Task Force on Diagnosis and Treatment of Pulmonary Arterial Hypertension of the European Society of Cardiology. *Eur. Heart J*, 2004; 25:2243–2278.

[2] Regős L: ECG. Incomplete Combined Ventricular Conduction Disturbances. White Golden Book Kft. Budapest 2010.

[3] Lenegre J: Etiology and pathology of bilateral bundle branch block in relation to complete heart block. *Progr. Cardiovascular Disease,* 1964: 6: 409-444.

[4] Lepeschkin E: Electrocardiographic diagnosis of bilateral bundle branch block in relation to the heart block. *Progr. Cardiovascular Disease*, 1954; 6: 445-471.

[5] BS: Bertram S Nissé, Congenital Heart Disease associated with Arborization Block of the Left Branch Bundle. *Proc R Soc Med,* 1929 February; 22 (4): 405–406.

[6] Watt Jr. TB, Freud G.E, Durrer, D. Pruitt, RD: Left Anterior Arborization Block Combined with Right Bundle Branch Block in Canine and Primate Hearts. An Electrocardiographic Study. *Circ. Res,* 1968; 22**:** 57-64

2. Clinical Electrocardiography

NORMAL LIMITS OF THE P WAVE IN A NIGERIAN COHORT

[1]I. Katibi, [1]A. Omotoso, [1]P. Kolo, [1]J. Ogunmodede, [1]O. Aiyedun, [1]W. Alaofin, [1]A. Olokoba, [1]A. Salami, [1]T. Omoneyin, [1]R. Akim, [1]A. Peter, [1]A. Abimbola, [2]E. Clark, [2]B. Devine, [3]S. Lloyd, [2]P. Macfarlane

[1]Department of Medicine, University of Ilorin, Ilorin. Nigeria,
[2]Institute of Cardiovascular and Medical Sciences, University of Glasgow, Glasgow, UK,
[3]Robertson Centre for Biostatistics, University of Glasgow, Glasgow,UK
Email: iakatibi@unilorin.edu.ng

Abstract. *The normal limits of the P wave in Nigerians were derived using automated methods. Previous studies adopted manual analysis. This study included 782 and 479 apparently healthy males and females respectively, with ages between 20 and 87 years.A single upright P wave was the most common type found and was mostly seen in lead II (96.0%). A biphasic P wave with initial upright component was mainly seen in lead V1 (60.9%). A biphasic P wave with initial inverted component was uncommon in this study (0.2%).The upper normal limits of P wave amplitude varied with gender, Electrocardiogram (ECG) lead and age. They were found to be slightly higher than earlier reported upper limits of normal in the same population and indeed, British and Chinese populations. Age and gender trends were, however, not statistically significant for P wave duration which varied from 130 to 134ms in males and 126 to 138ms in females respectively.*

Keywords: Normal limits, ECG, P waves, Nigerians, Automated ECG analysis

1. Introduction

The P wave is often used to assess the size of the atria in the electrocardiogram (ECG), a parameter that has both diagnostic and prognostic significance. Although the P wave of the normal ECG has been well studied for several racial groups using automated methods, it has not been investigated in indigenous Black Africans [1,2]. All previously reported ECG studies involving Nigerians have entailed using manual rather than automated analysis [3]. This is therefore the first report of P wave amplitudes in apparently healthy Nigerians with a view to comparing the findings with earlier documented reports in the same population using manual analysis, and with other racial groups using automated methods.

2. Methods

12 lead ECGs were recorded in apparently healthy Nigerians using a Burdick Atria 6100 electrocardiograph. ECGs were forwarded in digital form to the University of Glasgow and analysed using the Glasgow program [4]. Details of the methodology and statistical analysis used to derive normal limits have been published elsewhere [5]. Of particular relevance to the present study is that overall P wave duration is defined to be the same in all leads of an ECG but within the onset and termination, the amplitude and duration of P+ and P- components can vary by lead.

3. Results

The study included 782 males (mean age 43.1 ± 13.4 years) and 479 females (mean age 42.6 ± 14.5 years), all apparently healthy, with ages between 20 and 87 years. There were more males in the younger age groups than in the older groups.

A single upright P wave was the most common P wave morphology and was mainly seen in lead II (96.0%). A single inverted P wave was seen in lead aVR. A biphasic P wave with initial upright component was most commonly seen in lead V1 (60.9%). A biphasic P wave with initial inverted component was uncommon (0.2%) and was seen most frequently in females at the extremes of age.

Table. 1. P+ wave amplitude by age group and gender in all leads. Data are presented as Mean (SD), 2nd – 98th percentile of ranges and total no in the group.

	Age group (years)									
	20-29		*30-39*		*40-49*		*50-59*		*60+*	
Leads	*Male*	*Female*	*Male*	*Female*	*Male*	*Female*	*Male*	*Female*	*Male*	*Female*
I	79.68 (25.35)	89.04 (25.25)	85.38 (26.17)	94.31 (23.94)	80.26 (24.40)	92.03 (27.86)	85.21 (24.34)	94.02 (26.95)	79.20 (30.03)	89.46 (25.74)
	34 - 142	41 - 151	39 - 149	54 - 144	36 - 143	51 - 145	43 - 139	46 - 163	30 - 164	45 - 155
	n = 122	n = 97	n = 221	n = 110	n = 199	n = 107	n = 133	n = 89	n = 105	n = 74
II	176.35 (59.58)	148.51 (55.90)	162.55 (55.60)	159.53 (54.07)	176.66 (56.53)	158.24 (55.27)	162.10 (46.68)	175.21 (51.32)	179.04 (52.76)	164.45 (51.53)
	66 - 311	43 - 271	59 - 292	54 - 268	53 - 317	45 - 251	64 - 259	80 - 301	93 - 289	79 - 275
	n = 123	n = 97	n = 219	n = 110	n = 199	n = 107	n = 134	n = 90	n = 105	n = 74
III	127.22 (60.54)	95.72 (48.00)	106.82 (52.12)	91.88 (42.20)	121.61 (55.57)	95.73 (44.83)	104.66 (45.51)	106.70 (51.32)	122.46 (50.58)	102.75 (48.04)
	26 - 271	18 - 215	22 - 220	14 - 185	22 - 254	14.5 - 197	19 - 198	22 - 229	38 - 218	28 - 196
	n = 122	n = 89	n = 211	n = 103	n = 195	n = 100	n = 133	n = 89	n = 105	n = 72
aVR	-	-	-	-	-	-	-	-	-	-
	-	-	-	-	-	-	-	-	-	-
	-	-	-	-	-	-	-	-		
aVL	38.01 (19.54)	43.39 (24.14)	41.16 (24.45)	37.55 (21.46)	33.34 (20.09)	42.96 (23.09)	36.24 (18.66)	35.99 (20.71)	37.71 (19.44)	36.31 (23.45)
	14 - 81	9 - 96	11 - 105	7 - 84	9 - 90	7 - 97	10 - 82	8 - 80	12 - 78	6 - 102
	n = 70	n = 75	n = 159	n = 93	n = 120	n = 77	n = 94	n = 71	n = 52	n = 55
aVF	148.36 (59.92)	115.58 (54.22)	131.29 (53.79)	119.78 (49.84)	147.23 (55.04)	121.65 (49.83)	130.19 (45.56)	137.48 (51.23)	148.48 (50.64)	128.82 (50.98)
	42 - 286	16 - 236	36 - 254	21 - 218	40 - 283	24 - 226	34 - 227	30 - 267	65 - 246	37 - 232
	n = 123	n = 96	n = 217	n = 110	n = 197	n = 106	n = 134	n = 90	n = 105	n = 74
V1	97.93 (32.22)	80.77 (29.14)	80.56 (30.22)	91.64 (28.60)	72.91 (28.59)	84.49 (32.65)	61.79 (25.42)	78.50 (32.59)	60.22 (29.17)	76.04 (32.06)
	30 - 166	32 - 155	28 - 147	37 - 159	26 - 139	31 - 170	26 - 127	28 - 188	17 - 145	22 - 149
	n = 122	n = 97	n = 220	n = 110	n = 181	n = 106	n = 125	n = 90	n = 93	n = 72
V2	79.52 (28.90)	76.12 (22.41)	73.06 (29.88)	85.74 (27.73)	61.63 (27.58)	80.91 (33.45)	61.28 (30.83)	74.37 (34.07)	59.27 (27.66)	76.49 (29.65)
	31 - 148	43 - 145	24 - 162	45 - 154	20 - 137	35 - 164	20 - 124	26 - 207	14 - 131	33 - 169
	n = 122	n = 97	n = 218	n = 109	n = 190	n = 106	n = 130	n = 91	n = 98	n = 72
V3	77.81 (26.17)	76.78 (24.67)	69.72 (27.69)	86.47 (27.59)	62.97 (26.57)	87.16 (34.40)	65.36 (25.44)	86.40 (33.97)	63.27 (27.02)	88.54 (30.79)
	33 - 150	31 - 135	27 - 141	45 - 157	21 - 125	35 - 181	21 - 123	27 - 194	21 - 122	36 - 153
	n = 122	n = 97	n = 220	n = 109	n = 194	n = 107	n = 134	n = 91	n = 102	n = 74
V4	75.93 (25.36)	72.26 (24.16)	69.62 (25.55)	81.94 (25.74)	64.18 (25.28)	83.12 (28.52)	70.19 (25.10)	84.48 (24.84)	68.19 (26.57)	86.26 (29.13)
	29 - 140	31 - 138	29 - 132	40 - 140	19 - 131	41 - 147	22 - 129	40 - 136	20 - 124	34 - 169
	n = 123	n = 97	n = 220	n = 109	n = 197	n = 107	n = 134	n = 90	n = 104	n = 74
V5	78.28 (24.13)	71.59 (22.57)	71.52 (24.09)	79.27 (24.46)	68.29 (23.62)	81.92 (24.61)	73.42 (22.62)	86.07 (26.57)	76.32 (32.74)	90.47 (44.76)
	38 - 143	31 - 123	30 - 141	41 - 129	25 - 124	40 - 131	33 - 129	44 - 173	22 - 140	38 - 170
	n = 123	n = 97	n = 221	n = 110	n = 199	n = 107	n = 134	n = 90	n = 105	n = 74
V6	79.42 (23.73)	73.31 (22.91)	72.98 (21.79)	77.46 (23.19)	72.75 (21.51)	80.44 (23.45)	74.55 (21.79)	86.40 (23.73)	77.22 (26.78)	86.03 (25.64)
	39 - 134	32 - 136	36 - 144	39 - 133	28 - 122	35 - 131	36 - 123	47 - 149	33 - 142	37 - 159
	n = 123	n = 97	n = 219	n = 109	n = 199	n = 107	n = 134	n = 90	n = 105	n = 74

P Positive (P+) amplitude

The P+ wave amplitudes are presented in Table 1 for the various leads. P+ wave amplitude appears to vary with age, gender and ECG leads. The upper limits in lead II ranged from 259 to 317μV in males and 251 to 301μV in females respectively. There were no P+ wave amplitudes for lead aVR while lead II has the highest mean P+ wave amplitudes. While in lead II and some other leads, P+ wave amplitude was higher in males by 9.65μV, the converse

was true for lead I where females had higher amplitude (Mean difference =9.59μV at P <0.0001).

The upper limits of P+ wave amplitude varied with gender, ECG lead and age. After adjusting for both age and gender, the effect of age on P+ wave amplitude becomes statistically insignificant (P=0.22). Lead aVL generated the lowest P+ amplitude of all leads.

P+ wave duration

P+ wave duration was highest in Leads II, V5 and V6. The variations by age and gender were not found to be statistically significant. The upper limits of normal overall P wave duration in lead II ranged with respect to age groups, from 130 to 134ms in males and 126 to 138ms in females respectively. Detailed P wave duration by age group and gender for this population has previously been published [5].

P minus (P-) wave amplitude

In the normal ECG, a P- wave is seen in leads V1 and aVR. As such, the presentation of this aspect of the results focuses mainly on these two leads. In lead V1, the depth of the P- wave was consistently higher in males than females. The mean difference in P- wave amplitude was 8.95μV (P=<0.0001). P- wave amplitude increased progressively and significantly with aging in both genders (P=<0.0001). The converse was the case in lead aVR.

4. Discussion

This work has presented a comprehensive description of P waves in apparently healthy Nigerians. While no attempt was made to identify new morphologic categories, a detailed account has been given of the proportional representation of the various types by age group, gender and ECG leads. This does not tally exactly with earlier published work. Araoye generally reported lower proportions of single upright (60-70%) and biphasic P waves (58.9%) in leads II and V1 respectively than in this study. However, he independently reported, notched P waves in 17% and a flat P wave in 10% of the population he studied [3]. Clearly, Araoye's study did not bring to the fore the rising prevalence of biphasic P waves with advancing age as presented in this study. Perhaps, this reflects increased left atrial size. Araoye's study also reported that 31% and 28% of the subjects with biphasic P waves had a dominant upright and inverted morphology respectively while both phases were equal in 41%. This is totally at variance with the observation from our present study as the dominant inverted variety was very uncommon (0.2%). One possible reason for the difference in proportion is the poorer frequency response of the older equipment, making measurements less accurate than is possible with today's digital electrocardiographs. This has been a major draw-back in the methodology of earlier studies.

P wave amplitude

The upper limits of normal for P wave amplitude from this study ranged from 251 to 317μV. Macfarlane et al, in a Scottish population from the West of Scotland reported 242 to 305μV as upper limits of normal [1]. The difference between the means of P wave amplitudes between the Nigerian and British populations were statistically significant (P<0.0001). Chen et al [2], and Wu et al [6], at different times studying separate Chinese cohorts, reported upper limits of normal of 170-190μV and 150-200μV respectively, both of which are lower than either of the upper limits from this study or the Scottish population [1]. It is well known that Africans, particularly Blacks, generate higher ECG voltages than their Caucasian counterparts.

The P- wave amplitude in V1 has upper limits of 142 and 134μV in males and females respectively in this study. Macfarlane et al reported 91-117 and 79-105μV as upper limits of normal in their Caucasian population [1]. Both populations showed more negative P waves in males and with advancing age.

The differences between the different ethnic groups are probably of limited clinical significance.

P wave Duration

The upper normal limit for overall P wave duration has traditionally been set at 120ms. The 96th percentile upper limit of 138ms determined from this study is similar to the limits quoted from earlier studies [1, 2, 6]. The present study has the added advantage of presenting the age group, gender and lead-specific normal limits which had not been the case with earlier reported studies on an African population. Wu et al [6] had reported upper limits ranging from 125 to 141ms which is comparable to the result of 138ms obtained from this study. The higher value from both studies may be related to the fact that there was simultaneous recording of all ECG leads and the overall P wave duration was determined using the earliest P onset and the latest P offset. A Similar observation was made by Chen et al in their study of a Chinese population, wherein the upper limit ranged from 112 to 146ms, depending on the subject's age [3]. The mean P+ wave durations in lead II were 101 and 108ms in the British and Nigerian populations respectively with the difference in mean being statistically significant ($P<0.0001$).

Of utmost importance was the observation in this study that age and gender trends were not statistically significant in P wave duration just as was reported in studies from other parts of the world, with the exception of Wu et al, who reported a small but consistent difference between genders and an upward trend with increasing age [5]. Araoye had reported a normal reference range of 0.08 to 0.11s among Nigerians [3].

5. Conclusion

This is the first reported study on the normal limits of the P wave in healthy Blacks living in West Africa using automated methods. Some of the findings reported here are in sharp contrast to those earlier reported in the same population using manual analysis. Cognizance must therefore be taken of this observation in any attempt to improve the diagnostic accuracy of automated analysis of the ECG in this population.

References

[1] Macfarlane PW, Lawrie TDV. The normal electrocardiogram and vectorcardiogram, in: Macfarlane PW, Van Oosterom A, Pahlm O, et al, Editors. Comprehensive Electrocardiology. 2nd Edition, London, Springer, 2011, 457.

[2] Chen CY, Chiang B, Macfarlane PW. Normal limits of the electrocardiogram in a Chinese population. *J Electrocardiol*, 1989; 22: 1-15.

[3] Araoye MA. The 12-Lead scalar ECG in Negroes I: Normal values. *Nigerian Medical Practitioner*. 1984; 7: 59-65.

[4] Macfarlane PW, Devine B, Clark E. The University of Glasgow (Uni-G) ECG analysis program. *Comput. Cardiol*, 2005; 32: 451-4.

[5] Katibi IA, Clark E, Devine B, Lloyd S, Macfarlane P. Normal limits of the Electrocardiogram in Nigerians. *J Electrocardiol*, 2013; 46: 289-295.

[6] Wu J, Kors JA, Rijnbeek PR et al. Normal limits of the electrocardiogram in Chinese subjects. *Int J Cardiology*, 2003; 87: 37-51.

FREQUENT ELECTROCARDIOGRAPHIC ABNORMALITIES AND ASSOCIATED CONDITIONS IN CHAGAS DISEASE PATIENTS

[1]L. Ferreira, [1,2]M.S. Marcolino, [1,2]D.M.F. Palhares, [1,2]T.G.P. Assis, [2]M.B. Alkmim, [1,2]A.L. Ribeiro

[1]Medical School and University Hospital, Universidade Federal de Minas Gerais, Belo Horizonte, Brazil
[2]Telehealth Network of Minas Gerais, Belo Horizonte, Brazil
Email: tom@hc.ufmg.br

Abstract. *Our aim was to assess the prevalence of electrocardiographic abnormalities in a large sample of Chagas Disease (ChD) patients evaluated in the primary care setting. This retrospective observational study included all ChD patients whose digital 12-lead electrocardiogram (ECG) was analyzed by cardiologists of the Telehealth Network of Minas Gerais, Brazil, in 2011. Self-reported ChD patients (mean age 57.0±13.7 years, 64.1% female) comprised 7,590 (2.9%) of 264,324 patients whose ECGS were recorded during this period. Hypertension was the most common comorbidity (61.3%), followed by diabetes (9.1%). In 31.5% of the patients there was no ECG abnormality. The most frequent ECG abnormalities were nonspecific repolarization abnormalities (34.6) and right bundle branch block (22.7%). There was an increase in the proportion of patients with ECG abnormalities with increasing age. The mean number of ECG abnormalities per patient was 1.5 ± 1.5. In conclusion, most ChD patients evaluated in the primary care setting have abnormal ECGs.*

Keywords: Chagas Disease, Trypanosoma Cruzi, Electrocardiogram, Telehealth, Telecardiology

1. Introduction

Chagas disease (ChD) is an endemic disease in Latin America. It is a major cause of heart disease in those countries with an estimated 10 million South Americans chronically infected. In addition, it has become a worldwide problem due to the migration of infected individuals to developed countries, mostly Europe and North America [1].

The electrocardiogram (ECG) is a low cost and easily performed test, with diagnostic and prognostic value, and widely available in primary care settings [2]. Electrocardiographic abnormalities may precede the signs and symptoms of ChD [3].

In order to reduce the number of referrals to major centers and improve the quality of medical assistance, the Department of Health of the State of Minas Gerais funded the creation of the Telehealth Network of Minas Gerais (TNMG) [4], a public service that now provides support to primary care professionals of 660 state municipalities [5]. This service performs teleconsultation (second opinion) and telediagnosis, including ECG analysis [4, 5].

The objective of this study was to identify abnormalities prevalent in the ECG and common associated conditions in patients with ChD attended in primary care.

2. Methods

This retrospective observational study included all 12-lead digital ECGs analyzed by cardiologists from TNMG, from January 1st to December 31st, 2011. The digital ECGs are recorded in the municipalities and transmitted by means of the internet to the analysis center, and immediately reported by a team of cardiologists, trained and experienced in analysis and

interpretation ECG using standardized criteria [6]. This study was approved by the Research Ethics Committee of the Universidade Federal de Minas Gerais.

3. Results

During the study period, 264,324 patients underwent ECG analysis using the services of the TNMG. Of these, 7,590 (2.9%) patients reported having ChD. The ChD subjects have a mean age of 57.0 ± 13.7 years (ranging from 5.3 to 99.0 years old), of which 64.1% were female. Hypertension was the most common comorbidity (61.3%), followed by diabetes mellitus (9.1%) and dyslipidemia (6.9%). Smoking was reported in 10.7% of patients.

Regarding the analysis, in 31.5% of patients the ECG showed no abnormalities. Sinus rhythm was present in 86.9% of patients. The mean number of abnormalities per patient was 1.47 ± 1.45. The ECG abnormalities observed are reported in Table 1. The association of RBBB with left anterior hemiblock was observed in 13.75% of the patients.

Table 1 Prevalence of electrocardiographic abnormalities in Chagas disease patients who underwent electrocardiogram analyzed by the Telehealth Network of Minas Gerais (N = 7,590)

Electrocardiographic abnormalities	N (%)
Atrial fibrillation or Flutter	406 (5.3)
Supraventricular premature beats	192 (2.5)
Ventricular premature beats	412 (5.4)
First degree AVB	370 (4.9)
Second degree AVB*	18 (0.2)
Third degree AVB	18 (0.2)
Right bundle branch block	1723 (22.7)
Left bundle branch block	233 (3.1)
Left anterior hemiblock	1709 (22.5)
Ventricular repolarization abnormalities	2628 (34.6)

*AVB: atrioventricular block. * The advanced AVB and the 2:1 AVB was included with second-degree AVB.*

Patients who exhibited more than one abnormality represented 41.4% of the study sample, and 21.6% had three or more abnormalities. There was an increase in the proportion of patients with ECG abnormalities with increasing age (Fig. 1).

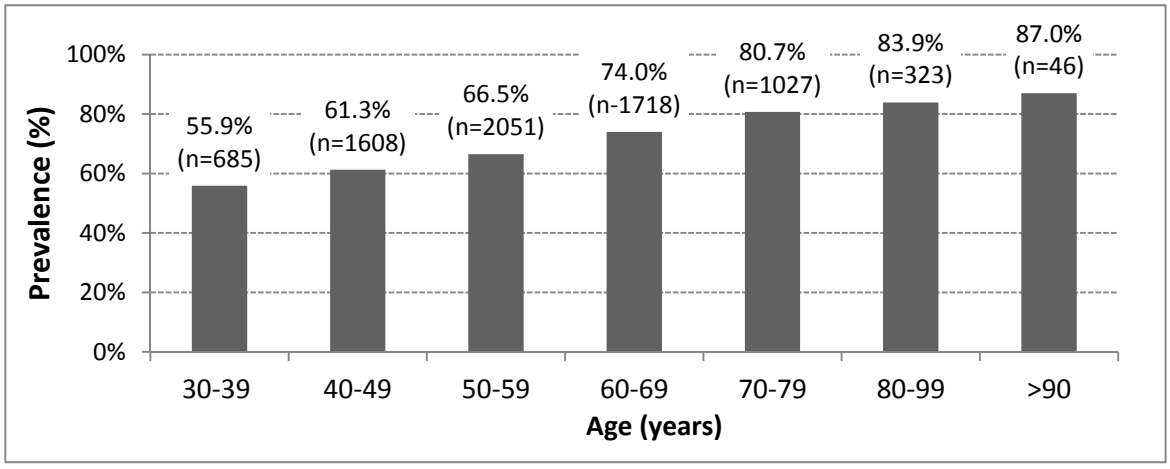

Fig. 1. Percentage of electrocardiogram abnormalities according to age groups, in patients with self-reported Chagas disease who underwent electrocardiography through the Telehealth Network of Minas Gerais service in 2011.

4. Discussion

This study included a large sample of ChD patients who were attended to in primary care and showed a high prevalence of ECG abnormalities: 68.5% of the patients had least one abnormality. Most of the previous series of non-selected patients with ChD showed a lower prevalence of ECG abnormalities, [3, 7, 8] probably related to lower mean age or to the fact that, in these studies, patients were members of the community [7, 8] or were asymptomatic blood donors [3].

Right bundle branch block (RBBB) and left anterior hemiblock were frequently observed in this sample, reinforcing the findings of previous studies in different populations.[3,7,8] RBBB is the most characteristic abnormality, as it is highly prevalent, fairly specific and of notable positive predictive value for *T. cruzi* infection[3,7–9]. There is evidence that RBBB is associated with more severe cardiac damage [3] and is an independent risk factor for mortality in patients with ChD [10].

Ventricular repolarization abnormalities were the most common finding in our study, affecting more than one third of patients. Indeed, since this study did not differentiate more pronounced ST-T wave abnormalities from minor repolarization abnormalities and most patients have concomitant diseases, it is difficult to attribute these abnormalities to the *T. cruzi* infection. However, it should stressed that repolarization abnormalities in ChD may be related to the presence of left ventricular dysfunction [3] and may have prognostic importance[11].

In this study, 5.3% of ChD patients had atrial fibrillation or flutter. The prevalence was higher than in the general population (1.9-2.5%)[12]. In ChD, it usually develops in patients with advanced heart involvement and severe ventricular dysfunction, as occurring in other heart diseases[1]. The presence of these arrhythmias and chagasic cardiomyopathy is associated with increased risk of cardioembolic events and constitutes an independent risk factor for the occurrence of embolic stroke [13].

It was also observed that there was an increase in the proportion of abnormalities with increasing age. This leads to two important considerations. Firstly, it may be a nonspecific finding, since older individuals tend to have other concomitant comorbidities beyond ChD, such as hypertension, which are primarily responsible for the effect in the ECG. Secondly, it may reflect the progression of the disease, observed even in the adult population: a large 10-year retrospective cohort study observed a moderate rate of progression to cardiomyopathy (1.85%/y) among adult persons infected with *T. cruzi* but without cardiomyopathy at baseline [14]. Indeed, the established concept that elderly patients with ChD tend to have a lower degree of cardiac dysfunction caused by disease and usually die from other causes [15] has been recently challenged with studies showing that *T. cruzi* infection remains an important cause of death in the elderly [16].

This study has some limitations. Screening tests for confirmed ChD were not performed routinely and only self-referred ChD subjects were studied. Furthermore, ECG findings on patients with ChD may not be specific and may be attributed to other causes.

In conclusion, this study, conducted in a large sample of patients treated ChD attended at primary care centers in Brazil, showed that the prevalence of ECG abnormalities was high in this population. Among the observed abnormalities, it is important to highlight RBBB, especially in association with left anterior hemiblock. By having a low cost and being easy to use and to interpret, the ECG is a very important tool to the primary care physicians in the evaluation of ChD patients, especially in remote areas without access to more sensitive tests where the disease is endemic.

References

[1] Ribeiro AL, Nunes MP, Teixeira MM, Rocha MO. Diagnosis and management of Chagas disease and cardiomyopathy. *Nat Rev Cardiol*, 2012; 9: 576-589.

[2] Varma N. Role of the surface electrocardiogram in developing countries. *J Electrocardiol*, 2010; 43: 612-614.

[3] Ribeiro AL, Sabino EC, Marcolino MS, Salemi VM, Ianni BM, Fernandes F, Nastari L, Antunes A, Menezes M, Oliveira CD, Sachdev V, Carrick DM, Busch MP, Murphy EL. Electrocardiographic Abnormalities in Trypanosoma cruzi Seropositive and Seronegative Former Blood Donors. *PLoS Negl Trop Dis*, 2013; 7: e2078.

[4] Ribeiro AL, Alkmim MB, Cardoso CS, Carvalho GG, Caiaffa WT, Andrade MV, Cunha DF, Antunes AP, Resende AG, Resende ES. Implementation of a telecardiology system in the state of Minas Gerais: the Minas Telecardio Project. *Arq Bras Cardiol*, 2010; 95: 70-78.

[5] Alkmim MB, Figueira RM, Marcolino MS, Cardoso CS, Pena de AM, Cunha LR, da Cunha DF, Antunes AP, Resende AG, Resende ES, Ribeiro AL. Improving patient access to specialized health care: the Telehealth Network of Minas Gerais, Brazil. *Bull World Health Organ*, 2012; 90: 373-378.

[6] Pastore CA, Pinho C, Germiniani H, Samesima N, Mano R. Diretrizes da Sociedade Brasileira de Cardiologia sobre Análise e Emissão de Laudos Eletrocardiográíficos. *Arquivos Brasileiros de Cardiologia*, 2009; 93: 1-19.

[7] Maguire JH, Hoff R, Sherlock I, Guimaraes AC, Sleigh AC, Ramos NB, Mott KE, Weller TH. Cardiac morbidity and mortality due to Chagas' disease: prospective electrocardiographic study of a Brazilian community. *Circulation*, 1987; 75: 1140-1145.

[8] Williams-Blangero S, Magalhaes T, Rainwater E, Blangero J, Correa-Oliveira R, VandeBerg JL. Electrocardiographic characteristics in a population with high rates of seropositivity for Trypanosoma cruzi infection. *Am J Trop Med Hyg*, 2007; 77: 495-499.

[9] Garzon SA, Lorga AM, Nicolau JC. Electrocardiography in Chagas' heart disease. *Sao Paulo Med J*, 1995; 113: 802-813.

[10] Rodriguez-Salas LA, Klein E, Acquatella H, Catalioti F, Davalos V, V, Gomez-Mancebo JR, Gonzalez H, Bosch F, Puigbo JJ. Echocardiographic and Clinical Predictors of Mortality in Chronic Chagas' Disease. *Echocardiography*, 1998; 15: 271-278.

[11] Salles GF, Xavier SS, Sousa AS, Hasslocher-Moreno A, Cardoso CR. T-wave axis deviation as an independent predictor of mortality in chronic Chagas' disease. *Am J Cardiol*, 2004; 93: 1136-1140.

[12] Andersson P, Londahl M, Abdon NJ, Terent A. The prevalence of atrial fibrillation in a geographically well-defined population in northern Sweden: implications for anticoagulation prophylaxis. *J Intern Med*, 2012; 272: 170-176.

[13] Lima-Costa MF, Matos DL, Ribeiro AL. Chagas disease predicts 10-year stroke mortality in community-dwelling elderly: the Bambui cohort study of aging. *Stroke*, 2010; 41: 2477-2482.

[14] Sabino EC, Ribeiro AL, Salemi VM, Di Lorenzo OC, Antunes AP, Menezes MM, Ianni BM, Nastari L, Fernandes F, Patavino GM, Sachdev V, Capuani L, de Almeida-Neto C, Carrick DM, Wright D, Kavounis K, Goncalez TT, Carneiro-Proietti

AB, Custer B, Busch MP, Murphy EL. Ten-Year Incidence of Chagas Cardiomyopathy Among Asymptomatic Trypanosoma cruzi-Seropositive Former Blood Donors. *Circulation*, 2013; 127: 1105-1115.

[15] Menezes M, Rocha A, da Silva AC, da Silva AM. Basic causes of death in elderly patients with Chagas' disease. *Arq Bras Cardiol*, 1989; 52: 75-78.

[16] Lima-Costa MF, Peixoto SV, Ribeiro AL. Chagas disease and mortality in old age as an emerging issue: 10 year follow-up of the Bambui population-based cohort study (Brazil). *Int J Cardiol*, 2010; 145: 362-363.

ELECTROCARDIOGRAPHIC CHANGES IN PATIENTS WITH SCHIZOPHRENIA

[1]M. Gegenava [2]T. Gegenava

[1,2]Tbilisi State Medical University Tbilisi, Georgia (Republic of)
Email: gegenavam@gmail.com

Abstract. *Some antipsychotics are associated with QT interval prolongation on the electrocardiogram (ECG), which increases the risk of sudden cardiac death. The aim of the present work was to reveal electrocardiographic changes in patients with schizophrenia. 71 patients diagnosed with schizophrenia were investigated. They all received neuroleptics and other psychotropic drugs. Electrocardiographic changes manifested in 44.3 % of the patients. PQ interval was slightly prolonged in the study group. QRS complex duration was also slightly prolonged in patients with schizophrenia. A high correlation between QTc prolongation and Haloperidol dosage with p<0,001 was revealed. As the results have shown, ECG changes occurred at quite a high rate among patients with schizophrenia. The use of the ECG is the most suitable way to monitor the safety of pharmacotherapy in psychiatric clinics. As neuroleptics affect cardiac repolarization, QTc interval has been found to be an accurate indicator of their effect on the heart.*

Keywords: schizophrenia, QTc prolongation, sudden cardiac death

1. Introduction

Drug-induced arrhythmia is a feasible mechanism by which antipsychotic drugs may increase the risk of sudden death. Some antipsychotics are associated with QT interval prolongation on the electrocardiogram (ECG), which increases the risk of sudden death in other populations from the potentially fatal ventricular arrhythmia known as torsade de pointes. What these drugs have in common is an action which prolongs cardiac repolarisation via blockade of the delayed rectifier within the potassium channel (I_{kr}) [1, 2]. The cloning of the human 'ether-a-go-go' (HERG) gene that encodes for this channel has resulted in studies confirming the specific I_{kr} blocking potential of haloperidol, droperidol, pimozide and sertindole. Antipsychotics bind to the I_{kr} with varying affinities, which may prove to be associated with their potential for arrhythmogenesis. I_{kr} blockade may be necessary for drug-induced QT prolongation and subsequent arrhythmia, but other factors also play a critical role [3, 4]. Although increasing antipsychotic dose has been linked to QT prolongation in psychiatric patients, other factors may operate, creating high-risk groups who develop QT prolongation and arrhythmias even at low doses. Old age, female gender and pre-existing ischaemic heart disease are all likely to increase risk. Hypokalaemia reduces the I_{kr} current, raising the likelihood that drug-induced QT prolongation will progress to arrhythmia. The metabolism of most psychotropic drugs is genetically determined, leading to differences of up to fivefold in steady state plasma levels. In the case of thioridazine, mutations of the gene coding for the CYP2D6 hepatic cytochrome p450 isoenzyme (debrisoquine hydroxylase) can result in an accumulation of metabolites that may be cardiotoxic. Pharmacodynamic variation may also determine risk. Mutations at the HERG locus produce a congenital 'long QT' syndrome (LQT2) in which I_{kr} current is reduced and torsade de pointes is frequent. Further blockade by drugs may then trigger the arrhythmia.

The prescription of two or more psychotropic drugs is common in psychiatric practice and interactions between them may increase the likelihood of a clinically significant effect. Tricyclic antidepressants also prolong the QT interval and block I_{kr} ([1, 5] but even some of

the relatively non-cardiotoxic selective serotonin reuptake inhibitors (SSRIs) such as fluoxetine and fluvoxamine can act to inhibit metabolism at CYP2D6, resulting in substantial increases in antipsychotic drug levels and a higher risk of QT prolongation and torsade de pointes[6, 7, 8]

The aim of the present work was to reveal electrocardiographic changes in patients with schizophrenia.

2. Methods

71 patients with the diagnosis of schizophrenia were investigated. They all received neuroleptics and other psychotropic drugs. Their age varied from 35 to 70 years. There was also a control group of 16 patients.

3. Results

Changes in the ECG were detected. Sinus tachycardia n=6 8,45 %; sinus bradycardia n=8, 11,26%; QTc was prolonged in 21.4 %, ST nonspecific changes in n=13 (18,3%) p=0.047, T wave nonspecific changes in n=7 (9,8%), ST depression in n=13, (9,85), p= 0.047, post infarction scarring Q wave and QS complex was detected in n=14 (19,71%). extrasystolic arrhythmia was revealed in n=6, 8,45%, ventricular extrasystoles in 2.8 %. Conduction block was detected in n=45, 63 %, mostly it was revealed as His bundle branch block. PQ interval is slightly prolonged in study group. QRS complex duration and QTc interval were also slightly prolonged in patients with schizophrenia. A high correlation was revealed between QTc prolongation and Haloperidol dosage p<0,001. There was no correlation detected between the other groups of psychotropic medication. ECG changes were marked in 44.3 % of the patients (Table 1, Fig. 1). Out of 30 healthy people only 2 (6.6 %) showed change in the ECG (p = 0.035). ECG changes were assessed in males and females.

4. Discussion and Conclusions

As the results have shown, ECG changes occurred in quite a high rate among the patients with schizophrenia. The use of ECGs is the most suitable way to monitor the safety of pharmacotherapy in psychiatric clinics. As neuroleptics can affect cardiac repolarization, the QTc measurement has been found to be an accurate indicator of their effect on the heart.

Electrocardiography prior to the initiation of drug therapy and during therapy may detect some patients at a higher risk owing to pre-existing repolarisation abnormalities or ischaemia and those with marked repolarisation abnormalities during treatment. Sudden unexplained death in psychiatric patients is uncommon, but many cardiac related deaths may go unrecognised. More post mortem examinations may be required if this is suspected. A higher index of suspicion and a lower threshold for the seeking of a postmortem examination are required.

Table 1. Statistical analysis of ECG changes in patients with schizophrenia

	Study Group	N	Control Group
	1	2	C
N =	32	39	16
	Mean ±SD	Mean ±SD	Mean ±SD
P	76.0±13.8 p_{1-2} = NS; p_{1-C} = NS; p_{2-C} = 0.002	79.6±11.2	72.6±4.2
PQ	0.16±0.02 p_{1-2} = NS; p_{1-C}<0.001; p_{2-C} = NS	0.15±0.03	0.14±0.02
QRS	0.07± 0.018 p_{1-2} = 0.032; p_{1-C}<0.001; p_{2-C} = 0.045	0.06±0.02	0.05±0.02
QT	0.39±0.04 p_{1-2} = 0.03; p_{1-C} = NS; p_{2-C}< 0.001	0.37±0.03	0.40±0.03

A proportion of sudden deaths may be related to antipsychotic-induced torsade de pointes. This is a rare adverse drug reaction, the risk of which may be outweighed for most antipsychotic drugs by their benefits.

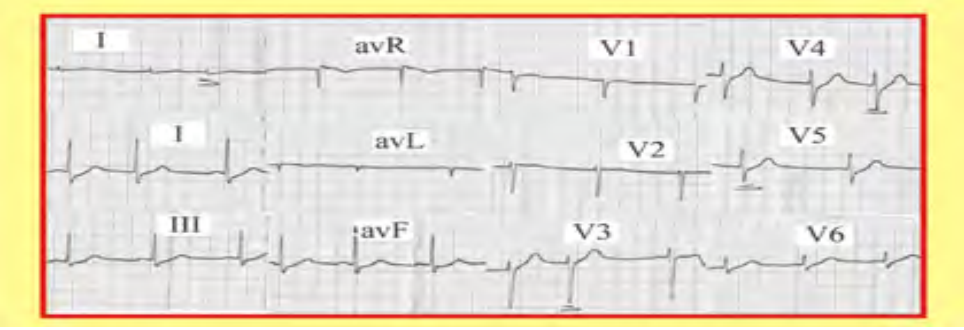

Fig. 1. ECG from a 65 year old patient with schizophrenia

However, an individual assessment is required for each drug as to whether it can be used safely, and whether restrictions are necessary. Current studies cannot yet reassure us that significant risks do not exist with other antipsychotic drugs. There is a need for more extensive pharmaco-epidemiological studies of current drugs, looking both at QT abnormalities and sudden death itself.

References

[1] Baker B, Dorian P, Sandor, P., et al. Electrocardiographic effects of fluoxetine and doxepin in patients with major depressive disorder. *Journal of Clinical Psychopharmacology*, 1997; 17: 15 -21.

[2] Buckley NA, Whyte IM, Dawson, AH. Cardiotoxicity more common in thioridazine overdose than with other neuroleptics. *Journal of Toxicology. Clinical Toxicology*, 1995; 33:3: 199-204.

[3] Carrillo JA, Ramos SI, Herraiz AG, et al. Pharmacokinetic interaction of fluvoxamine and thioridazine in schizophrenic patients. *Journal of Clinical Psychopharmacology*, 1999; 19:6: 494-499.

[4] Committee on Safety of Medicines & Medicines Control Agency QT interval prolongation and antipsychotics. *Current Problems in Pharmacovigilance*, 2001; 27:4.

[5] Teschemacher, EP, Seward, JC Hancox, HJ Witchel Inhibition of the current of heterologously expressed HERG potassium channels by imipramine and amitriptyline, *Br J Pharmacol*, 1999; 128: 479–485

[6] Rockville, MD Food and Drug Administration *Supplemental New Drug Applications for Mollaril (Thioridazine)*. US Department of Health and Human Services 2000. (http//www.fda.gov/cder/ogd/rld/17923s48.pdf).

[7] Kirchner, V, Kelly, CA, Harvey, R J. A systematic review of the evidence for the safety and efficacy of thioridazine in dementia (Cochrane Review). *The Cochrane Library*, 2001; 4: Oxford: Update Software.

[8] Prescription Pricing Authority Prescribing Cost Analysis Report, 1999 London: Department of Health. (http://www.doh.gov.uk/stats/pca99.htm)

CHANGES OF ELECTROCARDIOGRAM IN LOW-RENIN HYPERTENSION

[1]E. Blinova, [1]T. Sakhnova, [1]N. Chikhladze, [2]V. Trunov, [2]E. Aidu, [1]Z. Valieva, [1] M. Saidova, [1]A. Rogoza, [1]I. Chazova

[1]Cardiology Research Complex, Moscow, Russia
[2]Institute for Information Transmission Problems RAS, Moscow, Russia
Email: blinova2009.73@mail.ru

Abstract. *The aim of this study is to assess electrocardiogram (ECG) changes in hypertensive patients in comparison with the plasma renin activity (PRA), echocardiographic data and ambulatory blood pressure monitoring (ABPM). ECG parameters, echocardiography and ABPM were evaluated in 30 hypertensive patients in supine position with PRA < 1 ng/ml/hr and 10 with PRA >1 ng/ml/hr. The results show that patients with low PRA were characterized by significantly greater values of spatial QRS-T angle and significantly lower magnitude (G) and components X, Y, Z (Gx, Gy, Gz) of the "recovery acceleration" vector. We revealed statistically significant correlations between PRA and spatial QRS-T angle, G, Gx, Gy and Gz. Gy correlated with diastolic BP at ABPM. Gx correlated with left ventricular wall thickness and myocardial mass. In conclusion, hypertensive patients with low PRA in comparison with medium PRA are characterized by more pronounced changes in ECG parameters, describing cardiac repolarization in its relation to the preceding depolarization.*

Keywords: Left Ventricular Hypertrophy, Low-renin Hypertension, Electrocardiogram, Spatial QRS-T Angle

1. Introduction

Left ventricular hypertrophy (LVH) is a strong independent risk factor for cardiovascular morbidity and mortality. Early diagnosis of left ventricular hypertrophy in hypertensive patients can adequately assess the risk of cardiovascular complications and justify a focused selection of antihypertensive therapy (AH). Currently, there is no doubt that echocardiography compared with electrocardiography (ECG) can more accurately determine the mass of the left ventricular myocardium. However, it is shown that the ECG contains independent information, which indicates a more serious prognosis. ECG signs of regression of left ventricular hypertrophy during antihypertensive therapy can serve as a predictor of cardiovascular favourable outcomes [1]. In this regard, more and more attempts are made to attract the attention of scientists to study the relationships of mechanical and biochemical changes in complex bioelectrical interactions in LVH and their effect on prognosis [2]. In statements published by the International Working Group on the ECG diagnosis of left ventricular hypertrophy [3, 4] the researchers propose to move away from the old paradigm and focus efforts on clarifying mechanisms of ECG changes in LVH. It is assumed that, ideally, ECG should not "duplicate" echocardiography, but give additional information about the pathogenesis of the disease in the individual patient, which would increase the validity of the therapy and help to assess its effectiveness. The aim of our study was to study the changes of ECG in hypertensive patients in comparison with the plasma renin activity (PRA), echocardiographic data and ambulatory blood pressure monitoring (ABPM).

2. Methods

The study included 40 hypertensive patients (23 men and 17 women), aged 44.8 ± 2,4 years. A conventional clinical evaluation of patients was performed. Plasma aldosterone

concentration (PAC) and plasma renin activity (PRA) were evaluated at rest (at 9:00 in the morning) and after 4 hours of walking (at 13:00). PAC and PRA were measured by radioimmunoassay, using commercial kits («Immunotek», Czech Republic). Plasma electrolytes (potassium, sodium) levels were also determined. 10-14 days before the survey drug therapy that affects the performance of renin-angiotensin-aldosterone system was excluded. If necessary, verapamil was administered.

Conventional and orthogonal (McFee-Parungao lead system) 10-s electrocardiograms were recorded on a commercially available digital electrocardiograph and processed by means of software developed in the Cardiology Research Complex and Institute for Information Transmission Problems. On the 12-lead ECG, parameters analyzed were the duration of the complex QRS, Sokolow-Lyon voltage and Cornell product. Orthogonal ECG parameters under consideration were QRS maximal vector, spatial QRS-T angle, magnitude G (in ms) and spatial components Gx, Gy, Gz of the "recovery acceleration" vector (directed to the left, inferior, and anterior).

Blood pressure measurement was performed manually by the Korotkov method while patients were in the sitting position. All the patients underwent ambulatory blood pressure monitoring (ABPM) with measurement frequency 30 minutes during daytime and 60 minutes at night. The average systolic (SBP) and diastolic blood pressure (DBP) per 24 hours, day, night was analyzed. Transthoracic echocardiography was performed using Vivid 7 system (GE, USA). Estimation of the size of the left ventricular end-diastolic volume (EDV), interventricular septum thickness (IVST) and posterior wall thickness (PWT) was carried out using the standard method of the American Association of Echocardiography (ASE, 2006). Left ventricle myocardial mass (LVMM) was calculated using the formula $LVMM=0.8*(1.04*[(EDV+IVST+PWT)^3-(EDV)^3])+0.6$ g, with subsequent indexation for body surface area. Average thickness of the left ventricular walls (WT) was calculated as (IVST+PWT)/2. The relative thickness of the walls of the left ventricle (RWT) was calculated as (IVST+PWT)/EDV.

Statistical analysis was performed using Medcalc. Results are presented as mean and error of the mean (M±SE). To evaluate the differences between two independent samples, the unpaired nonparametric Mann-Whitney method was used. To identify the relationship between variables, the Pearson correlation coefficient was calculated. Differences were considered significant at $p < 0.05$.

3. Results

PRA in supine position at rest in 30 patients was less than 1 ng/ml/hr (group 1) and in 10 more than 1 ng/ml/hr (group 2). Excessive production of aldosterone was revealed in 11 of 40 (28%) patients. In 5 of them adrenal cortex aldosteromas were diagnosed. Characteristics of the groups are shown in Table 1.

Patients with low PRA were characterized by significantly greater values of spatial QRS-T angle and significantly lower magnitude (G) and components X, Y, Z (Gx, Gy, Gz) of the "recovery acceleration" vector.

We revealed statistically significant correlations between PRA and: spatial QRS-T angle ($r=-0.5$; $p<0.01$, Fig. 1); G, Gx and Gy ($r=0.5$; $p<0.01$); Gz ($r=0.4$; $p<0.02$). Gy correlated with diastolic BP at ABPM ($r=-0.4$; $p<0.02$). Gx correlated with WT and RWT ($r=-0.5$; $p<0.01$); LVMM and indexed LVMM ($r=-0.4$; $p<0.02$).

Table. 1 Characteristics of the groups.

	Group 1	Group 2	p
Age, years	47±15	35±12	0.02
AH duration, years	14±12	9±8	>0.1
SBP, mm Hg	153±25	140±13	>0.1
DBP, mmHg	91±14	86±12	>0.1
K+, mmol/l	4.5±0.7	4.8±0.6	>0.1
PRA, ng/ml/hr	0.34±0.29	1.78±0.92	<0.01
PAC, pg/ml	219±415	148±137	>0.1
SBP24hr, mmHg	141±15	141±11	>0.1
DBP24hr, mmHg	88±10	83±12	>0.1
EDV, mm	5.1±0.4	5.2±0.3	>0.1
WT, mm	1.07±0.23	0.93±0.11	0.09
RWT	0.42±0.07	0.36±0.05	0.03
LVMM, g	214±94	178±34	>0.1
ILVMM, g/m^2	109±41	92±19	>0.1
HR, bpm	66±10	65±14	>0.1
Sokolow-Lyon voltage, mV	2.50±0.79	2.87±0.60	>0.1
Cornell product, mm*ms	2293±1175	1669±599	0.07
QRS duration, ms	102.6±18.0	98.4±6.6	>0.1
QRS maximal vector, mV	2.15±0.80	2.33±0.52	>0.1

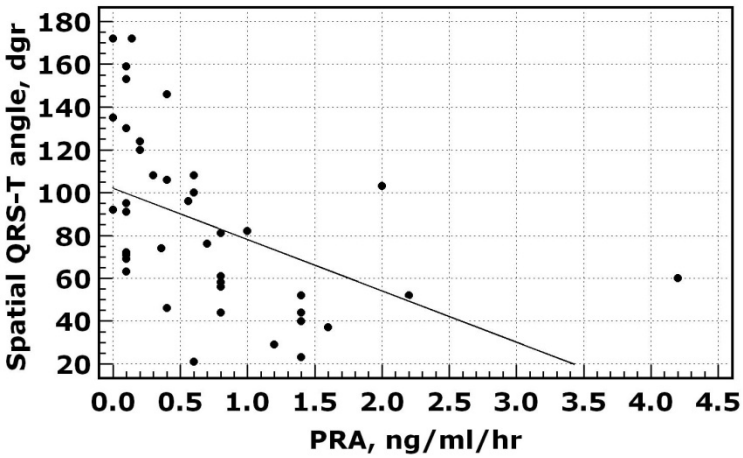

Fig. 1. Relationships between PRA and spatial QRS-T angle**.**

4. Discussion

Investigation of the influence of renin-angiotensin-aldosterone system on the myocardial state in hypertensive patients attracts a lot of attention. It was shown that patients with primary aldosteronism when compared with other forms of hypertension in comparable levels of blood pressure and disease duration have greater LVMM [5]. In our previous work we revealed that the changes of the "recovery acceleration" vector in patients with primary hyperaldosteronism, were especially pronounced in patients with adrenal cortex adenomas [6] and also found an increase in vectorcardiographic and decartographic parameters of ventricular depolarization in patients with high levels of PAC in the absence of significant correlations of these parameters with LVMM [7]. Data regarding the influence of PRA on

ventricular hypertrophy are contradictory [8, 9]. However, the changes of such an important parameter as a spatial QRS-T angle [10] in patients with low PRA are of particular interest.

Mechanisms of influence of renin on the processes of electrical remodelling require further study. Further research in this area will contribute to the development of new criteria for the evaluation of the heart state in hypertensive patients with different forms of hyperaldosteronism.

5. Conclusions

Hypertensive patients with low PRA in comparison with medium PRA are characterized by more pronounced changes in ECG parameters which describe cardiac repolarization in its relation to the preceding depolarization.

References

[1] Okin PM, Devereux RB, Jern S. Regression of electrocardiographic left ventricular hypertrophy by losartan versus atenolol: The Losartan Intervention for Endpoint reduction in Hypertension (LIFE) Study. *Circulation*, 2003; 108(6): 684-690.

[2] Rodriguez-Padial L, Bacharova L. Electrical remodelling in left ventricular hypertrophy - is there a unifying hypothesis for the variety of electrocardiographic criteria for the diagnosis of left ventricular hypertrophy? *J Electrocardiol,* 2012; 45(5): 494-497.

[3] Bacharova L, Estes H, Bang L, Mateasik A. The first statement of the Working Group on Electrocardiographic Diagnosis of Left Ventricular Hypertrophy. *J Electrocardiol,* 2010; 43(3): 197-199.

[4] Bacharova L, Estes EH, Bang LE, et al. Second statement of the working group on electrocardiographic diagnosis of left ventricular hypertrophy. *J Electrocardiol,* 2011; 44(5): 568-570.

[5] Muiesan ML, Salvetti M, Paini A, et al. Inappropriate left ventricular mass in patients with primary aldosteronism. *Hypertension,* 2008; 52(3): 529-534.

[6] Samedova HF, Chikhladze NM, Blinova EV, et al. Evaluation of the functional state of the myocardium in hypertensive patients on the background of hyperaldosteronism using orthogonal electrocardiography. *Kardiovaskulyarnaya terapiya i profilaktika,* 2006, 52 (2): 15 - 19.

[7] Sakhnova TA, Blinova EV, Chikhladze NM, et al. Changes of orthogonal electrocardiogram in hypertensive patients with hyperaldosteronism. *Kardioilogicheskiy vestnik,* 2013; 1: 41-44.

[8] Vlahakos DV, Hahalis G, Vassilakos P, et al. Relationship between left ventricular hypertrophy and plasma renin activity in chronic hemodialysis patients. *J Am Soc Nephrol,* 1997; 8(11): 1764-70.

[9] Bhattacharya SK, Gandhi MS, Kamalov G, et al. Myocardial remodeling in low-renin hypertension: molecular pathways to cellular injury in relative aldosteronism. *Curr Hypertens Rep,* 2009; 11(6): 412-20.

[10] Kardys I, Kors JA, van der Meer IM, et al. Spatial QRS-T angle predicts cardiac death in a general population. *Eur Heart J,* 2003; 24(14): 1357-64.

SPECIES SPECIFIC VENOM MANIFESTATIONS IN ECG

[1]R. Maheshwari, [2]V. Kumar, [3]H. K. Verma

[1]Rajasthan Technical University, Kota, India
[2]Indian Institute of Technology, Roorkee, India
[3]Sharda University, Noida, India
Email: ranjan_alpi@hotmail.com

Abstract. *Due to the hot and humid climate in Countries like India, a number of venomous species cohabit with human dwellings and in these countries, encounters and venom interactions are very common. The venom in the victim's body manifests certain symptoms that may be due to the synergistic effects of venom interacting with the body systems. In this study, electrocardiogram (ECG) signals of victims of four common venomous snakes of India and one scorpion species were obtained. As all the human body systems affect the functioning of the heart, venom interactions might result in some species specific and some common changes in the ECG signal. As these changes were found to be reversible with treatment, they may be attributed to the presence of venom in the body. This study may be useful in medical management of the victims, as well as in ascertaining the aggressor venomous species.*

Keywords: Venom, Species-specific, India, Venom interaction

1. Introduction

The Tropics and tropical countries are home to human and venomous species. This cohabitation results in frequent harmful encounters which may lead to venom interaction. Although, primarily venom is not intended to be used against human beings, but in conflicts in order to survive, a venomous species may inject venom into human beings. Venomous species use venom as a tool for survival and to digest their prey [1]. Based on their diet, habitat, size, age and physical condition, venomous species exhibit large variations in the constitution of their venom.

Heterogeneity in venom constituents is observed inter-species as well as intra-species. The vipers of India, Saw scaled viper or *Echis carinatus* (Merrem, 1820) and Russell's viper or *Vipera Russelli* (Laurenti, 1786) contain venom that is predominantly hemotoxic, whereas the elapids of India, Cobra or *Naja sp.* (Laurenti, 1768) and Common Krait or *Bungarus caeruleous* (Daudin, 1803) possess predominantly neurotoxic venom. In addition to these snakes, the Indian Red Scorpion or *Mesobuthus tamulus* (Fabricius, 1798) is also a potently venomous creature that often stings and introduces venom into human subjects [2].

When venom enters a human body, it may affect one or more body system and the interaction may result in specific symptoms. All the body systems work in synergy and the ECG is, directly or indirectly, affected by every system, including the cardiovascular system [3]. Thus, the ECG signals exhibit manifestations based on the quantity and constituents of the venom with some specific patterns of symptoms. This study proposes to observe specific symptoms in venom interacted victims' ECG signals that may be attributed to the presence of species specific venom in the victim's body.

2. Methods

As venom interaction is not predictable and is often accidental and random a number of subjects and other parameters could not be planned prior to the study. A protocol was developed, according to which, upon arrival of the victims in the hospital, the species would

be identified by standard techniques, including showing pictures of the snake species and identification of the remains of the species brought by the victim's attendants. Furthermore, the victims would be classified in four severity categories by the attending medical management team and as per the published work [4]. Meanwhile, the victim (if the victim would be a minor or not in a state to make a decision, then the attendant) would be briefed about this study. Consent would be obtained and the ECG signal would be obtained without any interference to medical management. Out of more than 300 cases, only a limited number of cases qualified under this protocol and only 97 victims' records could be obtained. The classification of the victims under this study is as given in Table 1.

Table 1 The classification of the species that interacted venom in the victims

Species	Mild	Moderate	Severe	Very Severe	Total
Cobra	1	1	6	5	13
Krait	0	0	7	9	16
Saw-scaled viper	12	8	5	2	27
Russell's viper	2	4	6	3	15
Scorpion sting	0	2	1	3	6
Others	13	5	2	0	20
Total	28	20	27	22	97

The ECG signals of the victims were acquired and stored in 16-bit simultaneous 12 channel integer ASCII format, sampled at 500 Hz with a least count of 1 microvolt. By default, the machine recorded 5008 samples, in each channel, for a period a little over 10 seconds.

Most of the victims presented without any medication following venom interaction. In order to identify how the venom manifesting parameters reversed, it was planned to record the ECG signal of the victim after one month post discharge. However, due to many socio-psycho and other constraints, many victims did not return for the post treatment ECG recording. Therefore the ECG signals during and at the time of discharge were obtained in most of the cases to identify any trend of change in the signals.

The ECG signals were analyzed using standard ECG analysis techniques. An approximate marking of the QRS onset and offset was performed using the Spatial Velocity Technique [5]. In each of the 12 leads, QRS onsets and offsets were identified with slope amplitude method and then their medians were identified as the final QRS onset and Offset.

Using the QRS offset as the starting point, T wave, U wave and T-U complex were identified using the Fiducial Segment Averaging technique [6]. In some cases, the P waves were difficult to identify, where P wave deflections were unclear in the power frequency of 50 Hz and artefact noise. A number of techniques were subsequently employed to find precise P wave boundaries. Medians of all the techniques across all the leads were obtained for the optimal estimation of P wave onset and offset.

The deflections were measured between onset and offset of all the wave components. Amplitudes, segments, intervals and durations were stored in a feature vector of each lead.

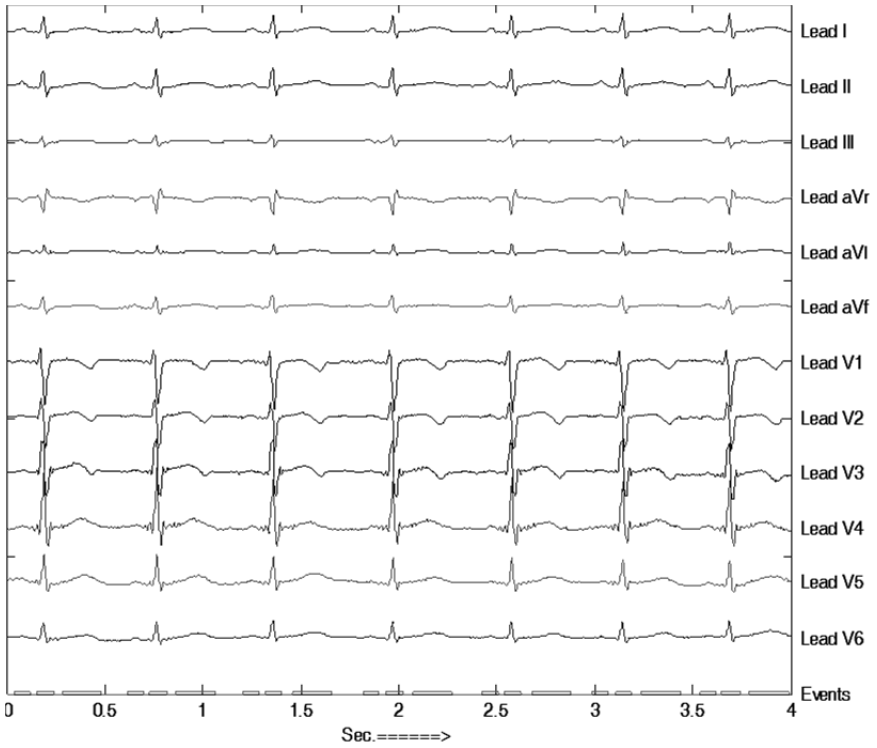

Fig. 1. ECG of a Scorpion sting (Female, 3 years) with a delay of four hours. Heart Rate 104.9/Min, QTc interval 0.44Sec and T wave inversion in right pre-cordial leads.

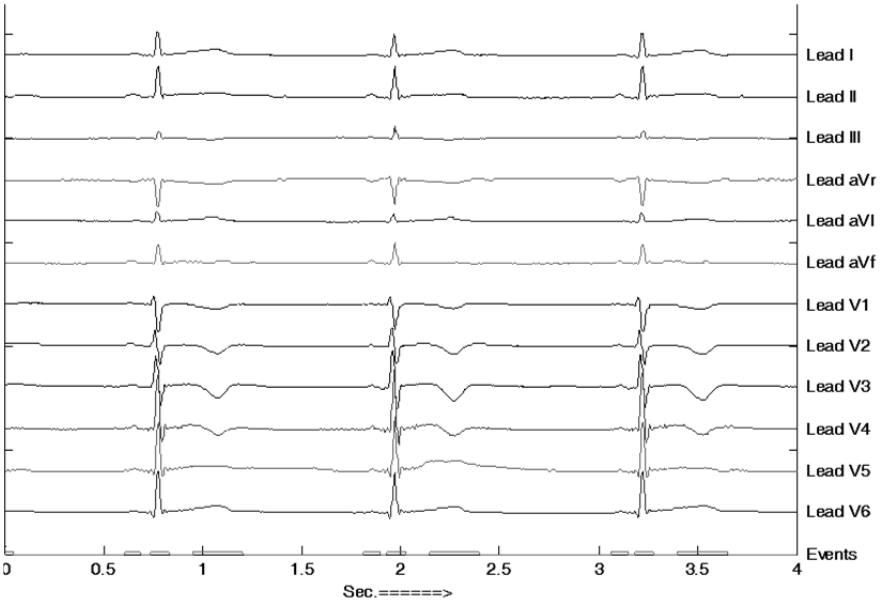

Fig. 2. ECG of a Saw scaled viper bite (Male, 11 years) with a delay of 5 hours. Heart Rate 52.45/Min, QTc interval 0.44 Sec, T wave inversion in right pre-cordial leads and V4. ST segment shift in V4 and V5

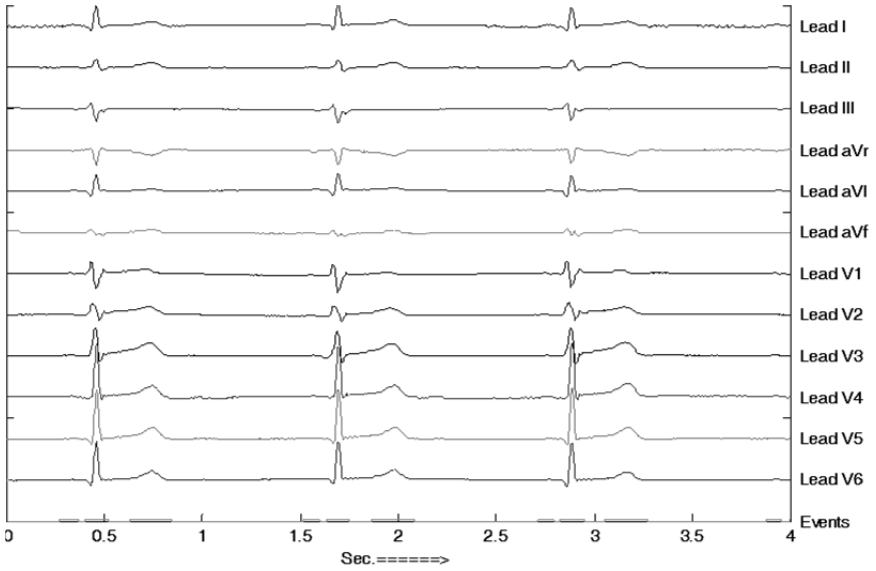

Fig. 3. ECG of a Russell's viper bite case (Male, 25) after a delay of 2 hours. Heart Rate 50.23/Min, QRS duration 0.12 Sec, QRS Axis -1.1 degree, QTc interval 0.41Sec, flat P waves in three limb leads, Q wave duration with little ST segment elevation in left pre-cordial leads.

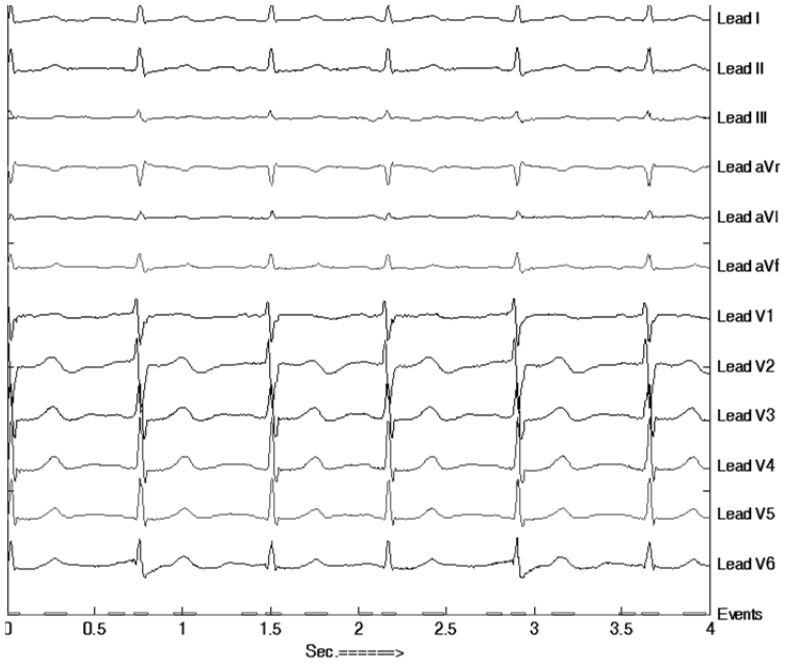

Fig. 4. ECG of a Krait bite (Male, 28 years) after a delay of 4 hours. QTc interval 0.41 sec. The T wave end was marked before the onset of U wave, the ST segment shifted downwards in the all the pre-cordial leads with significant U waves.

Using the frontal plane leads amplitudes, axes were derived. QTc was calculated using the median QRS onset and median T wave end. Where the RR interval exceeded 1 second, Fridericia formula was applied; otherwise Bazett's method was used. A visual presentation of one representative case from each species category is being presented here.

From an examination of the cases of severe and very severe Krait bite, it was observed that the ECGs manifested clear U waves which are often not seen in normal ECGs. U waves, alongwith the QTc prolongation and ST depression might be indicative of hypokalemia. In most of the Krait bite cases, renal failure was observed, which might enhance the cardiovascular load resulting in QRS axis deviation and augmentation in left ventricular voltages. In cases of delayed treatment, rhabdomyolysis may affect the electrophysiology with some more abnormalities, thereby masking the signs of hypokalemia [7].

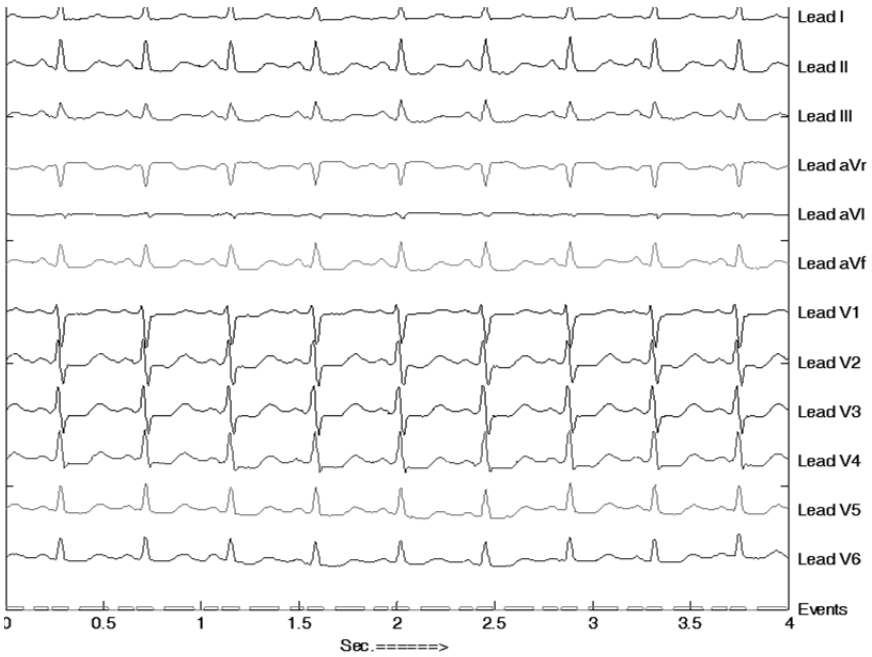

Fig. 5. ECG of a Cobra-bite case (Female, 33 years) after a delay of 5½ hours. Heart Rate 139.48/Min, PR interval 0.09 Sec, QTc interval 0.44Sec, ST segment shifted downwards in some chest leads, right pre-cordial leads and V4.

3. Results and Discussion

There were some species specific and some general features observed in the ECGs studied. It was observed that the right pre-cordial leads were more susceptible than their left counterparts in many venom interacted cases. It is proposed that higher susceptibility may be due to the wider surface area and thinner musculature of the right ventricle, compared to the left one. Hence, the direct contact of the venom mixed blood might have more prominently affected the right side of the heart, as compared to the left side. Furthermore, QTc elongation was observed with all types of venom. These symptoms vanished with therapy and thus may be attributed to the presence of venom in the body.

The scorpion venom causes ‘autonomic storm’ in the victim’s body and thus case to case features may vary [8]. Changes in features are also observed when treatment was delayed. Still, in many cases, tented T waves and tachycardia were observed, resembling the symptoms of hyperkalemia, as reported earlier.

Vipers are known to have venom with cytotoxic and hemotoxic effects, often leading to rhabdomyolysis [7].

The presence of these venoms resulted in bradycardia and non specific Q wave, T wave and ST level changes in cases of delayed treatment. These symptoms also reversed upon therapy and thus may not be indicative of any prior cardiac complication.

The elapid venoms, being neurotoxic, have a fast onset and might affect conduction at cellular level. Hypokalemic patterns were commonly observed in Krait bite cases with large U waves amalgamating with T waves and frequently making T-U complexes. In electrolyte tests, potassium deficiency was not observed in victims, so it is proposed that the Krait venom might affect the potassium channels mimicking hypokalemic patterns.

The Cobra bites exhibited patterns resembling myocardial ischemia with ST level changes and in some cases PR interval variation. The Cobra venom contains potent cardiotoxins and if therapy is not available to the victim in time, it might affect the heart. However, in all of the cases in this study, changes in the ECG returned to normal with therapy.

4. Conclusions

QTc Prolongation was commonly witnessed in the majority of cases. However, distinct species specific features could be observed in ECGs. Many typical morphological features were identified. It is concluded that due to the variation in constituents and composition of venoms, there are species specific features manifested in the ECG signal, that may reverse with therapy. It is also proposed that the ECG signal may provide significant clues in species identification.

Acknowledgements

The authors acknowledge Medical College Kota (INDIA) for the ethical clearance and guidance. Anurag Hospital and Research Centre Kota (INDIA) and Himalayan Institute Hospital Trust Dehradun (INDIA) are acknowledged for providing the ECG signal and other statistical information. All the subjects and their attendants are also acknowledged for their cooperation during the acquisition of the ECG signals.

References

[1] Harris JB, Goonetilleke A. Animal Poisons and the Nervous System: What the Neurologist Needs to Know. *Journal of Neurology, Neurosurgery & Psychiatry*, 2004; 75: 40-46.

[2] Kumar V, Maheshwari R, Verma HK. Toxicity and Symptomatic Identification of Species involved in Snakebites in the Indian Subcontinent. *Journal of Venomous Animals & Toxins including Tropical Disease*, 2006; 12(1): 3-18.

[3] Maheshwari R, Kumar V, Verma HK. Venom and ECG signal processing, in Intelligent Medical Technologies and Biomedical Engineering: Tools and Applications. Shukla A, Tiwari R. IGI Global, Hershey USA. 2011; 165-186.

[4] Maheshwari R, Kumar V, Verma HK. Neural Network Based Specie Identification in Venom Interacted Cases in India. *Journal of Venomous Animals & Toxins including Tropical Disease*, 2007; 13(4): 31-47.

[5] Maheshwari R, Vijaya G, Kumar V, Verma HK. Signal Analysis and a Heuro-logistic Interpretation of Multi-lead Electrocardiograms. *International Journal of System Sciences*, 1998; 29(3): 323-334.

[6] Ritsema HJ, Kors JA, Herpen G. Dispersion of Repolarization, Myocardial Iso-source Maps, and the Electrocardiographic T and U Waves. *Journal of Electrocardiology*, 2006; 39: S96-S100.

[7] Cheng AC, Curie BJ. Venomous Snakebites Worldwide With a Focus on the Australia-Pacific Region: Current Management and Controversies. *Journal of Intensive Care Medicine*, 2004; 19(5): 259-269.

[8] Joshi SR, Sapatnekar S M. Stings and Hopes: Toxinomics and Autonomic Storm in the Indian Red Scorpion (Mesobuthus Tamulus Concanesis, Pocock), *Journal of Association of Physicians of India*, 2007; 55: 11-13.

ECG QT INTERVAL MIGHT BE USEFUL FOR THE DETECTION OF MITRAL VALVE PROLAPSE SYNDROME IN TAIWAN

[1]C-H Hsu, [1]Y-C Chen, [2]L-W Tsai, [3]I-F Yang, [4]C-K Tseng, [1, 2]T-F Yang.

[1]National Chiao Tung University, Hsin Chu City, Taiwan
[2]Taipei Medical University and Hospital, Taipei City, Taiwan
[3]Jen Chi General Hospital, Taipei City, Taiwan
[4]China Medical University Hospital, Taichung City, Taiwan.
Email: tfy@tmu.edu.tw

Abstract. *Four corrected QT (QTc) formulae, namely Bazett, Fridericia, Framingham and Hodges, can be easily calculated by the modern electrocardiograph (ECG) to improve the detection of ventricular arrhythmia (VA) and Sudden Cardiac Death (SCD). Mitral Valve Prolapse Syndrome (MVPS) has been reported to have significantly more VA than normal. There has been no prior study concerning Taiwanese MVPS and normal QTc ranges published. The aim of this study is to evaluate if gender difference is a factor in QTc correction formulae in Taiwanese normal and MVPS. In Normal, all QTc were significantly longer in women than men. In MVPS, significant gender difference was only shown in Framingham and Hodges. There is no significant QTc difference between MVPS and normal in women. But in men, significant difference only exists in Bazett and Fridericia. QTc might be used to differentiate MVPS from normal. Gender dependent QTc criteria should be established for the diagnosis of MVPS.*

Keywords: QT interval, Normal, ECG, MVPS, QTc

1. Introduction

QT prolongation is a risk marker for polymorphic ventricular arrhythmia (VA) and sudden cardiac death (SCD). The QT interval is dependent on the heart rate (the faster the heart rate the shorter the QT interval) and may be adjusted to improve the detection of patients at increased risk of VA [1-5]. Besides this, QTc can be relatively easily calculated by computer-based ECG machines in real time to improve the detection of VA and SCD. There are a number of different correction formulas [6-10]. Four formulae are: Bazett, Fridericia, Framingham and Hodges [6, 7]. Patients with mitral valve prolapsed syndrome (MVPS) have been reported to have significant more repolarization abnormalities and VA than normal [3-5]. There are not many reports of ECG QTc intervals of MVPS and normal in Taiwanese [11-15]. Therefore, it is thought that the different ECG corrected QTc formulae might be a useful tool for evaluation of MVPS.

This study aims to investigate if the evaluation of gender dependent ECG QT interval difference is useful in the detection of MVPS in Taiwanese.

2. Methods

A total of 86 patients, 8 males and 78 females, who had been echocardiographically diagnosed as having MVPS at Taipei Medical University Hospital cardiology clinic from November 2008 to January 2012 were recruited. Data from another group of 581 healthy students from the College of Biological Science and Technology at National Chiao-Tung University and Taipei Medical University with no previous history of medical disease (239

males and 342 females) was collected as normal. All subjects signed the informed consent form and agreed to take part in this research.

12-lead ECG signals were measured and recorded by the BURDICK Atria 6100®ECG machine. The sampling rate adopted was 500 Hz and the interpretation software implanted is the Glasgow Programme developed by the University of Glasgow. ECG data measured from MVPS and normal subjects was statistically analysed on a Personal Computer.

The SPSS student's two tail t test was first adopted to differentiate the four QT corrected formulae in order to evaluate which was best to differentiate between MVPS and Normal. Independent-Samples T Test was used to characterize changes in four QTc formulae between normal male and normal female as well as the differences between male and female who were diagnosed with MVP. Subsequently, we separated the ECG data into two groups: Normal and MVPS. Independent-Samples T Test for statistical analysis was used again to find the most suitable QTc formula.

However we also wanted to investigate whether there is a difference between normal subjects and MVPS in the same gender. The male normal and MVPS as well as female normal and MVPS were used for comparison. P value less than 0.05 was regarded as statistically significant from this test.

These four QTc formulae are expressed mathematically as follows:

QTC	Formula
Bazett	$QTc\ Baz\ =\ QT\ /\sqrt{RR}$
Fridericia	$QTc\ Fri\ =\ QT\ /\sqrt[3]{RR}$
Framingham	$QTc\ Fra\ =\ QT + 154(1 - RR)$
Hodges	$QTc\ Hod\ =\ QT + 1.75(\frac{60}{RR} - 60)$

Gender differences of ECG QTc intervals

As it is difficult to show the widely varying QTc intervals resulting from the use of a range of formulae and to understand the varying impact of applying formulae at various heart rates of observed QT intervals, a simple graphical display of the results from the four different formulae was proposed by Rowlands et al [13].

This display is dependent on the concept of the absolute correction which infers the subtraction between QTc and QT interval. They introduced the absolute correction factor (ACF) defined as the correction to be added to the observed QT measurement to obtain the QTc. They suggested that the formulae can only be used for diagnosing during a narrow window of the resting heart rate which is good within the range from 40 to 100 beats per minute. It provides the representation in a useful graphical way to compare the different formulae.

However, it is not effective as an assessment tool to differentiate the normal from the abnormal. Therefore statistical analysis was used to differentiate between male and female and also to find the most suitable QTc correction formulae for gender differentiation. A P value <0.05 was determined as statistically significant. All QTc are expressed as mean ± SD. SPSS-19 software package, maintained by IBM was used for statistical analysis.

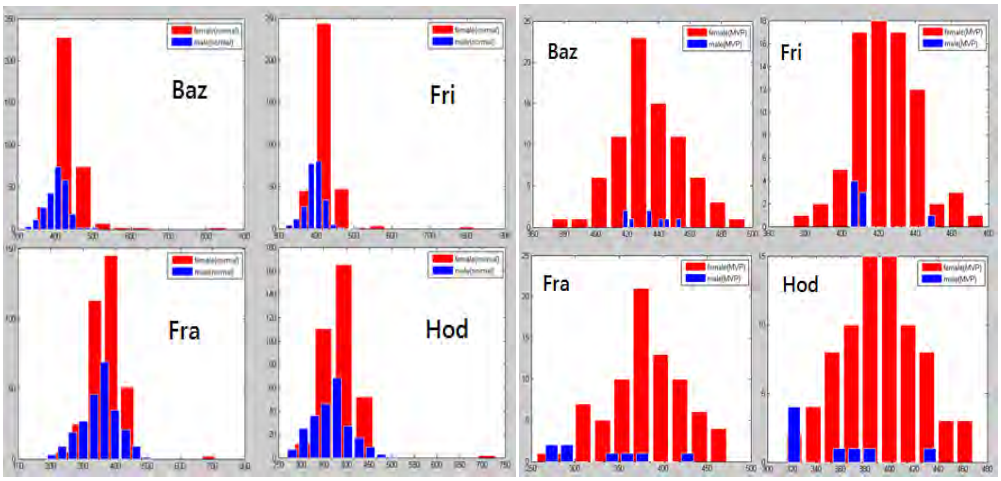

Fig. 1. Data based on four QTc equations. Males (blue) and females (red). Normals (left) and MVPS(right).

3. Results

The age and gender distribution of the participants are shown in Tables 1 and 2. In Tables 3 and 4, gender difference was demonstrated in the normal Taiwanese but only by Framingham and Hodges QTc correction formulae in MVPS. Nevertheless, all females have longer QTc than males in Taiwanese subjects. This trend is compatible with previous reports from Caucasians and Japanese studies.

Table. 1. Age and two ECG parameters of 239 normal males and 342 females.

Normal	Number	Age [year]	RR interval[ms]	QT interval[ms]
Male	239	26±10	882.40±147.14	378.79±2.00
Female	342	36±14	853.63±110.27	401.62±2.02

Table. 2. Age and two ECG parameters of 8 MVP males and 78 MVP females

MVP	Age[year]	RR interval[ms]	QT int[ms]
Male(8)	33±15	770.375±120.95	379.25±10.70
Female(78)	43±14	877.05±112.71	405.00±2.66

Table. 3. QTc in normal males and females. Four correction formulae were used.

Normal	QTint[ms]	QTcBaz[ms]	QTcFri[ms]	QTcFra[ms]	QTcHod[ms]
Male (239)	378.79±2.0	405.78±1.84	396.26±1.59	353.17±3.64	366.45±2.75
Female(342)	401.62±2.02	436.85±2.46	424.58±2.19	372.10±2.66	386.25±2.25
P value	<0.01	0.0001	0.0001	0.0001	0.0001

Table. 4. QTc in males and females with MVPS. Four formulae were used.

MVPS	Tint[ms]]	QTcBaz[ms]	QTcFri[ms]	QTcFra[ms]	QTcHod[ms)
Male(8)	79.25±10.7	433.43±4.70	414.31±5.35	329.06±21.21	355.13±14.9
Female(78)	05.00±2.66	434.01±2.37	423.92±2.01	380.45±4.92	392.09±3.71
P value	S	NS	NS	0.003	0.004

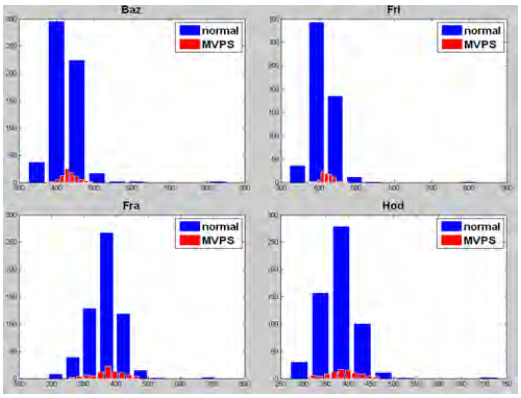

Fig. 2. The histograms from four QTc formulae. Normals (blue) and MVPS (red).

Table. 5. Comparison of QTc in all healthy individuals all those with MVPS.

	QTint[ms]	QTcBaz[ms]	QTcFri[ms]	QTcFra[ms]	QTcHod[ms]
Normal(581)	392.23	424.06±36.68	412.92±42.25	364.32±53.13	378.10±43.12
MVP(86)	402.60	433.96±25.16	423.03±37.62	375.68±47.23	388.65±35.18
P value	<0.01	<0.01	<0.01	<0.05	<0.05

Table. 6. Comparison of QTc in healthy females and females with MVPS.

	QTint[ms]	QTcBaz[ms]	QTcFri[ms]	QTcFra[ms]	QTcHod[ms]
Normal(342)	401.62±37.47	436.85±45.52	424.58±40.63	372.10±49.32	386.25±41.67
MVP(78)	405.00±23.50	434.02±20.93	423.93±17.73	380.46±43.44	392.09±32.78
P value	NS	NS	NS	NS	NS

Table. 7. Comparison of QTc in healthy males and males with MVPS.

	QTint[ms]	QTcBaz[ms]	QTcFri[ms]	QTcFra[ms]	QTcHod[ms]
Normal(239)	378.79±30.95	405.77±28.48	396.25±24.68	353.17±56.40	366.45±42.55
MVP(8)	379.25±30.36	433.43±13.30	414.31±15.13	329.06±60.00	355.14±42.38
P value	NS	<0.01	<0.05	NS	NS

From Table 5, in general, all four QTc correction formulae might be used to differentiate MVPS from normal. However, there is no significant difference of QTc between MVPS and normal in women of all four QTc formulae as illustrated from Table 6. Nevertheless, there were significant differences in QTc Bazett and Fridericia correction formulae in male. These two formulae might provide us with a useful tool for the investigation of MVPS in male Taiwanese.

4. Discussion

This research further demonstrated that gender dependent QTc criteria should be established for the evaluation of Normal and MVPS in Taiwanese. However, the disproportional male MVPS numbers of the male might have a significant influence for the present research. This issue mandates clarification in future study. Adoption of the specific QTc correction formulae might also be a major issue for future research in MVPS and normal ECG QT intervals.

References

[1] Tsai LW, Yang IF, Yang TF.An evaluation of Heart rate variability between MVP and a normal Taiwanese population. 17th Asian Pacific Congress of Cardiology Kyoto, Japan, 2009, May 20-23, S104. CVD Prevention and Control Vol.4 (Suppl.1): S104.

[2] Chen Y, Yang IF, Yang TF. Frequency Domain Heart Rate Variability Parameters Are Sex Dependent in an Apparently Healthy Taiwanese Population. 17th Asian Pacific Congress of Cardiology Kyoto, Japan, 2009, May 20-23. CVD Prevention and Control Vol.4 (supp)1, P102, May 2009.

[3] Chen YS, Chang CS, Lu CC, Tsai MJ,Chen Y, Yang IF, Yang TF. Standard 12-lead electrocardiogram in Taiwanese Mitral Valve Prolapse patients and normal healthy controls. The 37th International Congress on Electrocardiology (ICE). Lund, Sweden. June 3-5, 2010.P32, p104. *Journal of Electrocardiology*, 2011; 44:2:e44-e45.

[4] Chen Y, Chang CS, Lu CC, Tsai MJ, Chen YS, Yang IF, Yang TF, Postural Changes Influences on Heart Rate Variability in an apparently healthy Taiwanese population. The 37th International Congress on Electrocardiology (ICE). Lund, Sweden. June 3-5, 2010. P31, 103 *Journal of Electrocardiology*, 2011; 44~: 2:e42-e44.

[5] Yang IF, Yang TF. Use of short-term Heart Interval variability in Evaluation of angiotensin receptor blocker on cardiac autonomic modulation post hemodialysis. 17th Asian Pacific Congress of Cardiology, 101, Kyoto, Japan, 2009.

[6] Luo S, Michler K, Johnston P, Macfarlane PW. A comparison of commonly used QT correction formulae: the effect of heart rate on the QTc of normal ECGs. *J Electrocardiol*, 2004; 37 (Suppl): 81.

[7] Roden DM. Drug-induced prolongation of the QT interval. N *Engl J Med*, 2004; 350: 1013.

[8] Malik M, Garnett CE, Zhang J. Thorough QT studies: questions and quandaries. *Drug Saf*, 2010; 33: 1.

[9] Bazett HC. An analysis of the time relations of electrocardiograms. *Heart*, 1920; 7: 353.

[10] Malik M, Farbom P, Batchvarov V, Hnatkova K, Camm AJ. Relation between QT and RR intervals is highly individual among healthy subjects: implications for heart rate correction of the QT interval. *Heart*, 2002; 87: 220.

[11] Jacquemet V, Dube B, Knight R, et al. Evaluation of a subject-specific transfer-function-based nonlinear QT interval rate-correction method. *Physiol Meas*, 2011; 32: 619.

[12] Luo S, Michler K, Johnston P, Macfarlane PW. A comparison of commonly used QT correction formulae: the effect of heart rate on the QTc of normal ECGs. *J Electrocardiol*, 2004; 37(Suppl):81.

[13] Rowlands DJ, Graphical representation of QT rate correction formulae: an aid facilitating the use of a given formula and providing a visual comparison of the impact of different formulae. *J Electrocardiol*, 2012; 288-293.

[14] Mason JW, Florian Jr JA, Garnett CE, Moon TE, Selness DS, Spaulding RR. Pharmacokinetics and pharmacodynamics of three moxifloxacin dosage forms: implications for blinding in active-controlled cardiacrepolarization studies. *J Clin Pharmacol*, 2010; 50: 1249.

[15] Bazett HC. An analysis of the time relations of electrocardiograms. *Heart*, 1920; 7: 353.

SIGNAL AVERAGED ELECTROCARDIOGRAPHY IN ELDERLY HYPERTENSIVE PATIENTS

[1]I. Mozos, [1]M. Hancu, [2]L. Susan

[1]Victor Babes University of Medicine and Pharmacy,
Department of Functional Sciences, Timisoara, Romania
[2]Victor Babes University of Medicine and Pharmacy,
1st Department of Internal Medicine, Timisoara, Romania
Email: ioanamozos@umft.ro

Abstract. *Signal averaged electrocardiograms (SAECGs) detect late ventricular potentials (LVPs), as markers of the risk of sudden cardiac death. The present study hypothesized that aging increases the prevalence of LVPs in hypertensive patients. A total of 40 hypertensive patients, 73% males, aged 61±12 years, 43% of them being elderly (≥ 65 years), underwent SAECG. The positive criteria for LVPs were: QRS duration >120 ms, LAS40 (the duration of the signal at the end of the QRS complex with amplitude below 40 μV) >38 ms, and RMS40 (the square root of the last 40 ms of the signal) <20 μV. Elderly hypertensive patients were more likely to have longer SA-QRS and LAS40, lower RMS40 and late ventricular potentials than the younger patients. Aging increases the prevalence of abnormal SAECGs and LVPs in patients with hypertension which is also associated with left ventricular hypertrophy, coronary heart disease and an impaired renal function.*

Keywords: Ventricular late potentials, Signal averaged electrocardiogram, Aging, Hypertension, Left ventricular hypertrophy

1. Introduction

Abnormal signal averaged electrocardiograms (SAECGs) and late ventricular potentials (LVPs) are markers of ventricular arrhythmia vulnerability and sudden cardiac death. LVPs are low amplitude, high frequency waveforms, appearing in the terminal part of the QRS complex [1-3].

A high risk of sudden cardiac death was previously demonstrated in hypertensive patients, related to left ventricular hypertrophy, interstitial fibrosis, myocardial or subendocardial scars, silent myocardial ischemia, diastolic dysfunction and disturbances in cardiac autonomic balance [3-6].

Aging is considered a cardiovascular risk factor and is usually associated with increased cardiovascular pathology, the use of multiple drugs, structural, functional and vascular changes. The most important age-associated cardiovascular changes are: increased left ventricular wall thickness, focal collagen deposition, increased vascular stiffness, autonomic dysregulation and reduction of forward flow, limiting organ perfusion [7].

The present paper hypothesized that aging increases the prevalence of late ventricular potentials in hypertensive patients and aimed to identify factors significantly associated with LVPs in elderly hypertensive patients.

2. Methods

A total of 40 consecutively recruited hypertensive patients, from the CFR Hospital, from Timisoara, underwent SAECG and standard 12-lead ECG.

Patients

The most important inclusion criterion was hypertension, diagnosed according to the criteria of the European Society of Cardiology [8]. Patients with secondary hypertension, atrial flutter, bundle branch block, electrolyte imbalances and chronic obstructive pulmonary disease were excluded.

Ethical aspects

The investigations conformed to the principles outlined in the Declaration of Helsinki [10](Cardiovascular Research 1997; 35: 2-4) and were approved by the Ethics Committee of the University. A written informed consent was given by each patient.

SAECG

SAECG and standard 12-lead ECG were performed using a Siemens-Megacart electrocardiograph. The methodology for SAECG was previously described [3]. The positive criteria for LVPs were: QRS duration (SA-QRS) >120 ms, LAS40 (the duration of the signal at the end of the QRS complex with an amplitude below 40 μV - "Low Amplitude Signal") >38 ms and RMS40 (”Root Mean Square”- the square root of the last 40 ms of the signal) <20 μV. Abnormal SAECGs and LVPs were defined by one (LVP1) and two positive criteria (LVP2), respectively.

Left ventricular hypertrophy

The standard 12-lead ECG was used to diagnose left ventricular hypertrophy (LVH), if at least one of the following 5 criteria was positive: the Romhilt-Estes score [9], the Sokolov-Lyon index [11], Cornell voltage criteria and product [12], and the Mazzaro score [13].

Renal function and coronary heart disease

The glomerular filtration rate (GFR) was calculated using the Modification of Diet in Renal Disease equation (MDRD) [14].

A history of coronary heart disease was extracted from medical records.

Statistical methods

Categorical data are given as numbers and percentages, continuous data are given as means ± standard deviation. Linear and multiple regression analysis were used as statistical methods.

The minimum required sample size was 31, calculated for regression analysis with 2 predictors, 0.05 probability level and a desired statistical power of 0.8.

3. Results

The characteristics of the study population are described in Table 1. A total of 17 patients (43%) were included in the elderly group (≥65 years).

Prevalence of LVPs, abnormal SAECGs, LVH and impaired renal function in the two groups

Late ventricular potentials were detected in 16 patients (40%) (Table 1).

Prolonged SA-QRS, longer LAS40 and LVP2 were more prevalent in the elderly group compared to the other patients: 24% vs. 17%, 47% vs. 30% and 47% vs. 35%, respectively.

Left ventricular hypertrophy and an impaired renal function were also more prevalent in the elderly group (59% vs. 48% and 59% vs. 17%, respectively).

Regression analysis

Linear and stepwise multiple regression were performed. Significant associations were found between age and SAECG criteria, LVH, impaired GFR, and coronary heart disease, respectively (Table 2).

4. Discussion

The current study demonstrates the higher prevalence of LVPs and abnormal SAECGs in a comparison of elderly and younger hypertensive patients, associated with end-organ effects: LVH, CHD and impaired renal function.

LVPs were previously detected in hypertensive patients [6, 15 - 17], associated with left ventricular hypertrophy, low E/A ratios, withdrawal of parasympathetic tone, and in patients with an impaired renal function or coronary heart disease [1]. Palmiero et al. demonstrated a significant correlation between left ventricular hypertrophy and grade of arrhythmia and late potentials in patients with essential (primary) hypertension [16]. Aging and hypertension-related arterial stiffness promote left ventricular hypertrophy. Hypertensive LVH is both a pathologic response, emphasizing the imbalance between oxygen supply and demand and decreasing the coronary flow reserve, and a risk factor for sudden cardiac death risk in patients with elevated blood pressure values [18]. Arrhythmias in hypertrophyic hearts are facilitated by electrolyte imbalances, transient blood pressure peaks and the occurrence of myocardial ischemia [15]. The presence of LVPs was previously associated with a lower maximum oxygen uptake during ergospirometry [19].

Table 1. Characteristics of the study population

Variable	Results
Age	61±12 years
Gender	29 (73%) males
SA-QRS	108±21 ms (25%)
RMS40	22±12 microV (60%)
LAS40	44±22 ms (38%)
LVP1	24 (60%)
LVP2	16 (40%)
Left ventricular hypertrophy	21 (53%)
GFR<60 ml/min	14 (35%)
Coronary heart disease	18 (45%)

ECG left ventricular hypertrophy criteria were criticized due to lack of sensitivity. The use of multiple ECG criteria, especially combining QRS voltage and duration, increases sensitivity and specificity of LVH ECG diagnosis [20].

The direct relationship between aging and a higher incidence of late potentials was previously reported in patients with heart failure [18, 20]. The present study demonstates the association between LVPs and end-organ effects in elderly hypertensive patients.

Hypertension and aging both impair renal function. The aging kidney is characterized by progressive glomerulosclerosis and interstitial fibrosis, reducing the glomerular filtration rate

[18]. The current study demonstrates the association between LVPs and an impaired renal function in hypertensive patients.

Table 2. Linear and multile regression analysis. Significance F<0.01

Variable	Associated with	Multiple R	R square	Adjusted R
Age	SAQRS (p< 0.01)	0.978	0.957	0.930
	RMS40 (p= 0.0038)			
Age≥65 years	LVH (p= 0.033)	0.697	0.485	0.446
	GFR<60 ml/min (p< 0.01)			
LVP1	LVH (p=0.032)	0.572	0.328	0.284
	GFR<60 ml/min (p=0.031)			
LVP2	Age≥65 years (p=0.019)	0.705	0.498	0.458
	CHD (p< 0.01)			
SA-QRS>120 ms	Age≥65 years (p=0.037)	0.714	0.51	0.471
	CHD (p< 0.01)			
RMS40<20 microV	LVH (p= 0.032)	0.572	0.328	0.284
	GFR<60 ml/min (p= 0.031)			
LAS40 > 38 ms	LVH (p=0.003)	0.451	0.203	0.177

5. Conclusions

Elderly hypertensive patients are more likely to have longer SA-QRS and LAS40, lower RMS40 and late ventricular potentials than the younger patients. Aging increases the prevalence of abnormal SAECGs and LVPs in hypertensive patients, associated with left ventricular hypertrophy, coronary heart disease and an impaired renal function.

Further studies are needed to demonstrate that regression of left ventricular hypertrophy, improvement of coronary perfusion and slowing progression of chronic kidney disease in elderly hypertensive patients may reduce the risk of sudden cardiac death.

References

[1] Barbosa Benchimol PR, et al. Analysis of the prevalence of ventricular late potentials in the late phase of myocardial infarction based on the site of infarction. *Arq Bras Cardiol*, 2002; 78: 358-63.

[2] Olinic N, Zdrenghea D. Cardiopatia ischemica. Clusium Publishing House, Cluj-Napoca, Romania, 1998.

[3] Mozos I, et al. Late ventricular potentials in cardiac and extracardiac diseases, in Cardiac arrhythmias. Breijo-Marquez FR. Intech, Rijeka, Croatia, 2012, 227-256.

[4] Galinier M, et al. Prognostic value of arrhythmogenic markers in systemic hypertension. *Eur Heart J*, 1997; 18: 1484-1491.

[5] Brune S, et al. Prevalence of late ventricular potentials in hypertensive patients. *J Cardiovasc Pharmacol*, 1991; 17(Suppl 2): S46-7.

[6] Barison A, et al. Markers of arrhythmogenic risk in hypertensive subjects. *Curr Pharm Des*, 2011; 17(28): 3062-73.

[7] Beers MH, Berkow R. The Merck Manual of Geriatrics. Third Edition. Merck & Co, West Point, PA, USA, 2000.

[8] Mancia G, et al. 2013 ESH/ESC Guidelines for the management of arterial hypertension. *Eur Heart J*, 2013. doi: 10.1093/eurheartj/eht151.

[9] Romhilt DW, Estes EHJr. A point score system for the ECG diagnosis of left ventricular hypertrophy. *Am Heart J*, 1968; 75: 752-8.

[10] World Medical Association Declaration of Helsinki. Recommendations guiding physicians in biomedical research involving human subjects. *Cardiovascular Research* 1997; 35: 2-4.

[11] Sokolov M, Lyon TP. The ventricular complex in left ventricular hypertrophy as obtained by unipolar precordial and limb leads. *Am Heart J*, 1949; 37: 161-86.

[12] Casale PN, et al. Electrocardiographic detection of left ventricular hypertrophy development and prospective validation of improved criteria. *J Am Coll Cardiol*, 1985; 6: 572-805.

[13] Do Lago Mazzaro C, et al. Ventricular mass and electrocardiographic criteria of hypertrophy: Evaluation of new score. *Arq Bras Cardiol*, 2008; 90(4): 227-231.

[14] Levey AS, et al. A more accurate method to estimate glomerular filtration rate from serum creatinine: a new prediction equation. *Ann Intern Med*, 1999; 130(6): 461-70.

[15] Katholi RE, et al. Left ventricular hypertrophy: Major risk factor in patients withhypertension: Update and practical clinical applications. *Int J Hypertens*, 2011: 495349. doi: 10.4061/2011/495349.Epub 2011 jun 30.

[16] Palmiero P, Maiello M. Arrhythmic risk in essential hypertension: late potentials. *Minerva Cardioangiol*, 2004; 52(1): 1-8.

[17] Wojszwillo A, et al. Signal averaged ECG in different patterns of left ventricular hypertrophy and geometry in hypertension. *Kardiol Pol*, 2003; 58(5): 335-43.

[18] De Sousa Grell E, et al. Time domain analysis of the signal averaged electrocardiogram to detect late potentials in heart failure patients with different etiologies. *Arq Bras Cardiol*, 2006; 87(3): 241-7.

[19] Aronow WS, et al. ACCF/AHA 2011 expert consensus document on hypertension in the elderly: a report of the American College of Cardiology Foundation Task Force on Clinical Expert Consensus Documents. *J Am Coll Cardiol*, 2011; 57: 2037-114.

[20] Mozos I, et al. Ventricular arrhythmia risk in elderly heart failure patients. *Review of Global Medicine and Healthcare Research*, 2010; 1(1): 18-29.

CIRCADIAN VARIATION OF LATE POTENTIALS AND ASSOCIATION WITH AUTONOMIC NERVOUS SYSTEM IN NORMAL HEART SUBJECTS USING HOLTER AMBULATORY ELECTROCARDIOGRAM

[1]K. Hashimoto, [1]Y. Kasamaki,
[2]Y. Okumura, [2]T. Nakai, [2]S. Kunimoto, [2]I. Watanabe,
[2]A. Hirayama, [1]M. Soma

[1]Division of General Internal Medicine, Department of Medicine,
Nihon University School of Medicine, Tokyo, Japan
[2]Division of Cardiovascular Medicine, Department of Medicine,
Nihon University School of Medicine, Tokyo, Japan
E-Mail: Hashimoto.kenichi@nihon-u.ac.jp

Abstract. *It has been reported that late potentials (LP) were useful to detect malignant arrhythmias and identify the risk of sudden cardiac death in patients with organic heart disease and idiopathic ventricular fibrillation syndrome. Recently, it has been possible to measure LPs for 24 hours using a newly developed Holter ambulatory electrocardiogram (ECG). However, there are few studies describing referential intervals of LP through 24 hours, and little is known about its association with the autonomic nervous system in healthy subjects. LPs were recorded on 48 normal healthy subjects (24 men 24 women), aged 20 to 88 years (mean±SD, 45±7). LP parameters using Holter ambulatory electrocardiogram .were measured before and after each meal and going to bed (1 point in daytime and 1 point at night: total 2 points per 24 hours) in each indices (fQRS, RMS40, LAS40). We measured the RR interval and analyzed the component of HF, LF/HF for heart rate variability (HRV) at the same time on the 24-hour ambulatory ECG. FQRS and LAS40 in men were significantly longer at night time than those in daytime (FQRS; 106.5±5.5 vs. 110.6, P=0.02. LAS 40; 30.1± 3.0 vs. 37.8± 1.4, P=0.007. respectively) RMS 40 in men was significantly smaller at night time than those in daytime (28.3±6.1 vs. 21.2±4.6. P=0.007.) In women there are no differences in LP parameters between daytime and night time. There was significant negative correlation between FQRS, LAS40 and LF/HF in men (FQRS and LF/HF R=0.458, p=0.002, LAS40 and LF/HF; R=0.035, P=0012. respectively). There was significant positive correlation between RMS40 and LF/HF in men (R=0.35, p=0.0023) In conclusion, in cardiac normal subjects, there was circadian variation in LP which might be augmented by the autonomic nervous system. These factors should be taken into account in setting of the referential interval of LP parameters.*

Keyword: Circadian variation; Late Potential; Ventricular arrhythmias; Sudden Cardiac Death

1. Introduction

It has been reported that late potentials (LP) were useful to detect malignant arrhythmias (i.e. ventricular fibrillation, Ventricular tachycardia) and identify patients with organic heart disease [1-3] and idiopathic ventricular fibrillation syndrome (i.e. Brugada syndrome, J wave syndrome) at risk of sudden cardiac death [4].

Some investigators have described that LP of Brugada syndrome and J wave syndrome have circadian variation throughout 24 hours, and they note that vagal nerve activity affecting LP resulted in increased inducibility of malignant arrhythmias [5, 6].

Conversely, concerning organic heart disease such as ischemic heart disease, cardiomyopathy, and heart failure, circadian variation of LP through 24 hours and association with the autonomic nervous system has not been reported. Future study will be needed to elucidate the correlation between the circadian variation of LP and inducibility of malignant ventricular tachyarrhythmias.

Recently, it has been possible to measure LP throughout 24 hours using newly developed Holter ambulatory electrocardiogram [1-3]. In a previous study, Yakubo et al [7] describe the referential intervals of real time LP. However, there are few studies describing referential intervals of LP throughout 24 hours, and little is known about its association with the autonomic nervous system in cardiac normal subjects. It is important to assess the circadian variation in each LP parameter (FQRS, RMS 40, LAS40) in cardiac normal subjects to evaluate circadian variation of LP in patients with heart disease. The aim of this study is to measure LP parameter in daytime and at night time and to assess association with LP parameters and the autonomic nervous system.

2. Methods

Holter ECG monitoring analysis was performed on 48 persons (24 men and 24 women) who were referred to our hospital suffering from transient chest symptoms (i.e. chest pain, palpitation, chest discomfort) but abnormal evidence (X -ray, ECG, echocardiography, Holter 24 hour electrocardiogram) has not been identified.

We recorded the ventricular signal-averaged ECG using the newly developed 24-hour Holter ambulatory ECG system (Spider View; Ela medical Inc.) at 2 points (1 point in daytime and 1 point in night time).

LP by SAECG

Parameters were calculated using a computer algorithm: (1) filtered QRS duration (FQRS); (2) root mean square voltage of the terminal 40 msec in the filtered QRS complex (RMS40); and (3) duration of low-amplitude signals <40 μV in the terminal filtered QRS complex (LAS40). LP was considered positive when two of the three criteria (FQRS ≥114 msec, RMS40 <20 μV, LAS40 >38 msec) were met.

Heart Rate Variability (HRV) Measurement

The fast peaks of R waves of the electrocardiograms were detected, and R-R interval (RRI) was measured. The RRI data were analyzed by the maximum-entropy methods with high resolution (Memcalc; Suwa Trust, Tokyo, Japan).

For real-time analysis of HRV, data on RRI were obtained by on-line computer analysis with 2 ms sampling intervals.

The power of RRI (ms2) with LF (0.04 to 0.15 Hz) and HF (0.16 to 0.50 Hz) bands were calculated. LF/HF in RRI variability was also assessed.

As data were skewed, log transformation of HF power of heart rate variability was performed (LnHF).

Statistical analysis

Values were expressed as mean ±SE (Standard error). The difference in the parameter of LP between daytime and night time are examined by Wilcoxon signed rank test. Correlation

between LP parameters and indices of autonomic nerve activity were calculated by Spearman's rank correlation coefficient.

A value of $P < 0.05$ was considered to be statistically significant.

3. Results

Study population
The ages of subjects in the 24 men ranged from 20 to 82 years (mean±SD; 58.3 ±16.6), and in the 24 women, from 22 to 88 years (mean±SD; 57.1 ±17.8).

Circadian variation of LP
Table 1 shows the value of LP parameters in daytime and night time.

FQRS and LAS40 in men were significantly longer at night time than those in daytime (FQRS; 106.5±5.5 vs. 110.6, P=0.02. LAS 40; 30.1± 3.0 vs. 37.8± 1.4, P=0.007 respectively) RMS 40 in men was significantly shorter at night time than those in daytime (28.3±6.1 vs. 21.2±4.6. P=0.007).

FQRS and LAS40 in women tended to be longer at night time than those in daytime, however there was no significant difference (FQRS; 87.9±8.3 vs. 89.7±9.3 P=0.172. LAS 40; 29.1± 6.2 vs. 30.5± 7.8, P=0.3, respectively).

RMS 40 in women was tend to be smaller at night time than those in daytime, however there was no significant difference (56.5±8.0 vs.49.4±6.7, P=0.073).

Table 1 Correlation between LP parameters and autonomic nervous system activity

	Daytime	Night time	
			P value
FQRS (Men) ms	106±5.5#	110.6±5.4##	0.02
FQRS (Women) ms	87.9±8.3	89.7±9.3	0.172
RMS (Men) ms^2	28.3±6#	21.2±4.6##	0.023
RMS (Women) ms^2	56.5±8.0	49.4±6.7	0.07
LAS (Men) ms	30.1±3.0 †	37.8±1.4 ††	0.007
LAS (Women) ms	29±6.1	30.5±7.8	0.3

The Table shows comparison LP parameters between daytime and night time.
All data were expressed as Mean ± SE
P< 0.005 in comparison of value between # and ##
P< 0.001 in comparison of value between † and ††

Fig. 1 shows the correlation between LP parameters (FQRS, RMS40 and LAS40) and autonomic nervous system activity (LF/HF and LnHF)

There was significant negative correlation between FQRS, LAS40 and LF/HF in men (FQRS and LF/HF R=0.458, p=0.002, LAS40 and LF/HF; R=0.035, P=0012. respectively).

There was significant positive correlation between RMS40 and LF/HF in men (R=0.35, p=0.0023).

On the other hand, there were no negative significant correlation between FQRS, RMS 40 and LF/HF (FQRS and LF/HF R=0.03, p=0.8, LAS40 and LF/HF; R=0.07, P=0.5 respectively). There were no positive significant correlation between RMS 40 and LnHF (R=0.56, p=0.09)

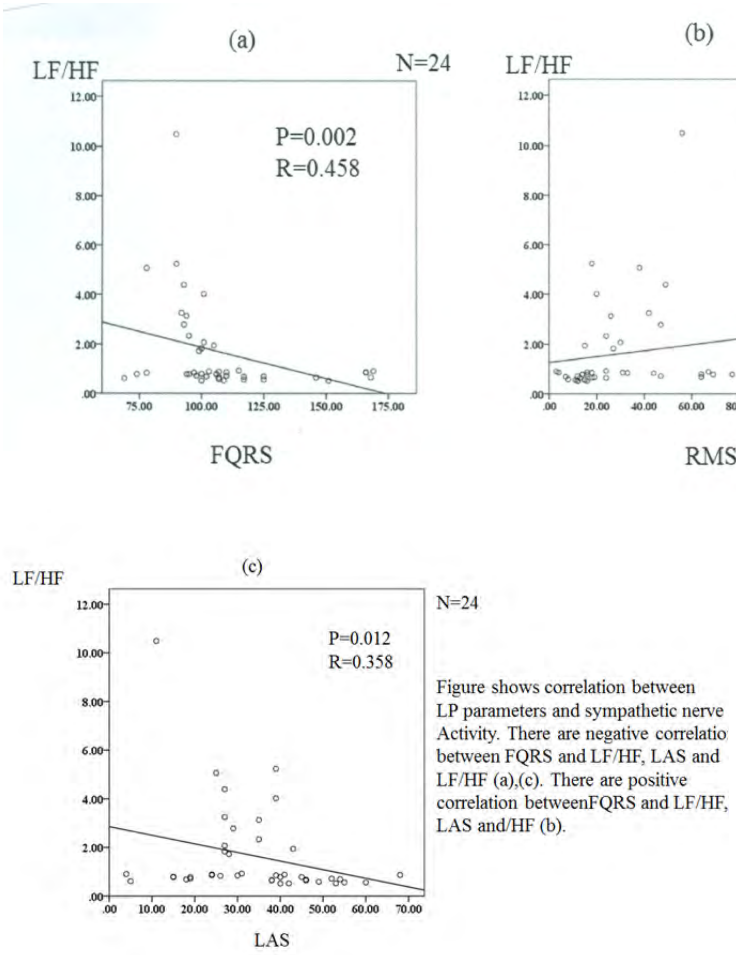

Fig. 1. Correlation between LP parameters (FQRS, RMS40 and LAS40) and autonomic nervous system activity (LF/HF and LnHF)

4. Discussion

In this article, we first report on circadian variation of LP in cardiac normal subject. Our main findings are firstly, each parameter of LP (FQRS, RMS 40 and LAS 40) was worsening at night time in men. However it was not the case in women. Secondly, LP parameters were augmented by vagal nerve activity.

Circadian variation of LP

It has been reported that in idiopathic ventricular fibrillation such as Brugada syndrome and J wave syndrome, the incidence of malignant arrhythmias is higher at night than in daytime [8].

Conversely, in a patient with organic heart disease (e.g. IHD.) the incidence of VT and VF which result in SCD are higher in daytime than night time [9-11].

The time peaks derived from malignant arrhythmias were different for each type of heart disease. Therefore it is important to research the factors contributing to all arrhythmias occurring throughout the day.

On the other hand, LP represents low-amplitude, fragmented signal from the myocardium and is associated with ventricular tachyarrhythmias related to SCD in IHD and IVF [1-3]. In addition, the existence of LP indicates that there are substrates inducible to ventricular arrhythmias.

Several studies carried out since the 1980s, have reported on the usefulness of LP in clinical practice for predicting SCD. However there are limitations in that sensitivity for VT is in the

range of 64-100%, and Specificity is 46-89% [12.]Therefore LP might be useful to detect low-risk patients who are suspected to have occurring ventricular tachyarrhythmias for predicting SCD.

Recent newly developed 24-hour Holter monitoring can detect LP all day. And the device might be used to help to increase sensitivity to predict ventricular tachyarrhythmias.

Abe et al [13] ,reported that LP parameters exacerbation were observed in night tendency in patients with Brugada syndrome and J wave syndrome, but not in patients with arrhythmogenic right ventricular cardiomyopathy (ARVC). Our data is useful to evaluate LP as reference, particularly at night time. Moreover the patients of Brugada syndrome and J wave syndrome and ARVD patients were men, little data showed LP circadian variation in women. Thus our data is useful to evaluate LP as reference particularly at night time.

Our data suggest that each parameter of LP (FQRS, RMS 40 and LAS 40) were worsening at night time in men, however the same effect did not occur in women.

Late potential is considered to be a depolarization abnormality. On the other hand, it has been reported that QT reflect repolarization and in the situation of bradycardia at night, a prolongation of QT in women are greater than that of in men [14-16]. This fact might reflect a gender discrimination phenomenon between depolarization and repolarization in the circadian variation.

Correlation between LP parameters and autonomic nerve activity

In our present study, RMS 40 was positively correlated with LF/HF, and FQRS and LAS 40 was negatively correlated with LnHF.

LF/HF is believed to reflect sympathetic nerve activity and LnHF to reflect parasympathetic nerve activity.

Recently Abe et al and Mizumaki et al [5-6] reported vagal activity modulates a spontaneous increase of the amplitude of the J wave. These findings suggest that vagal activity plays an important role in the occurrence of ventricular tachyarrhythmias.

In the male cardiac normal subject, it might be suggested that LP parameter is influenced only by sympathetic activity, and not by vagal activity. Moreover, in female cardiac normal subjects LP parameters are not influenced by the autonomic nervous system.

In further studies, this data could be useful to assess the correlation between arrhythmogenesis and the autonomic nervous system.

5. Conclusions

In cardiac normal male subject, there was circadian variation in LP which might be augmented by the autonomic nervous system. These factors should be taken into account in setting of the referential intervals of LP parameters.

Acknowledgements

This Study was supported by a grant for scientific research Nihon University School of Medicine

The authors express their thanks to Mr H Shimabukuro, Nihon University for reading the manuscript.

References

[1] Simson MB. Use of signals in the terminal QRS complex to identify patients with ventricular tachycardia after myocardial infarction. *Circulation*; 1981; 64(2): 235-242.

[2] Breithardt G, Schwarzmaier J, et al. Prognostic significance of late ventricular potentials after acute myocardial infarction. *Eur Heart;* 1983; J 4(7): 487-495.

[3] Breithardt G, Cain ME, et al. Standards for analysis of ventricular late potentials using high-resolution or signal-averaged electrocardiography. A statement by a Task Force Committee of the European Society of Cardiology, the American Heart Association, and the American College of Cardiology. *Circulation*, 1991; 83(4): 1481-1488.

[4] Ikeda T, Sakurada H, et al. Assessment of noninvasive markers in identifying patients at risk in the Brugada syndrome: insight into risk stratification. *J Am Coll Cardiol,* 2001; 37(6): 1628-1634.

[5] Abe A, Ikeda T, et al. Circadian variation of late potentials in idiopathic ventricular fibrillation associated with J waves: insights into alternative pathophysiology and risk stratification. *Heart Rhythm*, 2010; .7(5): 675-682.

[6] Mizumaki K, Nishida K, et al. Vagal activity modulates spontaneous augmentation of J-wave elevation in patients with idiopathic ventricular fibrillation. *Heart Rhythm*, 2012; 9(2): 249-255.

[7] Yakubo, S, Ozawa Y, et al. Normal limits of high-resolution signal-averaged ECG parameters of Japanese adult men and women. *J Electrocardiol*, 2000; 33(3): 225-231.

[8] Matsuo K, Kurita T, et al. The circadian pattern of the development of ventricular fibrillation in patients with Brugada syndrome. *Eur Heart J*; 1999; 20(6): 465-470.

[9] Anand K, Aryana A, et al. Circadian, daily, and seasonal distributions of ventricular tachyarrhythmias in patients with implantable cardioverter-defibrillator, 2007. *Am J Cardiol*, 2007; 100(7): 1134-1138.

[10] Muller JE., Ludmer PL, et al. Circadian variation in the frequency of sudden cardiac death. *Circulation*, 1987; 75(1): 131-138.

[11] Willich SN, Levy D, et al. Circadian variation in the incidence of sudden cardiac death in the Framingham Heart Study population. *Am J Cardiol*, 1987; 60(10): 801-806.

[12] Malik M. Risk of arrhythmia and sudden cardiac death, Malik M, Editor .BMJ Books, London, 2001,168-169

[13] Abe A, K. Kobayashi K, et al. Comparison of late potentials for 24 hours between Brugada syndrome and arrythmogenic right ventricular cardiomyopathy using a novel signal-averaging system based on Holter ECG. *Circ Arrhythm Electrophysiol,* 2012; .5(4): 789-795.

[14] Smetana P, Batchvarov VN, et al. Sex differences in repolarization homogeneity and its circadian pattern. *Am J Physiol Heart Circ Physiol*, 2002; 282(5): H1889-1897.

[15] Yan GX, Antzelevitch C, Cellular basis for the normal T wave and the electrocardiographic manifestations of the long-QT syndrome. *Circulation*, 1998; 98(18): 1928-1936.

[16] Nakagawa M, Ooie T, et al. Gender differences in the dynamics of terminal T wave intervals. *Pacing Clin Electrophysiol,* 2004; 27(6 Pt 1): 769-774.

DECARTOGRAPHIC DETECTION OF PRESENCE AND SEVERITY OF RIGHT VENTRICULAR OVERLOAD IN PATIENTS WITH PULMONARY HYPERTENSION

[1]T. Sakhnova, [1]E. Blinova, [2]V.Trunov, [2]E. Aidu, [1]E. Yurasova, [1]M. Saidova, [1]T.Martynyuk, [1]I. Chazova

[1]Cardiology Research Complex, Moscow, Russia
[2]Institute for Information Transmission Problems RAS, Moscow, Russia
Email: tamara-sahnova@mail.ru

Abstract. *The objectives of the study were to review the possibilities of decartographic repolarization parameters for the assessment of right ventricular overload severity in pulmonary arterial hypertension (PAH).The magnitude G and spatial components Gx, Gy, Gz of the "recovery acceleration" vector were studied in 120 PAH patients and 120 controls. Moderate PAH was defined as systolic pulmonary artery pressure (SPAP) 30-50 mm Hg; severe - as SPAP > 50 mm Hg. We found that in 30 patients with moderate PAH G, Gx and Gz were lower than in normal; G, Gx and Gy were greater than in severe PAH. For the discriminating of moderate PAH and normal group Gz had the area under the ROC curve (AUC) 0.83, SE 0.05; for the discriminating of moderate and severe PAH Gy had AUC 0.87, SE 0.04. In conclusion, in PAH patients' decartographic repolarization parameters may be helpful for detection of right ventricular overload and assessment of its severity.*

Keywords: Pulmonary Arterial Hypertension, Right Ventricular Overload, Electrocardiogram, Repolarization

1. Introduction

Detection of chronic right ventricular pressure overload is a difficult diagnostic challenge. It is known that the ability of the conventional 12-lead ECG parameters to detect right ventricular hypertrophy (RVH) is relatively low [1]. At the same time, an echocardiogram in RVH is also less definitive than in left ventricular hypertrophy due to the complex 3-dimensional shape of the right ventricle, while measuring difficulties frequently occur. In recent years some experimental and clinical studies [2, 3] demonstrated that the development of pulmonary arterial hypertension (PAH) may induce the marked changes of ventricular gradient, a 3-D measure of ventricular action potential duration heterogeneity. Decartographic "recovery acceleration map" or "recovery acceleration vector" shows the distribution of the dipole component of the depolarized state duration shortening over the heart surface. Concerning the electrophysiological meaning, this characteristic is very close to ventricular gradient. The aim of our work was to study the possibilities of decartographic "recovery acceleration vector" parameters for the assessment of right ventricular overload severity in patients with PAH.

2. Methods

We examined 120 patients, in whom the presence of PAH was verified with clinical and instrumental methods. 120 healthy subjects comprised the control group. Systolic pulmonary artery pressure (SPAP) was calculated using Doppler echocardiography. Moderate PAH was defined as SPAP 30-50 mm Hg; severe PH as SPAP > 50 mm Hg. Digital orthogonal (McFee-Parungao lead system) 10-s electrocardiograms were recorded on a commercially available electrocardiograph and processed by means of software developed in Cardiology Research Complex and Institute for Information Transmission Problems.

We studied the magnitude G (in ms) and spatial components Gx, Gy, Gz of the "recovery acceleration" vector (directed to the left, inferior, and anterior).

Statistical analysis was performed using Medcalc. Results are presented as mean±standard deviation. To evaluate the differences between two independent samples unpaired t-test was used. To identify the relationship between variables, Pearson correlation coefficient was calculated. To determine the diagnostic value of parameters receiver operating characteristic (ROC) analysis was used. Differences were considered significant at $p < 0.05$.

3. Results

Among the PAH patients studied, 30 had moderate PAH and 90 – severe PAH. Characteristics of the groups are presented in Table 1. In patients with moderate PAH G, Gx and Gz were lower as compared with the normal group, and G, Gx and Gy were greater as compared with severe PAH.

Table. 2 Characteristics of the groups.

	Normal	moderate PAH	severe PAH
Age, years	33.5±10.5	47.4±14.3*	36.9±12.2#
% males	32.5	30	26.8
SPAP, mm Hg	< 30	39.4±6.7	95.2±29.4#
G, ms	82.2±22.4	72.7±25.4*	53.6±26.3#
Gx, ms	42.4±13.2	23.2±20.2*	5.7±22.8#
Gy, ms	34.2±12.4	36.2±16.6	9.9±20.2#
Gz, ms	26.6±17.6	-6.1±31.7*	-18.5±26.9#

*p<0.05 as compared with normal group; # p<0.05 as compared with moderate PAH

When used for the discriminating of moderate PAH and normal group Gz had the area under the ROC curve 0.83, SE 0.05; the threshold Gz < 10 ms provided 77% sensitivity and 83% specificity. For the discriminating of moderate and severe PAH Gy had the area under the ROC curve 0.87, SE 0.04; the threshold Gy < 25 ms provided 82% sensitivity and 90% specificity (Fig. 1). Gx and Gy had moderate correlation with SPAP (r=-0.5; p<0.01 – Fig. 2).

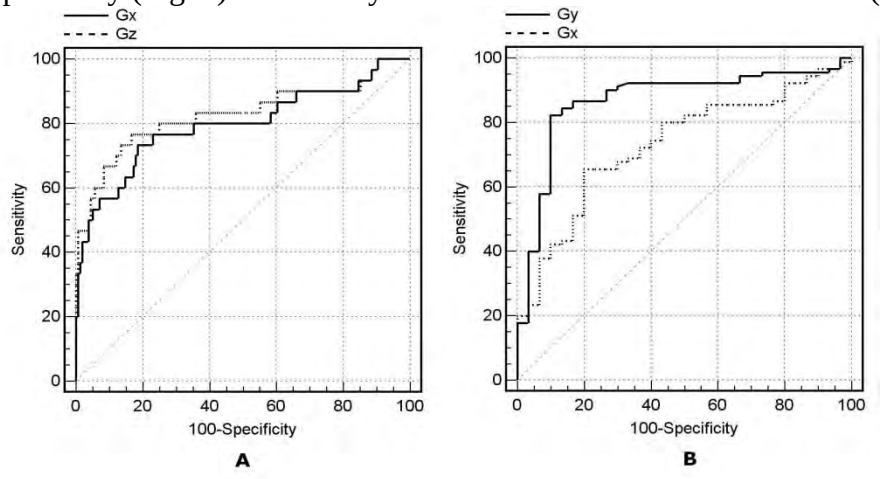

Fig. 1. ROC curves for the discriminating of moderate PAH and normal group (a) and for the discriminating of moderate and severe PAH (b).

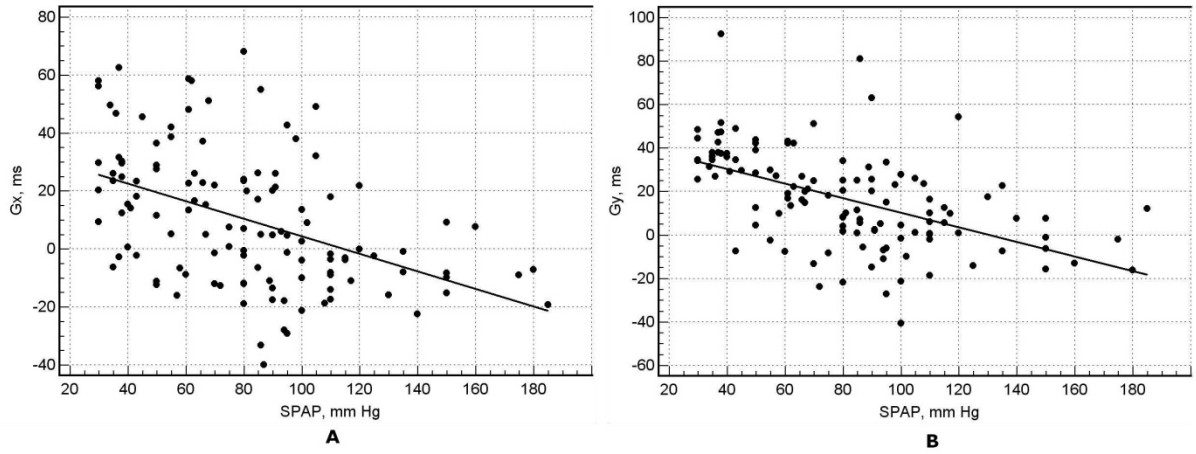

Fig. 2. Relationships between Gx and SPAP (a) and Gy and SPAP (b).

Typical decartograms of normal subject and patients with different SPAP values are shown in Fig. 3. Decartographic "recovery acceleration map" visually shows a gradual change in the direction of the "recovery acceleration" vector with the rise of SPAP values. In patient with SPAP 150 mm Hg "recovery acceleration" vector takes the direction opposite to that observed in normal.

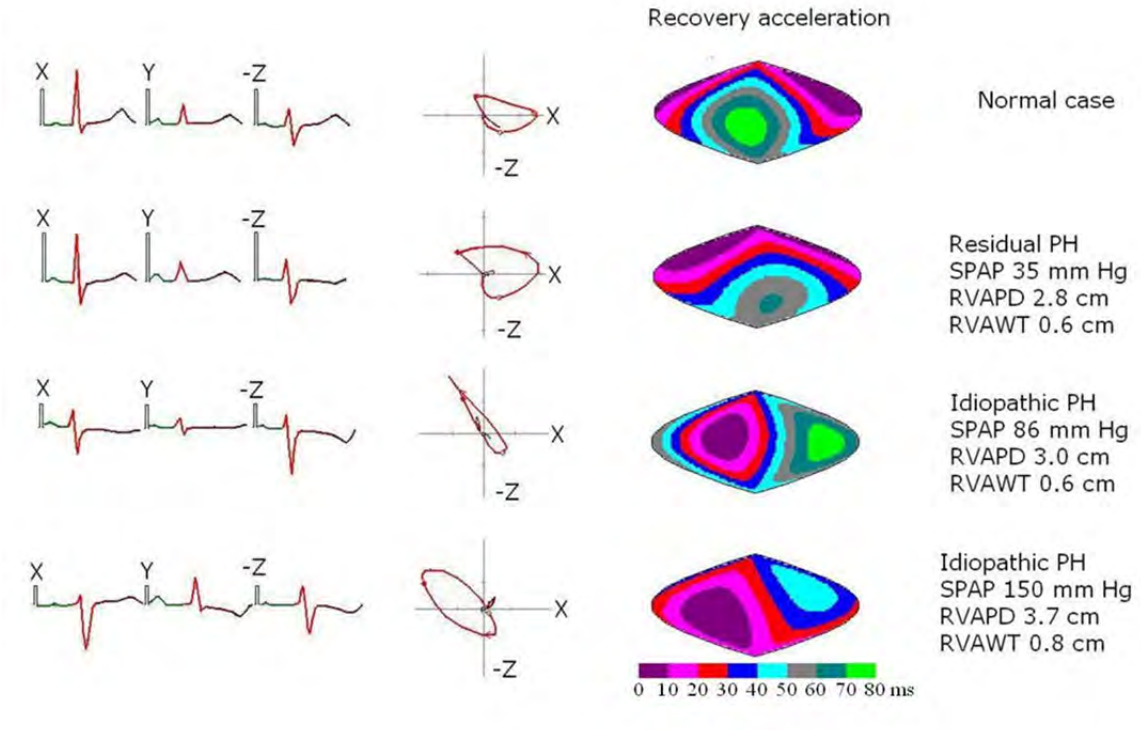

Fig. 3. Typical decartograms of normal subject and patients with different SPAP values.

4. Discussion

Data from our study are consistent with those of Henkens et al [2] in that the ECG-derived ventricular gradient is accurate in detecting chronic increase in right ventricle pressure load, and can be used to distinguish between normal right ventricle pressure load, mildly to moderately increased right ventricle pressure load, and severely increased chronic right ventricle pressure load. In patients included in our study, X component of "recovery acceleration" vector progressively decreased with the increase of SPAP. Besides that, it was

found that Y component of “recovery acceleration” vector remaining unchanged in patients with moderate PAH changes significantly in patients with severe PAH. Z component of “recovery acceleration” vector in moderate PAH was lower as compared with normal group, but with a further increase of SPAP has not changed so dramatically.

In statements from the International Working Group on the ECG diagnosis of left ventricular hypertrophy [4, 5] it is proposed to focus efforts on clarifying mechanisms of ECG changes in ventricular hypertrophy, that may potentially give additional information about the pathogenesis of the disease. From this point of view, ventricular gradient is an interesting parameter, which theoretically reflects the changes in myocardial electrophysiological properties, namely, the alteration in action potential duration heterogeneity in the ventricles. The decartographic “recovery acceleration map” provides a convenient three-dimensional graphic representation of this quantity, facilitating the analysis and comprehension of the received information. Right ventricular hypertrophy is an interesting object for the study, since the range of the load on the right ventricle is much wider than in the left ventricular hypertrophy. Further research of the mechanisms of ECG changes in right ventricular hypertrophy may contribute not only to the development of new criteria for the improved ECG detection of right ventricular pressure load, but also to the more accurate evaluation of state of the heart in such patients.

5. Conclusions

The use of decartographic parameters which describe cardiac repolarization in its relation to the preceding depolarization may be helpful, not only for detection of right ventricular overload in patients with PH, but also for the assessment of its severity.

References

[1] Hancock EW, Deal BJ, Mirvis DM, et al. AHA/ACCF/HRS recommendations for the standardization and interpretation of the electrocardiogram: part V: electrocardiogram changes associated with cardiac chamber hypertrophy: a scientific statement from the American Heart Association Electrocardiography and Arrhythmias Committee, Council on Clinical Cardiology; the American College of Cardiology Foundation; and the Heart Rhythm Society: endorsed by the International Society for Computerized Electrocardiology. *Circulation*, 2009; 119(10): e251-61.

[2] Henkens IR, Mouchaers KT, Vonk-Noordegraaf A, et al. Improved ECG detection of presence and severity of right ventricular pressure load validated with cardiac magnetic resonance imaging. *Am J Physiol Heart Circ Physiol*, 2008; 294(5): H2150-7.

[3] Henkens IR, Mouchaers KT, Vliegen HW, et al. Early changes in rat hearts with developing pulmonary arterial hypertension can be detected with three-dimensional electrocardiography. *Am J Physiol Heart Circ Physiol*, 2007; 293: H1300–H1307.

[4] Bacharova L, Estes H, Bang L, Mateasik A. The first statement of the Working Group on Electrocardiographic Diagnosis of Left Ventricular Hypertrophy. *J Electrocardiol*, 2010; 43(3): 197-199.

[5] Bacharova L, Estes EH, Bang LE, et al. Second statement of the working group on electrocardiographic diagnosis of left ventricular hypertrophy. *J Electrocardiol*, 2011; 44(5): 568-570.

CT ANGIOGRAPHY IDENTIFIES CORONARY VENOUS ANOMALY RESULTING IN SUCCESSFUL ABLATION OF AN EPICARDIAL ACCESSORY PATHWAY

[1]H. Roukoz; [1,2]C. W. Shepard [1,2]P. Dorostkar

[1]University of Minnesota, Cardiovascular Division,, Minneapolis, USA
[2]University of Minnesota, Pediatric Cardiology Division, Minneapolis, USA
Email: pcd@umn.edu

Abstract. *Venous anomalies of the coronary sinus can be associated with symptomatic epicardial postero-septal accessory pathways. We present a pediatric case where a Computed Tomography angiogram of the heart helped guide the ablation of a rare epicardial accessory pathway.*

Keywords: Fragmented QRS, Granulomatous Myocarditis, Cardiac Sarcoidosis, Cardiac Tuberculosis, Ventricular Tachycardia

1. Introduction

Difficult accessory pathways (AP) have been associated with Ebstein's anomaly, L-Transposition of the great Arteries, and especially with venous anomalies of the coronary sinus (CS). The latter are usually asymptomatic and can be difficult to visualize with conventional angiography during the ablation procedure of the AP. Surface electrocardiogram (ECG) features can suggest an epicardial pathway associated with such a CS anomaly. We present a pediatric patient where computerized tomography angiogram (CTA) helped with the ablation of a rare AP.

2. Methods

We report the case of a 10 year old boy with no prior cardiac history. He presented in January 2013 with frequent palpitations and was found to have Wolf-Parkinson-White (WPW) syndrome and documented supra-ventricular tachycardia. He had an ablation in 2008 but his palpitations recurred within days. During the first ablation attempt, the accessory pathway was targeted at the anterior wall of the proximal coronary sinus about 0.5 cm from the ostium. A follow-up surface ECG was suggestive of an epicardial postero-septal pathway (Fig. 1).

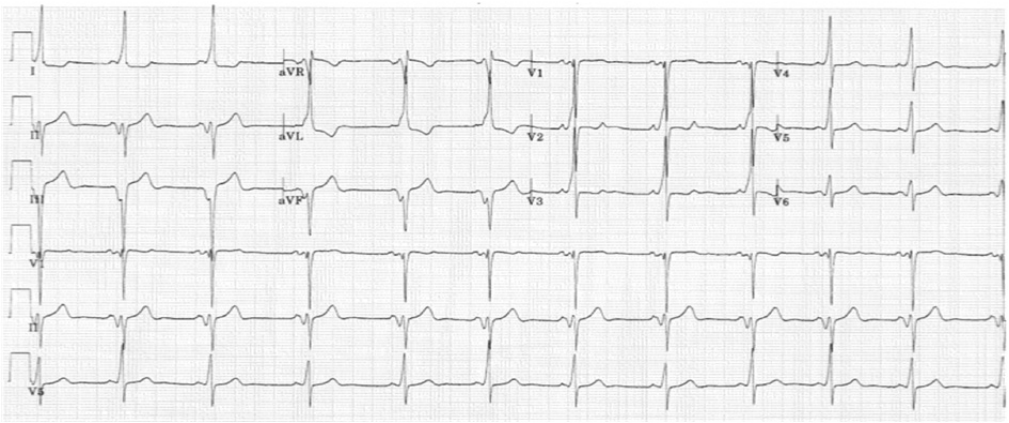

Fig. 1. Surface ECG of patient at presentation. The delta wave is iso-electric in V1 and negative in the inferior leads suggesting a postero-septal pathway. It is also steeply negative in lead II with no iso-electric line between the P wave and delta wave, positive in AVR with R≤S in lead V6, suggesting an epicardial pathway.

To further evaluate for suspected coronary sinus anomalies, a CTA was performed on a dual source Siemens SOMATOM Definition scanner using contrast enhancement according to previously reported protocols [1, 2]. Pediatric Flash modality was used with prospective ECG triggering, following dose reduction protocols (3). The CTA demonstrated diverticular dilation of the proximal segment of the middle cardiac vein (MCV) (Fig. 2). Whole volume CTA data was loaded into the 3D mapping system and utilized as a guide during the ablation. The patient underwent a repeat ablation procedure and the pathway was easily located at the proximal part of the dilated segment of the MCV and successfully ablated with the one application of radiofrequency energy (Fig. 3). There was no recurrence of the pathway at 7 month follow-up.

3. Discussion

This report presents the rare case of an epicardial AP associated with dilation of the proximal end of the MCV. The surface ECG suggested the presence of a postero-septal accessory pathway with findings of an isoelectric delta wave in V1 and a negative delta wave in the inferior leads [4]. The features suggesting that the AP was epicardial consisted of a steep negative delta wave in lead II with no iso-electric line between the P wave and delta wave, a positive delta wave in AVR and a deep S wave with R≤S in lead V6 [4, 5].

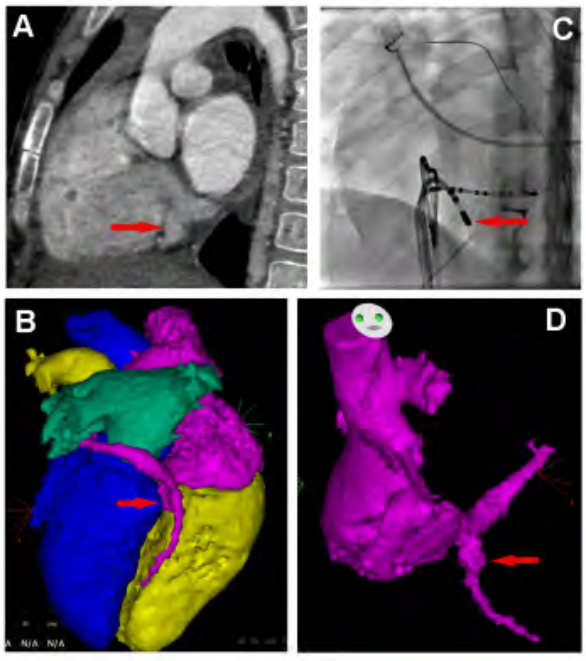

Fig. 2. Cardiac CTA with segmentation. The red arrow in all figures shows the diverticular dilation of the proximal MCV. **(A)** Sagittal view of the heart. **(B)** Segmentation of the cardiac CTA using the Carto 3 mapping system. The heart is shown in a posterior inferior view. The right atrium and coronary venous system are presented in purple, the right ventricle and pulmonary artery in yellow, the left atrium in green and the left ventricle and aorta in blue. **(C)** Left anterior oblique fluoroscopic view of the intracardiac catheters with the ablation catheter at the proximal portion of the CS diverticulum (successful site of ablation). **(D)** The segmented right atrium and coronary venous system shown alone. CTA = computed tomogram angiography; MCV = middle cardiac vein.

Epicardial postero-septal pathways consist of CS to left ventricle muscular extensions. They constitute less than 20% of postero-septal pathways. A diverticulum is present in 21% of cases within the proximal 1.5 cm of the CS [6]. When present, the pathway is usually located at the mouth of the diverticulum.

A conventional CS angiogram during the procedure can be difficult or unclear. An ECG gated CTA of the heart can help diagnose and localize CS anomaly with high definition. The CTA can be segmented and merged with the 3D mapping system as was done in this case. The hybrid map can then facilitate the localization and ablation of the accessory pathway by targeting the proximal end of the ectatic venous segment.

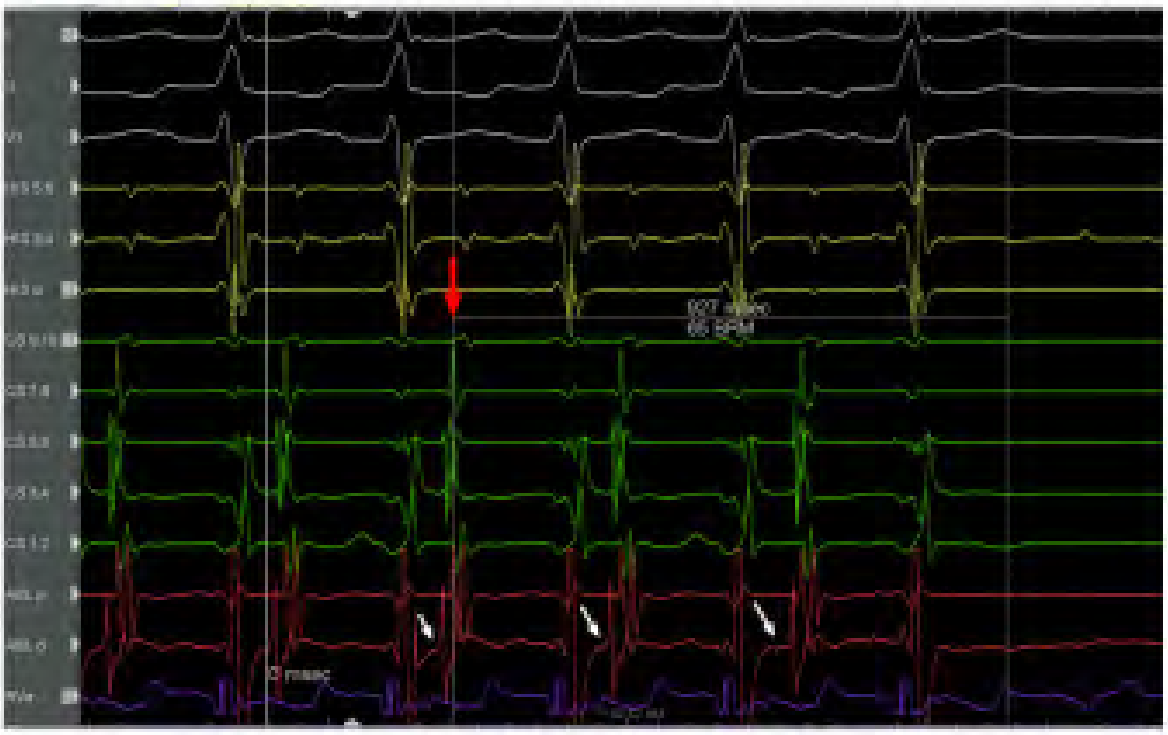

Fig. 3. Successful ablation of the accessory pathway. The ablation catheter was placed on the mouth of the middle cardiac vein diverticulum during tachycardia. Note a sharp potential between the local ventricular and atrial electrograms (white arrows) suggesting accessory pathway potential. The tachycardia was terminated less than one second after the start of radiofrequency ablation (red arrow). ABL = ablation catheter recording (p=proximal and d=distal); CS = coronary sinus (CS 1, 2 is the distal CS recording, CS 9, 10 is the proximal CS recording); HIS = His recording; RVa = right ventricular apex recording.

4. Conclusions

CTA of the heart can be used as an adjunct for planning and guiding the ablation of the substrate(s) that support tachycardia in patients with congenital heart anomalies.

References

[1] Siripornpitak S, Pornkul R, Khowsathit P, Layangool T, Promphan W, Pongpanich B. Cardiac CT angiography in children with congenital heart disease. *Eur J Radiol*, 2013; 82: 1067.

[2] Kim JE, Newman B. Evaluation of a radiation dose reduction strategy for pediatric chest CT. *Am J Roentgenol*, 2010; 194: 1188.

[3] Goske MJ, Applegate KE, Boylan J, et al. The 'Image Gently' campaign: increasing CT radiation dose awareness through a national education and awareness program. *Pediatr Radiol*, 2008; 38: 265**.**

[4] Arruda MS, McClelland JH, Wang X, et al. Development and validation of an ECG algorithm for identifying accessory pathway ablation site in Wolff-Parkinson-White syndrome. *J Cardiovasc Electrophysiol*, 1998; 9: 2.

[5] Takahashi A, Shah DC, Jais P, Hocini M, Clementy J, Haissaguerre M. Specific electrocardiographic features of manifest coronary vein posteroseptal accessory pathways. *J Cardiovasc Electrophysiol*, 1998; 9: 1015.
[6] Sun Y, Arruda M, Otomo K, et al. Coronary sinus-ventricular accessory connections producing posteroseptal and left posterior accessory pathways: incidence and electrophysiological identification. *Circulation*, 2002; 106: 1362.

COMPARISON OF RR-INTERVALS IN RABBIT HEART *IN-VIVO*, *EX-VIVO*, AND UNDER ISCHEMIA

[1,2]O. Janoušek, [1,2]M. Ronzhina, [1,2]J. Kolářová, [1,3]M. Nováková, [1]P. Scheer, [1,2]I. Provazník

[1]International Clinical Research Center - Center of Biomedical Engineering, St. Anne's University Hospital Brno, Brno, Czech Republic
[2]Brno University of Technology, Brno, Czech Republic
[3]Masaryk University, Brno, Czech Republic
Email: janouseko@feec.vutbr.cz

Abstract. *Changes of RR interval duration in the in-vivo heart are compared with those in a completely denervated heart and those in a denervated ischemic heart. Five New Zealand rabbits were included in the study. The in-vivo heart beats almost periodically, with RR interval close to 260 ms. Prolongation of RR interval to 350 ms caused by denervation of the heart is statistically significant ($\alpha = 0.05$), as well as subsequent prolongation to 680 ms caused by global ischemia. The heart rhythm remains periodic, even without the presence of the nervous system, until the global occlusion of perfusion.*

Keywords: In-vivo Heart, Ex-vivo Heart, Ischemia, Isolated Heart, Rabbit

1. Introduction

It is well known that the analysis of RR interval changes is one of the most frequently used non-invasive methods for assessing cardiac autonomic regulation [1]. Under physiological conditions, heart cycles are controlled by innervation from both sympathetic and parasympathetic branches of the autonomic nervous system [2]. The sympathetic system increases heart rate, whereas the parasympathetic system inhibits the pacemaker, and thus slows down the heart. The resulting sinus rhythm reflects balanced sympathetic and vagal states.

However, in the diseased heart this balance is impaired. Mechanisms of this impairment have not been completely clarified. Changes in the autonomic nervous system and several other mechanisms (i.e. release of adrenomedullary catecholamines, humoral factors including variation of the renin-angiotensin system, stretch-induced mechanical effect, etc. [3]) may influence heart rhythm.

The aim of this study was to compare changes of heart rhythm in denervated heart with those in denervated and simultaneously diseased heart. It focused on the probability distribution of RR interval duration. We believe that assessing global changes of RR interval, reflected by its probability distribution, is more informative and robust than assessing of individual arrhythmia occurrence.

2. Methods

In-vivo hearts

ECG signals from five New Zealand rabbits were included in the study. The signals were recorded using a SEIVA recording system. Body surface wire electrodes were attached to the skin with miniature clips. The location of electrodes did not restrict the posture of the animal in the sitting position. In order to get stable signals from conscious animals, they were placed

in a plastic box. The box was sufficiently high to prevent the rabbit from looking out, which could make the animal restless.

Isolated hearts

All experiments followed the guidelines for animal treatment approved by local authorities and conformed to EU law. Five New Zealand rabbits were included in the study. In deep i.m. anaesthesia with xylasin and ketamin, the hearts were excised and fixed on perfusion apparatus filled with Krebs-Henseleit (K-H) solution (1.25 mM Ca^{2+}, 37°C) and placed in a thermostatically-controlled bath. The isolated hearts were perfused according to Langendorff at constant perfusion pressure (85mmH) mode. The hearts were stabilized for 30 minutes. Then, each heart underwent a 15-minutes long episode of coronary artery occlusion, followed by a reperfusion period of the same duration. Global ischemia was achieved by a complete restraint of perfusion (s.-c. flow ischemia). The ECG signal was recorded using a method which involved no contact with the heart [4, 5]. Briefly, Ag-AgCl disc electrodes in three orthogonal directions x, y, and z were placed in the walls of the bath which is a part of the perfusion system. ECG signals were recorded by a data acquisition multifunction card PCI-6111E (National Instruments, USA) with sampling frequency fs=2000Hz. The signals were acquired by our own application designed in LabView 7.1 software (Texas Instrument, 2008). The 12-bit analogue to digital conversion was used. The digital signal was stored on a hard disk for off-line processing.

Data processing and statistical analysis

ECG signals degraded by noise were excluded from further processing. R-peaks were detected automatically by our own R-wave detector designed in Matlab R2006a (MathWorks, 2006). The results of automatic analysis were reviewed and any errors in detection were corrected manually. RR interval parameters were computed from the RR series histogram.

Four parameters of the histogram were analysed: (1) Median of histogram represents a typical value of RR interval; (2) Triangular interpolation of RR intervals (TINN) represents range of variability; which has been evaluated by the baseline width of the RR histogram evaluated through triangular interpolation [1]; (3) Kurtosis represents sharpness of the RR intervals distribution; (4) Skewness reveals the ratio between the number of short and long RR intervals.

The Wilcoxon signed rank test has been used for distinguishing statistically significant ($\alpha = 0.05$) differences between consecutive phases of experiment. Only the relevant phases (*in-vivo* vs. *ex-vivo*; *ex-vivo* vs. ischemia; ischemia vs. reperfusion) of the experiment were compared.

3. Results

The histogram and boxplot have been used for the comparison of RR-intervals of *in-vivo* and *ex-vivo* hearts and RR-intervals of the isolated hearts under normal and ischemic condition.

Representative histograms of RR intervals are shown in Fig. 1. All four consecutive phases of experiment are shown: *in-vivo* (Fig. 1A), *ex-vivo* (Fig. 1B), ischemia (Fig. 1C), and reperfusion (Fig. 1D) periods. Each histogram is shown at the same scale. Prolongation of RR interval after each phase of experiment is clearly visible. Beside prolongation of RR interval, the shape of histogram changes dramatically over consecutive parts of experiment.

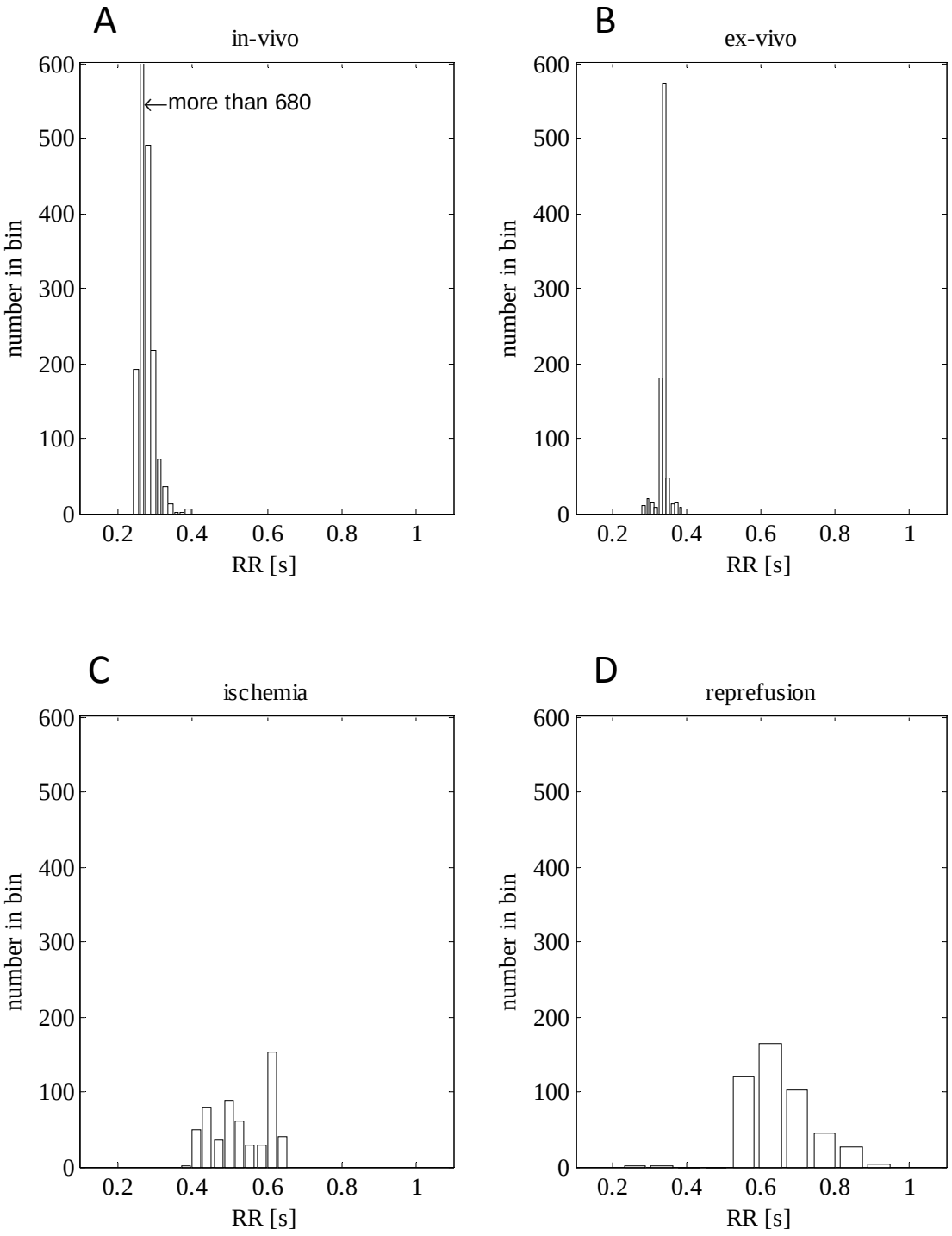

Fig 1. Histogram of RR intervals in A: *in-vivo* period; B: *ex-vivo* period; C: ischemia period; D: reperfusion period.

Boxplots of the medians of RR intervals in each phase of experiment are shown in Fig. 2A. *In-vivo* hearts beat almost periodically with RR interval close to 260 ms. Prolongation of RR interval to 350 ms caused by denervation of the heart is statistically significant ($\alpha = 0.05$), as well as subsequent prolongation to 680 ms caused by global stoppage of perfusion. There is no statistically significant change of RR interval caused by reperfusion, although median of RR interval decreases to 640 ms.

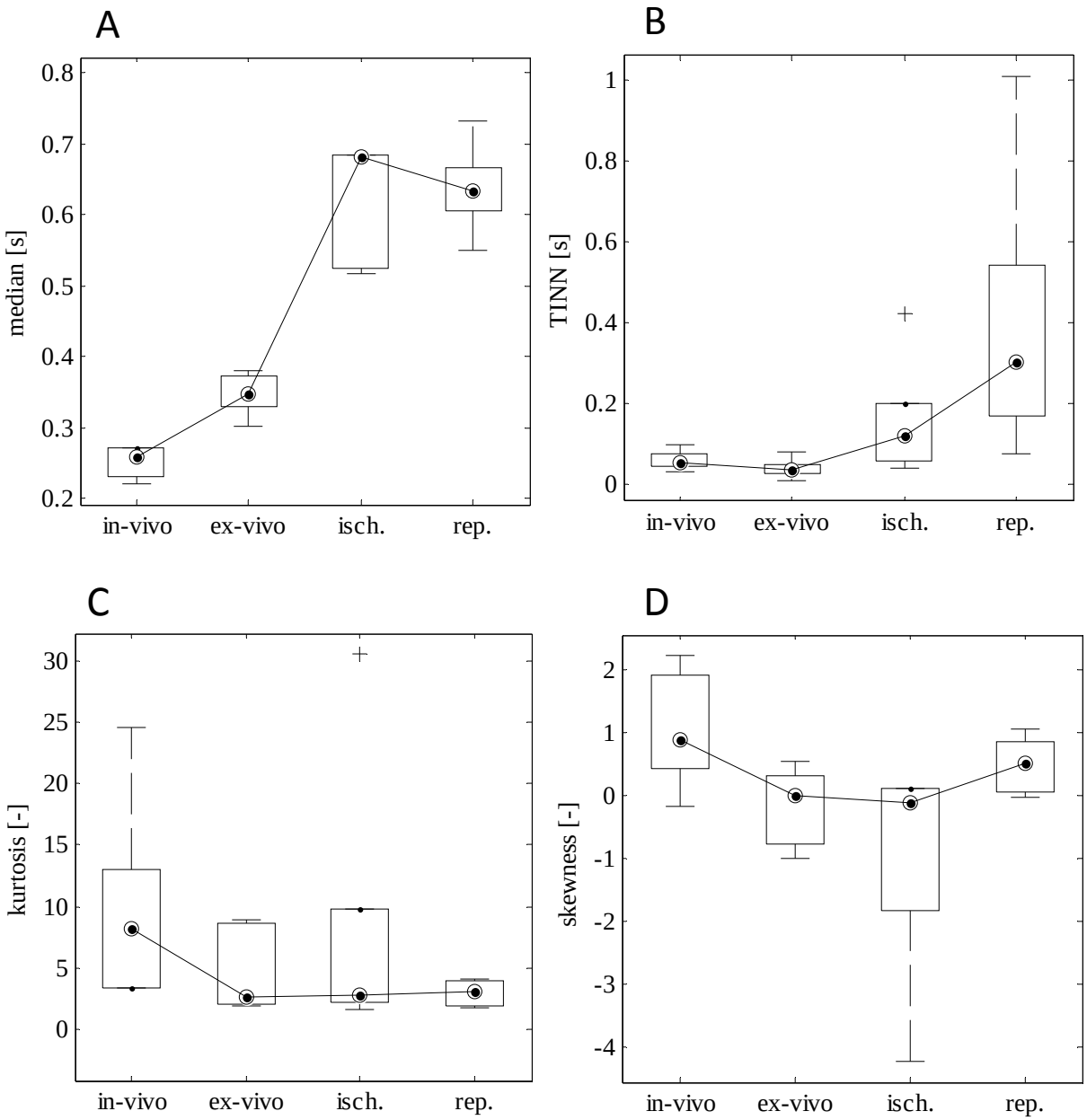

Fig 2. A: Median of RR intervals; B: TINN of RR intervals; C: Kurtosis of RR intervals; D: Skewness of RR intervals. Boxplots of TINN are presented in Fig. 2B. The low variability of RR intervals in in-vivo and ex-vivo hearts become substantial and statistically significant (α=0.05) in ischemic phase. Further broadening of RR interval range has been observed in the reperfusion period; however, this broadening is not statistically significant with regard to ischemic phase values.

Boxplots of kurtosis are presented in Fig. 2C. The highly leptokurtic shape of RR interval histograms in in-vivo hearts become to be slightly platykurtic in ex-vivo hearts and under the global ischemia. Mesokurtic shape of the RR interval histogram in reperfusion period is close to a Gaussian distribution. No changes of kurtosis are statistically significant.

Fig. 2D represents boxplots of histogram skewness. Positive skewness in in-vivo hearts reflected the obvious longer right tail of the histogram (see Fig. 1). This is in contrast with ex-vivo hearts behavior, where negative skewness has been observed. Negative skewness has

also been observed in the ischemic phase, and during subsequent reperfusion it again becomes positive. All changes of skewness were statistically insignificant.

Statistical significance of changes in histogram distribution is summarized in Table 1. Statistically significant changes are presented by their p-values; insignificant changes are presented by hyphen. Only subsequent pairs of experimental phases are depicted.

Table. 3 Statistical significance of histogram parameters

	in-vivo and *ex-vivo*	*ex-vivo* and ischemia	ischemia and reperfusion
median	$\alpha < 0.01$	$\alpha < 0.01$	-
TINN	-	$\alpha < 0.05$	-
kurtosis	-	-	-
skewness	-	-	-

4. Discussion

The aim of this study was to examine changes of RR intervals between the in-vivo and ex-vivo situation of a heart, and to examine the effect of global ischemia in isolated heart model.

Parameters of the RR interval histogram show that the heart in-vivo beats almost periodically, with a small variation, represented as low value of TINN. Periodicity of the in-vivo heart can be also deduced from the highly leptokurtic shape of histogram. Only a few exceptions from periodic rhythm have been observed, predominantly comprised of prolonged RR intervals.

Denervation of the heart, associated with extraction from the body, significantly prolongs RR intervals. Heart rhythm remains periodic, even without the presence of the nervous system. The range of variability slightly lowers in comparison with the in-vivo situation. It can be concluded that extraction of the heart does not influence heart rate variability. Denervation causes both shortening and prolongation of RR intervals with equal ratio.

Global occlusion of perfusion has a dramatic effect on heart rhythm. Duration of RR intervals increases by a factor of two in comparison with ex-vivo ones. Heart is beating non-periodically under global ischemia and RR interval variability rapidly increases. Arrhythmias caused by global ischemia are mainly represented by shorter RR intervals, which causes an imbalance of ratio between short and long RR intervals. The majority of shorter RR intervals under ischemia contrasts with its minority in in-vivo hearts.

Reperfusion shortens RR intervals, but not to the same extent of the ex-vivo intervals. Reperfusion therefore is not able to fully reinstate behavior of the heart before ischemia. A wide range of variability together with mesokurtic shape of histogram reveals that both intrinsic and extrinsic control mechanisms of the heart are weakened. Skewness of right-tailed histograms in the reperfusion period shows that there are more prolonged than shortened RR intervals . This imbalance corresponds with the in-vivo condition.

Acknowledgements

This work was supported by European Regional Development Fund - Project FNUSA-ICRC (No. CZ.1.05/1.1.00/02.0123), grant projects of the Grant Agency GACR 102/12/2034, and MUNI/A/0951/2012.

References

[1] Task Force of The European Society of Cardiology and The North American Society of Pacing and Electrophysiology. Heart Rate Variability, Standards of measurement, physiological interpretation and clinical use. *Europ Heart Journal*, 1996; 354-381.

[2] Berntson GG, Bigger JT Jr, Eckberg DL, Grossman P, Kaufmann PG, Malik M, Nagaraja HN, Porges SW, Saul JP, Stone PH, van der Molen MW. Heart rate variability: origins, methods, and interpretive caveats. *Psychophysiology* 1997; 34(6): 623-48.

[3] Bernardi L, Salvucci F, Suardi R, Soldá PL, Calciati A, Perlini S, Falcone C, Ricciardi L. Evidence for an intrinsic mechanism regulating heart rate variability in the transplanted and the intact heart during submaximal dynamic exercises. *Cardiovascular research* 1990; 24(12): 969-981.

[4] Nováková M, Moudr J, Bravený P. A modified perfusion system for pharmacological studies in isolated hearts. Analysis of Biomedical Signals and Images. *15th Biennial International Eurasip Conference Biosignal* 2000;162-164.

[5] Kolářová J, Fialová K, Janoušek O, Nováková M, Provazník I. Experimental methods for simultaneous measurement of action potentials and electrograms in isolated heart. *Physiol Res* 2010;59(S1):71-80.

ARRHYTHMIA TELEMONITORING IN ASYMPTOMATIC PATIENTS

T. Gegenava, M. Gegenava, Z. Kirtava

Tbilisi State Medical University Tbilisi, Georgia (Republic of)
Email: gegenavat@yahoo.com

Abstract. *Asymptomatic arrhythmias can be a challenge to diagnose. The goal of the present study was to assess asymptomatic episodes of arrhythmia with the help of mobile telemonitoring, which facilitates the continuous monitoring and recording of arrhythmias. We investigated 54 outpatients in Georgia (Republic of) with different types of arrhythmia, among which were patients with unexplained syncope, with epilepsy, asymptomatic patients who underwent radiofrequency catheter ablation, asymptomatic patients after aorto-coronary bypass graft surgery and healthy sportsmen. Investigations were made with a 3-lead electrocardiograph-ECG loop recorder in automatic recording/transmitting mode.* Cases *of sinus brady- and tachyarrhythmia, sick sinus syndrome, atrial fibrillation, supraventricular tachycardia, supraventricular premature complexes (SPCs) and ventricular premature complexes (VPCs) have been correctly recognized by automatic recognition software and recorded. Asymptomatic episodes were detected in the majority of cases with p=0.001. We concluded that mobile telecardiology is a useful tool to detect a relapse or symptomatic and asymptomatic episodes of life-threatening arrhythmia.*

Keywords: Asymptomatic Arrhythmias, Mobile Telemonitoring, Syncope

1. Introduction

The concept of telemedicine was introduced more than 30 years ago. However, the technology to enable its application has grown considerably in the past decade. Although, telemedicine could potentially affect all medical specialties, the greatest current applications are found in radiology, pathology, cardiology and medical education. The term telecardiology, in short refers to the utilization of telecommunication technology for cardiac disease diagnosis, treatment and patient care. The common telecardiologic devices include the ambulatory Holter monitor, event-triggered monitor, electrocardiographic-ECG telemeter monitor and loop event recorder etc.

Recently, continuous mobile cardiac outpatient telemetry has become available as an alternative to conventional ambulatory monitoring. It is a promising telecardiologic device which features continuous, real-time outpatient electrocardiographic monitoring for extended time periods and autodetects asymptomatic arrhythmias [1, 2].

Telecardiology enables a cardiologist at one site to diagnose patients, deliver health care, provide therapy, or consult with another physician or paramedical personnel at a remote site. Perhaps the greatest impact of telemedicine may be in fulfilling its promise to improve the quality, increase the efficiency, and expand the access of the healthcare delivery system to the rural population and developing countries. Now wireless cellular systems will offer video telephony that can facilitate the transfer of real-time images, such as ECG reports strips or echocardiograms, to help with communications between a patient or a caregiver and a health-care professional.

It is superior for detecting suspected myocardial ischemic events or transient arrhythmic episodes, i.e. tachycardia, fibrillation or flutter, which are difficult to determine with routine ECG or ambulatory 24-hour monitoring [3, 4].

Many studies with telecardiology have been employed on coronary heart disease, heart failure and syncope where the cause is unknown. The majority has been documented and contrasted with common follow-up methodology, such as ECG and ambulatory 24-hour ECG monitoring. Furthermore, telecardiology is suitable for some special cohorts, such as elderly and pediatric patients who find it inconvenient or are reluctant to visit a physician. But its more promising aspect lies in the diagnosis of specific arrhythmias, for instance atrial fibrillation and syncope without an underlying cause or symptom.

A classical example demonstrating the impact of telemedicine on diagnosis is in the event recording of arrhythmias. Documentation of the event is a prerequisite for the subsequent diagnosis and therapy. Event recording also enables the correlation between the arrhythmia and the symptoms of the patient and allows the evaluation of the quantity and quality of clinically relevant arrhythmias. Finally, the documentation of the recording of the clinical arrhythmia allows the comparison with an artificially induced tachycardia by electrostimulation [5, 6].

In the field of ischemia related events, transient or nocturnal ischemias can be documented. The progress after coronary interventions (e.g. CABG, PTCA, stent, rotablation) can also be observed. In the research literature it has been shown that the cause of syncope with the aid of Holter ECG can be evaluated in only 10 % of patients. After complete non invasive examination, 50 % of syncope episodes remain unexplained. For out-of-hospital monitoring of cardiovascular patients, loop recorders and event recorders are available. Studies have shown that the use of event recorders which can directly transmit ECGs can reduce the time of admission to hospital for groups at risk, facilitate the diagnosis on an ambulant basis and reduce health costs.With regard to the new concept of Disease Management, telemedical devices for measuring ECG, blood pressure and blood glucose are useful tools in connection with a Service Center Concept for patient monitoring, patient compliance and memory function in cooperation with physicians and general practitioners [7].

Asymptomatic arrhythmias can be a challenge to diagnose. The goal of the present study was to assess asymptomatic episodes of arrhythmia with the help of mobile telemonitoring, which facilitates the continuous monitoring and recording of arrhythmias.

2. Methods

The Vitaphone Tele-ECG-Loop-Recorder weighs only 85 grams. It can be attached to a belt or strapped to the chest, and is able to record an ECG continuously under the conditions of normal everyday life. The intelligent software automatically detects pathological anomalies (supraventricular and ventricular tachycardias, bradycardias, pauses and atrial fibrillation). The memory of the Vitaphone Tele-ECG-Loop-Recorder is large enough for continuous recording of 40 minutes of a 3-channel ECG. The oldest ECG data are overwritten (using a loop function). When an ECG anomaly is automatically detected, the software immediately sends the ECG via a Bluetooth wireless connection to a Bluetooth-enabled mobile phone without the patient having to do anything. Bluetooth wireless transfer allows the recorder and mobile telephone to be positioned up to 50 meters apart. The mobile phone transmits the ECG digitally and completely automatically to the Tele-ECG system REMOS. If a mobile telephone is unavailable, data can be transmitted to the patient via a landline telephone by means of an integrated acoustic coupler. The post-hospital use of Remos ECG 100/300 BT significantly shortens in-patient hospitalizations for clinical cardiology diagnostics and treatment.

The employment of telecardiological functional diagnosis in pre- and post-hospital care opens new economic horizons: Therapy based on its data and findings can lead to tangible rewards in the long term.

During June-December, 2010, we investigated 54 outpatients with different types of arrhythmia (Male/Female=32/22, age range – 12-80 y); among them were 10 patients with concomitant epilepsy, 6 patients who had undergone radiofrequency catheter ablation, 4 patients following aorto-coronary bypass graft surgery and 10 patient with unexplained syncopes. The control group consisted of recording 7 clinically healthy athletes (all – male aged 15-17 y), during a 30 minute veloergometer stress-test. Investigations were made with a 3-lead ECG Loop Recorder (Vitaphone BT 3300, Vitasystems GmbH, Germany) in automatic recording/transmitting mode, using special LRMA software (MDT, Czech Republic) and Nokia6730 symbian phone. Patients' ECGs after automatic recording by loop recorder were transmitted by Bluetooth to phone and then by 3G communication (supported by partner mobile operator - MagtiCom Ltd.) to VitaSystems server in Germany and available to a Georgian physician via e-mail/Internet (time from recording – 30-70 seconds).

3. Results

Arrhythmias were registered/monitored during 7 to 68 hours of observation. The number of automatically recorded ECG events varied between 3 and 170 per observation or 0.4-10.7 hourly. Minor artifacts have been recorded, occurring mainly in the first minutes of recording (in <4%) or during vigorous physical exercise (around 12%, largely - in the control sportsmen group).

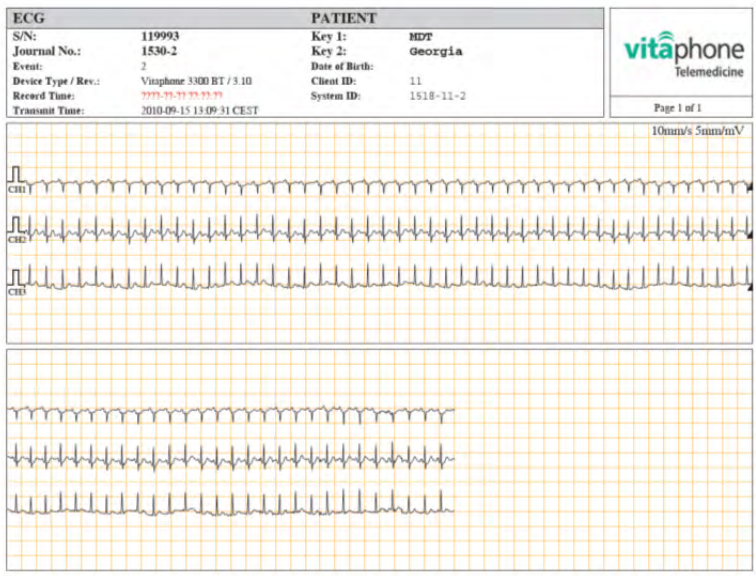

Fig. 1. 53 year old woman with palpitations. 24h Holter monitoring was performed twice, without diagnosis. We discovered paroxysmal supraventricular tachycardia after 48h of investigation

Cases of sinus brady- and tachyarrhythmia, sick sinus syndrome, atrial fibrillation (AF), supraventricular tachycardia (SVT) - (Fig-1), supraventricular premature complexes (SPC) and ventricular premature complexes (VPCs) have been correctly recognized by automatic recognition software and recorded.

Arrhythmias were registered during 7-68 hours of observation. 52% of arrhythmia episodes were asymptomatic. Arrhythmia relapse was detected in n=3 (from n=6) patients who

underwent radiofrequency catheter ablation (SVT, SVPCs) - (Fig 2), but mostly they were asymptomatic. Asymptomatic episodes of ventricular premature complexes (Fig.3) were detected in patients who underwent aorto-coronary bypass graft surgery.

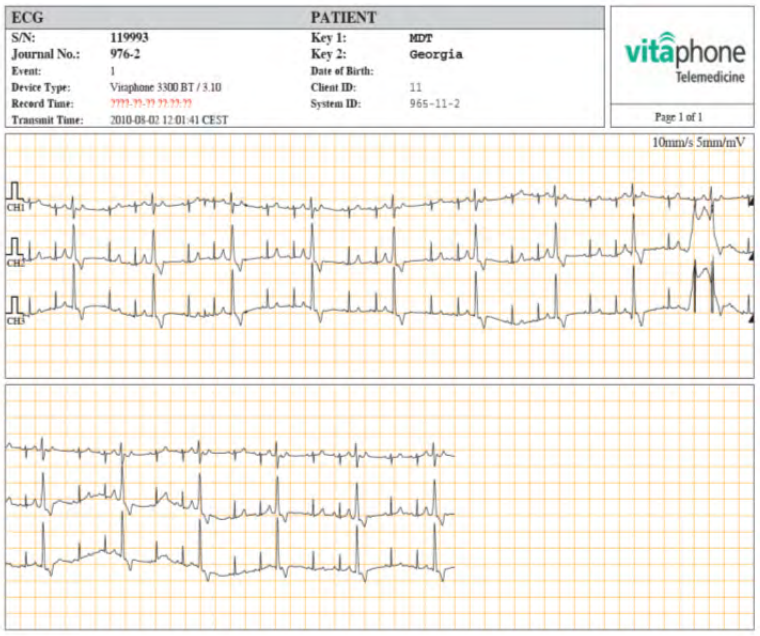

Fig. 2. 39 year old woman (asymptomatic). She was diagnosed with atrial tachycardia and had a radiofrequency catheter ablation procedure 1 year before .We have discovered 2 episodes of supraventricular tachyarrhythmia.

From n= 10 patients with epilepsy we discovered n=3 patients with supraventricular tachycardia (SVT) and n=2 patients with sinus tachycardia. Among n=10 patients with unexplained syncope,we revealed n=2 patients with sinus tachycardia, n=2 patients with SVT and n=1 patient with sick-sinus syndrome.

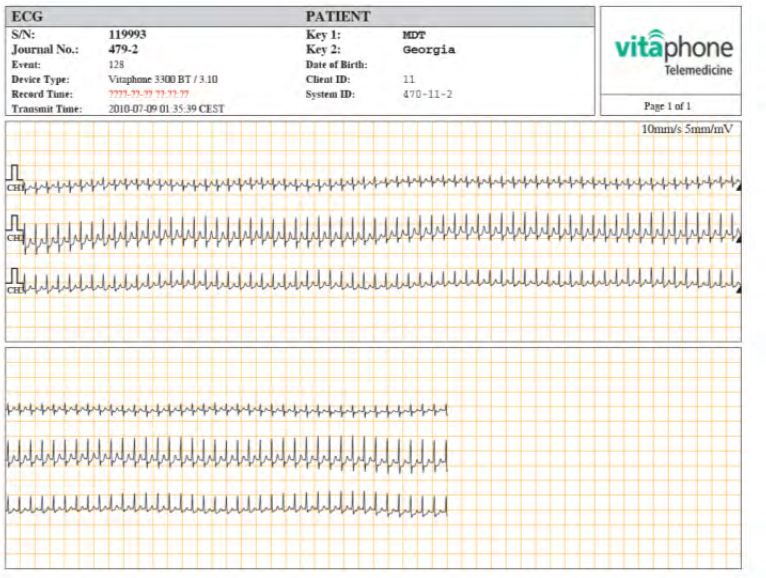

Fig. 3. 67 year old woman, with the diagnosis of nodular hyperthyroidism. Ventricular trigeminy **was noted.**

Asymptomatic episodes of supraventricular tachycardia were detected in n=1 sportsmen. Asymptomatic episodes were detected in the majority of cases with p=0.001. No differences were revealed relating to gender.

4. Discussion

Telemonitoring of arrhythmias on an ambulant basis seems to be cost effective and a promising concept for homecare and rehabilitation. Telemonitoring on wards has been shown to enhance the mobility of patients who need to be supervised during an in-hospital stay. Telemedical arrhythmia monitoring allows the patient to move freely on the ward. The advantages for physicians and medical staff is the combined monitoring of different patients, an alarm management for different parameters (heart rate, blood pressure, respiration and oxygen saturation), online-diagnostics of arrhythmias and post procedural supervision. Mobile telecardiology represents a feasible methodology to monitor arrhythmia, especially asymptomatic episodes of arrhythmia, outpatients in Georgia, promoting earlier discharge of non-life-threatening cases, improving patients' comfort of life and increasing their mobility with enhanced safety. mHealth might also represent significant cost-saving for insurance companies (ongoing study). Finally, in remote areas patients monitoring by mHealth methodology will improve quality of care by the timely provision of a second opinion in cases, when local expertise is not always sufficient.

References

[1] Kirtava Z, Gegenava T. Gegenava M. Mobile Telemonitoring of Arrhythmias in Outpatients in the Republic of Georgia. *Journal of Telemedicine and e-Health* 2012; 18: 7.

[2] Khoor S, Nieberl J, Fugedi K, Kail E. Telemedicine ECG Telemetry with Bluetooth Tecnology. *Computers in Cardiology*, 2001; 28: 585-588.

[3] Molinari G, Valbusa A, Terrizzano M et al. Nine years' experience of telecardiology in primary care. *J Telemed Telecare* 2004; 10: 249-253.

[4] Joshi AK, Kowey PR, Prystowsky EN et al. First experience with a Mobile Cardiac OutpatientTelemetry (MCOT) system for the diagnosis and management of cardiac arrhythmia. *Am J Cardiol*, 2005; 95: 878-881.

[5] Dowie R, Mistry H, Young TA et al. Telemedicine in pediatric and perinatal cardiology: economic evaluation of a service in English hospitals. *Int J Technol Assess Health Care*, 2007; 23: 116-125.

[6] Tually P, Janssen J, Cowell S, Walker J. A preliminary assessment of Internet-based nuclear telecardiology to support the clinical management of cardiac disease in a remote community. *J Telemed Telecare*, 2003; 9 Suppl 1: S69-71.

[7] Vassilikos VP, Vogas V, Giannakoulas G, Mantziari L, Lekka I, Dimitrakopoulos K, Paraskevaidis S, Konias S, Maglavelas N, Chouvarda I, Styliadis H, Styliadis IH. The Use of Transtelephonic Loop Recorders for the Assessment of Symptoms and Arrhythmia Recurrence after Radiofrequency Catheter Ablation. *Telemedicine and e-Health*, 2010; 16 (7): 792-798. doi:10.1089/tmj.2010.0018.

GENDER DIFFERENCES OF HEART RATE VARIABILITY BETWEEN TAIWANESE SYMPTOMATIC MITRAL VALVE PROLAPSE SYNDROME AND NORMAL

[1]Y.C. Chen, [1]C.H. Shu, [2]L.W. Tsai, [3]I.F. Yang, [4]C.K. Tseng, [1, 2]T.F. Yang

[1]National Chiao Tung University, Hsin Chu, Taiwan
[2] Taipei Medical University Hospital, Taipei, Taiwan
[4] China Medical University Hospital, Taichung, Taiwan
[3]Jen Chi General Hospital, Taipei, Taiwan
Email: tfy@tmu.edu.tw

Abstract. *Short Term (5-15 min) Heart rate variability (HRV) can provide non-invasive evaluation of the autonomic nervous system (ANS). The purpose of this study is to evaluate the gender effect and influence of postural changes in symptomatic Mitral Valve Prolapse Syndrome (MVPS) patients and normal subjects. A total of 118 MVPS patients and 148 healthy students were recruited. A HRV system with modified lead II ECG was used. Subjects were asked to rest 5 minutes before recording HRV in a lying, sitting and standing posture. Paired Student t test was used to characterize changes in HRV variables. Normal and symptomatic MVPS can be differentiated by Time domain's SDNN and Frequency domain's Total Power. In Frequency domain all parameters were shown to have significant differences except in the lying position. Although time domain parameters may not be beneficial for the evaluation of MVPS, frequency domain with postural changes could be a useful tool.*

Keywords: Heart rate variability, Mitral Valve Prolapse Syndrome, posture change, normal, ECG.

1. Introduction

Heart rate variability (HRV) is the temporal variation between sequences of consecutive heartbeats. On a standard electrocardiogram (ECG), the duration between two adjacent R wave peaks is termed the R-R interval. The resulting period between adjacent QRS complexes resulting from sinus node depolarization is termed the N-N (normal-normal) interval, and HRV is the measurement of the variability between the N-N intervals [1-6]. The last two decades have witnessed the recognition of a significant relationship between the autonomic nervous system and cardiovascular mortality, including sudden cardiac death [4-7]. HRV investigation has its use in the prediction of long-term survival in patients who have suffered from congested myocardial infarction, or had valvular or congenital heart disease [5-7]. Depressed HRV is a predictor of mortality [4-6]. In addition, arrhythmic complications independent of other recognized risk factors. HRV assessed from short-term recordings may be used for initial screening of all survivors of an acute myocardial infarction [5, 6, 8, 18]. The purpose of this study is to evaluate the gender and postural effects in HRV parameters between symptomatic Mitral Valve Prolapse Syndrome (MVPS) patients and an apparently healthy population.

2. Methods

Materials

A total of 118 patients, 7 males and 111 females, who had been echocardiographically diagnosed as having MVPS at Taipei Medical University Hospital cardiology clinic from November 2008 to January 2012, and 148 healthy students, 54 males and 94 females with a

normal 12-lead ECG with no previous history of medical disease from the College of Biological Science and Technology of National Chiao-Tung University were recruited for the study. All subjects had given informed consent and agreed to take part in the research.

Methods of HRV Recording

A locally developed Taiwanese machine (Daily Care BioMedical ReadMyHeart) was used to record the HRV. One ECG lead (modified lead Ⅱ) was used for signal collection and analysis. The QRS complexes were detected and labelled automatically. The results of the automatic analysis were reviewed subsequently, and any errors in R-wave detection and QRS labelling were then edited manually. The subjects were asked to rest 5 minutes before each HRV recording (lying, sitting and standing) (Fig. 1) All the recordings were taken during the day (between 9:00 AM to 4:00 PM) to avoid any difference due to the diurnal influence of the autonomic nervous system [9-17].

Analysis of HRV

HRV was assessed automatically from the calculation of the mean R-R interval and its standard deviation measured on short-term 5 minute ECG recordings. Normal-to-normal R-R interval data obtained from the edited time sequence of R-wave and QRS labelling were then transferred to a personal computer. For time-domain HRV measures, the mean normal-to normal R-R intervals (NN) and the standard deviation of normal-to normal R-R intervals during 5 minutes (SDNN) were then calculated [7]. For frequency-domain HRV parameters analysis, spectral power was quantified by fast Fourier transformation and autoregressive method for the following frequency bands: 0.15-0.4 Hz (high frequency), 0.04-0.15 Hz (low frequency). Time domain parameters used were SDNN, RMSSD and NN50. Frequency domain parameters selected were LF, HF and LF/HF (Fig. 2). These parameters were defined in accordance with the 1996 ACC/AHA/ESC consensus [7].

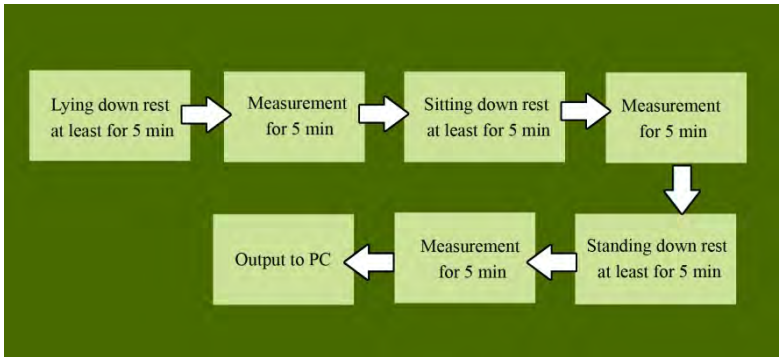

Fig. 1. Steps of the HRV experiment.

Statistical Analysis

To make sure our data has a normal distribution, the Kolmogorov–Smirnov test was used at first. Then the Paired Student t test was used to characterize differences in HRV variables. All HRV variables were expressed as mean ± SD. All statistical analyses were performed using Microsoft Excel 2007. A P value <0.05 was determined as statistically significant.

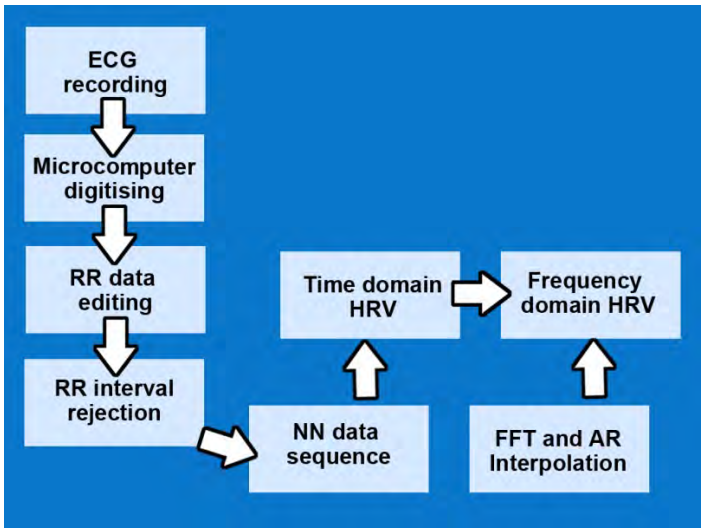

Fig. 2. . Steps of data analysis.

Table. 1. Age and Gender distribution between 118 Symptomatic MVP and 148 Normal Group

	Symptomatic MVPS Average Age(years)		Normal Average Age(years)
Male (7)	39±7	Male (54)	28±4
Female (111)	42±13	Female (94)	26±6

Table. 2. Time domain HRV Parameters between Symptomatic MVP and Normal Group

HRV parameters	Posture	Symptomatic MVP (n=118)	Normal Group (n=148)	P value
SDNN(ms)	Lying	42.43 ± 37.75	51.06 ±33.75	0.03
	Sitting	36.67 ±17.35	50.67 ± 22.15	<0.01
	Standing	32.27 ±16.74	36.56 ±14.61	0.03
RMSSD(ms)	Lying	41.20 ± 50.84	46.84 ±43.83	NS
	Sitting	28.84 ±16.12	35.09 ±15.95	0.005
	Standing	20.62 ±16.26	18.70 ± 9.55	NS
NN50	Lying	37.36 ± 53.89	60.24±57.75	<0.01
	Sitting	34.65 ±48.14	51.64 ±45.14	<0.01
	Standing	11.49±22.37	10.79 ±18.54	NS

Table. 3.Frequency domain HRV Parameters between Symptomatic MVP and Normal Group.

HRV parameters	Posture	Symptomatic MVP (n=118)	Normal Group (n=148)	P value
FFT				
TP	Lying	1213.50 ±719.13	1707.00 ± 241.83	<0.01
	Sitting	1379.50 ±1590.28	965.00 ±958.84	<0.01
	Standing	980.00 ±107.48	619.50 ±251.02	<0.01
HF(nu)	Lying	55.53 ± 15.90	53.96±16.11	NS
	Sitting	49.24 ±17.89	41.76 ±18.53	<0.01
	Standing	37.09 ±18.29	26.37 ±15.12	<0.01
LF(nu)	Lying	44.46 ± 15.90	45.95±16.11	NS
	Sitting	49.87 ±18.03	57.69 ±18.66	<0.01
	Standing	62.90 ±18.30	73.63 ±15.12	<0.01
LF/HF	Lying	1.03 ± 0.89	1.10 ±1.00	NS
	Sitting	1.34 ±1.08	2.00 ±1.89	<0.01
	Standing	2.97 ±4.19	4.45 ±3.55	<0.01
AR				
TP	Lying	1306.00 ± 650.54	1783.50 ± 256.68	<0.01
	Sitting	1400.00 ±1596.65	1121.00 ±1166.73	<0.01
	Standing	1344.50 ±581.95	627.50 ±252.44	0.04
HF(nu)	Lying	55.43 ± 15.99	53.91 ±16.32	NS
	Sitting	49.17 ±17.90	43.36 ±19.02	0.02
	Standing	37.02 ±18.33	26.41 ±15.94	<0.01
LF(nu)	Lying	44.56 ±15.98	46.08 ±16.33	NS
	Sitting	50.08 ±17.93	57.22 ±18.55	<0.01
	Standing	62.99 ±18.39	73.81 ±15.35	<0.01
LF/HF	Lying	1.04 ±0.90	1.11 ±0.99	NS
	Sitting	1.42 ±1.16	2.06 ±2.02	<0.01
	Standing	2.89 ±3.75	4.56 ±4.10	<0.01

3. Results

In time domain analysis, only SDNN between MVPS and the Normal group was statistically significantly different in all positions, and as in the frequency domain Total Power. In

frequency domain analysis, with the exception of the lying posture, all parameters were shown to have significant differences particularly in the sitting position. There were statistically significant differences of RMSSD and NN50 in the lying posture both in MVPS and Normal groups between the male and female gender in the time domain. In the frequency domain, all parameters were statistically significantly different in all postures both in MVPS and normal with Total Power as an exception.

4. Conclusions

The SDNN is compatible with Total Power as demonstrated in the previous reports. Gender specific HRV variation had been reported in our previous study in normal Taiwanese. It is further strengthened the digenetic criteria for HRV should be gender specific in MVPS as well. Moreover, more male MVPS cases should be recruited for further clarification of this issue.

Although time domain parameters might not be of use for the evaluation MVPS, frequency domain with postural changes might be a useful tool in MVPS diagnosis risk stratification.

References

[1] Kleiger RE, Miller JP, Bigger JT, Moss JA, and the Multicenter Post-infarction Research Group. Decreased heart rate variability and its association with increased mortality infarction. *Am J Cardiol*, 1987; 59:256-262.

[2] Kleiger RE, Bigger JT, Bosner MS, Chung MK, Cook JR, Rolnitzky LM, Steinman R, Fleiss JL. Stability over time variables measuring heart rate variability in normal subjects. *Am J Cardiol* 1991; 68: 626-630.

[3] McSayers BA: Analysis of heart rate variability. *Ergonom*, 1973; 16: 85-97.

[4] Malliani A, Pagani M, Lombardi F and Cerutti S: Cardiovascular neural regulation explored in the frequency domain, *Circulation*, 1991; 84: 482-492.

[5] Moser M, Lehofer M, Sedminek A, Lux M, Zapotoczky H-G, Kenner T and Noordergraaf A. Heart rate variability as a prognostic tool in cardiology, *Circulation*, 1994; 90: 1078-1082.

[6] Cavalcanti S, Chiari L, Severi S, Avanzolini G, Enzmann G, Lamberti C: Parametric analysis of heart rate variability during hemodialysis. *International Journal of Bio-Medical Computing*, 1996; 42(3): 215-24.

[7] Task Force of the European Society of Cardiology and the North American Society of Pacing and Electrophysiology. Heart rate variability. Standards of measurement, physiological interpretation, and clinical use. *Eur Heart J.* 1996; 17: 354-81.

[8] Login E, Schaible T, Lenz T, Konig S. Short term heart rate variability in healthy neonates: normative data and physiological observations. *Early Hum Dev*, 2005; 81: 663-71.

[9] Tsai LW, Yang IF, Chen MN, Yang TF. A preliminary study of short term HRV analysis of a MVPs Population. International Congress on Electrocardiology (ICE), 2008. St. Petersburg, Russia. (Abstract).

[10] Yang IF, Tsai LW, Yang TF. Comparison between angiotensin converting enzyme inhibitor and angiotensin receptor blocker on cardiovascular tolerance after hemodialysis: Heart Rate Variability and QT Interval analysis. *International Congress on Electrocardiology (ICE)*, 2008. St. Petersburg, Russia. (Abstract).

[11] Chen Y, Yang IF, Yang TF. Frequency Domain Heart Rate Variability parameters are

sex dependent in an apparently healthy Taiwanese Population in Conference Proceedings of *Asian Pacific Congress of Cardiology (APCC),* S96, 2009.

[12] Chen Y, Chen YS, Lu CC, Tsai MJ, Chang CS, Yang IF, Yang TF. Postural changes influences on Heart Rate Variability in an apparently healthy population. *International Congress on Electrocardiology*, 2010. Lund, Sweden (Abstract).

[13] Yang IF, Yang TF. Use of short-term heart interval variability in evaluation of angiotensin receptor blocker on cardiac autonomic modulation post hemodialysis. *17th Asian Pacific Congress of Cardiology Kyoto, Japan*, 2009, May 20-23. *CVD Prevention and Control*, Vol.4 (sup.1), P101, May 2009.

[14] Tsai LW, Yang IF, Yang TF. An evaluation of heart rate variability between MVP and a normal Taiwanese population. 17th Asian Pacific Congress of Cardiology Kyoto, Japan, 2009, May 20-23, S104. *CVD Prevention and Control* Vol. 4 (Suppl.1):S104.

[15] Chen Y, Yang IF, Yang TF. Frequency Domain Heart Rate Variability parameters are sex dependent in an apparently healthy Taiwanese population. 17th Asian Pacific Congress of Cardiology Kyoto, Japan, 2009, May 20-23. *CVD Prevention and Control* Vol.4 (suppl.1) P102, May 2009.

[16] Chen YS, Chang CS, Lu CC, Tsai MJ, Chen Y, Yang IF, Yang TF. Standard 12-lead electrocardiogram in Taiwanese Mitral Valve Prolapse patients and normal healthy controls. *The 37th International Congress on Electrocardiology (ICE)*. Lund, Sweden. June 3-5, 2010.P32, p104. *Journal of Electrocardiology Vol. 44*, Issue 2, Pages e44-e45.

[17] Chen Y, Chang CS, Lu CC, Tsai MJ, Chen YS, Yang IF, Yang TF. Postural changes influences on Heart Rate Variability in an apparently healthy Taiwanese population. *The 37th International Congress on Electrocardiology (ICE).* 2010. P31, p103. *Journal of Electrocardiology,* 2011; 44: 2: e42-e44.

[18] Xhyheri B, Manfrini O, Mazzolini M. Heart Rate Variability today. *Progress in Cardiovascular Diseases,* 2012; 55: 321-331.

LINEAR – NONLINEAR HEART RATE VARIABILITY ANALYSIS AND SVM BASED CLASSIFICATION OF NORMAL AND HYPERTENSIVE SUBJECTS

[1]M. G. Poddar, [1]V. Kumar, [2]Y. P. Sharma

[1]Indian Institute of Technology, Roorkee, India,
[2]Post Graduate Institute of Medical Education and Research, Chandigarh, India
Email: mohangpoddar@gmail.com

Abstract. *Recent study has shown, one of the major causes of mortality is hypertension which can affect the whole body or damage organs even before diagnosis. Heart rate variability (HRV) analysis provides the best non-invasive diagnostic tool to detect hypertensive (HTN) subjects when compared with normal (NOR) subjects. The goal of this study is to analyze and compare HRV ontology of NOR and HTN subjects using time domain (TD), frequency domain (FD) and nonlinear methods. Thereafter, all features are classified using a support vector machine (SVM). For short term HRV analysis, a five minutes duration electrocardiogram (ECG) of 57 NOR and 56 HTN subjects was recorded. Most TD features of HTN have more reduced values over NOR subjects. FD features, like power in different spectral bands also have distinguishable decreased values whereas sympathovagal balance has a clearer edge in HTN than NOR as it is the ratio of low frequency to high frequency and non linear parameters of Poincare plot. Approximate entropy (APEN), sample entropy (SAMPEN) too have higher values in NOR in comparison with HTN. SVM based binary system classifies these two groups with 100 percent accuracy and 100 percent sensitivity when all TD, FD and non linear features are used together rather than individual classification hence, it may work as a better predictor for all causes of mortality in patients with HTN.*

Keywords: RR Tachogram, Heart Rate Variability, Normal, Hypertension, Time Domain, Frequency Domain, Nonlinear, Support Vector Machine Classifier

1. Introduction

Hypertension is the condition in which blood pressure (BP) in the arteries is consistently elevated, hence also called high blood pressure, generally exceeding 140/90 mm Hg. Since it can have no symptoms for many years or even decades, high BP is a silent killer as it damages critical organs of the human body. Recent studies in the literature [1, 2] indicate that HTN is one of the major causes of mortality in the elderly and the stressed middle aged. Heredity, stress, exercise, obesity, ethnicity alcohol intake, and smoking are the major causes of HTN. In recent years, HRV analysis has been considered as a popular non-invasive diagnostic tool in cardiology to assess the behaviour of the autonomic nervous system. HRV is the subsequent RR interval variation of the electrocardiogram (ECG) in a particular duration which maintains sympathovagal balance by correlating sympathetic and parasympathetic activities. HRV analysis has been used for many years to measure ANS activities due to its simplicity, accuracy, and noninvasive application. Though it is widely discussed in the standard literatures a value for HRV normal range in the healthy population has still not been identified [3], since, there are lots of influencing factors which affect the normal RR interval significantly such as age, gender, race, region, diet, habits etc. Earlier research studies reported comparison of HRV analysis of normal subjects considering different age groups and gender as well as comparison of HRV analysis of normal subjects with respect to subjects suffering from particular diseases by time domain and frequency domain methods. In the present study, the comparison of HRV analysis of normal and HTN

subjects is carried out using features derived from time domain, frequency domain and nonlinear methods. Sensitivity analysis is carried out for feature selection to determine the most discriminatory features between normal and HTN groups. It is observed that combined features such as variance of RR interval (Variance), Standard Deviation of Normal to Normal RR intervals (SDNN), Root Mean Square of Successive Difference of RR intervals (RMSSD), Percentage of number of adjacent RR intervals having more than 50msec (pNN50) of time domain, power in very low frequency (P-VLF) in ms2, power in low frequency (P-LF) in ms2, power in high frequency (P-HF) in ms2, power in total frequency range (P-Total) in ms2, LF/HF of frequency domain by Fast Fourier Transform (FFT) analysis, standard deviations SD1, SD2 (Poincare plot), coefficient of APEN and coefficient of SAMPEN of non linear method features provide maximum class separability, these selected features are used to design the binary support vector machine (SVM) classifier.

2. Methods

In the present work, an electrocardiogram (ECG) of Lead –II was recorded using a sixteen channel BIOPAC^{TM} MP 150 system in cooperation with AcqKnowledge 4.0 software using 500 Hz sampling frequency and its ECG amplifier module 100C. The module was kept in its normal mode with amplifier's gain at 1000 and the channel to be used was calibrated prior to recording. An approximately seven minutes duration of data was recorded in supine rest condition, in noise free and calm ambience, whereas only five minutes of clean data after manual inspection, is used for short term HRV analysis as per standard guidelines [1]. ECGs of 56 HTN patients were recorded in relaxed conditions at the Post Graduate Institute of Medical Education and Research, Chandigarh, India, following consultation with the cardiologist regarding the study group symptoms. ECGs of 57 NOR healthy subjects were recorded after medical examination and confirming no cardiac disorders and no prior medical history. An informed written consent was taken from each subject prior to data recording, making the patients fully aware that their recorded data will be used only for research purpose. Out of 57 NOR subjects, 20 subjects were in the range of 18 to 30 years, 20 subjects were in the range of 30 to 45 years and 17 subjects were in the range of 45 to 65 years. We analysed and extracted the features in different age ranges of all groups separately and then combined all ranges to single NOR category to avoid any kind of biasing. In case of HTN, all 56 subjects were in the age group of 36 to 65 years, as HTN in the lower age group is very rare. In both NOR and HTN, RR tachogram is the pictorial representation of successive RR intervals with respect to progressive beats. Such RR tachogram is generated using the acqknowledge 4.0 software of BIOPAC system. This generated tachogram contains unevenly placed samples as RR interval varies from one beat to another beat in both cases of NOR and HTN, hence resampling is carried out with 4 Hz frequency to maintain the uniformity among the entire length tachogram data. This resampled RR interval tachogram in text format is now ready to use as a dataset for the HRV analysis by Time Domain (TD), Frequency Domain (FD) and Non linear methods. Fig. 1 shows the generalized block diagram of different stages involved in HRV analysis using TD, FD and non linear methods, beginning with ECG data recording. In TD, we calculated the parameters such as Number of RR intervals (RR_{no}), Maximum value of RR intervals (RR_{max}), Minimum value of RR intervals (RR_{min}), Mean value of RR interval (RR_{mean}), Median value of RR intervals (RR_{median}), Mean value of Heart Rate (HR_{mean}), SDNN, Variance value of the RR intervals, Coefficient of Variance value of RR intervals (CV%), Standard Deviation of Successive Difference RR intervals (SDSD), RMSSD and pNN50. After calculating above said TD parameters for both NOR and HTN, a sensitivity analysis is carried out where the parameters which have similar ranges are excluded for classification thus, excluded parameters are RR_{no}, RR_{max}, RR_{min}, RR_{mean}, RR_{median}, HR_{mean}, CV%, SDSD and included parameters are Variance, SDNN, RMSSD and

pNN50. Similarly in FD, we calculated the power using power spectral density (PSD) in all frequency ranges i.e. P-VLF in ms^2 (0 to 0.04 Hz), P-LF in ms^2 (0.04 to 0.15 Hz), P-HF in ms^2 (0.15 to 0.4Hz) and P-Total in ms^2 (0 – 0.4 Hz), normalised powers P_n-VLF, P_n-LF, P_n-HF, P_n-Total in the same said frequency ranges and LF/HF ratio which signifies the sympathovagal balance [4]. These PSD are calculated by two methods 1). Non-parametric: FFT analysis with 256 samples, Welch periodogram and Hann windowing by 50% overlapping which provides the smoother PSD curve with in different frequency bands 2). Parametric: Autoregressive (AR) analysis where final prediction error (FPE) technique is used to determine the order of the model and Yule-Walker method is used to estimate the variance predictor. The prediction error is calculated for different model orders, and the one with least error is selected for given data.

$$\mathbf{FPE}\ [\mathbf{p}] = \boldsymbol{\sigma}_{\mathbf{p}}^{\mathbf{2}} \left[\frac{\mathbf{N+(p+1)}}{\mathbf{N-(p-1)}}\right] \tag{1}$$

Where σ_p^2 is the variance of the predictor, p is the model order and N is the number of samples. By both these parametric and nonparametric methods, a sensitivity analysis is carried out similar to TD method to all the features calculated. The parameters excluded for classification are P_n-VLF, P_n-LF, P_n-HF and P_n-Total and also all the parameters AR modelling to avoid possible redundant features hence, included features in FD are P-VLF in ms^2, P-LF in ms^2, P-HF in ms^2, P-Total in ms^2 and LF/HF. In non linear methods, the considered algorithms to calculate the features are Poincare plot, approximate entropy and sample entropy. Poincare plot is the graphical representation of present and next RR interval, if x and y are the present and next state RR interval series respectively then From equation (2), the features SD1 and SD2 can be calculated which represents the standard deviation (dispersion) short term and long term variability respectively of data point perpendicular to the axis of line-of-identity i.e. SD1 and SD2 are the standard deviation of x_1 and x_2 respectively. APEN is a measure of the complexity or irregularity of a signal where there is a more regular or predictable RR interval series, the lower will be the value of APEN and vice versa [4].

$$\begin{bmatrix} x_1 \\ x_2 \end{bmatrix} = \begin{bmatrix} \cos\frac{\pi}{4} & -sin\frac{\pi}{4} \\ sin\frac{\pi}{4} & cos\frac{\pi}{4} \end{bmatrix} \begin{bmatrix} x \\ y \end{bmatrix} \tag{2}$$

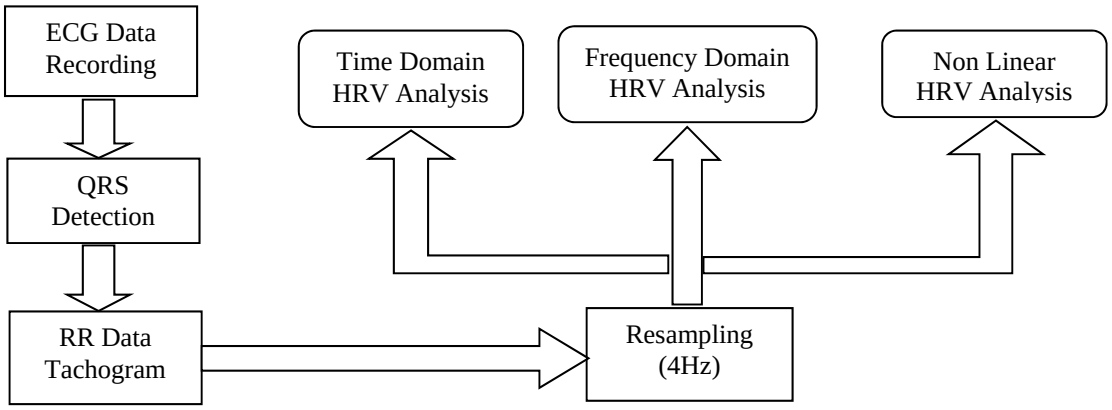

Fig 1. Generalized block schematic of linear and non linear analysis of heart rate variability

The steps involved to understand APEN are as follows. Consider the data sample sequence with *N* as length of the data and two fixed parameters must be determined, which are m and r**.** The parameter m means the embedding dimension of the vector formed, and r is the similar tolerance. In the present work, the considered values of m and r are 2 and 0.2 of standard deviation respectively. By considering the data sample sequence RR_{Total} = (RR_1, RR_2, . . . , RR_N) can be represented as RR (i), i = 0, 1, …….., N. From RR(i), m dimension vectors X(1) to X(N-m+1) can be formed as X(i) = [x(i), x(i+1), ..., x(i+m-1)], where i = 1 to N-m+1 and X(j) = [x(j), x(j+1), ..., x(j+m-1)], j = 1 to N-m+1. Define d(X^m(i), X^m(j)) the distance between vector X^m(i) and vector X^m(j) as the maximum absolute difference between their corresponding scalar elements as

$$d(X^m(i), X^m(j)) = \max_{k=0 \sim m-1}[|x(i+k), x(j+k)|]. \quad (3)$$

Note that all the other differences between the corresponding elements will then be less than d.

Hence, N^m(i) = no. of d[X(i), X(j)]≤ r **,** then C^m(i)= N^m(i)/(N- m + 1).

Take the natural logarithm of each C^m_i(r), and average it over i, denoted as Φ^m (r):

$$\Phi^m(r) = \sum_{i=1}^{N-m+1} \ln C_i^m(i) \quad (4)$$

Increase the dimension m to m +1, and repeat steps and find Φ^{m+1}(r), Then ApEn is

$$ApEn(m, r) = \lim_{N\to\infty}[\Phi^m(r) - \Phi^{m+1}(r)] \quad (5)$$

Hence, In general for finite length N, APEN is represented as

$$\text{ApEn}(m, r) = \Phi^m(r) - \Phi^{m+1}(r) \quad (6)$$

SAMPEN is another similar type of algorithm which measures the complexity in the time series data in which it avoids the self similarity as compared to APEN. The values of m and r are considered in the same way as that of APEN. The extracted features after the sensitivity analysis are variance of RR interval, SDNN, RMSSD, pNN50 of time domain, P-VLF, P-LF, P-HF, P-Total, LF/HF of frequency domain by FFT analysis, SD1, SD2 (Poincare plot), APEN and SAMPEN of non linear method used for classification by support vector machine (SVM) classifier separately for TD, FD, non linear and combined all together. In the present work, SVM classifier is implemented using LibSVM library in which it attempts to construct an optimum hyper plane in the higher dimensional feature space to separate the training data with minimum expected risk. Kernel functions are used for nonlinear mapping of the training data from input space to higher dimensional feature space Initial normalization is done between 0 and 1 with min - max normalization procedure to avoid bias caused by unbalanced feature values. To obtain good generalization performance in the correct choice of the regularization parameter C and kernel parameter γ, since C attempts to maximize the margin while keeping low value for training error, hence in this case, an extensive search is carried out in the parameter space for the values of C ϵ {2^{-4},.., 2^{15}} and γ ϵ {2^{-12},.., 2^5} using 10-fold cross-validation on training data [5]. 25 data sets of both case of NOR and HTN for training and testing have been used to maintain uniformity among training and testing data set.

3. Results

Initially all the TD features are compared in normal healthy subjects with different age groups

Table. 1 Comparison of time domain features for normal subjects with different age group and NOR with HTN

Features	NOR Age Group 18 - 30 (Mean ± SD)	NOR Age Group 30 - 45 (Mean ± SD)	NOR Age Group 45 – 65 (Mean ± SD)	NOR All Age Group (Mean ± SD)	HTN (Mean ± SD)
Rrno	316.77 ± 4.52	326.88 ± 4.52	302.06 ± 4.11	316.01 ± 4.44	311.50 ± 6.32
RRmin	679.33 ± 9.34	689.66 ± 8.58	768.66 ± 19.17	709.25 ± 14.09	763.03 ± 17.20
RRmax	991.77 ± 13.67	912.00 ± 18.85	1010.26±11.43	969.05 ± 14.47	945.28 ± 13.81
RRmean	827.01 ± 10.06	797.35 ± 11.34	837.78 ± 13.33	830.30 ± 10.03	857.33 ± 14.95
RRmedian	828.5 ± 11.08	797.16 ± 12.89	874.86 ± 14.33	831.07 ± 11.34	857.39 ± 15.63
HRmean	74.12 ± 1.04	76.50 ± 1.02	70.64 ± 1.31	73.93 ± 1.12	72.89 ± 15.07
Variance	2637.58±158.7	1218.06± 53.5	1276.30± 68.1	1736.20±101.48	1117.75±119.14
SDNN	49.76 ± 1.05	34.14 ± 1.44	34.27 ± 1.41	37.69 ± 1.78	30.19 ± 1.47
SDSD	40.39 ± 1.64	28.00 ± 1.72	26.35 ± 1.60	31.83 ± 1.45	26.40 ± 1.43
RMSSD	40.32 ± 1.73	27.96 ± 1.54	26.30 ± 1.17	31.83 ± 1.45	26.36 ± 1.43
CV%	6.03 ± 1.51	4.31 ± 0.95	3.96 ± 1.21	4.82 ± 1.52	3.50 ± 1.57
pNN50	19.59 ± 1.59	9.33 ± 1.74	6.10 ± 5.59	12.00 ± 1.83	8.99 ± 1.95

which shows the decrease in almost all parameters with increasing age and then combined all age groups to compare with HTN to avoid the age factor, the HTN still has reduced values of all parameters as shown in the table 1. In the same way, the comparison of all FD features by FFT method also shows decreased values in parameters. Table 3 shows the distinguishable difference in comparison of NOR with HTN from extracted features of all methods. SVM classifier provides an accuracy of 58%, 64% and 66% also HTN sensitivity as 92%, 92, and 80% when classified separately with TD, FD and nonlinear methods respectively when classified with combined features, it shows 100% accuracy with 100% both NOR and HTN sensitivity.

Table. 2 Comparison of all extracted features

Methods	Features	NOR (Mean ± SD)	HTN (Mean ± SD)
Time Domain	Variance	1736.20±101.4	1117.75±119.1
	SDSD	37.69 ± 1.78	30.19 ± 1.47
	RMSSD	31.83 ± 1.45	26.36 ± 1.43
	pNN50	12.00 ± 1.83	8.99 ± 1.95
Frequency Domain	P-VLF (ms^2)	269.36 ± 49.47	139.15 ± 10.24
	P-LF (ms^2)	183.93 ± 12.3	70.13 ± 24.50
	P-HF (ms^2)	108.37 ± 9.82	45.09 ± 5.12
	P-Total (ms^2)	561.66 ± 51.93	254.38 ± 22.41
	LF/HF	2.19 ± 0.42	2.54 ± 0.63
Poincare Plot	SD1	22.99 ± 2.56	18.67 ± 1.76
	SD2	51.87 ± 6.00	37.39 ± 3.43
Approximate Entropy	APEN	1.0885 ± 0.02	0.9902 ± 0.02
Sample Entropy	SAMPEN	1.5541 ± 0.01	1.5152 ± 0.02

Table. 3 The classification results obtained by SVM

Features	Confusion Matrix		C	γ	Acc (%)	Sen (%)
TD		NOR HTN	1.0	0.001	58	
	NOR	6 19				24
	HTN	2 23				92
FD		NOR HTN	1.0	0.001	64	
	NOR	9 16				36
	HTN	2 23				92
Non Linear		NOR HTN	1000	0.001	66	
	NOR	13 12				53
	HTN	5 20				80
All		NOR HTN	10000	0.1	100	
	NOR	25 0				100
	HTN	0 25				100

Acc=Accuracy, Sen= Sensitivity

4. Discussion

In the TD Method, other features such as Mean, Median of RR, Mean HR, SDSD, and NN50 are also analyzed but excluded by carrying out sensitivity analysis and including features such as Variance, SDNN, RMSSD and pNN50. Similarly, in the FD method, normalized power of all spectral band are also excluded and the entire set of features obtained from AR modelling excluded by considering the redundant features of similar trends in value. In Nonlinear Methods, SD1 and SD2 both provides the Elliptical structure of Poincare plot and have higher values in NOR case and lower values in HTN. The Coefficients of both APEN and SAMPEN are also higher, though marginally, in NOR case as compared to HTN, since the overall range is much less. SVM classification approach is one of the suitable techniques for binary classification, hence in our case, SVM provides less accuracy and sensitivity when we classify TD, FD, & Non linear features separately but when all these features are used in a combined way then it gives 100 percent accuracy with 100 percent sensitivity of both Normal and Hypertension subjects as we considered the equal data set for cases to train and test.

5. Conclusions

Time domain and frequency domain methods remain the basic building blocks of heart rate variability analysis and these features can be utilized for classification to differentiate normal healthy subjects from hypertensive subjects. Nonlinear Methods such as Poincare Plot, Approximate entropy and Sample Entropy provide the additional information to clearly distinguish normal healthy subjects from hypertensive subjects. Support Vector Machine based classification technique is simple, yet most effective specifically in binary classification which gives a clear separability of hypertensive subjects with normal healthy subjects.

References

[1] Virtanen R, Jula A, Kuusela T, Helenius H, Voipio – Pulkki LM. Reduced heart rate variability in hypertension association with life style factors and plasma renin activity. *J Hum Hypertens*, 2003; 17: 171–9.

[2] Schroeder E, Liao D, Chambless L, Prineas R, Evans G and Heiss G. Hypertension, blood pressure, and heart rate variability. The Atherosclerosis Risk in Communities (ARIC) Study. *Hypertension*, 2003; 42: 1106-1111.

[3] Task Force Report: Task Force of the European Society of Cardiology and the North American Society of Pacing and Electrophysiology. Heart Rate Variability: standards of measurement, physiological interpretation and clinical use. *Circulation*, 1990; 93: 1043-1065.

[4] Pichon A, Nuissier F, Chapelot D. Heart rate variability and depressed mood in physical education students: A longitudinal study. *Autonomic Neuroscience: Basic and Clinical*; 2010; 156: 117–123.
[5] Virmani J, Kumar V, Kalra N, Khandelwal N: SVM based charecterization of liver cirrhosis by singular value decomposition of GLCM matrix. *International Journal of Artificial Intelligence and Soft Computing*; 2013; 3: 276-96.

CARDIAC ARRHYTHMIA INDUCED BY HYPOTHERMIA IN A CARDIAC MODEL *IN VITRO*

[1]B. Xu, [2]S. Jacquir, [2]S. Binczak, [1]O. Pont, [1]H. Yahia

[1]Géostat, INRIA Bordeaux Sud-Ouest, France
[2]CNRS UMR 5158, LE2I Université de Bourgogne, Dijon, France
Email: Binbin.xu@inria.fr

Abstract. *Patients that have survived Out-of-Hospital Cardiac Arrest usually develop some degree of neurological problems. A common treatment to mitigate neurological damage is mild therapeutic hypothermia (MTH). However, MTH has adverse effects, including arrhythmia. In order to explore the mechanisms of arrhythmia linked to MTH, we took measurements on a temperature controlled experimental model which simulates MTH. These measurements consisted of extracellular potential of cardiac culture on a multi-electrode array and we analysed them in terms of nonlinear dynamics. The results showed that cardiac arrhythmia is induced around temperature 35°C (spiral waves at T~35°C against plane waves at other temperatures). A period-doubling phenomenon is also observed around T=35°C, confirmed with the analysis methods. All results showed that 35°C is a critical temperature triggering arrhythmia. This suggests that the re-warming / cooling speed could affect arrhythmia generation after MTH.*

Keywords: Cardiac Arrest, Therapeutic Hypothermia, Detrended Fluctuation Analysis, Phase Space Reconstruction

1. Introduction

The neurological damage following Cardiac Arrest (CA), caused by ischemia-reperfusion cerebral injury 0, constitutes a big health challenge. Many clinical trials with specific drugs which act against these damages have been conducted. However the problem remains far from being solved. Therapeutic hypothermia therapy (34°C–32°C) has shown its benefit in reducing cerebral oxygen demand and improving neurological outcomes after CA 0. Nevertheless, it can have some adverse effects, among which cardiac arrhythmia represents an important part (in up to 34% of cases, according to a number of different clinical studies 0). Compared to studies *in vivo*, cardiac culture *in vitro* provides a better spatial resolution at cellular level, which could bring additional insights on the mechanisms of post-hypothermia arrhythmia generation.

2. Methods

Monolayer cardiac culture is prepared with cardiomyocytes (CM) from a new-born Wistar rat (process see in Fig. 1, Left, and details of culture preparation in 0). The extracellular potential (EP) of the CM culture is acquired with a multi-electrode array (MEA) system allowing real-time recording of the extracellular potential. The MEA has 60 electrodes aligned in a 8 × 8 matrix (see in Fig. 1, Right) with a diameter 30µm, inter-electrodes distance 100µm. When it is compared to other conventional electrophysiological methods (intracellular recording or by patch-clamp), this method can provide a better spatial resolution, as it is non-toxic and non-invasive at cellular level [5, 6] The acquired extracellular potential (EP) shares almost the same electrophysiological properties as cardiac muscular cell *in situ* 0, and corresponds to a combination of 1st and 2nd order derivatives of the action potential. In consequence, the results obtained from EP could indirectly bring some insights at the *cellular action potential* level.

The experiments consist of culture cooling (37°C→30°C) and re-warming (30°C→37°C). The acquired signals are then analysed with detrended fluctuation analysis (DFA) and phase space reconstruction (PSR).

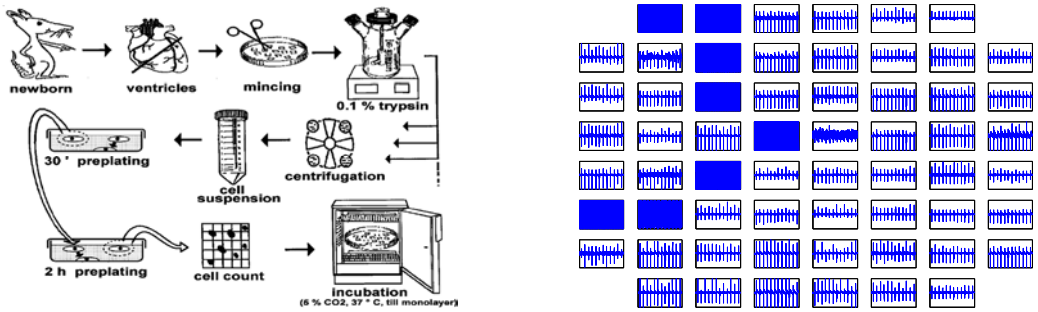

Fig. 1. **Left**: Preparation of monolayer cardiac culture; **Right**: extracellular potential acquired by MEA, 60 signals according to the positions of corresponding electrode on the MEA.

3. Results

Arrhythmia induced by hypothermia

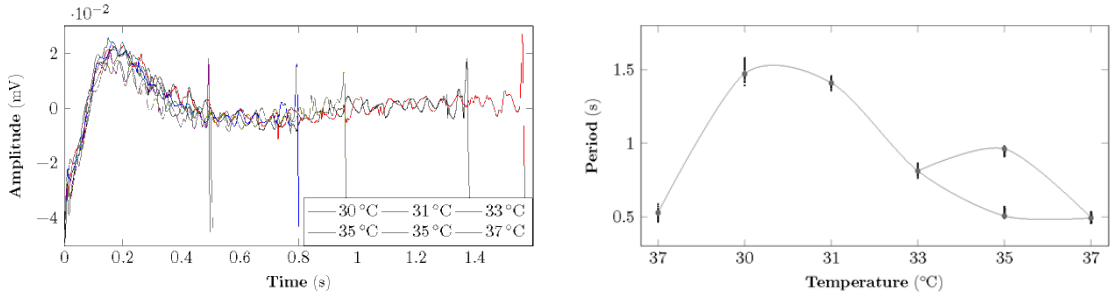

Fig. 2. **Left**: typical single period EP signals at different temperatures; **Right**: evolution of EP signal periods, periods doubling happened at T=35°C. The small black dots show actual values, while the bigger ones are medians at each temperature.

At temperatures other than 35°C, the EP signals are in general regular and stable. From a two-dimensional view, they can be represented by the propagation of plane waves. However, at 35°C, acquisitions show arrhythmia type signals. Spiral waves are observed in the reconstructed activation map which is commonly considered as a sign of cardiac arrhythmia. Both experiments (re-warming and cooling) showed that period-doubling phenomena happened at this temperature (see Fig. 2), which can be interpreted as a transition point from a normal state to a chaotic state. We also observed an inflection point between 30°C–33°C, which could indicate another regime transition of a different nature than the first one; in accordance to other studies showing that hypothermia below 32°C induces arrhythmia 0. These signals are then analysed by DFA and PSR methods.

Detrended fluctuation analysis

DFA is a method for determining the statistical self-affinity of a signal, which is often used to analyze electro-physiological signals 0. DFA characterizes the degree of complexity of the EP signals. This property is expressed as a parameter D which gives a measure of the effective (fractal) dimension of the system. As shown in Fig. 3, the result confirmed that a doubling of values occurred at 35°C, almost exactly as observed in Fig. 2.

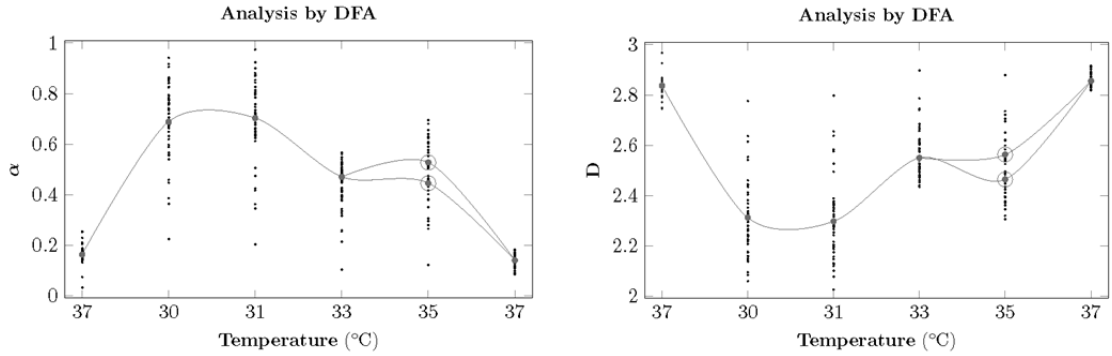

Fig. 3. Detrended fluctuation analysis for EP signals, showing the values for parameters α and D (which equals $3 - \alpha$). Parameter doubling happened at T~35°C.

Phase space reconstruction

Another method derived from chaos theory and nonlinear dynamics, which is suitable to study the complex dynamics of physiological signals, is the phase space reconstruction. Its principle is to transform the properties of a time series into topological properties of a geometrical object which is embedded in a space, wherein all possible states of the system are represented. Each state corresponds to a unique point, and the reconstructed space shares the same topological properties as the original phase space of the system behind the observed time series 0.

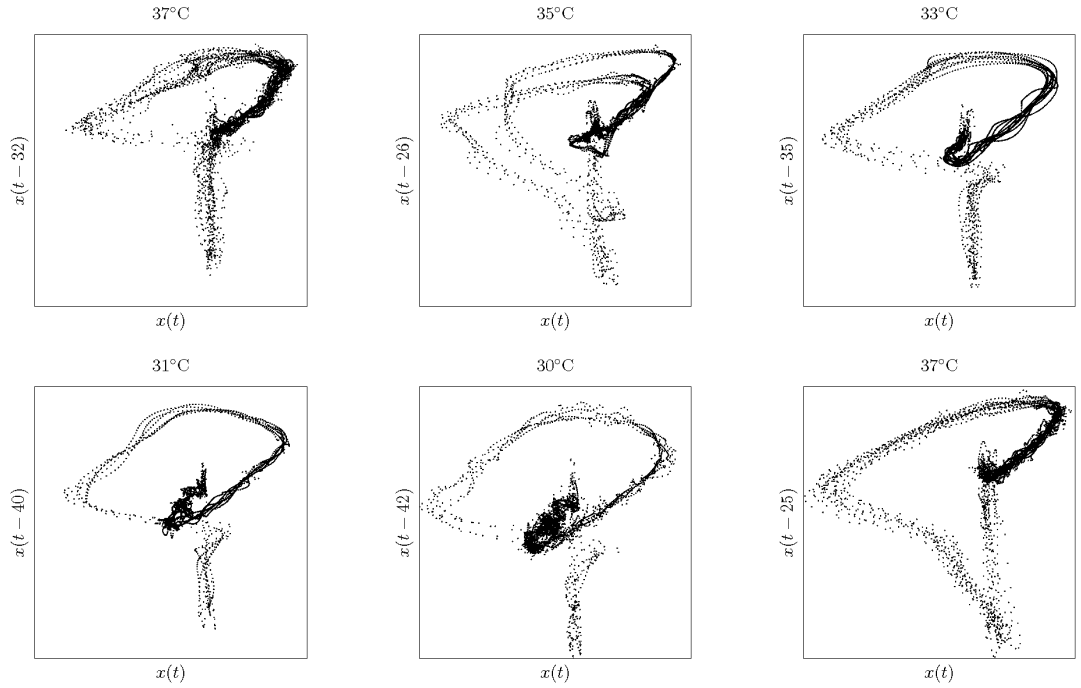

Fig. 4. Phase space reconstruction for signals at different temperatures (37°C→30°C→37°C). A trajectory-doubling is observed at T=35°C.

The trajectories of EP signals are represented in the reconstructed phase space (Fig. 4). Their general forms are similar. The width of these trajectories is tight, which signifies that the system is stable. However around T~35°C, a bifurcation of trajectories is observed which reflects the fact of signal periods-doubling as shown in Fig. 1. These results further confirmed in a more concrete way that T~35°C could be a critical temperature for arrhythmia generation after the therapeutic hypothermia.

4. Conclusions

In this experimental study, the action potentials during the process of therapeutic hypothermia (cooling and re-warming) are generally stable except around T~35°C. At this temperature, cardiac arrhythmia type signals are induced and spiral waves can be observed in the culture against plane waves at other temperatures. Also at this temperature, the activation periods are doubled, which indicates a transition to chaotic dynamics. Both analysis methods DFA and PSR confirmed a singular behaviour around T~35°C. General hypothermia therapy uses a constant rate of cooling and re-warming. From our observations, we propose that varying this rate, especially when passing around 35°C, could reduce the possibility of post-hypothermia arrhythmia generation.

Acknowledgements

We acknowledge the Institute of Cardiovascular Research (Dijon, France) and the NVH Medicinal (Dr. David VANDROUX, Dijon, France) for our collaboration in the experimental data acquisition.

References

[1] de Vreede-Swagemakers JJ, Gorgels AP, Dubois-Arbouw WI, van Ree JW, Daemen MJ, et al. Out-of-hospital cardiac arrest in the 1990s: A population-based study in the maastricht area on incidence, characteristics and survival. *Journal of the American College of Cardiology*, 1997; 30: 1500-1505.

[2] Group W, Nolan J, Morley P, al Therapeutic hypothermia after cardiac arrest: An advisory statement by the advanced life support task force of the international liaison committee on resuscitation. *Circulation*, 2003; 108: 118-121.

[3] The Hypothermia after Cardiac Arrest Group. Mild therapeutic hypothermia to improve the neurologic outcome after cardiac arrest. *New England Journal of Medicine*, 2002; 346: 549-556.

[4] Athias P, Vandroux D, Tissier C, Rochette L Development of cardiac physiopathological models from cultured cardiomyocytes. *Annales de Cardiologie et d'Angeiologie*, 2006; 55: 90-99.

[5] Stett A, Egert U, Guenther E, Hofmann F, Meyer T, et al. Biological application of microelectrode arrays in drug discovery and basic research. *Analytical and Bioanalytical Chemistry*, 2003; 377: 486-495.

[6] Hescheler J, Halbach M, Egert U, Lu ZJ, Bohlen H, et al. Determination of electrical properties of es cell-derived cardiomyocytes using MEAs. *Journal of Electrocardiology* 2004;37: 110-116.

[7] Watanabe T, Delbridge LM, Bustamante JO, McDonald TF. Heterogeneity of the action potential in isolated rat ventricular myocytes and tissue. *Circulation Research*, 1983; 52: 280-90.

[8] Kantelhardt JW, Zschiegner SA, Koscielny-Bunde E, Havlin S, Bunde A, et al. Multifractal detrended fluctuation analysis of nonstationary time series. *Physica A: Statistical Mechanics and its Applications*, 2002; 316: 87–114.

[9] Takens F. Detecting strange attractors in turbulence, in Dynamical Systems and Turbulence, Lecture Notes in Mathematics. Rand D., Young L.-S., Editors. Springer Berlin, Heidelberg, 1981, 366–381.

T WAVE ALTERNANS DETECTION, QUANTIFICATION AND PATTERN DEFINITION

[1]A. Deogire, [2]S. Hamde

[1]MET's Institute of Engineering, Nashik, India
[2]SGGSIT&E, Nanded, Vishnupuri, India
Email: arunadeogire@gmail.com

Abstract. *The work discussed here is about a multi-lead TWA detection algorithm, implemented in three stages; first, checking presence or absence of alternans, second quantification and third, detection of patterns. The algorithm makes use of eight independent leads (I, II, V1-V6), and is therefore called Multilead. The Principal Component Analysis (PCA) technique is used for enhancement of T wave quality. For positive TWA cases, a quantification process based on magnitude estimation and the pattern of alternans, like ABAB or BABA is defined. The algorithm was tested on 100 records of the Physionet TWA database. Results are presented in the form of positive predictivity and sensitivity, for correct detection of TWA cases, and are further compared with those of a combined method, proposed by others. The quantification results are compared with the actual magnitude provided by challenge organizers and the alternans pattern results are compared visually.*

Keywords: TWA, ECG, Multilead, PCA, SCD

1. Introduction

T-Wave Alternans (TWA) is a cardiac repolarization phenomenon defined as beat to beat alteration in morphology and amplitude of the ST segment or T wave. It represents a spatiotemporal heterogeneity of repolarization [1-7]. In recent years, the TWA detection procedure has proved to be a potential method of identifying patients with a high risk of sudden cardiac death (SCD) and cardiovascular mortality. This is supported by evidence in more than one hundred studies and in more than 1200 patients [6, 8]. The presence of TWA may be detected at the micro or macro level. Macro alternans is easily visible to the eye while micro - volt alternans is not visually detectable and therefore presents a challenge on which to work.

Numerous algorithms have been proposed to detect and/or quantify TWA, among which Spectral (SM) and Modified Moving Average (MMA) methods are common and commercially available. SM is an FFT based method which determines alternans based on a periodogram. MMA is a recently developed method which separates the ECG beats under study continuously as odd, even and calculates a moving average of both the odd and even beats [2]. SM require stationary alternans for a fixed period and is also sensitive to noise, so the MMA method is preferred over SM, under noisy conditions, specifically in ambulatory or stress test data. Other methods like Correlation, Complex Demodulation, KL transform, Periodicity Transform, Poincare Mapping, Generalized Likelihood Ratio test (GLRT) are also available. A detailed review of some important techniques and methodological processes of TWA detection is discussed by Martinz etc [2]. In addition, recently introduced methods like Wavelet transform [3, 4], periodic component analysis [4] show that this is a continuously evolving research area where efforts are made either to provide added value to existing methods or to explore new possibilities which will give detailed insight into the phenomenon. The present work is about TWA detection using a multilead PCA approach whereby an attempt is made to detect alternans presence and pattern and quantify the findings.

2. Methods

The Physionet/CinC TWA 2008 challenge database was used, which is a collection of 100 ECG records, out of which 30 synthetic records are with known alternans values, ranging from 2 to 60 micro-volts. A pre-processing step is performed to remove baseline wander and noise using zero mean filter and wavelet de-noising technique. A multilead approach as explained by Violeta [1] with eight independent leads is used.

T Wave Peak Detection and Separation

The TWA phenomenon, by definition, relates to alternans in the T wave or ST segment of the ECG. Therefore, for TWA analysis, the T waves are separated out. The procedure starts with detection of R peaks, using a threshold method. The detected R peaks are taken as reference with which to find T peaks. Finally T wave separation is done by selecting a fixed portion of the signal from both sides of the T peak of around 350ms duration. The procedure is repeated for every T peak of all the eight leads. Fig. 1 shows an example of separated T waves in the eight leads.

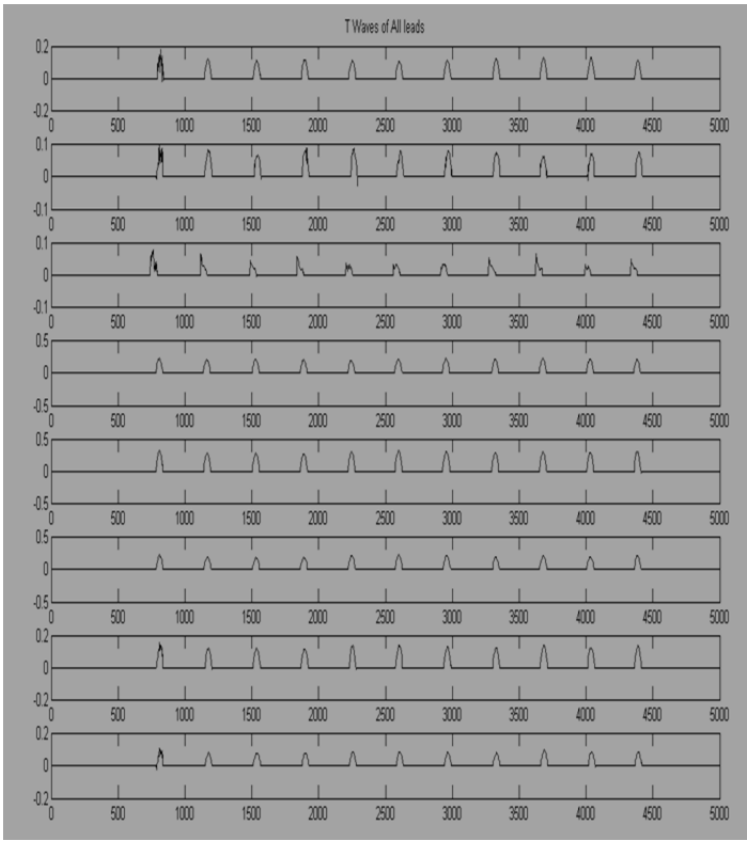

Fig. 1. T waves separation in Eight Independent Leads

PCA Analysis

Thus T waves separated from the eight leads as in the previous step differ in shape, size as well as noise contamination. Therefore results of the TWA detection algorithm may change based on the lead selected for analysis. To overcome this limitation, the separated T waves from each lead are subjected to Principal Component Analysis (PCA). PCA is an eigenvalue based technique which can tackle redundancy very effectively. This stage will transform the signal into eight orthogonal principal components, starting from the highest independent component as first to the lowest as last. Fig. 2 shows only the first three PCA components out of eight, as the remaining components show very little information about the signal. The first

component has a very similar appearance to the original T wave. The T waves obtained in this way are very clear and with uniform scale as compared to T waves taken directly from any lead of the original recorded signal.

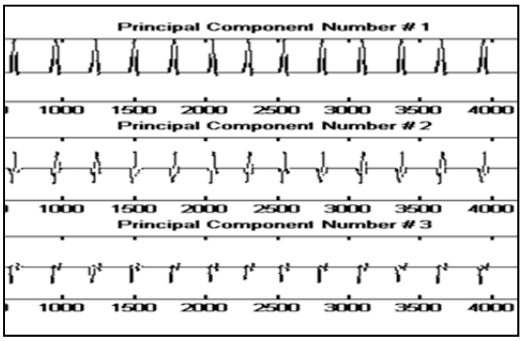

Fig. 2. First Three Principal Components

Alternans Detection

Thus the first PCA component of the previous stage will labelled as the transformed T wave and henceforth will be considered as the signal for alternans analysis. Following normalization, peak detection is executed on the transformed T wave signal and corresponding amplitudes are recorded. A stem plot of these detected peaks is as shown in Fig. 3. As the TWA phenomenon is supposed to appear on every alternate T wave, so the presence or absence of TWA is decided by comparing amplitudes of alternative beats. If there is a difference in amplitude following the same pattern consecutively for at least one fourth of the total T waves detected, then TWA is considered to be present. The average amplitude difference for the beats in which alternans is detected is calculated and taken as the final TWA amplitude.

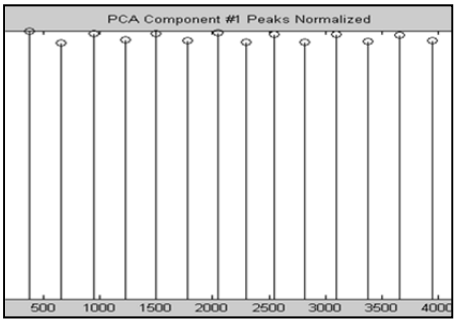

Fig. 3. Stem Plot of transformed T Wave

Pattern Detection

TWA can appear as simple ABAB or BABA patterns or in more complex patterns. This pattern makes a difference between other ST and T wave variations and TWA [1-8]. As a first step in the direction of pattern detection, an attempt is made by comparing amplitudes of the alternate T waves on the TWA alternans database. As shown in Fig 3, a clear pattern of ABABAB can be easily visualized. Similarly in some cases, pattern BABA is also identified. Further extension of this work will be to identify more complex or variable alternans patterns like ABBABB or ABABBABA.

3. Results and Discussions

Results are presented in three stages. First is the detection of TWA positive cases from available dataset; second, is the estimation of TWA magnitude and third, the alternans pattern detection. Regarding the first stage, after examining all of the 100 records, 29 records were

found to be TWA positive, where 30 are expected. The records that are detected as very noisy after the first pre-processing stage have the noise filtered out further at a second stage. Even after second stage filtering, if the signal seems to be noisy, then it not considered as valid for analysis. Two parameters, sensitivity and accuracy, are calculated as percentages.

The results of this stage are compared with the combined method proposed by Bortolan and Christov [5] because of the similarity used in the dataset as shown in Table 1.

Table. 1. T Wave Alternans Presence Result

Method	Sensitivity %	Accuracy %
Proposed	96.66	96.66
Bortolan G, Christov I. [5]	86.7	87.5

The sensitivity for the proposed method is 96.66 % (29/30), while for Bortolan it is a maximum of 86.7%. The accuracy here means percentage of true classification, which is also 96.66% for the proposed method, compared to 87.5% reported by Bortolan [5]. The result shows a definite improvement in both sensitivity and accuracy. That only one record could not be detected is possibly due to a very low amplitude and noise (2 micro-volts). The second part of the result, i.e. the TWA magnitude of the true cases which are actually detected as positive, is compared with the actual magnitude values provided in the Challenge dataset. The magnitude of the TWA ranges from 2 to 60 micro-volts and is provided for 30 synthetic records. The 30 records are divided into five groups, from A to E, and the amplitude varies from low to high values, as presented in Table 2.

Table. 2. TWA Magnitude, Actual vs Measured

Record	Model	TWA Magnitude (μV)		Record	Model	TWA Magnitude (μV)	
		Actual	Measured			Actual	Measured
twa76	A	2	2	twa15	C	15	7
twa64	A	4	4	twa01	C	45	21
twa51	A	8	8	twa91	C	60	27
twa50	A	15	16	twa30	D	2	ND
twa79	A	30	32	twa67	D	6	6
twa34	A	60	61	twa70	D	8	8
twa78	B	2	3	twa21	D	10	10
twa98	B	6	7	twa06	D	17	18
twa33	B	10	12	twa09	D	30	30
twa17	B	13	17	twa35	E	2	2
twa97	B	17	22	twa25	E	4	4
twa29	B	45	56	twa82	E	8	9
twa28	C	2	1	twa73	E	13	15
twa69	C	4	2	twa72	E	17	20
twa88	C	6	3	twa13	E	60	59

From the results obtained, it can be seen that, in all the groups except group C, the TWA detection accuracy is good. The statistics show that there are 9 records with 0% error, 12

records with less than 25% error, 2 records with 30% error and 6 records are with 50% error (from group C), out of the total of 29 detected records.

The graphical representation of actual versus measured TWA magnitude for each group is plotted which in Fig. 4. The graph shows that the relation is almost linear for every group, even for group C, especially for alternans values above 15 micro-volts.

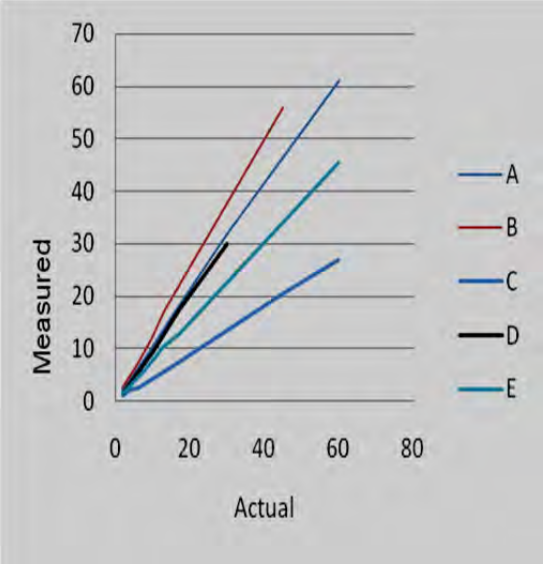

Fig. 4. TWA Magnitude, Actual vs Measured

The third stage of results relates to pattern detection. The main intention of this stage is basically to understand the internal changes in the behaviour pattern of TWA, which may lead to fibrillation and if detected earlier, can be used as an indicative marker of risk. The primary work of detecting simple patterns like ABAB or BABA is done at this stage. For example, from the output generated in Fig. 3, it can be seen that the pattern is ABAB.

4. Conclusions

Thus TWA is a potential test for detecting the risk of sudden cardiac death but still there is a room for improvement to make it robust by reducing the cases of indeterminate results. Also, combining the other SCD markers with TWA can give new insights into SCD risk analysis. The present work is a step into the direction of understanding and contributing to the TWA research whereby an attempt has been made to detect the presence or absence of TWA, and to quantify and to define the pattern of alternans. Further work is going on to improve the detection accuracy of T wave magnitude. In addition, the pattern detection methodology needs further attention.

References

[1] Monasterio V. Laguna, P. Mart J. P.,Multilead Analysis of T-Wave Alternans in the ECG Using Principal Component Analysis. *IEEE Transactions on Biomedical Engineering*, 2009; 56 (7): 1880–1890.

[2] Martínez JP, Olmos S. Methodological Principles of T Wave Alternans Analysis: A Unified Framework. *IEEE Transactions on Biomedical Engineering*, 2005; 52 (4): 599–613.

[3] Wan X, Yan K, Luo D, Zeng Y.A combined algorithm for T-wave alternans qualitative detection and quantitative measurement. Journal of Cardiothoracic Surgery, 2013; 8: 1–7.

[4] Janusek D. Comparison of T wave detection methods. *Biocybernetics and Biomedical Engineering*; 24 (4): 31–41.
[5] Bortolan G, Christov I. T-wave alternans detection by a combined method of principal component analysis and T-wave amplitude. *Physiological Measurement*, 2012; 33 (3): 333–43.
[6] Narayan SM., T-wave alternans and the susceptibility to ventricular arrhythmias. *Journal of the American College of Cardiology*, 2006; 47 (2): 269–81.
[7] Langley P, Bowers EJ, Murray A. Principal Component Analysis as a Tool for Analyzing Beat-to-Beat Changes in ECG Features: Application to ECG-Derived Respiration. *IEEE Transactions on Biomedical Engineering*, 2010; 57 (4): 821–829.
[8] Nieminen T, Verrier RL. Usefulness of T-wave alternans in sudden death risk stratification and guiding medical therapy. *Ann Noninvasive Electrocardiol*, 2010; 15 (3): 276-88.

3. Modelling

ACCURACY OF ELECTROCARDIOLOGICAL INVERSE SOLUTIONS: A MODEL STUDY

[1]G. Tuboly, [1]G. Kozmann, [1]I. Maros, [2]D. Wei, [2]X. Zhu

[1]University of Pannonia, Veszprém, Hungary,
[2]University of Aizu, Aizu-Wakamatsu, Japan
Email: tuboly.gergely@virt.uni-pannon.hu

Abstract. *The principal aim of this work is the investigation of the accuracy of the widely used Tikhonov regularization in electrocardiological inverse solutions by the study of the achievable quality of epicardial potential estimation. Reference epicardial and body surface electrocardiograms were generated in 1003 epicardial and 344 body surface points by the Wei model. The inverse problem has been solved for homogeneous and inhomogeneous chest models by the zero-order Tikhonov regularization formula with various regularization parameters and linear equation system solvers. The results were correlated with the original epicardial potential distribution. The highest correlations (> 0.9) occurred in the first half of the QRS interval and the correlation fell below 0.6 at the end of the QRS. While the result was highly dependent on the chosen regularization parameter and equation system solver, the largest source of error proved to be the inadequate volume conductor model when the correlation fell below 0.4.*

Keywords: Electrocardiological Inverse Solution, Modelling, Tikhonov Regularization, QRS Interval

1. Introduction

The epicardial potential distribution contains essential diagnostic information related to the functioning of the heart. This can be important for example in the assessment of malignant ventricular arrhythmia risk, which is closely related to the action potential heterogeneity of the heart muscle cells [1]. There are two possible ways to obtain the epicardial potential distribution: performing epicardial measurements or estimating the epicardial distribution based on high resolution body surface potential measurements by solving the inverse problem of electrocardiography. Since the former is an invasive procedure, it is not considered to be practical in human diagnostics. Therefore, developing and improving inverse solution methods is very important.

One of the most widely used inverse solution methods is the zero-order Tikhonov regularization which tries to transform the ill-posed problem into a well-posed problem by a special regularization parameter [2]. This method has also been frequently used in electrocardiological inverse computations [3]. The efficiency of the inverse solution methods is characterized mostly by the correlation coefficient of the measured and estimated potential distributions and by the relative error.

The aim of this paper is the study of the achievable epicardial potential distribution quality in the QRS interval by using the Tikhonov method with various regularization parameters and linear equation system solver algorithms. These tests have been performed for both an inhomogeneous and a homogeneous chest model.

2. Methods

Heart and chest model

The reference epicardial and body surface ECG signals were generated in 1003 epicardial and 344 body surface points by the Wei-Harumi forward model [4]. The body surface potential distributions were calculated by solving the forward problem of electrocardiography according to Eq. 1:

$$\mathbf{\Phi}_b = \mathbf{Z}\mathbf{\Phi}_h \tag{1}$$

where

$\mathbf{\Phi}_b$ vector of body surface potential distribution (344 x 1)

$\mathbf{\Phi}_h$ vector of epicardial potential distribution (1003 x 1)

$\mathbf{Z}$ transfer matrix between the epicardial and thoracic surfaces (344 x 1003, related to the homogeneous chest model) [5].

Tikhonov regularization

Equation 2 represents the inverse solution according to the zero-order Tikhonov regularization:

$$\mathbf{\Phi}_h = \left[\mathbf{Z}^T\mathbf{Z} + \gamma\mathbf{I}^T\mathbf{I}\right]^{-1}\mathbf{Z}^T\mathbf{\Phi}_b \tag{2}$$

where

$\mathbf{I}$ identity matrix

γ regularization parameter.

The regularization parameter is responsible for making the singular matrix to be regular, thus transforming the ill-posed problem into a well-posed one. The optimal value of γ is usually chosen empirically [2].

Solving the linear equation system

After rearranging Eq. 2 and substituting **A**, **x** and **b**, we get the linear equation system of Eq. 3:

$$\mathbf{Ax} = \mathbf{b} \tag{3}$$

where

$\mathbf{A} = \mathbf{Z}^T\mathbf{Z} + \gamma\mathbf{I}^T\mathbf{I}$

$\mathbf{b} = \mathbf{Z}^T\mathbf{\Phi}_b$

$\mathbf{x} = \mathbf{\Phi}_h$.

We chose six methods offered by the MATLAB library: the default linear equation system solver of MATLAB ("mldivide" command which equaled to the Cholesky factorization in our case) and five iterative methods (conjugate gradients, minimum residual, quasi-minimal residual, least-squares QR and symmetric LQ).

3. Results

We tested the Tikhonov regularization with various γ values. The results are summarized in Fig. 1, using homogeneous chest model during the forward and inverse computations (homogeneous case).

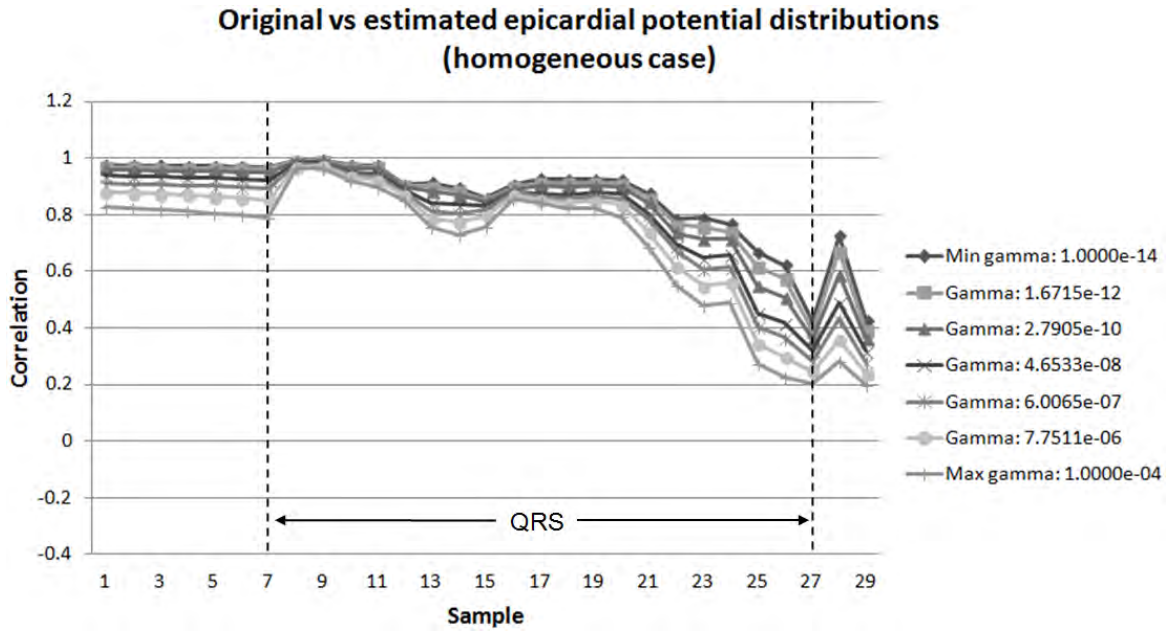

Fig 1. Efficiency (correlations) of the Tikhonov regularization with 7 different γ parameters in homogeneous case.

We performed the computations by also using an inhomogeneous chest model during the forward computations (inhomogeneous case). By using the homogeneous chest model in the inverse computations, we were able to test the sensitivity of the Tikhonov regularization for an inadequate chest model. As expected, this case produced poorer quality results, but using higher regularization parameters (γ > 1e-7) the correlations were not much lower than in the homogeneous case in the first half of the QRS interval (see Fig. 2).

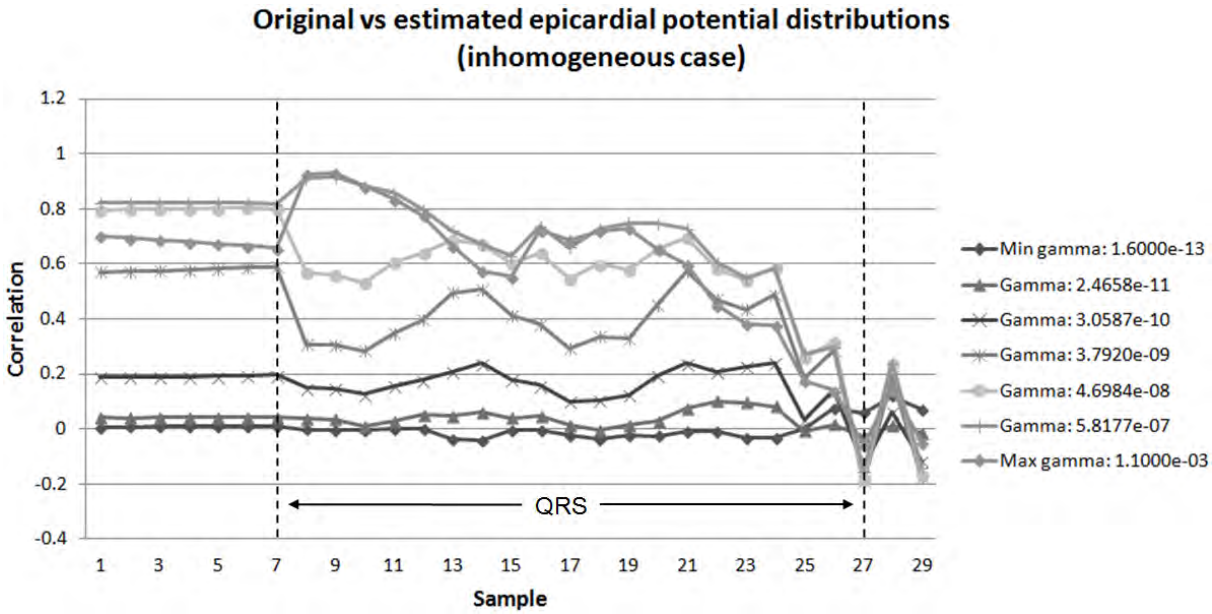

Fig 2. Efficiency (correlations) of the Tikhonov regularization with 7 different γ parameters in inhomogeneous case.

Performing the Tikhonov regularization with a fixed γ value by using different linear equation system solver algorithms, we found significant differences between the accuracy of the algorithms in the homogeneous case as shown in Fig. 3.

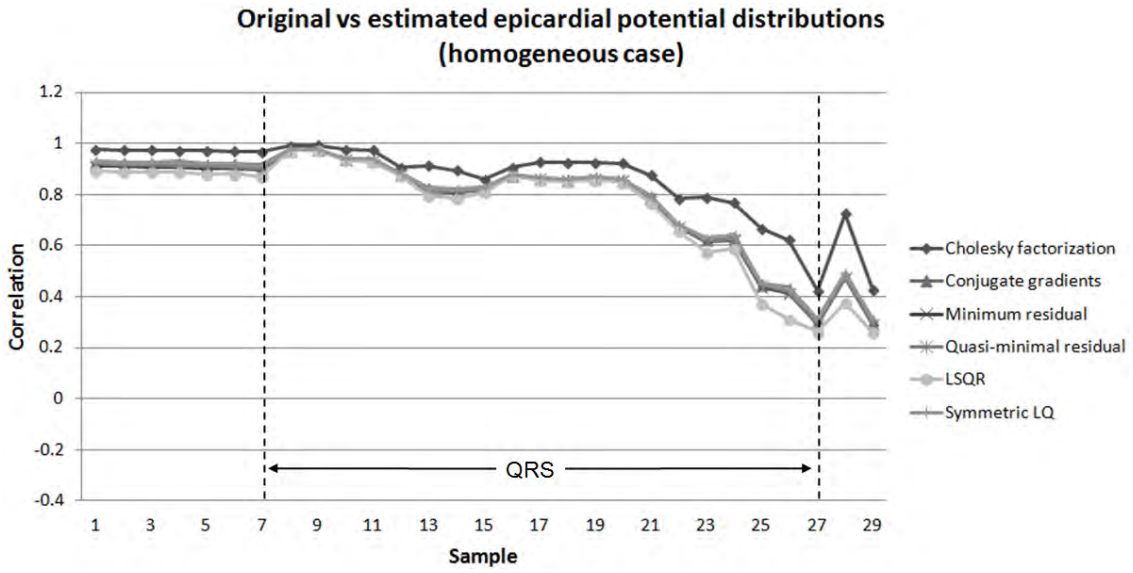

Fig 3. Efficiency (correlations) of the Tikhonov regularization with 6 different linear equation system solver algorithms in homogeneous case. The chosen γ value is 1e-14.

4. Discussion

The results show that the efficiency of the Tikhonov regularization highly depends on the chosen chest model, regularization parameter and the linear equation system solver algorithm. The Cholesky factorization proved to be the best algorithm, while the least-squares QR resulted in the worst correlations. In our experience, using the inadequate volume conductor model (inhomogeneous case) seems to result in the greatest source of error. It is interesting that at the end of the QRS interval none of the configurations could produce correlations higher than 0.8. This is probably due to the high complexity of the epicardial potential maps that show activation in the posterior side of the heart at the end of the QRS.

Acknowledgements

This research has been supported by the European Union and co-funded by the European Social Fund. Project title: “Telemedicine-focused research activities in the field of Mathematics, Informatics and Medical sciences”. Project number: TÁMOP-4.2.2.A-11/1/KONV-2012-0073.

References

[1] Geselowitz DB. The ventricular gradient revisited: relation to the area under the action potential. *IEEE Trans. Biomed. Eng.*, 1983; 30: 76-77.

[2] Tikhonov AN. Solution of Ill-posed Problems. Winston & Sons, Washington, 1977.

[3] Shahidi AV, Savard P, Nadeau R. Forward and Inverse Problems of Electrocardiography: Modeling and Recovery of Epicardial Potentials in Humans. *IEEE Trans. Biomed. Eng.*, 1994; 41: 249-256.

[4] Wei D. Whole heart modeling: progress, principles and applications. *Prog. Biophys. Molec. Biol.*, 1997; 67: 17-66.

[5] Barr RC, Ramsey M, Spach MS. Relating Epicardial to Body Surface Potential Distributions by Means of Transfer Coefficients Based on Geometry Measurements. *IEEE Trans. Biomed. Eng.*, 1977; 24: 1-1.

IMPACT OF TORSO MODEL FIDELITY ON THE INVERSE LOCALIZATION OF ISCHEMIA

J. Lenkova, J. Svehlikova, M. Tysler

Institute of Measurement Science, Slovak Academy of Sciences, Bratislava, Slovakia
Email: tysler@savba.sk

Abstract. *The accuracy of non-invasive localization of an ischemic lesion was investigated using different approximate heart models together with a patient-adjusted common torso model. Surface ECGs corresponding to 18 ischemic lesions were simulated in 7 realistic torso models. Difference QRST integral maps were then used as input for the inverse solution to find the position of each lesion represented by a single dipole. With a common heart model the mean lesion localization error was 3.4 cm, if the model was vertically shifted to an inversely estimated position, the error increased to 3.9 cm. For equally shifted but properly shaped heart models based on MRI scans, the error decreased to 2.4 cm. Finally, for MRI-based and properly positioned heart models the mean error achieved was1.0 cm, slightly bigger than the error of 0.7 cm obtained with the use of MRI-based torso and heart models. It can be concluded that the use of a patient-adjusted common torso model with a properly positioned and shaped heart model can lead to acceptable accuracy of the inverse localization of an ischemic lesion.*

Keywords: Ischemic Lesion, Body Surface Potential Mapping, Inverse Solution, TorsoModel

1. Introduction

Local cardiac ischemia caused by occlusion of a single coronary artery can be non-invasively assessed by finding a solution to the inverse problem with electrocardiology using the multichannel surface electrocardiogram (ECG) and a proper torso and heart model [1]. However, the accuracy of this solution can be influenced by many factors, such as the number of ECG leads, noise, model of the cardiac generator used and the inverse method or the fidelity of the geometrical torso and heart model. Whilst an accurate whole-torso model based on computer topography (CT) or magnetic resonance imaging (MRI) would be desirable, in practical situations, often only partial imaging of the heart area is available and the approximate torso model has to be used.

In a previous study [2] it was concluded that a common torso shape adjusted according to patient-specific chest dimensions with an “accurate” heart model yields acceptable accuracy of the lesion localization. In this simulation study we investigated how accurate is the inverse solution if a patient-adjusted torso shape, containing lungs and different heart models is used instead of the whole-torso MRI-based model.

2. Methods

Forward simulation of surface ECGs

Surface ECGs in 62 leads, generated by a normal heart and by a heart with one small ischemic lesion were simulated (using the boundary element method (BEM)) in 7 realistic inhomogeneous torso models based on real MRI scans (6 men, 1 woman) [3]. The original hearts were substituted by simplified models with shape and position adjusted in agreement with the original hearts (Fig. 1). In each heart 18 lesions were modeled by shortening the action potential by 20% in three areas typical for stenosis of the main coronary vessels: anterior - in the region supplied by left descending artery, posterior - in the region supplied by

the left circumflex artery, and inferior - in the region supplied by the right coronary artery. Three sizes of lesions from 0.5 - 14% of the ventricular myocardium, located at the epi- or endocardial surface were modeled (Fig. 2).

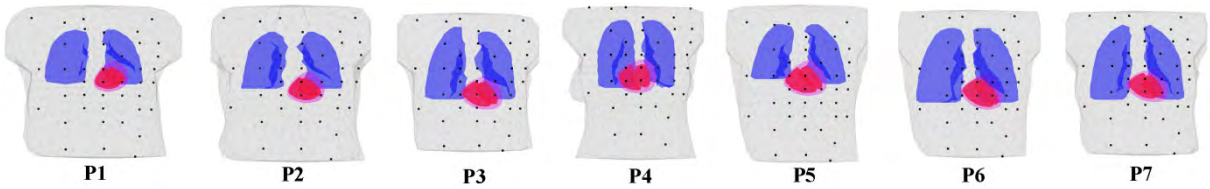

Fig. 1. : Seven realistic torso models based on MRI scans that were used in the study.

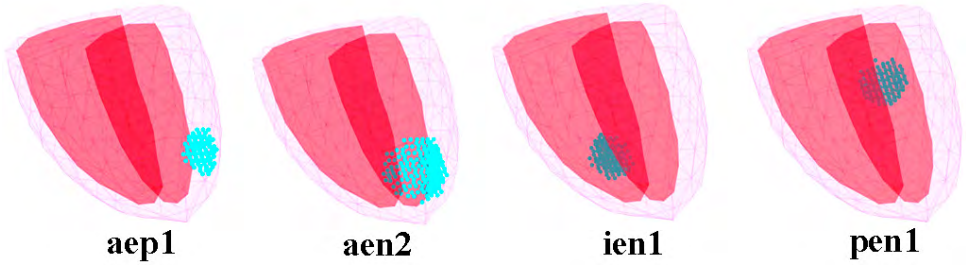

Fig. 2. Four examples of the 18 simulated ischemic lesions: small anterior epicardial (aep1), medium anterior endocardial (aen2), small inferior endocardial (ien1) and small posterior endocardial (pen1) lesion.

Assessment of an ischemic lesion by the inverse solution with single dipole model.

A Difference QRST integral map computed as the difference between integral maps generated by the pathologically changed and normal heart was used as input for the noninvasive assessment of the ischemic lesion. This map represents the pathological electrical source Δs in the ischemic lesion:

$$\Delta im = \int_{QRST} pm_P(t) - \int_{QRST} pm_N(t) = \int_{QRST} \mathbf{A}\, g_P(t) - \int_{QRST} \mathbf{A}\, g_N(t) = \mathbf{A}\left(s_p - s_N\right) = \mathbf{A}\,\Delta s \quad (1)$$

where $pm_P(t)$ and $pm_N(t)$ are surface potentials generated by pathological and normal activation of the ventricular myocardium, $g_P(t)$ and $g_N(t)$ are corresponding multiple dipole generators, $\boldsymbol{A}$ is time independent transfer matrix representing the relation between electrical generators and surface potentials, s_P and s_N represent the integral multiple dipole generators of the ischemic and normal heart and Δs characterizes only the pathological sources in the modeled lesion.

The equivalent integral generator (EIG) representing the original pathological integral multiple dipole generator Δs in equation (1) can be then computed as:

$$EIG = \mathbf{A}^{+}\Delta im \quad (2)$$

where $\boldsymbol{A}+$ is the pseudo-inverse of the transfer matrix $\boldsymbol{A}$.

Finding the *EIG* is a complex problem. However, if the EIG represents only a small volume of myocardium, it can be approximated by single dipole defined by 6 parameters. In the method used in this study [1], only three *EIG* parameters - components of the dipole moment - are computed. The other three parameters - dipole coordinates - are determined so that the dipole moments are computed for many predefined positions within the ventricular volume that are several millimeters apart (their spacing determines the resolution of the method) and the position of the lesion is then determined as the location in which the *EIG* best represents the input data Δim. This position is defined by the criterion that the root mean squared difference between the map generated by the *EIG* and the input integral map Δim is minimal.

Torso and Heart Models Used in the Inverse Solution

Four heart models in a common torso shape (taken from the Dalhousie torso model [4]) and adjusted according to 10 patient-specific anthropometric parameters were tested (Fig. 3):

A - common heart model in standard vertical position defined by the position of the ECG lead V2 and with "standard" rotation,
B - common heart model vertically shifted to an inversely estimated position by locating the site of the initial ventricular activation to the mid septal region, as proposed in [5],
C - heart model vertically shifted as in B but properly shaped and rotated in agreement with the MRI-based model used in the forward computation,
D - heart model properly shifted, shaped and rotated in agreement with the MRI-based model used in the forward computations.

The results for these torso models were compared with the results obtained for inverse solution using the original MRI-based torso models used in the forward calculations.

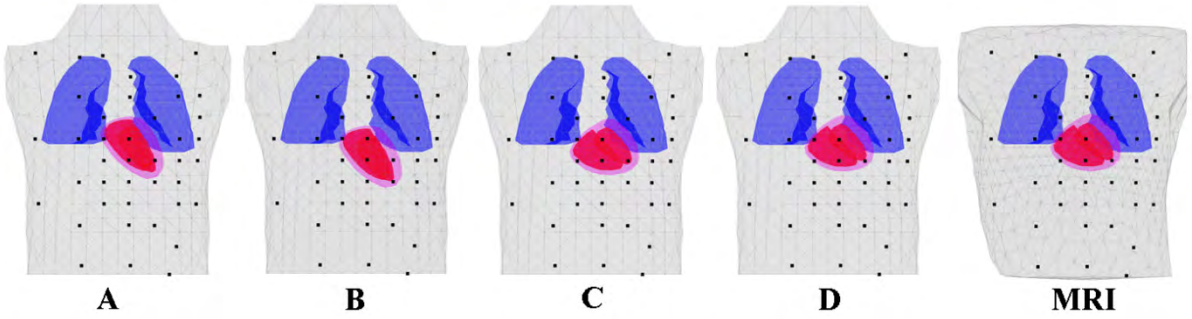

Fig. 3. Example of 4 torso and heart models A, B, C, D used in the inverse computations (for torso P5 in Fig. 1). The fifth model (MRI) is the reference realistic MRI-based model used also in the forward computations.

For each torso model used in the inverse computations two parameters were evaluated: (1) the mean error of the heart model vertical position measured relatively to the position used in the forward computation and (2) the mean lesion localization error defined as the distance between the gravity center of the simulated lesion and the inversely estimated position of the dipole representing the lesion.

3. Results

The mean values for the error of the vertical position of the heart model and error of the lesion localization for different torso and heart models are shown in Table 1.

Table. 4 Mean errors of the vertical heart position and lesion localization for the tested torso models.

Torso and heart model:	A	B	C	D	MRI
Error of vertical heart position:	1.1 ± 2.3	0.6 ± 0.9	0.6 ± 0.9	0.0	0.0
Error of lesion localization:	3.4 ± 1.1	3.9 ± 1.2	2.0 ± 0.9	1.0 ± 0.7	0.7 ± 0.7

The worst results were achieved with the unadjusted common heart models (model A). With the vertically shifted heart model (model B), the error of the vertical heart position decreased substantially but the lesion localization error even increased. Proper shaping and rotation of the shifted heart model (model C) did not change the vertical position error but decreased the lesion localization error significantly. Positioning the shaped heart model in accordance with the MRI scan (model D) decreased the lesion localization error to an acceptable value of 1.0

cm what is comparable with the intrinsic error of 0.7 cm of the used method (model MRI). Example of the results is illustrated in Fig. 4, right.

There were no substantial differences between results for the 7 realistic torsos (see Fig. 4, left). For all lesion positions the mean lesion localization errors were less than 1.0 cm if torso models D or MRI were used, except anterior endocardial lesions with mean errors of 2.2 ± 1.2 cm and 1.4 ± 1.3 cm for the D and MRI models, respectively.

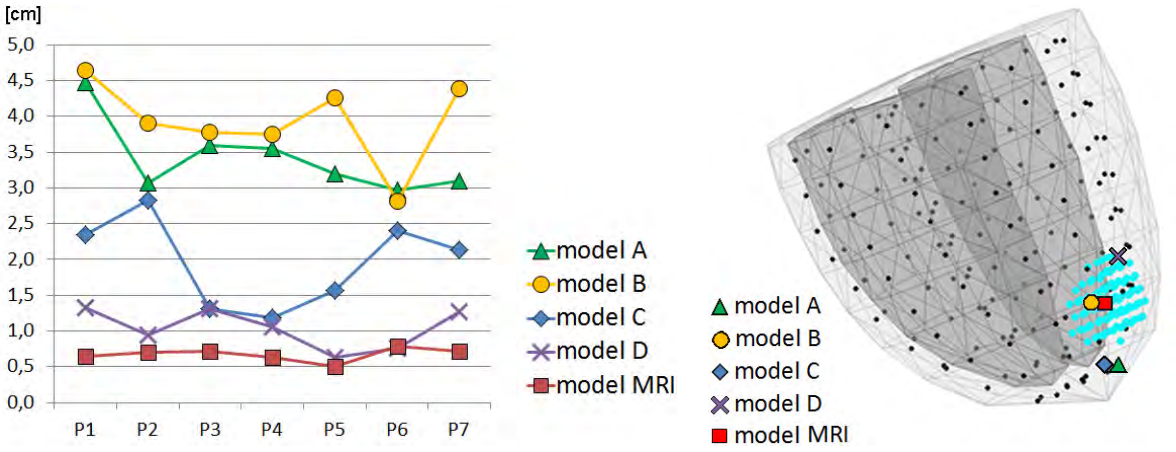

Fig. 4. Left: Mean lesion localization errors for investigated torso models and for all 7 individual patient torsos. Right: Example of medium anterior endocardial lesion (aen2) localization (in position with largest errors).

4. Discussion

As the inverse method used enables us to locate the dipoles only to predefined positions, the intrinsic error of this method depends on their volume density. In our study the distances between the positions were around 1 cm which led to a reasonable "grid error" of around 0.7 cm.

The individual results also showed that the method is not optimal for larger lesions; in such cases a modified method using a cluster of dipoles instead of one dipole performs better [6].

5. Conclusions

Both position of the heart model in the torso and its proper shaping and rotation appear to be crucial for inverse calculations. Torso models with shape adjusted to the patient's chest dimensions and with properly shaped and positioned heart models give acceptable accuracy of the inverse localization of small ischemic lesions represented by a single dipole. However, the precision of the localization may vary depending on the lesion position within the heart.

Acknowledgements

This study was supported by the research grant 2/0131/13 from the VEGA Grant Agency and by the grant APVV-0513-10 from the Slovak Research and Development Agency.

References

[1] Tyšler M, Kneppo P, Turzová M, Švehlíková J, Karas S, Hebláková E, Hána K, Filipová S. Non-invasive assessment of local myocardium repolarization changes using high resolution surface ECG mapping. *Physiological Research*, 2007; 56, Suppl 1: S133-S141.

[2] Lenkova J, Svehlikova J, Tysler M. Individualized model of torso surface for the inverse problem of electrocardiology. *J. of Electrocardiology*, 2012; 45: 231-236.

[3] Hoekema R, Uijen GJH, van Erning L et al. Interindividual variability of multilead electrocardiographic recordings - influence of heart position. *J. of Electrocardiology*, 1999; 32: 137-148.

[4] Horacek BM, Warren JW, Penney CJ et al. Optimal electrocardiographic leads for detecting acute myocardial ischemia. *J. of Electrocardioliogy*, 2001; 34: Suppl. 97-111.

[5] Švehlíková J, Lenková J, Drkošová A, Foltín M, Tyšler M. ECG based assessment of the heart position in standard torso model. *IFMBE Proceedings*, 2012; 37: 474-477.

[6] Svehlikova J, Lenkova J, Tysler M. Modified Inverse Solution to one dipole for location of lesions with changed repolarization. *Computing in Cardiology*, 2012; 39: 841-844.

SIMULATION STUDY OF VENTRICULAR RATE CONTROL THERAPY DURING ATRIAL FIBRILLATION USING A ONE-DIMENSIONAL CABLE MODEL WITH TWO CONDUCTION PATHWAYS

[1]S. Inada, [2]T. Ono, [3]N. Shibata, [1]M. Iwata, [1]R. Haraguchi, [4]T. Ashihara, [5]A. Abe, [5]T. Ikeda, [2]K. Mitsui, [6]M. R. Boyett, [6]H. Dobrzynski, [1]K. Nakazawa

[1]National Cerebral and Cardiovascular Center, Suita, Osaka, Japan
[2]Tokyo Denki University, Tokyo Japan
[3]Shinjuku Mitsui Building Clinic, Tokyo, Japan
[4]Shiga University of Medical Science, Otsu, Shiga, Japan
[5]Toho University Faculty of Medicine, Tokyo, Japan
[6]Institute of Cardiovascular Sciences, University of Manchester, Manchester, UK
Email: inada.shin.ri@ncvc.go.jp

Abstract. *The atrioventricular (AV) node lies between the atria and ventricles and is the only excitation conduction pathway between the upper and lower chambers. During atrial fibrillation (AF), the AV node plays an important role in adjusting the ventricular rate. Ionic channel blockers and beta-blockers are used clinically to control the ventricular rate. However, the mechanisms of these drugs on excitation conduction have not been clarified. To investigate the mechanisms by which these drugs affect excitation conduction in the AV node, we conducted computer simulations using a one-dimensional model with fast and slow conduction pathways in the AV node. Due to long refractoriness in the fast pathway, high-frequency excitations in the right atrium were partially blocked in the AV node. As a result, the ventricular rate decreased during AF. When calcium channel blockers were applied to the AV node, the ventricular rate decreased even further. Although all of the drugs used in this study could adjust ventricular rate, their mechanisms might differ.*

Keywords: Atrioventricular Node, Atrial Fibrillation, Ventricular Rate Control, Computer Simulation

1. Introduction

The atrioventricular (AV) node lies between the atria and ventricles and is the only excitation conduction pathway between the upper and lower chambers. During atrial fibrillation (AF), the AV node plays an important role in adjusting the ventricular rate. In addition, calcium blockers and beta-blockers are used clinically to control the ventricular rate. However, the mechanisms by which these drugs affect excitation conduction in the AV node have not been clarified. To investigate the effects of these drugs on AV nodal conduction, we constructed a mathematical model of the AV node and simulated excitation conduction between the right atrium and the bundle of His.

2. Methods

We recently developed action potential models for the rabbit AV node myocyte [1]. Using these models with an action potential model for the rabbit atrial muscle (AM) cell [2], we have constructed a one-dimensional (1D) multicellular model from the right atrium to the bundle of His via the AV node (Fig. 1). There are fast and slow conduction pathways in the AV node region. Atrial cells are connected to these pathways. Two pathways are connected to

a central region of the AV node, a compact node and nodal-His myocytes. Neighbouring cells are connected by a coupling conductance (g_j). The two conduction pathways are composed of atrial, atrio-nodal and nodal myocytes in the fast pathway and atrial and nodal myocytes in the slow pathway (Fig. 1C). All cells are assigned cell numbers from 0 to 249 in the atrial region, atrio-nodal and nodal regions in the fast pathway and nodal-His region and from 250 to 499 the atrial and nodal regions in the slow pathway. To simulate excitation conduction from the right atrium to the bundle of His in a sinus rhythm that represents physiological pacemaking generated from the sinoatrial (SA) node and high-frequency excitations corresponding to atrial tachycardia, inward currents of constant cycle length were applied to the end of the atrial string (cell 0).

There are two approaches for the treatment of AF: one involves treatment with antiarrhythmic drugs to terminate AF and recover sinus rhythm (rhythm control), while the other uses ventricular rate-controlling drugs that do not convert the sinus rhythm (rate control). Many studies, including the AFFIRM study [3] have reported that rate control therapy appears to be at least equivalent to or better than rhythm control using currently available pharmacological therapeutic options.

The AV node may play an important role in rate control therapy. Ca^{2+} channel blockers, digitalis and beta-blockers are generally used to control the ventricular response in patients with AF. However, the ionic basis of the underlying mechanisms of rate control therapy is not clear. A better understanding of how these drugs control the ventricular response during AF may facilitate the development of new clinical treatment strategies. In this study, the effects of Ca^{2+}, Na^{+} and K^{+} channel blockers and beta-blockers on excitation conduction from the right atrium to the bundle of His during AF were simulated. To simulate AF, an atrial cell (cell 24) was stimulated, and the intervals of stimuli were changed randomly from 75 to 150 ms, as in an experimental study by Mazgalev et al [4].

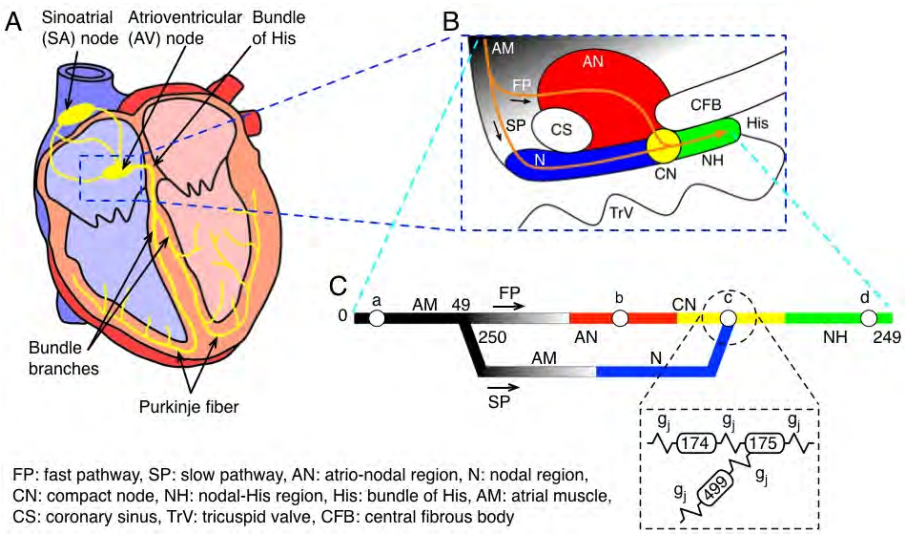

Fig. 1. Cardiac conduction system of the heart (A); schematic diagram of the AV node (B); and the cable model from the right atrium to the bundle of His through the AV node (C).

3. Results

Responses of the AV node to high frequency excitations in the atrium

During high-frequency excitations in the atrium corresponding to atrial tachycardia, conduction block was observed in the AV node. Fig. 2 shows representative results. Action potentials at selected cells through the AV node (Fig. 1C) are displayed.

When stimuli with a pacing cycle length of 210 ms were applied, conduction times from the atrium to the bundle of His corresponding to the PR intervals in the electrocardiogram were gradually prolonged beat by beat until excitation conduction was blocked completely in the AV node (Fig. 2A). These phenomena are known to the Wenckebach periodicity, which is frequently observed clinically. At higher pacing rates, intermittent conductions in the AV node were observed. For example, Fig. 2B shows a 3:1 conduction ratio with a pacing cycle length of 100 ms.

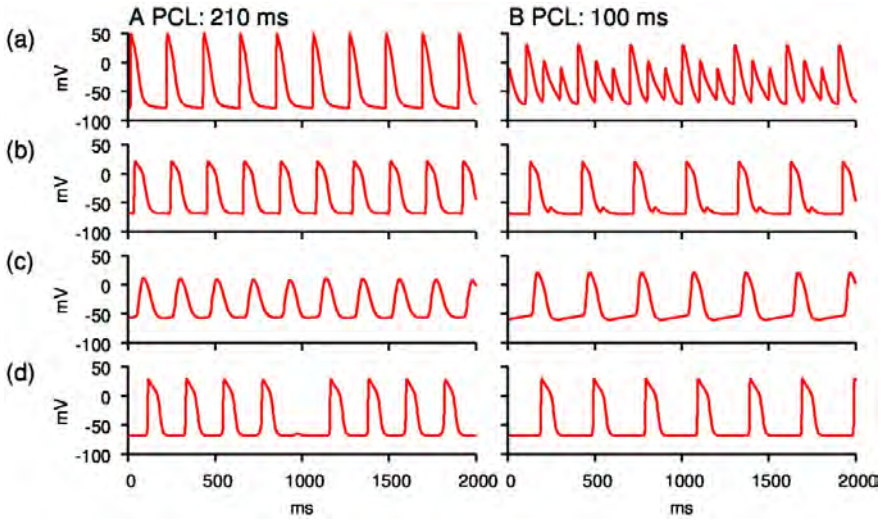

Fig. 2. Responses of the AV node to high-frequency excitations in the atrium.

Excitation conduction in the AV node and ventricular rate control with ionic channel blocking during atrial fibrillation

During AF, the AV node protects the ventricles from high-frequency excitations in the atrium (Fig. 3A). Activities within the conduction pathway were irregular, and frequent local conduction blocks occurred. Consequently, the excitation rate at the bundle of His (d) corresponding to ventricular excitation rate was decreased.

To investigate the possibility of adjusting the ventricular rate during AF through the use of drugs, we conducted simulations. After partial blocking of the L-type Ca^{2+} current (I_{CaL}), conduction blocks in the AV node occurred more frequently (Fig. 3B) compared to the control condition (Fig. 3A) due to decreasing excitability in the nodal region. At a high degree of blocking of I_{CaL}, a complete AV node block was observed.

Blocking the Na^+ current (I_{Na}) and delayed rectifier K^+ current (I_{Kr}) could also affect the ventricular rate during AF. Fig. 4A shows the relationships between channel conductances (g_{Na}, g_{CaL} and g_{Kr}) and the ventricular rate. Beta-blockers could also control the ventricular rate during AF. To simulate the effects of beta-blockers on the ventricular rate, the L-type Ca^{2+} current (I_{CaL}) and delayed rectifier K^+ current (I_{Kr}) were decreased simultaneously. Fig. 4B shows the relationships between the channel conductance of the delayed rectifier K^+ current (g_{Kr}) and the ventricular rate at various conductances of the L-type Ca^{2+} current (g_{CaL}). The simulation results suggest that the mechanisms by which ionic channel blockers adjust the ventricular rate during AF may differ.

4. Conclusions.

Our simulation results suggest that different drugs may control the ventricular rate during AF via different mechanisms. Our model contributes to the understanding of the complex phenomena that occur in the AV node.

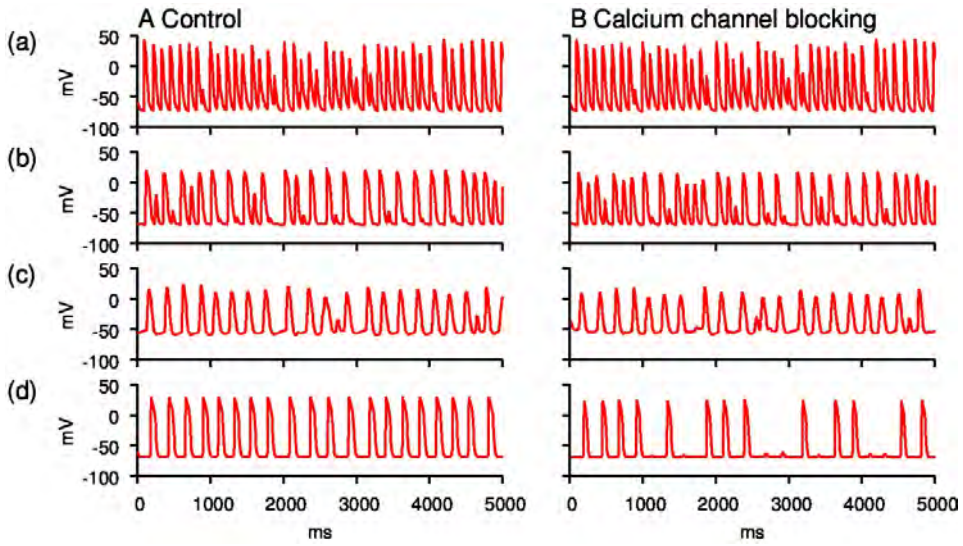

Fig. 3. Excitation conduction of the AV node during atrial fibrillation before (A) and after (B) application of calcium channel blockers.

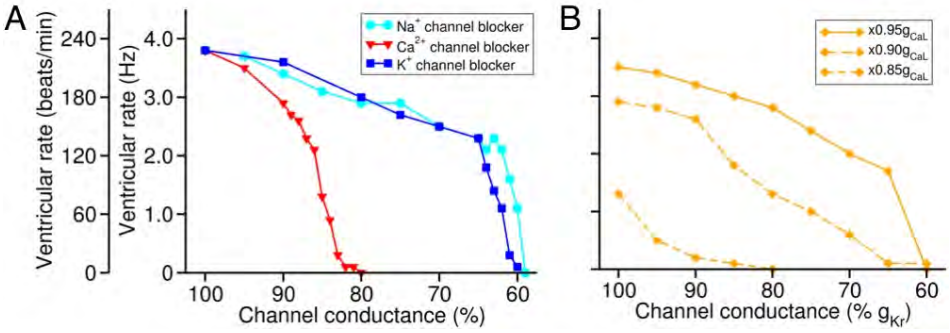

Fig. 4. Effects of ionic channel blockers (A) and beta-blockers (B) on the ventricular rate during atrial fibrillation.

Acknowledgements

This study was financially supported by Grants-in-Aid 22136011 and 25282138 from the Ministry of Education, Sports, Science and Technology, Japan, and is a project in the Graduate School of Applied Informatics, University of Hyogo.

References

[1] Inada S, Hancox JC, Zhang H, Boyett MR. One-dimensional mathematical model of the atrioventricular node including atrio-nodal, nodal, and nodal-His cells. *Biophys J*, 2009; 97: 2117-2127.

[2] Lindblad DS, Murphey CR, Clark JW, Giles WR. A model of the action potential and underlying membrane currents in a rabbit atrial cell. *Am J Physiol Heart Circ Physiol*, 1996; 271: H1666-H1696.

[3] The Atrial Fibrillation Follow-up Investigation of Rhythm Management (AFFIRM) Investigators. A comparison of rate control and rhythm control in patients with atrial fibrillation. *N Engl J Med*, 2002; 347: 1825-1833.

[4] Mazgalev TN, Garrigue S, Mowrey KA, Yamaguchi Y, Tchou PJ. Autonomic modification of the atrioventricular node during atrial fibrillation: role in the slowing of ventricular rate. *Circulation*, 1999; 99: 2806-2814.

TOWARDS COMPUTATIONAL MODELLING OF THE HUMAN FOETAL ELECTROCARDIOGRAM: NORMAL SINUS RHYTHM, HEART BLOCK AND RE-ENTRANT VENTRICULAR TACHYCARDIA

[1]A. P. Benson, [2]B. Hayes-Gill, [3]S. Hodgson, [1]A. V. Holden, [1]E. Pervolaraki

[1]School of Biomedical Sciences, University of Leeds, UK,
[2]Electrical & Electronic Engineering, University of Nottingham, UK,
[3] Division of Medical Sciences, University of Oxford, UK.
Email: a.v.holden@leeds.ac.uk

Abstract. *A biophysically detailed, one dimensional computational model for propagation during normal sinus rhythm in the foetal heart during gestation is constructed, with parameters that reproduce the intervals of foetal ECG at 16, 24 and 38 weeks gestational age. Spatially uniform reduction of the L-type calcium conductance mimics the effects on ECG intervals of congenital heart block, with 2:1 atrio-ventricular block preceded by bradycardia occurring at 50%, and complete block at 75% reduction of the L-type calcium conductance in the model. Self terminating and persistent re-entrant ventricular activity with a period of 240ms can be initiated in the model during a vulnerable window of 2ms duration 275ms after ventricular depolarisation during normal sinus rhythm with a cycle length of 420ms in a foetal ventricle with diameter > 10mm, i.e. about 14 weeks gestational age. The simple model may be used to quantitatively predict changes, produced by pharmacological agents or pathologies, in foetal ECG intervals during gestation.*

Keywords: Foetal ECG, Congenital Heart Block, Foetal Arrhythmia, Computational model

1. Introduction

The 10-100μV foetal electrocardiogram (fECG) can be recorded from the maternal abdominal surface from approximately 12 weeks gestational age (WGA) onwards. In addition, signal processing allows the extraction of RR, PR, QR and QT intervals, and T and P wave dispersions [1]. These non-invasive measures provide quantitative information on sino-atrial node pacemaking rate (*via* RR), propagation times and hence velocities (*via* PR, QT), and ventricular action potential duration (QR) and its restitution (QT-RR) during foetal normal sinus rhythm (NSR). Foetal arrhythmias are infrequently observed, may be benign, or may be life-threatening and require *in utero* therapy [2].

Computational modelling of the heart has provided a quantitative, predictive coupling between cell and tissue electrophysiology and the ECG [3] and allows the interpretation of the body surface ECG in terms of cardiac surface activity [4]. Cardiac modelling requires detailed models of cell electrophysiology, anisotropic tissue architecture and heart geometry. The anisotropic geometry of the foetal heart has been mapped by diffusion tensor MRI [5] and there are several models of the electrophysiology of adult human cardiac cells from the pacemaking and conducting system, and atrial and ventricular myocardium.

Here we modify the parameters of models of adult human nodal [6], atrial [7], Purkinje [8] and ventricular [9] cells, incorporate them into a simple 1-D model of propagation in the foetal heart, and compute propagation patterns that reproduce normal sinus rhythm during gestation, provide a predictive model for congenital heart block, and the characteristics of foetal ventricular tachycardia. This preliminary 1-D model for the foetal heart is modular, and

therefore other models for human cardiac cell electrophysiology, their parameters, and their changes during gestation may readily be incorporated.

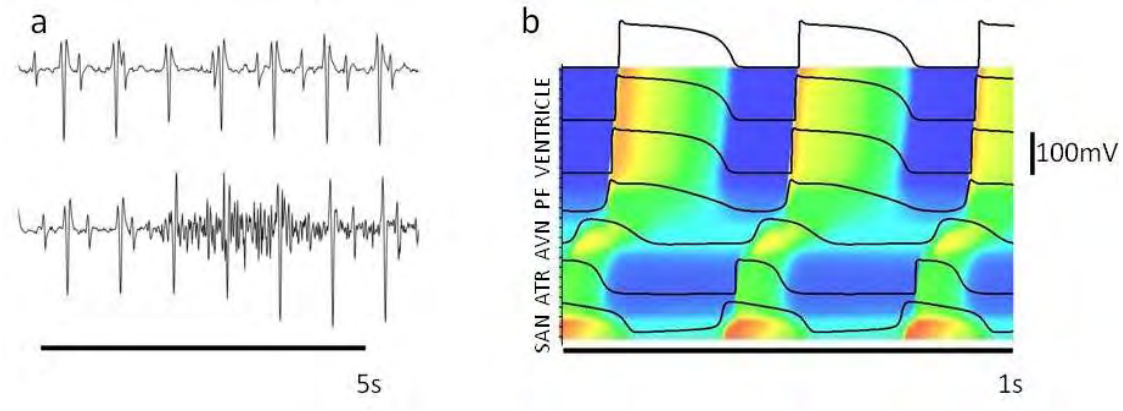

Fig 1. (a) Abdominal surface recordings of maternal and fECG NSR (upper) and putative self-terminating foetal ventricular tachycardia (lower) in same subject. (b) Space time plot of computed NSR for 20 mm, 1-D model of 24 WGA foetal heart, with cycle length 400 ms, and with V(t) for representative sino-atrial, atrial, atrio-ventricular, Purkinje and ventricular cells overlaid on the space-time display.

2. Methods

Propagation of electrical excitation in heterogeneous cardiac tissue can be described by the nonlinear partial differential equation [3] :

$$\frac{\partial V}{\partial t} = \nabla(D\nabla V) - I_{\mathbf{ion}}. \qquad (1)$$

where V (mV) is the membrane potential, ∇ is a spatial gradient operator and t is time (ms). D is the diffusion coefficient tensor ($mm^2.ms^{-1}$) that characterises the electrotonic spread of voltage via local circuit currents, through cell-to-cell coupling by gap junctions, and the extracellular and intracellular resistances. I_{ion} is the total membrane ionic current density. Heterogenity is introduced by segmenting the strand into sinoatrail node, atrial, atrioventricular node, Purkinje and ventricular tissue, each with different parameter value sets for I_{ion}, and intercellular coupling. The programs and parameters used for the figures in this paper are available from the authors.

One-dimensional partial differential equation models of SAN, atrial, AVN, Purkinje and ventricular tissue, with lengths from MRI data and intercellular coupling informed by PR and QR intervals, were constructed for hearts from 15-40 WGA. Numerical solutions, with zero-flux boundary conditions, were obtained by a forward-time central-space scheme (with space steps of $\Delta x = 0.1$ mm) in conjunction with an operator splitting and adaptive time step method (to give time steps between $\Delta t = 0.01$ and $\Delta t = 0.05$ ms).

3. Results

Normal Sinus Rhythm

The 1D model, illustrated in Fig. 1b at 24 WGA, and with parameters for 16, 24, 38 WGA gave NSR intervals RR (cycle length) : 390, 400, 415; and PR (first atrial to first ventricular

depolarisation) and QRS (first to last ventricular depolarisation) all within 10 ms of the means values for these gestational ages [1].

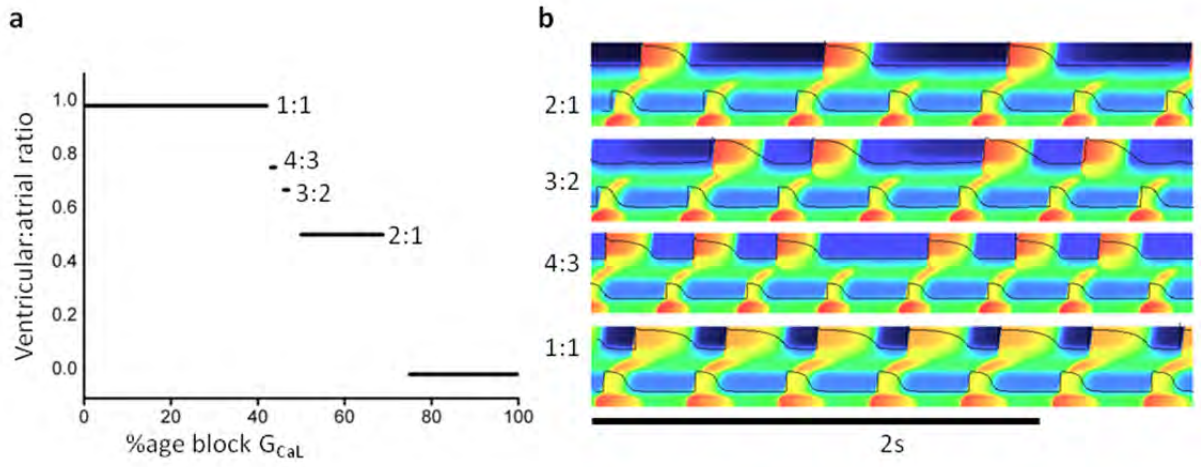

Fig 2. (a) Ratio of ventricular: atrial periodic activity in 1D, 24 WGA model during spatially uniform block of G_{CaL}, estimated during 6 s of 10s of activity (b) Space time plots for 20 mm, 1-D model of 26 WGA foetal heart illustrating normal 1:1 sinus rhythm, and 4:3, 3:2 and 2:1 conduction blocks produced by 43, 47 and 50% block of G_{CaL}.

Atrioventricular block

Spatial heterogeneities (different cell properties and diffusion coefficients) can give rise to partial (Wenckebach-like) and complete conduction block. These can be produced in the 1-D foetal heart models at the atrio-ventricular node by spatially uniform reduction in the maximal L-type calcium conductance, $G_{Ca,L}$, as illustrated in Fig. 2. In the 24 WGA model, reduction of $G_{Ca,L}$ by up to 42% prolongs the cycle length from 399 to 442 ms, and further reduction leads to atrio-ventricular conduction blocks that appear in a typical Farey sequence, with (n+N):(m+M) regions between n:m and N:M regions.

Ventricular tachycardia

Excitation initiated at different sites S1 and S2 in a ring can lead to re-entry if the S2 excitation occurs in a narrow (~2ms wide) window 275 ms after the upswing of the ventricular action potential, as in Fig. 3. The period of re-entry in the model is 240ms, and increases with ring circumference and decreases with ring diffusion coefficient.

4. Discussion and conclusions

This 1-D family of models is preliminary, is engineered from current models of adult cardiac cells by changes only in expression (channel density): differences in kinetics (due to channel isoforms, microenvironment) are omitted. These can readily be incorporated if and when experimental data is available. This family of models reproduces the observed timings of fECG intervals from 15-40 WGA, and quantitatively predicts the characteristics of foetal AV

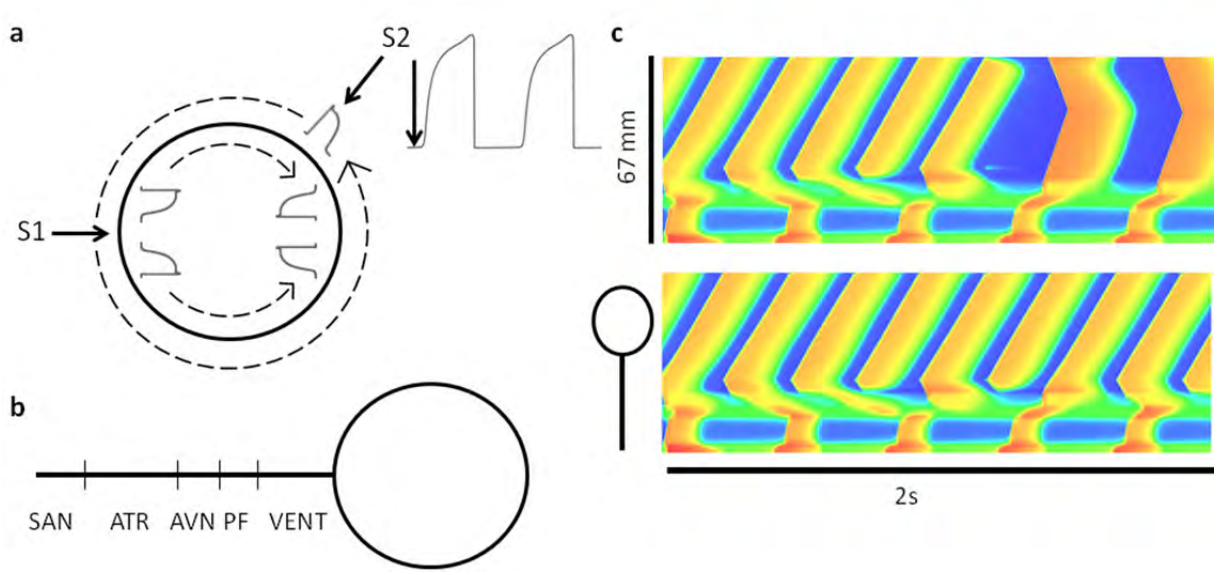

Fig 3. (a) Re-entry in a 1-D ring. Excitation at S1 produces pairs of action potentials that propagate around the ring and collide. An ectopic excitation at S2, within the vulnerable window, produces a solitary action potential that circulates counter-clockwise around the ring. (b) Construction of a 1-D strand-ring model that reproduces normal sinus rhythm, atrio-ventricular conduction block, and re-entrant ventricular tachycardia (c) Space time plot of self-terminating and persistent ventricular tachycardia in 24 WGA strand-ring model; the ventricle has been extended to give a 40mm ring, where the circumference of the is ~π times the ventricular diameter.

block due to spatially uniform reduced G_{CaL}, and the vulnerable window for, and existence of, self terminating and persistent re-entrant ventricular tachycardia.

Congenital heart block (CHB) is an autoimmune disease where maternal antibodies produce irreversible foetal AV block, due to reduction in L- and T- type Ca^{++} current expression [10]. FECGs during the development of congenital heart block could be used to fine-tune the parameters of the model, and the bradycardia predicted by the model could monitor the development of CHB before AV node block develops.

The period of the model ventricular re-entry is consistent with the period of the "putative ventricular tachycardia" illustrated in Fig. 1, and consequently such fECG recordings may result from re-entrant tachycardia in the foetus. If they self-terminate, they are benign; if not, they could be a cause of death *in utero*.

References

[1] Sato N, Hoshiai T, Ito T, A *et al*. Successful detection of the fetal ECG waveform during various states of singletons. *Tohoku J.Exp. Med*, 2011; 225: 89-94.

[2] Strasburger JF, Wakai RT. Fetal cardiac arrhythmia detection and *in utero* therapy. Nat. Rev. Cardiology, 2010:7 (5): 177-290.

[3] Panfilov AV, Holden AV Editors. The Computational Biology of the Heart. John Wiley, Chichester, 1997, 416.

[4] Ramanathan C, Ghanem RN, Jia P, Ryu K, Rudy Y. Noninvasive electrocardiographic imaging for cardiac electrophysiology and arrhythmia. *Nat. Med.* 2004; 10 (4): 422-8.

[5] Pervolaraki E, Anderson RA, Benson AP, Hayes-Gill B, Holden AV, *et al.* Antenatal architecture and activity of the human heart. *Interface Focus* 2013 3 (2) 20120065

[6] Chandler NJ, Greener ID, Tellez JO, Inada S, Musa H, Molenaar P *et al*. Molecular architecture of the human sinus node insights into the function of the cardiac pacemaker. *Circulation* 2009; 119 (12): 1562-1575.

[7] Courtemanche M, Ramirez RJ, Nattel S. Ionic mechanisms underlying human atrial action potential properties. *Am. J. Physiol.* 1998; 275: H301-21.

[8] Stewart P, Aslaidi OV, Noble D, Mathematical models of the electrical action potential of Purkinje fibre cells. *Phil Trans. Roy. Soc. (London) A* 367:2225-2255.

[9] Ten Tusscher Panfilov KHWJ, Noble D, Noble PJ, Panfilov AV: A model for human ventricular tissue. *Am. J. Physiol.* 2004; 286: H1573-H1589.

[10] Qu Y, Baroudi G, Yue Y, Boutjdir M: Novel molecular mechanism involving α_{1D} (Cav1.3) L-type calcium channel in autoimmune-associated sinus bradycardia. *Circulation*, 2004; 111:3024-3034.

BIOPHYSICAL MODELLING OF ST-T ALTERATIONS UNDER MYOCARDIAL ISCHEMIA

[1]O.V. Baum, [1]V.I. Voloshin, [1]L.A. Popov, [2]G.A. Muromtseva

[1]Institute of Theoretical and Experimental Biophysics, Pushchino, Russia,
[2]National Research Centre for Preventive Medicine, Moscow, Russia
Email: baum@iteb.ru

Abstract. *With the use of mathematical models, some tendencies of alterations of the morphological characteristics of the T wave on the changing parameters of the transmembrane action potential in an "ischemic" zone have been investigated. Computer experiments were executed on a system for 3D-modelling of the cardiac electrical activity with the aid of our model of ECG genesis which we have developed. Methods of segmentation of the model hearts on separate segments, as well as calculation of the partial contribution of any segment, including "ischemic" segments, into the potential of the chosen lead have been developed and were used. For the modelled ECG, a set of characteristics, parameters similar to that of the in vivo ECG, have been measured and analyzed. A new diagnostic parameter Kg has been suggested.*

Keywords: Ischemia, Repolarization, Action Potential, T wave, Mathematical Modelling

1. Introduction

The most important risk factor for sudden death in patients with coronary heart disease is myocardial ischemia (Isch). It is important to develop methods of noninvasive diagnostics of Isch, especially at the early stage of the disease, on the basis of new data on heart biophysics and physiology. Research methods in this area of knowledge involve mathematical and computer modelling. A systemic approach is necessary to the problem, combining methods of modelling with investigations of the electric field of the human heart.

The main objective of the study is to investigate with the aid of computer models trends of alterations of the morphological characteristics of the electrocardiographic T wave when changing parameters of the transmembrane action potential (AP) in the ischemic area for the purpose of increasing an information content of diagnostic algorithms. In the course of our work, we were also developing a method for segmentation of the model heart and a method for determination of the partial contribution of any segment, including "ischemic" segments, into the potential of the modelled ECG.

2. Methods

Computer experiments were executed on a system for 3D-modelling of the cardiac electrical activity with the aid of our model of ECG genesis [1]. The parameters of the model are electrophysiological, anatomical, and biophysical characteristics of the heart muscle. The current implementation of the model is presented in [2].

For modelling of the emergence and development of any pathology it is necessary to describe characteristic changes occurring in the heart muscle within the space of parameters of the chosen model. In the case of myocardial ischemia – these are mainly characteristics of the AP within the limits of its various phases. Initially (conditionally "normal") durations of AP on the outer and inner surfaces of the electrically active myocardium were chosen to 250 and 300 ms respectively. A change of AP characteristics relative to a model-accepted "conditional

norm” were treated as a degree of intensity of ischemia. Please note that we are discussing the “internal” intensity as a degree of change in the electrophysiological state of myocardium, as distinct from “external” intensity, i.e. the degree of influence of ischemia on the ECG, which presents itself in the given case as an object of investigation.

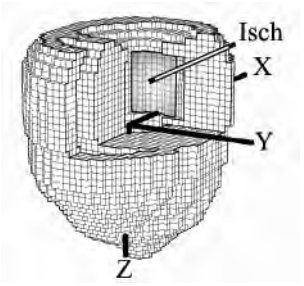

During modelling of an ischemic region of myocardium its localization was chosen on the inner surface of the free wall of the left ventricle. The expanse of the subendocardial zone of lateral Isch constituted 80 msu (model space unit) cubic elements with an edge of 2 mm, in the first experiments which corresponds approximately to 10% of the total surface of endocardium in the left ventricle for the model of small resolution (Fig. 1).

Fig. 1. Incision in the simulated ventricles, which consist of tightly packed elements msu (model space unit) of "Myocardium", "His" and "Purkinje" types. Shown is an “ischemic” area (Isch) on the endocardial surface of the left lateral wall.

For a rough estimate of tendencies of change in T-wave shape, at the first step of computer experiments, along with an AP close to a real shape, use was made also of a simplified trapezoidal approximation (Fig. 2): after an instant jump of potential there followed a plateau phase (phase 2) and a phase of fast repolarization (phase 3). For such an approximation some variants of change of model AP in the two phases were considered. For each of the variants, we conducted a set of computer experiments, in which for corresponding, step by step, changes of AP we obtained model ECGs and then “measured” their repolarization parameters. Temporal and amplitude parameters of AP phases were changing in the experiment with steps of 25 ms and 20 mV respectively. For checking hypotheses emerging in the process of modelling we used our data base (DB) of real ECGs, from which samples “Norm” and “Ischemia” were obtained.

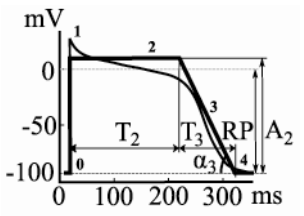

Fig. 2. Transmembrane action potential (phases 0, 1, 2, 3, 4) and its trapezoidal approximation (resting potential RP; phase of plateau 2 with duration T_2 and amplitude A_2; phase of fast repolarization 3 with duration T_3 and slope α_3).

3. Results and Discussion

Method of segmentation

An important result of the work in a methodological aspect appeared as development of a method for segmentation of the model heart into separate segments for coordinate binding of a “focus of ischemia” to geometry of the model by the type of representation for a tomographic image of the heart [3] (in our case, the heart is divided into segments in each of four macro-layers (basal, mid, apical, and apex)) along its own longitudinal axis. The left ventricle is divided into 17 sectors. In 16 sectors there are inner (endo) and outer (epi) surfaces, in the apex (17th sector) – only an outer one. Two more surfaces belong to the right ventricle. In total we obtained 35 surfaces for the entire model heart [3].

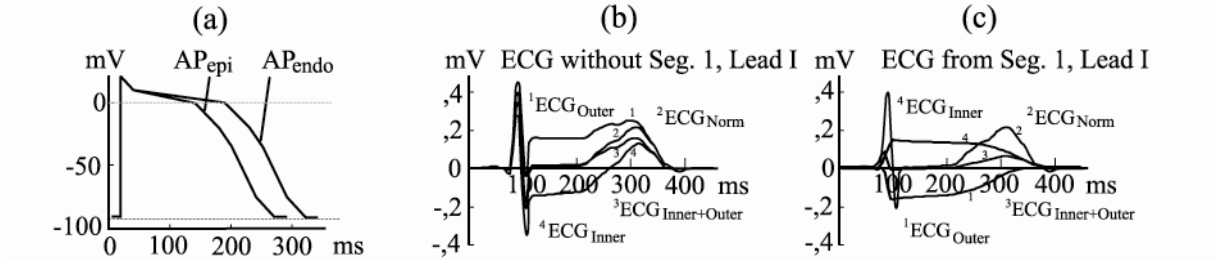

Fig. 3. Example using the joint methods of segmentation and partial contributions. For APs, specified on epicardium and endocardium (a), shown are normal ECG (ECG_{Norm}) and different variants of partial "ECG" with and without participation of outer and inner surfaces of the segment 1 (b and c).

In the simplest case, when modelling ECG curves, all msu-elements belonging to each of the surfaces constitute one compartment and work through upon excitation as one and the same variant of the AP.

Method of partial contributions

A method for calculation and visualization of the partial contribution of any segment, including "ischemic" ones, into the potential of the chosen ECG lead was also developed and used in the given work. As an example of using the joint methods of segmentation and partial contributions, in Fig. 3 two forms of AP (a), specified on the epicardium and endocardium, shown against the background of conditionally normal ECG (ECG_{Norm}) demonstrate different variants of partial "ECG" in lead I with and without participation of outer and inner surfaces of the segment 1 (b and c).

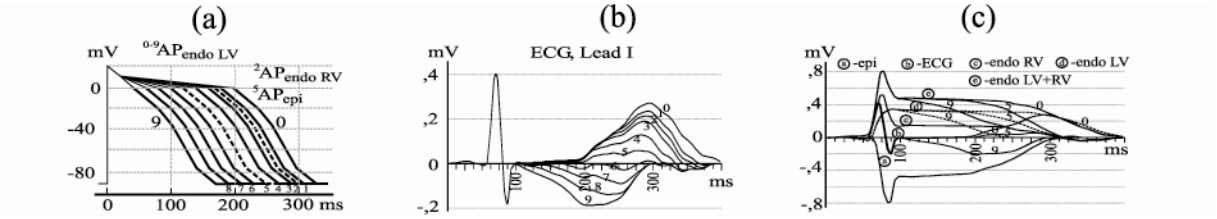

Fig. 4. Changing duration of the plateau phase in computer experiment for a close-to-original AP shape (a) and corresponding alterations of the T wave and ST segment (b), as well as patterns of the partial curves (c).

Modelling and analysis of changes in the ST-T interval of ECG

For original shape (Fig. 4a) and for trapezoidal approximation (Fig. 5, first row, curves "0") of the AP form the following four variations for changing parameters were used (Fig. 5): (a) modification of duration of the horizontal plateau phase at the constant slope of the phase 3; (b) change in the amplitude of the plateau phase at the constant durations of this phase and the whole of the AP; (c) modification in the slope of the fast repolarization phase at the constant duration of the plateau phase; (d) reduction in the duration of phase 2 at constant AP duration.

We studied (outside of scenarios developed formerly) the separate effects caused by changing these parameters (see, for instance, Fig. 4a for duration of the plateau phase) on alterations of the T wave and ST segment (Fig. 4b), as well as patterns of the partial curves (Fig. 4c). With the aid of a special program for model cardiosignals obtained we have conducted "medical" evaluation of changes in the ST-T interval in terms of the Minnesota Code and have "measured" and calculated model parameters of ECG, analogous to parameters of the real ECG, both generally accepted and newly developed (see [4] for full details).

The character of changes for the simplified shape of AP, modeled in the ischemic area, and generalized results of their influence on some parameters of the repolarization part of the cardiocycle are compiled in the matrix-picture (Fig. 5), where the columns (a, b, c, d) pertain to specified variants of changing AP, while the rows demonstrate considered changes in the AP shape for each columns (1st row), changes of the ST-T pattern in lead I (2nd row) and so on – alteration of some ECG parameters in the same lead as functions of stepwise changes of the AP parameter being the main given variant of the computer experiment.

At the chosen anatomical position of the model heart and localization of the Isch zone perceptible changes in the shape of the T wave were observed in frontal leads (except lead III), and also in leads V_3, V_4, V_5. The most sensitive parameters of ECG in this case turned

out to be β_T (ratio of maximal absolute values of the derivatives at the left and right of the T wave apex), G (scalar interpretation of the ventricular gradient), and ssST80 (shift of the ST segment at time moment removed by 80 ms from J point).

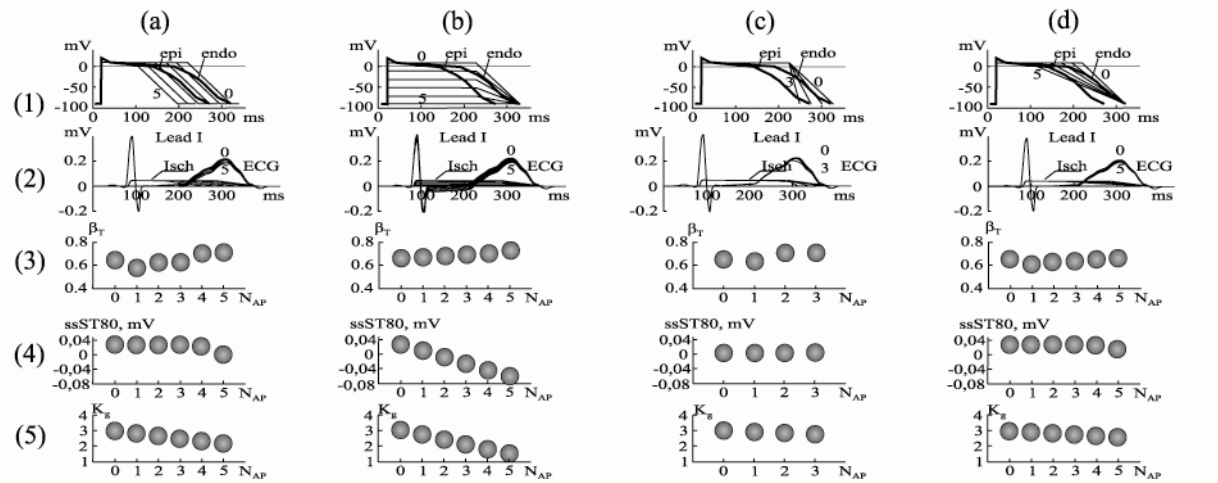

Fig. 5. Generalized results of the computer experiment for the trapezoidal AP. Columns pertain to specified variants (a, b, c, d) of changing AP. The rows demonstrate considered changes in the AP shape (1st row), changes of the ST-T pattern (2nd row) and so on – alteration of some ECG parameters as functions of stepwise changes in the corresponding AP parameter.

As a result of analysis we proposed a K_g parameter, which represents a ratio of areas, determined with or without taking into account the sign of signal, under the ECG curve on QRS and JT intervals. The K_g behavesmore regularly than G and appears, as shown by investigations on real ECGs, more stable in conditions of practical measurements.

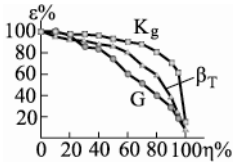

Fig. 6. Calculated values of sensitivity ε at different specified values of specificity η for three tested parameters (G, β_T, K_g) of ECG description in a diagnostic threshold type algorithm

For parameter K_g, the sensitivity ε and specificity η of the following algorithm (Alg: {If $K_g \leq$ some chosen threshold, then → "Ischemia"}) were counted for samples "Norm" and "Lateral ischemia" from the DB of real ECGs. In Fig. 6 for several chosen values of η we show for comparison the calculated values of ε in algorithms of a similar kind for the three parameters mentioned above (G, β_T, K_g).

Results presented at this stage of the work are interesting for the identification of the cardiac electrophysiological state. Further systematic comparative investigations on the basis of modelling ischemia of various localization, expanse and degree of intensity are necessary.

References

[1] Baum OV. Transmembrane potential and genesis of electrocardiogram: physical - mathematical model. In proceedings of the Symposium Biophysics of membranes. Babsky EB, Editor. Kaunas Medical Institute Press, Moscow-Kaunas, 1969, 32-35.

[2] Baum OV, Voloshin VI, Popov LA. Biophysical models of the heart electrical activity. *Biofizika*, 2006; 51(6): 1069-1087.

[3] Cerqueira MD, et al Standardized Myocardial Segmentation and Nomenclature for Tomographic Imaging of the Heart A Statement for Healthcare Professionals From the Cardiac Imaging Committee of the Council on Clinical Cardiology of the American Heart Association. Circulation, 2002; 105: 539-542

[4] Baum OV, Voloshin VI, Popov LA. Electrocardiographic Image of Myocardial Ischemia: Real Measurements and Biophysical Models. Part II. *Biofizika*, 2012; 57(5), 860-869.

IMPROVED EASI ECG MODEL AS A RESULT OF USING VARIOUS REGRESSION AND MACHINE LEARNING TECHNIQUES

[1]W. Oleksy, [2]E. Tkacz, [2]Z. Budzianowski

[1]Institute of Informatics, Faculty of Automatic Control, Electronics and Computer Science, Silesian University of Technology, Gliwice, Poland
[2]Institute of Electronics, Faculty of Automatic Control, Electronics and Computer Science Silesian University of Technology, Gliwice, Poland
Email: wojciech.oleksy@polsl.pl

Abstract. *The main idea of this study was to increase efficiency of the EASI ECG method introduced by Dover in 1988 using various regression techniques. EASI was proven to have a high correlation with the standard 12 lead ECG. In addition, it is less susceptible to artefact, increases the mobility of patients and is easier to use due to a smaller number of electrodes. Linear Regression, Artificial Neural Network, Support Vector Regression, Pace Regression, Least Median of Squares Regression, Gradient Boosting and Isotonic Regression methods were used to improve the quality of the 12-lead electrocardiogram derived from four (EASI) electrodes.*

Keywords: EASI, ECG, Linear Regression, Artificial Neural Network, Support Vector Regression.

1. Introduction

In 1988 Dower and his team introduced the EASI ECG system, which derives a standard 12 lead ECG using only 5 electrodes. The E electrode is on the sternum while, the A and I electrodes are at the left and right mid-auxiliary lines, respectively. The S electrode is at the sternal manubrium. The fifth electrode is a ground electrode and is typically placed on one or the other clavicle, see Fig. 1. EASI was proven to have a high correlation with the standard 12 lead ECG, as well as with the Mason-Likar 12-Lead ECG. Besides that, it is less susceptible to artefact, it increases the mobility of patients, it is easier and faster to use due to the smaller number of electrodes. What is more, the smaller number of electrodes reduces the cost of a device.

The electrodes are positioned over readily identified markers which can be located with minimal variability, independent of the patient's physique, assuring high repeatability. The electrode placement allows the chest to be largely unencumbered, allowing physical or imaging examination of the heart and lungs without the need for removing the electrodes.

Problem description

In the classical approach introduced by Dower, using the EASI lead configuration, 3 modified vectorcardiographic signals are recorded from the following bipolar electrode pairs:

– A-I (primarily X, or horizontal vector component)

– E-S (primarily Y, or vertical vector component)

– A-S (containing X, Y, Z, the anterior-posterior component)

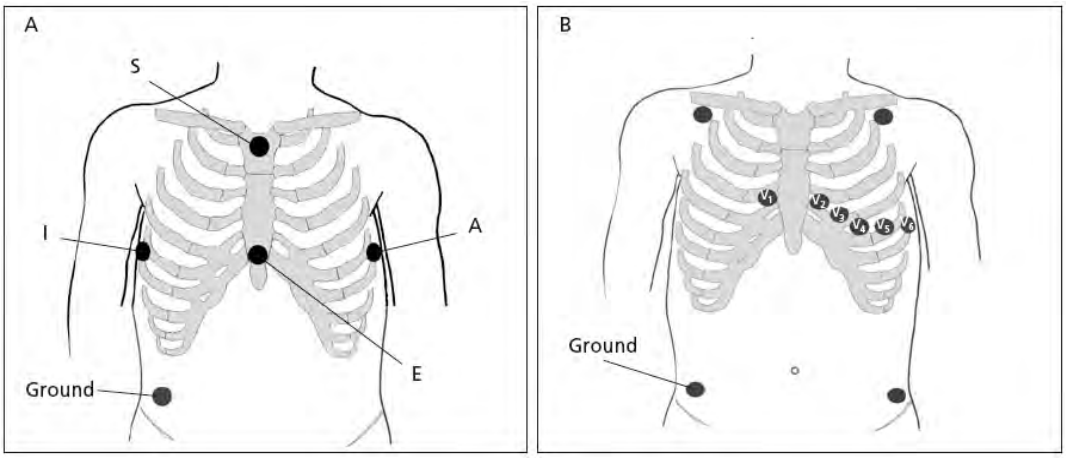

Fig 1. A. The electrode positions of the EASI lead system. B. The Mason-Likar modification of the electrode positions for the 12 lead ECG system.

Each of the 12 ECG leads is derived as a weighted linear sum of these 3 base signals using the following formula:

$$L_{derive} = a(A–I)+b(E–S)+c(A–S)$$

Where L represents any surface ECG lead and a, b, and c represent empirical coefficients. These coefficients, developed by Dower, are positive or negative values, accurate to 3 decimal places, which result in leads very similar to standard leads. Our idea on how to improve EASI ECG performance was to find a new model used for 12 ECG leads calculation. To do that we treated the system as a black box with 4 input variables: E, A, S, I and 12 output variables: I, II, III, aVR, aVL, aVF, V1, V2, V3, V4, V5 and V6 using various regression techniques to build a model.

2. Methods

Our work was focused on improving the Dower model by using some regression and machine learning techniques to obtain a new EASI model and as a result improve the EASI method. Seven different regression methods were tested to find a best fitting model, namely Linear Regression, Artificial Neural Network, Support Vector Regression, Pace Regression, Least Median of Squares Regression, Gradient Boosting and Isotonic Regression.

3. Results

Each model calculation was 10 fold cross validated. All results are based on data from PhysioNet database and also on artificial data. Calculated models were compared with results obtained using the classical Dower approach and also with Improved EASI Coefficients described in the paper “Improved EASI Coefficients: Their Derivation, Values, and Performance” by Dirk Q. Feild, Charles L. Feldman, and B. Milan Horacek. To determine performance of all systems, for each of them root mean squared error (Table 1) was calculated. Sample plot obtained for all models is shown in Fig 2.

Table. 1 RMSE comparison for all 12-leads.

	aVF	aVL	aVR	I	II	III
Obtained model	27.45	22.02	16.03	18.01	26.13	31.41
Dower model	28.41	35.45	31.86	40.75	32.57	37.19
Another test model	66.29	34.22	55.30	42.47	78.20	60.03
	V1	V2	V3	V4	V5	V6
Obtained model	21.01	40.54	46.62	55.60	24.66	10.77
Dower model	99.24	177.75	120.25	144.60	119.93	93.17
Another test model	86.42	119.61	141.69	129.96	49.90	33.10

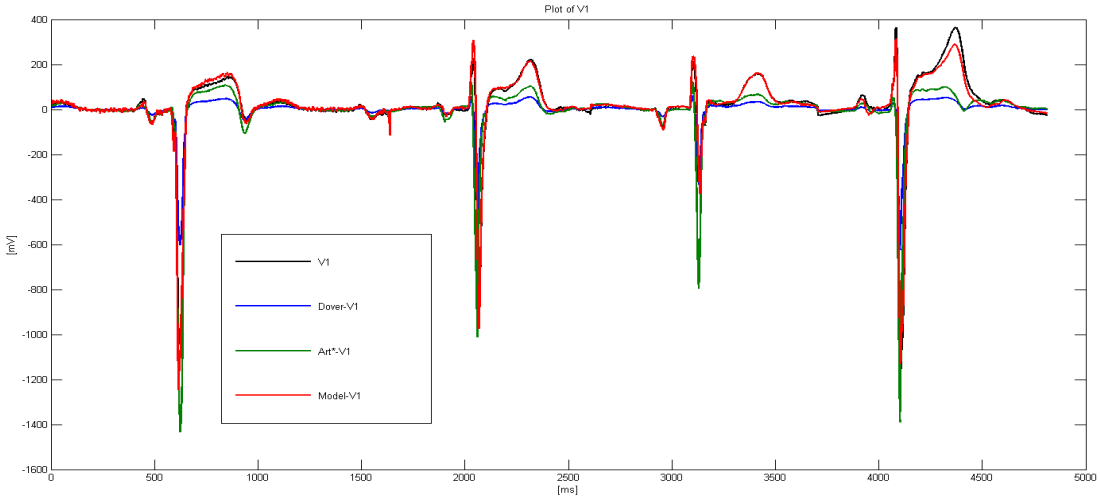

Fig 2. Plot of V1 signal measured using standard ecg method, derived using the EASI ECG method developed by Dower, improved EASI ECG method (art*) and regression based EASI ECG method. V1 = black; Dower V1 = blue; Art* V1 = green; Model V1 - red.

4. Conclusions

The results above show that the best performance was obtained for the linear model built using regression techniques. The second best performance model was one created by Dower. Surprisingly low performance was observed for the model that uses improved EASI coefficients. Further work in the topic of improving EASI ECG coefficient using various regression techniques should be continued.

Acknowledgements

This work was supported by the European Union from the European Social Fund (grant agreement number: UDA-POKL.04.01.01-00-106/09)

References

[1] Dower GE, Yakush A, Nazzal SB, Jutzy RE, Ruiz CE. Deriving the 12-lead electrocardiogram from four (EASI) electrodes. *J Electrocardiol*, 1988; 21(suppl): S182-S187.

[2] CL Feldman, G MacCallum, LH Hartley. Comparison of the Standard ECG with the EASIcardiogram for Ischemia Detection During Exercise Monitoring *J Facts* 1991; 21:201-9.

[3] Klein MD, Key-Brothers I, Feldman CL. Can the vectorcardiographically derived EASI ECG be a suitable surrogate for the standard ECG in selected circumstances? In Computers in Cardiology. IEEE Computer Society Press, Piscataway, NJ: 1997; 721-724.

[4] Chantad D, Krittayaphong R, Komoltri C. Derived 12-lead electrocardiogram in the assessment of ST-segment deviation and cardiac rhythm. *Journal of Electrocardiology*, 2006; 39: 7 – 12.

[5] Drew BJ, Pelter MM, Wung SF, Adams MG, Taylor C, G. Evans T, Foster E. Accuracy of the EASI 12-Lead Electrocardiogram Compared to the Standard 12-Lead Electrocardiogram for Diagnosing Multiple Cardiac Abnormalities. *Journal of Electrocardiology*, 1999; 32: S.

[6] Welinder A, Sfrnmo L, Feild DQ, et al. Comparison of signal quality between EASI and standard Mason-Likar 12-lead electrocardiograms during physical activity. *Am J Crit Care*, 2004; 13: 228.

[7] Dower GE. EASI 12-Lead Electrocardiography. Totemite Publishers, Point Roberts, WA,1996.

[8] G. Cybenko. Approximations by superpositions of sigmoidal functions. *Mathematics of Control, Signals, and Systems,*1989; 2: 303-314.

[9] Smola AJ, Scholkopf B. A Tutorial on Support Vector Regression. 2003.

[10] Wang, Y, Witten I.H. Pace Regression. 1999 (Working paper 99/12). Hamilton, New Zealand: University of Waikato, Department of Computer Science.

[11] Feild DQ, Feldman CL, Horacek BM. Improved EASI Coefficients: Their Derivation, Values, and Performance. *Journal of Electrocardiology* , 2002; 35 Suppl: 22-33.

MODELLING OF PRESYMPTOMATIC AND SYMPTOMATIC STAGES OF PARKINSONISM IN MPTP-TREATED MICE: HEART CONTRACTION, ADRENERGIC REGULATION AND CATECHOLAMINES CONTENT IN BLOOD

[1,4]R.R. Nigmatullina, [1]T.S. Fedoseeva, [2]G.R. Khakimova, [2,3]V.S. Kudrin, [1]S.N .Zemskova, [2]M.V. Ugrumov

[1]Kazan State Medical University, Kazan, Russia;
[2]Institute of Developmental Biology RAS, Moscow, Russia;
[3]Institute of Pharmacology RAMS, Moscow, Russia;
[4]Kazan (Volga region) Federal University, Kazan, Russia.
Email: razinar@mail.ru

Abstract. *Parkinson's disease (PD) is characterized by a long-term development at the preclinical stage. The testing of peripheral manifestations of the systemic pathology might be useful for a preclinical diagnosis of PD, and the peripheral markers should be sought in Parkinsonian animals at the pre-symptomatic (PSS) and the early symptomatic stage (ESS). The goal was to evaluate the catecholaminergic regulation of the heart. PSS and ESS models of Parkinsonism were recently developed. The left ventricle (LV) contraction force was not changed at the PSS compared to the control, whereas a norepinephrine (NE) stimulating effect on its contraction increased significantly. Conversely, at the ESS, contraction of the LV decreased and was accompanied by a decrease of a noradrenaline (NA) effect. Transition of the PSS to the ESS was manifested by the development of heart failure as well as by an increase of the NA in plasma.*

Keywords: Parkinson's Disease, Heart Contraction, Adrenergic Regulation, Model of Parkinsonism, Mouse

1. Introduction

Parkinson's disease (PD) is an incurable, chronic neurodegenerative disease that is linked with the death of DA-ergic neurons in the nigrostriatal system of the brain. Parkinson's disease can occur without symptoms for twenty to thirty years, i.e. in the preclinical stage, due to the inclusion of the brain plasticity mechanism, designed to compensate for the functional failure of degenerating DA-ergic neurons. Only after the death of the majority (70-80%) of neurons and the exhaustion of compensatory mechanisms the first symptoms appear and the disease enters the relatively short clinical stage, which ends with death or disability of the patient. PD is a systemic disease, and in PD patients a sympathetic denervation of the heart occurs [1]. Lewy bodies and alpha-synuclein-positive neurons were identified in the heart of PD patients, suggesting the involvement of post-ganglionic sympathetic and intracardiac neurons in the PD process [2]. Vagal baroreflex heart failure and cardiac sympathetic denervation in patients with Parkinson's disease may occur before the onset of motor disorders [2]. PD leads to the deficit of adrenergic innervation, which may play an important role in the myocardial fibrosis mechanism due to changes of the responsiveness to adrenoreceptor agonists. Sympathetic dysfunction is also observed in mice injected with the 1-methyl-4-phenyl- ,2,3,6-tetrahydropyridine (MPTP), which was shown in the modelling of clinical stages of the PD [4]. However, data regarding the changes of the myocardial contractility and its adrenergic regulation at the pre-symptomatic and early symptomatic stages of Parkinson disease are absent.

This article presents the results of determination of atrial and ventricular myocardial inotropic function responses to the norepinephrine, as well as data on the norepinephrine concentration in the blood of mice in an experimental model of the pre-symptomatic and early symptomatic stages of the Parkinson's disease.

2. Methods

MPTP reproduces almost all of the most essential characteristics of Parkinson's disease [3]. Pre-symptomatic and early symptomatic stages of PD were reproduced by two-fold and four-fold neurotoxin MPTP injections at a dose of 12 mg / kg [5]. The study was performed on male mice C57BL line / 6 aged 2.5-3 months, weighing 22-26 g. Three groups of 8 mice each were created: two groups characterized by different developmental stages of Parkinsonism, one group served as a control (injection of the saline solution). The myocardial inotropic function of the atria and ventricles was studied using the force sensors MLT 050 / D, and ADC PowerLab MLA410 (IDInstruments). For this task the following parameters were determined: the amplitude, duration of contraction and relaxation, the total contraction time, the velocity of the contraction and relaxation. Due to the fact that in patients with PD, the failure of heart adrenergic innervation was shown, one of the tasks of our study was to determine the response of cardiomyosytes to the norepinephrine in concentrations of 0.1, 1.0, and 10 mM / l. The concentration of catecholamines in blood was determined by high performance liquid chromatography (HPLC) with electrochemical detection. Results were statistically processed, and the significance of differences was estimated by the t- Student’s test.

3. Results

At the presymptomatic stage of Parkinson's disease there was no significant change in the concentration of epinephrine, norepinephrine and dopamine in the mice blood plasma (Fig.1). During the transition from the presymptomatic to the early symptomatic stage of Parkinson's disease the plasma concentration of NE increased by 46% and epinephrine - by 44%, while the level of dopamine tripled, which may be caused by the dysfunction of the catecholamines’ degradation enzymes, or increased catecholamine synthesis which serves as a compensatory reaction.

At the presymptomatic stage of PD there is no significant change of the left ventricular weight, while the early symptomatic stage of PD showed the decreasing of the left ventricle weight by 19% when compared with the controls.

At the presymptomatic stage of Parkinsonism, the force of left ventricle contraction does not change significantly, but myolysis of individual cardiomyocytes was revealed on the histological slices. It should be noted that while the contraction time characteristics are already changing at the presymptomatic stage, the contraction and relaxation duration decrease compared with the control, while at the early symptomatic stage significant decreasing of the left ventricular contraction force was revealed with synchronous decreasing of the contraction duration.

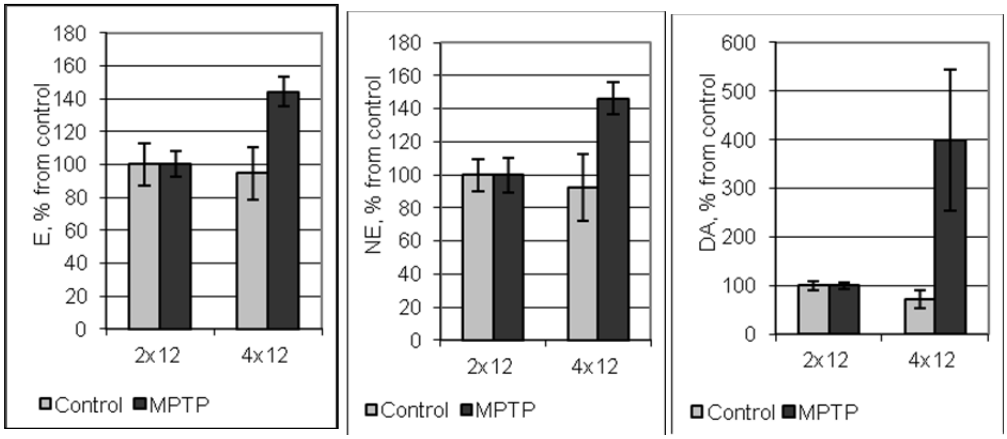

Fig. 1. The changing of catecholamines concentration in mice plasma at presymptomatic (2 x 12) and early symptomatic (4 x 12) stages of the Parkinsonism.

At the presymptomatic stage of Parkinsonism, the response of the left ventricle to 1 mM and more of norepinephrine was three times higher than in the control. However, at the early symptomatic stage of PD, the left ventricular myocardial contractile force decreased in response to the 0,1 mM NE by 66,0%, and to the 1 and 10 mM by 53,6% and 84,0% respectively. It was found that, in the control, NE increased the myocardial contraction force.

4. Discussion

Parkinson's disease is a systemic neurodegenerative disease, in which not only dopaminergic neurons die in the brain, but also degeneration of adrenergic neurons innervating the heart occurs. Adrenergic denervation of the heart, revealed by scintigraphy, develops in patients with PD for 5to 6 years before clinical manifestation of the disease [1, 2]. Neurotoxin MPTP produces almost all of the most important characteristics of Parkinson's disease and is used to simulate the onset of the clinical stage of PD [4]. The models of presymptomatic and early symptomatic stages of Parkinson's disease with the use of MPTP were elaborated in the laboratory of academician M.V. Ugrumov [5]. In our study, it was necessary to identify the changes in adrenergic regulation of the inotropic myocardial function during the transition from the presymptomatic to the early symptomatic stages of PD. After Parkinsonism simulation by MPTP administration, oxidative stress was observed, associated with mitochondrial dysfunction [6], which can lead to heart failure due to fibrosis and hypertrophy /malnutrition of the myocardium. It was found, that at the presymptomatic stage of PD the force of left ventricle contraction does not change significantly, but the myocardial response to norepinephrine increased, reflecting the beginning of sympathectomy of the myocardium. It should be noted that at this stage of PD, changes in the humoral part of adrenergic regulation were not expressed, i.e. the norepinephrine, epinephrine levels were not changed. At the early stages of symptomatic Parkinsonism the reverse, opposite effect of norepinephrine on the strength of the left ventricle contraction was found – the strength is reduced. We have shown that at the early symptomatic stage, the levels of norepinephrine, epinephrine and dopamine in the blood significantly increased. The increasing concentration of catecholamines in the blood is a consequence of sympathectomy and can be explained by adrenal hypertrophy and the release of a large amount of catecholamines into the blood. Such changes in the adrenal glands and the concentration of catecholamines in the blood have been proved in classical models of sympathectomy. It is likely that we have identified the negative inotropic effect of norepinephrine in animals at an early symptomatic stage of Parkinson's disease, which can be explained by the replacement of the G-protein subunits of metabotropic adrenoceptor-Gs by another - Gi, as it was revealed for beta-adrenergic receptors in heart

failure. It is well known that the inhibitory G protein subunit triggers the negative effect of the receptor agonists. It is also possible that at high concentrations of catecholamines in the blood at this PD stage, adrenoceptor desensitization occurs. Therefore, we found a significant alteration in the adrenergic regulation of myocardial contractility in the transition from the presymptomatic to the early symptomatic stage of Parkinson's disease, which is comparable with findings in studies on chronic heart failure.

5. Conclusions

Our studies have shown that the model of presymptomatic and early symptomatic stages of PD reflects the changes in adrenergic regulation observed in patients at the preclinical stage of the disease. It is possible to investigate the molecular-cellular mechanisms of neurodegeneration, which characterize PD, in the cardiovascular system. This approach will allow us to identify and to substantiate the validity of peripheral markers for the diagnosis of the preclinical stage of PD. The prerequisites are elaborated for the preclinical diagnosis, the approbation of pharmaceutical products for the preventive treatment of PD.

Acknowledgements

This study was supported by (a) the Program of the Presidium of RAS "Fundamental science for medicine" project "Presymptomatic and early symptomatic stages of Parkinsonism: compensatory processes in the brain and neurodegeneration on the periphery", (b) the grant RFBR 12-04-01219 "Monoaminergic regulation of the heart functions in the model of the presymptomatic and early symptomatic stages of Parkinsonism", (c) the grant “Leading Scientific School” 4670.20124 “Molecular mechanisms intra- and extracellular signalling in excitable tissues in norm and pathology“.

References

[1] Goldstein DS. Dysautonomia in Parkinson's disease: neurocardiological abnormalities. *Lancet Neurol.*, 2003; 2(11): 669-76.

[2] Goldstein DS. Cardiac denervation in patients with Parkinson disease. *Cleve Clin J Med*., 2007; 74 Suppl 1: S91-4.

[3] Nakahara T, Yamamoto T, Endo K, Kayama H.. Neuronal ectopic expression of tyrosine hydroxylase in the mouse striatum by combind administration of 1-methyl-4-phenyl-1,2,3,6-tetrahydropyridine and 3-nitropropionic acid. *Neuroscience* 2001; 108: 601-610.

[4] Ren J, Porter JE, Wold LE, et al. Depressed contractile function and adrenergic responsiveness of cardiac myocytes in an experimental model of Parkinson disease, the MPTP-treated mouse. *Neurobiol Aging*, 2004; 25(1): 131-8.

[5] Ugrumov MV, Khaindrava VG, Kozina EA, et al. Modeling of presymptomatic and symptomatic stages of parkinsonism in mice. *Neuroscience*, 2011;5: 181: 175-88.

[6] Usha R, Muralikrishnan D, Thomas B, et al. Region-specific attenuation of a trypsin-like protease in substantia nigra following dopaminergic neurotoxicity by 1-methyl-4-phenyl-1,2,3,6-tetrahydropyridine. *Brain Res.* 2000; 882(1-2): 191-5.

4. Signal Processing

FEATURE EXTRACTION OF ECG SIGNAL USING SUPPORT VECTOR MACHINE

[1]I. Saini, [2]V. Kumar, [1]A. Khosla

[1]Dept. of Electronics & Communication Engineering, Dr B R Ambedkar National Institute of Technology Jalandhar, India
[2]Dept. of Electrical Engineering
Indian Institute of Technology, Roorkee, India
Email: indu.saini1@gmail.com

Abstract. *Identification and delineation of clinically important parameters such as occurrence, amplitude and duration of P, QRS-complex and T-wave of the electrocardiogram (ECG) to predict clinical conditions and for diagnostic purposes is well established. In this work, a Support Vector Machine (SVM), a classifier informed by statistical learning theory, has been successfully applied for locating the fiducial points along with their waveform boundaries. The algorithm was evaluated on two standard databases (i) CSE DS-3 (ii) QT and also on ECG dataset acquired using BIOPAC®MP100 in laboratory settings. The mean error and standard deviation of P-on, P-off, QRS-on, QRS-off and T-end were calculated as the average of the time difference between the algorithmic results and the referee cardiologist annotations. The delineation results of CSE and QT databases have been compared with the accepted two-standard deviation (2sCSE) tolerances as recommended by the CSE working party and were found to be well within tolerance limits.*

Keywords: ECG Delineation, Support Vector Machine, Feature Extraction, Classifier, Gradient

1. Introduction

The main objective of ECG signal analysis is to deliver accurate, fast and reliable estimation of parameters such as occurrence, amplitude and duration of the P, QRS and T-wave. Most of the clinically useful information in ECGs can be obtained from intervals, amplitudes, or wave morphology of the ECG. Therefore, the development of efficient and robust methods for automatic ECG delineation is a subject of major importance. During the past five decades, a number of computer programs have been developed for the automatic interpretation of cardiac disorders using ECG signals. However, the state of perfection is yet to be reached. All ECG computer analysis programs are basically composed of two parts. The first part deals with the accurate identification and measurement of the characteristic fiducial points of the ECG signal and the second part deals with diagnostic interpretation. In recent years, many algorithms have been developed for the detection and delineation of the ECG signal. Some of these algorithms are:

Martinez et al. [1] developed and evaluated a robust single-lead ECG delineation system based on Wavelet Transform (WT). Goutas et al. [2] presented a new algorithm based on digital fractional order differentiation for P and T-waves detection and delineation. Yan et al. [3] proposed a multiscale morphological derivative transform for the detection of fiducial points in the ECG signal. Andriao et al. in [4] developed an original Hidden Markov model approach for online beat segmentation and classification of ECGs. Mehta and Lingayat [5] presented the application of SVM for QRS detection in single and 12-lead ECGs using entropy and combined entropy criterion. Chauhan et al. [6] proposed an accurate and efficient

method for detection and delineation of QRS-complexes, P-waves and T-waves in the 12-lead ECG. Arzeno et al. [7] analyzed traditional first-derivative based squaring function and Hilbert transform-based methods for QRS detection. In [8], the authors have used WT based ECG delineator for detection of P, Q, R, S and T waves. Lin et al. [9] proposed Bayesian inference to represent a priori relationships among ECG wave components. The proposed strategy is evaluated on the annotated QT database.

In this paper, the SVM algorithm has been used for locating the fiducial points along with their waveform boundaries. Use of the SVM is a useful technique for data classification. In general, the classification task usually involves training and testing data which consist of some data instances. Each instance in the training set contains one target value and several attributes. The goal of SVM is to produce a model which predicts the target value of data instances in the testing set where only the attributes are given [10].

2. Overview of SVM

SVM is an algorithm of machine learning introduced by Vapnik, based on the structural risk minimization principle from statistical learning [11]. SVM is a method for finding a hyperplane in high dimensional space that separates training samples of each class which maximizes the minimum distance between that hyperplane and the training samples. SVM identifies those samples that are closest to the hyperplane and thus play a greater role in classifying a test sample. However classification rate is not very high when samples are close to the hyperplane. The training data samples along the hyperplanes near the class boundary are called support vectors and the margin is the distance between the support vectors and the class boundary hyperplanes. A decision plane is one that separates sets of objects having different class memberships [10]. The solution gives rise to the decision function of the form [10-11].

$$f(x) = \mathrm{sgn}\left[\sum_{i=1}^{l} y_i \alpha_i (x.x_i) + b\right] \qquad (1)$$

where α_i are Lagrange multipliers.

The accuracy of the SVM model is largely dependent on the selection of the kernel method applied. By replacing the inner product with kernel function the input data are mapped to a higher dimensional space that requires the construction of a separating hyperplane to maximize the margin. There are a number of kernel functions resulting in different kinds of SVMs with different performance levels. These include linear, polynomial and radial basis functions [11].

3. Methods

In this section, we describe the methodology of the proposed algorithms for the delineation of ECG signal using SVM classifier, for datasets, (i) CSE database and (ii) QT database and (iii) ECG data acquired using BIOPAC®MP100.Data Acquisition.

The 12-lead ECG records have been acquired from CSE data libraries. All the data of 10 second duration have been sampled at 500Hz. Here, CSE DS-3 dataset has been used for this work. The onsets and offsets of P, QRS and T of these beats have been analyzed by a group of cardiologists. The CSE committee has published measurement results of 25 of the records out of 125; hence the proposed algorithms have been evaluated only for 25 records. In the QT database, 30 out of 105 ECG recordings have been used for validation. Each one has a duration of 15 minutes and is sampled at 250Hz(http://www.physionet.org/cgi-bin/atm/ATM). Within each record, between 30 and 100 representative beats were manually annotated by cardiologists, who identified the beginning, peak and end of the P-wave QRS and T-wave. 30

records of Lead-II ECG data acquired using BIOPAC®MP100 our own laboratory have been used in this work for validation of algorithms for ECG delineation.

Signal Processing

In order to attenuate the noise present in the raw ECG, the acquired signal is passed through a band-pass filter which is composed of cascaded high-pass and low-pass filters. The band-pass filter reduces the influence of muscle noise, baseline wander, 50 Hz and T-wave interferences. Feature extraction is an essential element of any classification system. In this work, the gradient of the signal is used as feature vector, as any part of the signal which has an elevated slope will have a higher value of gradient. Thus, slope or gradient of the signal at every sampling instant is calculated and normalized. After feature extraction, the SVM classifier is trained with training data along with class labels. Here, a training matrix is formed, consisting of m training instances of n features. The number of training instances (m) is equal to the number of samples of selected portions of ECGs and (n) is the number of normalized gradient curves for respective data. If the training instance belongs to the QRS region the training label vector is set to 1 and if it belongs to a non-QRS region it is set to -1.

After training of SVM, 25 records of CSE database, 30 records of QT database and 30 records of locally recorded datasets are tested for the detection of the QRS-complex. The testing data is also formatted as per training data. Testing records picked from the QT database depends upon the number of annotated beats present in that particular record. Here, testing labels are not known, hence any random value can be used either 1 or -1 for SVM classifier. After testing, a train of 1's is obtained at the output of SVM classifier. Then this train of 1's is picked and by using their duration, the average pulse duration of 1's is evaluated. Those trains of 1's, whose duration turns out to be more than the average pulse duration are detected as QRS-complex and the other are discarded.

The starting instance of QRS-complex is depicted as QRS-onset and end point of QRS-complex is treated as QRS-offset point. QRS-complex duration has been calculated by using their onset and offset points. The R-peak is obtained from the raw ECG signal by detecting the absolute maximum in the predefined QRS-on and QRS-off locations. Heart rate is also determined after identifying all the R-peaks. The QRS-complexes obtained are removed from the ECG signal by replacing them with the baseline value.

The slope at every sampling instant of QRS less ECG signal is then calculated and normalized. The SVM is again trained and tested for T-wave as explained above respectively. The detected output of the classifier is the T-wave locations. The starting instance of T-wave is depicted as T-on and end point of T-wave is treated as T-end point. The T-peak is obtained from the raw ECG signal, by detecting the absolute maximum peak in the predefined T-on and T-end locations. QT-interval has been calculated from the onset point of QRS-complex and offset point of T-wave. The T-waves obtained are removed from QRS less ECG signal by replacing them with the baseline value. The slope at every sampling instant of ECG signal without QRS and T-wave is calculated and normalized.

The SVM is again trained and tested for P-wave as explained above, respectively and the detected output is the P-waves present in the signal. The starting instance of P-wave is depicted as P-onset and end point of P-wave is treated as P-offset point. The P-peak is obtained from the raw ECG signal, by detecting the absolute maximum peak in the predefined P-onset and P-offset locations. P wave duration is calculated by using onset and offset point of P-wave. PR-interval has also been calculated from onset of P-wave and onset of QRS-complex.

4. Results

An algorithm was developed for reliable detection of the QRS-complex. It then measures the fundamental ECG parameters by using the QRS location as a sharp time reference. The delineation performance of the proposed algorithm is validated using referees' annotations and the combined program median provided in CSE multi-lead measurement results [12]. The accuracies of five wave fiducial points (P-on, P-off, QRS-on, QRS-off and T-end) were evaluated using the proposed algorithm resulting in an average accuracy of 94.4% for CSE DS-3 database [13].

The mean (m) of five fiducial points is calculated as the average of the variation, taken as the time difference between the algorithmic results and the referee cardiologist annotations. Standard deviation in milliseconds (ms) is also calculated. The algorithm performance has been compared with other delineation algorithms which have been validated with the CSE database and also compared with the accepted two-standard deviation (2sCSE) tolerances as recommended by CSE working party as shown in last row of Table 1 [14]. The results show that standard deviations of the variation obtained with the proposed algorithm are well within the tolerance limits.

For further validation, QRS-complexes, P and T-wave peaks along with their onsets and offsets have been computed using 30 records from the QT database. For assessment of the accuracy of the algorithm, the computed instants have been compared with manually annotated instants available in the QT database. The mean and standard deviation of the differences between automatic detection and cardiologists' annotations are computed in order to quantify the performance of the ECG delineation algorithm. The performance of the proposed algorithm is compared with other delineation algorithms which have been validated with the whole QT database: Martinez et al., [1]; Jane et al., [18]. The results of Table 2 show that, in terms of standard deviation, the proposed algorithm has tolerances accepted by cardiologists and slightly outperform the other compared algorithms, when evaluated on the QT database.

Table. 1. Comparison of the delineation results using SVM algorithms on the CSE database

Method	P-on m±std(ms)	P-off m±std(ms)	QRS-on m±std(ms)	QRS-off m±std(ms)	T-end m±std(ms)
SVM Algorithm (25 records)	-0.16±4.2	-1.2±6.2	-1.8±5.8	0.4±6.0	2.6±10.4
Martinez *et al.*, 2004 [1]	-4.9±5.4	-1.0±6.4	1.3±6.3	5.8±10.9	1.3±21.8
Laguna *et al.*, 1994 [15]	1.0±7.9	-1.0±5.1	-2.1±7.4	-0.2±3.6	2.6±10.5
Chazal *et al.*, 1996 [16]	N/A	N/A	0.9±3.6	-0.6±7.1	N/A
Sahambi *et al.*, 1997 [17]	N/R±4.0	N/R±6.0	N/R±2.0	N/R±4.0	N/R±20.0
Tolerances (2_{sCSE})	10.2	12.7	6.5	11.6	30.6

N/A: Not Applicable, N/R: Not Reported

Table. 2. Comparison of delineation results using SVM algorithm on the QT database

Method	P-on m± std(ms)	P-off m± std(ms)	QRS-on m± std(ms)	QRS-off m± std(ms)	T-end m± std(ms)
Proposed Algorithm (30 records)	0.2±13.2	1.3±12.4	-1.4±7.6	4.2±8.6	2.7±17.2
Martinez *et al.*, 2004 (105 records) [1]	2.0±14.8	1.9±12.8	4.6±7.7	0.8±8.7	-1.6±18.1
Jane *et al.*, 1997 (105 records) [18]	14.0±13.3	-0.1±12.3	-3.6±8.6	-1.1±8.3	13.5±27.0
Tolerances (2_{sCSE})	10.2	12.7	6.5	11.6	30.6

For further verification, SVM algorithm has also been implemented on 30 recordings of 10-sec duration acquired using BIOPAC®MP100. The results of QRS duration, heart rate, QT-interval, P-wave duration and PR-interval using SVM algorithm are given in Table 3. The comparison of the value of heart rate computed by the proposed algorithm measurement results referred as 'Algo.' with the results estimated by the Acknowledge 4.0 Software of BIOPAC®MP100 referred as 'Soft.' has also been listed in Table 3. The value of five wave parameters given in Table 3, show that all the value are well within the normal limits as suggested by [19]. Thus the overall accuracy of the algorithm in the measurement of five wave parameters is 100%.

Table. 3. Summary of ECG analysis results of 30 records of BIOPAC®MP100 using SVM algorithm

Sr. No.	Record No.	Heart Rate		P-Duration	PR-Interval	QRS-Duration	QT-Interval
		Algo.	*Soft.*				
1	JAL 2001	79.51	79.15	94.6	152	85.6	300
2	JAL 2003	89.66	89.02	98.2	156	88.4	292
3	JAL 2004	82.06	82.87	86.4	150	80.6	296
4	JAL 2014	52.82	53.57	88.6	164.6	76.2	328
5	JAL 2015	79.21	78.12	90.2	160.2	82.6	314
6	JAL 2017	81.04	80.53	96.4	162	88.2	284
7	JAL 2018	68.20	68.02	84.2	170.5	80.4	340.5
8	JAL 2019	72.84	72.72	82.2	178	74.6	304
9	JAL 2020	61.35	61.34	92.4	134.8	88.8	330.6
10	JAL 2023	66.08	65.50	90.5	160	82.8	346.4
11	JAL 2025	73.21	73.26	94.2	154.4	88.6	338
12	JAL 2027	76.63	76.72	86.2	140.6	84.6	320
13	JAL 2029	75.59	75.56	90.6	150.5	88.2	308.8
14	JAL 2030	79.15	79.72	86.8	144	84.6	297.6
15	JAL 2031	75.02	74.90	74.8	166	70.6	314
16	JAL 2032	79.69	79.89	80.4	152	76.4	288
17	JAL 2035	81.63	80.97	82.6	148.2	78.4	320
18	JAL 2037	70.97	72.46	96.2	160.5	88.2	320.4
19	JAL 2039	68.41	69.50	87.4	170	84.6	336.4
20	JAL 2040	76.98	76.82	90.2	138	86.4	375.5
21	JAL 2045	87.37	86.20	84.2	126.4	82.8	306
22	JAL 2046	57.79	56.60	102.2	184	80.4	362.8
23	JAL 2124	75.78	76.04	95.6	158	99.6	296.5
24	JAL 2127	59.03	59.40	96.8	152.6	86.8	288.4
25	JAL 2128	79.48	79.36	96.0	148.8	88.0	314
26	JAL 2130	87.87	87.97	81.2	146	76.4	318
27	JAL 2131	74.47	73.98	86.3	132.6	82.6	330
28	JAL 2132	95.38	92.14	90.0	150.8	82.4	316.5
29	JAL 2133	85.15	84.15	100.4	148	92.2	300.7
30	JAL 2134	67.74	67.18	80.2	150	78.6	324

5. Conclusions

The P and T-wave is the most important feature of the ECG after the QRS-complex. In general, the automated disease diagnostic is being carried out by observing limits of the ECG parameters. Therefore, the reliability of the disease diagnosis is totally dependent on accuracy of the ECG parameter estimates. The method which is presented here for ECG wave delineation is efficient, simple and easily adaptable to different ECG wave morphologies. The proposed algorithm has been validated on two standard ECG databases and ECG records acquired in laboratory settings. The statistical parameters, i.e., mean and standard deviation

have been computed for both the standard databases and compared with tolerance limits given by the CSE working party.

References

[1] Martinez JP, Almeida RS, Olmos S, Rocha AP and Laguna P. A Wavelet-based ECG delineator: Evaluation on standard databases. *IEEE Transactions on Biomedical Engineering*, 2004; 51 (4): 570–581.

[2] Goutas A, Ferdi Y, Herbeuval JP, Boudraa M, Boucheham B. Digital fractional order differentiation-based algorithm for P and T-waves detection and delineation. *ITBM-RBM*, 2005; 26: 127–132.

[3] Yan S, Chan KL and Krishnan SM. Characteristic wave detection in ECG signals using morphological transform. *BMC Cardiovascular Disorders*, 2005; 5 (28).

[4] Andreao RV, Dorizzi B, and Boudy J. ECG signal analysis through hidden markov models. *IEEE Transactions on Biomedical Engineering*, 2006; 53(8): 1541-1549.

[5] Mehta SS and Lingayat NS. Comparative study of QRS detection in single lead and 12-lead ECG based on entropy and combined entropy criteria using support vector machine. *Journal of theoretical and applied information technology*, 2007; 3(2): 8-18.

[6] Chouhan VS and Mehta SS. Threshold-based detection of P and T wave in ECG using new feature signal. *International Journal of Computer Science and Network Security*, 2008; 8(2): 144–152.

[7] Arzeno NM, Deng ZD, and Poon CS. Analysis of first-derivative based QRS detection algorithms. *IEEE Transactions on Biomedical Engineering*, 2008; 55(2): 478-484.

[8] Dumont J, Hernandez A I and Carrault G. Improving ECG beats delineation with an evolutionary optimization process. *IEEE Transactions on Biomedical Engineering*, 2010; 57(3): 607-615.

[9] Lin C, Mailhes C, and Tourneret JY. P- and T-wave delineation in ECG signals using a bayesian approach and a partially collapsed gibbs sampler. *IEEE Transactions on Biomedical Engineering*, 2010; 57(12): 2840-2849.

[10] Vikramaditya J. Tutorial on Support Vector Machine (SVM). School of EECS, Washington State University, Pullman, 2010.

[11] Vapnik V. The nature of statistical learning theory. New York: Wiley, 1988.

[12] Saini I, Singh D and Khosla A. P- and T-wave delineation in ECG signals using support vector machine. *IETE Journal of Research*, 2013 (Accepted for publication).

[13] Willems JL, Arnaud P, van Bemmel JH et al. A reference data base for multilead electrocardiographic computer measurement programs. *Journal American College Cardiology* 1988; 10: 1313-21

[14] Willems JL. Recommendations for measurement standards in quantitative electrocardiography. *European Heart Journal*, 1985; 6 (10): 815-825.

[15] Laguna P, Jane R and Caminal P. Automatic detection of wave boundaries in multilead ECG signals: Validation with CSE database. *Computers and Biomedical Research*, 1994; 27(1): 45-60.

[16] Chazal P de and Celler B. Automatic measurement of the QRS onset and offset in individual ECG leads. Presented at the 18th Annual International Conference IEEE Engineering in Medicine and biology Society, Amsterdam, The Netherlands, 1996;. 1399-1400.

[17] Sahambi JS, Tandon SN and Bhatt RKP. Using wavelet transforms for ECG characterization - An on-line digital signal processing system. *IEEE Engineering in Medicine and Biology*, 1997; 16(1): 77-83.

[18] Jane R, Blasi A, Garcia J and Laguna P. Evaluation of an automatic detector of waveforms limits in holter ECG with the QT database. Computers in Cardiology, Los Alamitos, CA: *IEEE Computer Society Press*, 1997; 24: 295–298.

[19] Yanowitz FG. Introduction to ECG interpretation V8.0. July 2012.

INVESTIGATION OF INTERRELATION BETWEEN HEART RATE AND BLOOD PRESSURE USING WAVELET TRANSFORM COHERENCE

[1]K. Rajinder, [2]S. Dilbag

[1]Sant Longowal Institute of Engineering and Technology, Longowal, Punjab, India
[2]Dr. B. R. Ambedkar National Institute of Technology, Jalandhar, Punjab, India
Email: rk_nandra2002@yahoo.co.in

Abstract. *Coherence analysis is an efficient tool for assessing the existence and strength of linear coupling between cardiovascular signals in the frequency domain.. The continuous wavelet transform is specifically efficient in the analysis of transient and non-stationary signals. In the present work, the continuous wavelet transform is used to evaluate the coherence between R-R interval and systolic blood pressure signals of the subjects of the Eurobavar dataset using complex Morlet wavelet transform coherence for both lying and standing postures in the Low Frequency and High Frequency bands.*

Keywords: Continuous Wavelet Transform, Wavelet Transform Coherence, Morlet wavelet, bivariate spectral analysis

1. Introduction

Spectral analysis of heart rate (HR), respiration and blood pressure (BP) signals is a well-established procedure for the non-invasive investigation of cardiovascular control mechanisms. The spontaneous assessment of different physiological phenomenon can be inferred from the bivariate spectral analysis of variability in the R-R interval (RRI) and systolic blood pressure (SBP) signals. The most important are (a) respiratory sinus arrhythmia (RSA) due to breathing, at High Frequency (HF) between 0.2 to 0.35 Hz, (b) Mayer waves of blood pressure in Low Frequency (LF), at a frequency of about 0.1 Hz, the so-called 10s rhythm, and (c) oscillations at the Very Low Frequency (VLF) (0.003 to 0.04 Hz), which may possibly be due to long-term fluctuations in the thermoregulatory system. However, the physiological basis for VLF fluctuations is still under study [1]. The Coherence function is a straightforward method to quantify the existence and strength of the linear coupling between the signals in the frequency domain. Coherence is a well-established standard tool to analyze the linear relation between two signals by determining the correlation between their spectra [2].

The Fourier transform is limited as it does not take into account any temporal structure of the signal, beyond phase information and requires the signal to be stationary. Therefore, coherence cannot be used to give any information on the dynamically varying dependence between the signals, which is useful in the study of cardiovascular dynamics. [3, 4]. To overcome the shortcomings of the Fourier transform, various time-frequency methods are used for the analysis of dynamically varying signals, such as Wigner-Ville distribution (WVD), time dependent autoregressive models, Choi-Williams distribution (CWD), the short time Fourier transform (STFT) and the Wavelet transforms. In STFT, the coherence is calculated around a number of time instants using a fixed size window. The problem with such an approach is that, while it removes the assumption of wide sense stationarity inherent in the coherence measure, it still requires stationarity within each time interval i.e. window length [5]. The Wavelet transform is an efficient method to overcome the shortcomings of Fourier transform and STFT, specifically for the analysis of transient and non-stationary

signals by enabling simultaneous optimal interpretation of spectral and temporal information using a window of variable length [6]. The wavelet transform coherence (WTC) using Continuous Wavelet Transform (CWT) has been used by various researchers in recent years for the bivariate analysis of cardiovascular signals due to its potential to offer additional information about the complex functioning of autonomic regulatory mechanisms. A conceptually simple wavelet that has already proven useful for coherence analysis is the complex Morlet wavelet. In the present work, continuous wavelet transform using Morlet wavelet has been used to evaluate the coherence between R-R interval and systolic blood pressure variability signals.

2. Methods

Data

Holter recordings of 10-12 minutes duration in both lying and standing positions obtained from 21 subjects from the Eurobavar dataset (4 males and 17 females) aged 20 to 68 years (38±14.7, mean±SD) were considered for the estimation of WTC between RR interval and SBP signals. In the Eurobavar dataset, there were 4 healthy volunteers, 2 with hypercholesterolemia that was treated, 1 with hypertension, 2 with hypertension that was treated, 8 outpatients, 1 with diabetes without neuropathy, 1 with diabetes with evident cardiac autonomic neuropathy, 1 was a recent recipient of heart transplant, and 1 pregnant woman in her first term [7]. RR interval and systolic pressure time series were taken from this standard dataset and resampled at a frequency of 4 Hz after cubic splines interpolation. The aim of this study is to find the coherence between RR interval and SBP signals of all the subjects of Eurobavar dataset in two postures viz. lying and standing in two frequency bands i.e. LF band (0.04 - 0.15) Hz and HF band (0.15 – 0.4) Hz.

The Continuous Wavelet Transform

There are two classes of wavelet transform; the CWT and its discrete counterpart (DWT). The DWT is a compact representation of the data and is particularly useful for noise reduction and data compression whereas the CWT is better for feature extraction purposes and therefore is a common tool for analyzing localized intermittent oscillations in a time series. Many real valued wavelets have already been developed for different applications, but coherence is most strongly influenced by linearity in phase which makes it necessary to use complex wavelets in order to compute meaningful wavelet coherence. A conceptually simple wavelet that has already proven useful for coherence analysis is the complex Morlet wavelet [8, 9], and the present work applies continuous wavelet transform to evaluate coherence between R-R interval and SBP by using complex Morlet wavelet. The continuous wavelet function Ψ based on the Morlet wavelet function, consisting of a plane wave modulated by a Gaussian, is

$$\Psi_0(\eta) = \pi^{-1/4} e^{j\omega_0\eta} e^{-1/2\eta^2} \qquad (1)$$

where ω_0 is the dimensionless frequency and is called the Morlet wavelet coefficient which shifts the balance between frequency resolution and time resolution. η is the dimensionless time and is equal to t/s, t is the time and s is the scale. The Morlet coefficient is limited to $\omega_o \geq 6$ owing to the admissibility condition. It has been found that, for physiological signals, the preferable choice for good balance between time and frequency resolution combination is with ω_0 in the range 6-20 [2, 6, 8].

The CWT is defined as the convolution of a scaled parent wavelet function with the analyzed function g(t) [2, 6],

$$W(s,\tau) = \int g(t)\Psi_s(t-\tau)dt \qquad (2)$$

where s and τ are scale and time respectively, $\Psi_s(t-\tau)$ is the shifted and scaled version of mother wavelet $\Psi_s(t)$.

Wavelet Transform Coherence

The coherence function of two time series is defined as their cross-correlation also known as the cross-spectral density normalized by the auto-spectral density of the two signals. Following Torrence and Compo [9], the wavelet coherence of two time series is defined as

$$R_n^2(s) = \frac{\left|S\left(s^{-1}W_n^{XY}(s)\right)\right|^2}{S\left(s^{-1}\left|W_n^X(s)\right|^2\right)\cdot S\left(s^{-1}\left|W_n^Y(s)\right|^2\right)} \qquad (3)$$

where S is a smoothing operator and is achieved by a convolution in time and scale. It is natural to design the smoothing operator so that it has a similar path as the wavelet used. For the Morlet wavelet, the time convolution is performed with a Gaussian $e^{-t^2/2s2}$, which is the absolute value of the wavelet function in each scale. The scale convolution is performed by a rectangular window with a length of $\delta j_o.s$, where $\delta j_o = 0.6$ is the empirical scale decorrelation length for Morlet wavelet [2, 5, 6 ,8, 9].

3. Results

The wavelet transform coherence has been evaluated between RR interval and SBP time series for all the subjects of the Eurobavar dataset in the LF and HF bands for both lying and standing positions as per A. Grinsted et al [10] with some modifications according to the analysis required. For healthy volunteers, high coherence is seen in the LF band with SBP leading RRI by an angle less than 90^o.

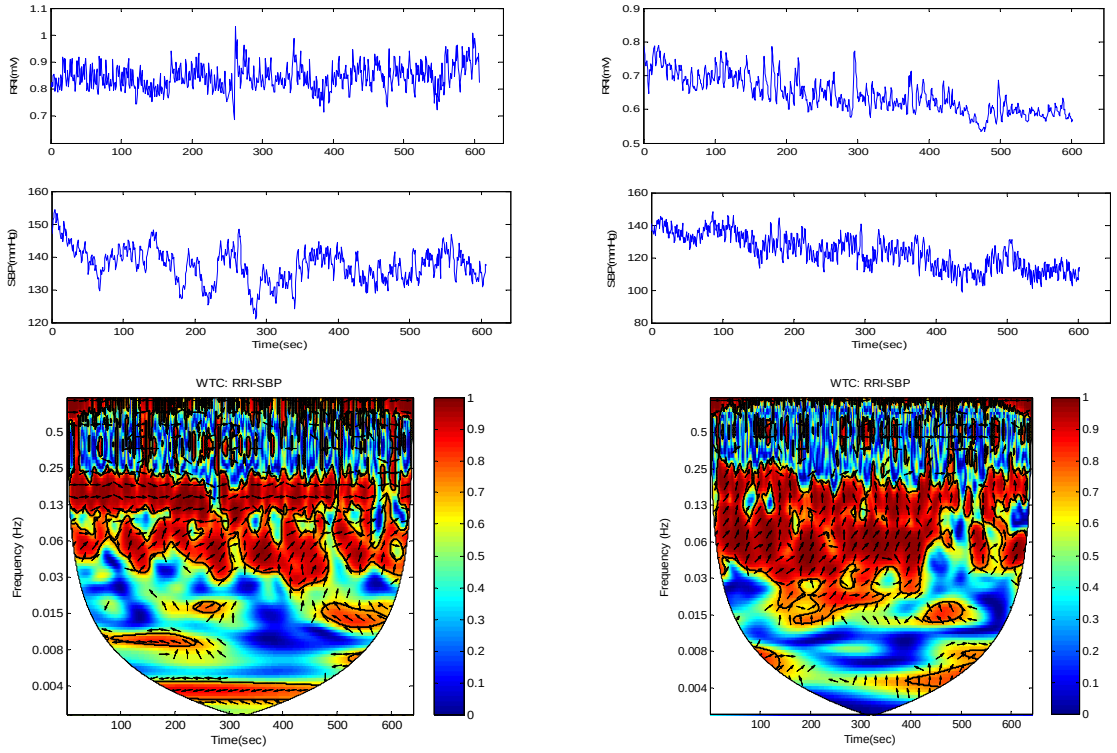

Fig 1. The RRI and SBP signals along with the wavelet coherence plot between these two signals (from top to bottom) for one of the healthy volunteer in the lying position (left) and standing position (right).

Somewhat high coherence (less than in the LF band) is observed in the HF band for both postures, while SBP is almost in-phase with RRI for the lying position and SBP leads by an angle almost equal to 90^o for the standing position in the HF band. The coherence is observed more in the lying posture when compared to standing for the healthy volunteers. Fig. 1 shows both the RRI and SBP time series with wavelet coherence plot in the lying and standing position for one of the healthy volunteers.

The results of all the healthy volunteers and rest of the subjects of the Eurobavar dataset are concluded in Table 1.

Table 1. Results for all the subjects of Eurobavar dataset.

	Lying		Standing	
Subjects	LF Band	HF Band	LF Band	HF Band
Healthy Volunteers	high coher., SBP leads<90^o	high coher., almost inphase	high coher., SBP leads<90^o	high coher., SBP leads~90^o
Hypercholesterolemia	high coh., SBP leads<90^o	less coh., SBP leads<90^o	high coh., SBP leads<90^o	almost neglig. Coherence
Hypertension	very less coh. SBP leads<90^o	high coh., small lead RRI	less coh., SBP leads>90^o	very less coh., RRI leads<90^o
Hypertension Treated	very high coh., SBP leads<90^o	negligible coherence	high coh., SBP leads<90^o	negligible coherence
Diabetes without Neuropathy	very less coh., small led SBP	very high coh., almost inphase	very less coh., SBP leads<90^o	significant coh almost inphase
Diabetes with Neuropathy	negligible coh, small lead RRI	high coh., RRI leads<90^o	very less coh., SBP leads>90^o	significant coh RRI leads<90^o
Recent Heart Transplant Recipient	very less coh., at some instant RRI leads<90^o	very less coh., RRI leads<90^o	very less coh., almost anti-phase	very less coh., almost in-phase
Pregnant Woman (3 months)	significant coh SBP leads<90^o	high coh., small led SBP	very high coh., SBP leads<90^o	high coh., small led SBP
Outpatients	significant coh SBP leads<90^o	very high coh., almost inphase	significant coh SBP leads<90^o	less coh., almost inphase

4. Discussion

The wavelet coherence has been found to be an efficient tool specifically for the analysis of transient and non-stationary signals by enabling simultaneous optimal interpretation of spectral and temporal information using a window of variable length. In this study, the WTC using complex Morlet wavelet, has successfully analyzed the interrelation between RR interval and SBP by providing the magnitude and phase information simultaneously on the

wavelet coherence plot. The duplicate pairs in the Eurobavar dataset are b014, a003 and b015, a008 which give the identical results for wavelet coherence with appropriate analysis.

Acknowledgements

The authors are thankful to the Department of Instrumentation and Control Engineering of Dr. B. R. Ambedkar National Institute of Technology, Jalandhar, Punjab (India) for providing the necessary laboratory facility to carry out this research work.

References

[1] Berntson G, Bigger Jr JT, Eckberg DL, Grossman P, Kaufmann G, Malik M, Nagaraja H N, Porges SW., Saul JP, Stone PH, Van Der Molen MW, Heart rate variability: origins, methods, and interpretive caveats. Psychophysiology,1997; 34: 623-648.

[2] Keissar K, Davrath LR, Akselrod S, Time-frequency wavelet transform coherence of cardio-respiratory signals during exercise. *Computers in Cardiology*, 2006; 33: 733-736.

[3] Klein A, Sauer T, Jedynak A, Skrandies W. Conventional and wavelet coherence applied to sensory-evoked electrical brain activity. *IEEE Trans. Biomedical Engg*. 2006; 53: 2: 266-272.

[4] Postolache G, Rocha I, Girao PS. Phase shift, coherence, BPV and HRV before and during self-terminating cardiac arrhythmia. In Proceedings of IEEE International Workshop on Medical Measurements and Applications (MeMeA), 2011, 525-531.

[5] Saab R., McKeown MJ, Myers L J, Abu-Gharbieh R. A wavelet based approach for the detection of coupling in EEG signals. In Conference Proceedings, 2nd International IEEE EMBS Conference on Neural Engineering, 2005; 616-620.

[6] Keissar K, Davrath LR. Akselrod S. Coherence analysis between respiration and heart rate variability using continuous wavelet transform. *Philosophical Transactions of the Royal Society A, Mathematical Physical and Engineering Sciences*2009; 367: 99: 1393-1406.

[7] Westerhof BE, Gisolf J, Stok WJ, Wesseling K H, Karemaker JM. Time-domain cross-correlation baroreflex sensitivity: Performance on the EUROBAVAR data set. *Journal of Hypertension*, 2004; 22: 1371–1380.

[8] Grinsted A, Moore JC Jevrejeva S. Application of the cross wavelet transform and wavelet coherence to geophysical time series. *Nonlinear Processes in Geophysics*, 2004; 11:561-566.

[9] Torrence C, Compo GP. A Practical Guide to Wavelet analysis. *Bulletin of the American Meterological Society* 1998;79: 61-78.

[10] Grinsted A, Moore JC, Jevrejeva S. Cross Wavelet and Wavelet Coherence. [Online]. Available: http://noc.ac.uk/using-science/crosswavelet-wavelet-coherence.

FRACTAL DIMENSION OF ELECTROCARDIOGRAM: DISTINGUISHING HEALTHY AND HEART-FAILURE PATIENTS

H.M.C. Mary, D. Singh

Dr B R Ambedkar National Institute of Technology, Jalandhar, India
Email: helenmarymc@gmail.com

Abstract. *Determining the complexity of the cardiovascular system is a difficult task since it cannot be split into a simpler subsystem without affecting the dynamic properties. The electrocardiogram (ECG) signal is self-replicating, which means it looks similar at different level of magnification. Hence the ECG signal is referred to as a fractal signal. Fractal dimension is an index for characterizing fractals and can reveal the complexity of the cardiovascular system. Fractal dimension can be calculated using Detrended Fluctuation Analysis and can be applied to healthy and heart failure patients to obtain the ranges of fractal dimension. Fractal dimension for healthy patients is 1.66±0.02 and for heart failure patients it is 1.09±0.03. It indicates that as the complexity of signal increases the fractal dimension increases. Thus, fractal dimension can reflect changes in adaptability of physiological processes and can lead to successful diagnosis of pathological conditions. Fractal analyses are therefore promising diagnostic tools in cardiovascular disease diagnosis and evaluation.*

Keywords: Electrocardiogram, Detrended Fluctuation Analysis, Fractal Dimension

1. Introduction

Determining the complexity of the cardiovascular system is a difficult task since it cannot be split into simpler subsystems without tampering with its dynamic properties. Linear methods of analysis are unable to handle the irregularity present in the signal, simply disregarding it or consider it as originating from a naturally occurring external source. Recent results strongly suggest that such irregularity actually reveals a more complex behavior of the system [1, 2]. It seems evident that any biological system responds better to description by a non-linear system. Non linear analysis is mainly composed of a non linear method and fractal method. A non linear method cannot be applied to raw data. It is necessary to carry out a transformation of the data with the aim of reproducing the conditions of the system under study [3]. However, the fractal analysis method can be applied to any set of data. The cardiovascular system is comprised of multiple subsystems that exhibit highly nonlinear deterministic, stochastic characteristics and is subject to hierarchical regulations. As a result, signals generated by cardiovascular systems are highly nonlinear, non-stationary, random and complex. Standard linear analysis methods may not be able to detect the irregular components. This irregularity can be identified only by using non-linear analysis.

The ECG signal is self-replicating, which means that it looks similar at different levels of magnification. Hence the ECG signal is referred to as a fractal signal. Thus fractal analysis can be applied to obtain fractal features to distinguish between healthy and heart failure patients. Fractal dimension is an index for characterizing fractals and can reveal the complexity of the cardiovascular system. Fractal Analysis can be understood as a technique that elaborates on, extends and enriches the notion of variability analysis, thus potentially providing practitioners with a more accurate, efficient and versatile statistical tool. Therefore it provides a new statistical tool for variability analysis and can reflect changes in adaptability of physiological process and can lead to successful diagnosis of pathological condition.

Fractal analyses are therefore a promising tool in cardiovascular disease diagnosis and evaluation.

2. Methods

ECG recordings were made from 10 healthy young subjects (age: 25±3) in the supine posture, who were free from diabetes mellitus, hypertension, alcohol dependence, and other diseases that can affect autonomic function. ECG data of standard Lead II were obtained from the selected subjects in Biomedical Instrumentation Laboratory, National Institute of Technology Jalandhar using Biopac MP100C module with Acqknowledge 3.9 DAQ software under standardized conditions in a quiet room, at comfortable light and temperature level. The ECG was converted by ADC at 500 Hz sampling frequency, 12-bit resolution, and then stored. ECG data of heart failure patients were taken from physioBank ATM database [4].

Detrended Fluctuation Analysis

Detrended Fluctuation Analysis (DFA) is a well-established method for determining scaling behaviour of fractals in the presence of possible trends without knowing their origin and shape [5-6]. Since the time series is based on the random walk theory, the noise level due to imperfect measurements in most records is reduced [5]. As implied by its name, it was conceived as a method for detrending local variability in a sequence of events and hence providing insight into long term variation in the data sets.

Steps:

1. For ECG signal (X_j), $j = 1, \ldots, N$, obtain the global profile $Y(j)$, i.e. the cumulative sum of the signal and represents the normalized signal. N represents the length of the signal.

$$Y(j) = \sum_{i=1}^{j} X_i - < X > \quad (1)$$

where

$< X >$ mean of signal

$Y(j)$ global profile

2. Splitting of the global profile $Y(j)$ of N elements into N_s, $N_s = int(N/s)$ non-overlapping segments of size s, starting from the beginning and another N_s non-overlapping segments of size s, starting from the end of the considered signal. This way neither data at the end nor at the beginning of the record is excluded.

3. Trend is the unwanted noise in the time-series which is unlikely to be part of a process on the time scale of that window and may be removed by subtracting the polynomial trend in the window. Estimating the polynomial trend $y_{v,s}^{m}(j)$ within each segment v by least-square fitting and subtracting this trend from the original profile (`detrending') to obtain the detrended profile $Y_s(j)$

$$y_{v,s}^{m}(j) = [Y(N - (v - N_S)s) - Y(N - (v + 1 - N_S)s)]^m \quad (2)$$

$$Y_s(j) = Y(j) - y_{v,s}^{m}(j) \quad (3)$$

The degree of the polynomial can be varied in order to eliminate constant ($m = 0$), linear ($m = 1$), quadratic ($m = 2$) or higher order trends of the profile function. Detrending of the signal profile essentially reveals the true scaling with a super imposed trend both for uncorrelated and correlated signals [7].

4. The variance of the detrended profile $Y_s(j)$ in each segment yields the mean-square fluctuations

$$F^2_{DFAm}(v,s) = \frac{1}{s}\sum_{j=1}^{s} Y_s^2\ (j) \quad (4)$$

The fluctuation function depends on the scales in a power-law fashion $F(s) = s^H,\ H$, is the Hurst exponent.

5. Fractal Dimension (FD), D of signal can be obtained. FD is related to Hurst exponent [8] as:

$$H = 2 - D \quad (5)$$

3. Results

In order to study the alteration in the fractal dimension of the signal in association with pathological conditions, ECG data of healthy and heart failure patients was analyzed and DFA applied separately for various segment sizes. After obtaining the global profile of the signal, root-means-square (RMS) variation of the signal is calculated. The fast changing fluctuations in the time-series will influence the overall RMS, for segments with large sample size (i.e., large scale). The overall RMS should therefore be computed for multiple segments sizes (i.e., multiple scales) to emphasize both fast and slow evolving fluctuations that influence the structure of the time-series. By using small scale ($s = 16$) the identified fluctuation is more as when compared with large scale ($s = 1024$) and is represented in Fig. 1.

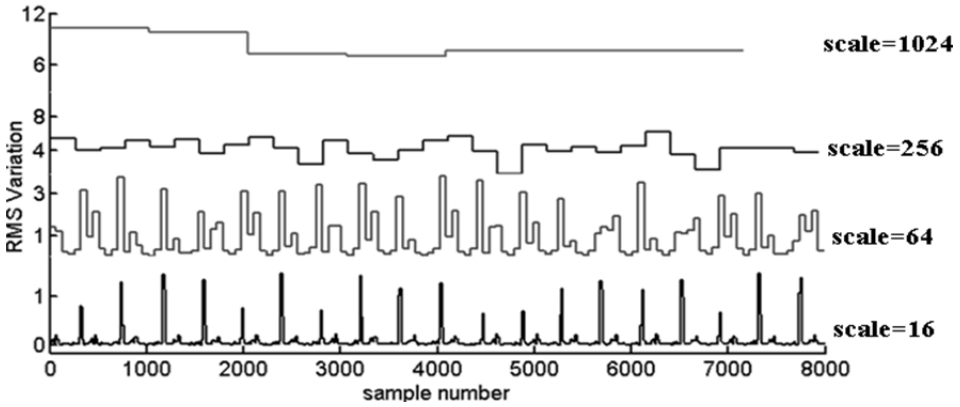

Fig. 1. RMS variation of signal profile with respect to scale variation

The fluctuation function was computed as mean standard deviation of all identically sized windows of signal profile (second order statistics). Fluctuation function is calculated from equation (4) and observed that it varies in a power-law fashion:$F(s) = s^H,\ H$ determines the DFA exponent. Logarithmic scales are used for plotting the graph since it gives equal weight to all segment sizes. The plotted signal obtained with respect to fluctuation function and scale and is indicated on Fig. 2. The straight line is fitted using linear regression and the slope of the line indicates the DFA exponent (Hurst exponent) H.

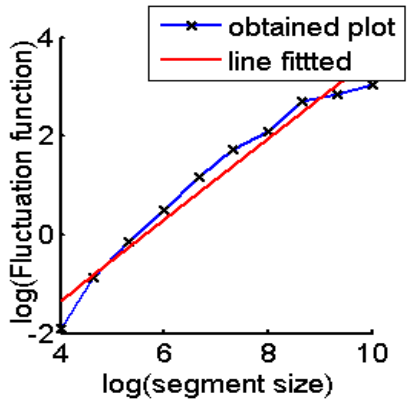

Fig. 2. Obtained DFA plot

4. Conclusions

Estimating fractal dimension from a signal is one way to detect and quantify the self organizational properties that affect the human heart. Fractal dimension can reflect changes in adaptability of physiological processes and can lead to successful diagnosis of pathological conditions. As we know the dimension of the line is one and plane is two, a signal is made up of small lines that indicate the dimension obtained will be between one and two. The complexity of signal changes as the dimension changes. The dimension obtained for a healthy patient is more when compared to heart failure patients. Thus, fractal dimension can reflect changes in physiological processes and can lead to the successful diagnosis and evaluation of cardiac diseases. Therefore it can help in identifying the health status of patients.

References

[1] Butler GC, Yamamoto Y, Hughson RL. Fractal nature of short-term systolic BP and HR variability during lower body negative pressure. *American journal of Physiology, Regulatory Integrative and Comparative Physiology*, 1994; 267: R26-33.

[2] Elbert T, Ray WJ, Kowalik ZJ, Skinner JE, Graf KE, Birbaumer N. Chaos and Physiology: Deterministic Chaos in Excitable cell assemblies. *Physiological reviews,* 1994; 74: 1-47.

[3] Gonzalez Julian J. and Pereda Ernesto. Applications of Fractal and Non-linear Time-series Analysis to the Study of Short-term Cardiovascular Control. *Current Vascular Pharmacology*, 2004; 2: 149-162.

[4] Goldberger AL, Amaral LAN, Glass L, Hausdorff JM, Ivanov PC, Mark RG, Mietus JE, Moody GB, Peng CK, Stanley HE. PhysioBank, PhysioToolkit, and PhysioNet: Components of a New Research Resource for Complex Physiologic Signals. *Circulation*, 2000; 101: e215-e220.

[5] Kantelhardt JW, Konscienly-Bunde E, Rego HHA, Havlin S, Bunde A. Detecting long range correlations with detrended fluctuation analysis. *Physica A*, 2001; 295: 441-454.

[6] Peng CK, Buldyrev SV, Havlin S, Simons M, Stanley H E, Goldberger A L. Mosaic Organization of DNA Nucleotides. *Physical Review E*, 1994; 49: 1685-1689.

[7] Hardstone R, Poil SS, Schiavone G, Jansen R, Nikulin VV, Mansvelder HD, Linkenkaer-Hansen K. Detrended fluctuation analysis: a scale-free view on neuronal oscillations. *Frontiers in physiology*, 2012; 3(450): 1-13.

[8] Bassingthwaighte JB, Raymond GM. Evaluating rescaled range analysis for time-series. *Annals of Biomed. Eng.*, 1994; 22: 432-444.

5. Miscellaneous

A SYSTEM FOR ANALYSING THERMALLY-INDUCED EFFECTS OF PROPAGATION DIRECTION DEPENDENT FEATURES IN FIELD POTENTIALS OF CARDIOMYOCYTE MONOLAYERS USING MULTI-ELECTRODE ARRAYS

[1]R. Kienast, [1]M. Handler, [1]M. Stöger[1], [2]G. Fischer, [1]F. Hanser, [1]C. Baumgartner

[1]Institute of Electrical and Biomedical Engineering, UMIT, Hall in Tyrol, Austria
[2]AFreeze GmbH, Innsbruck, Austria
Email: roland.kienast@umit.at

Abstract. *Microelectrode array (MEA) technology opens a new opportunity for investigating electrophysiological changes of cooled myocardial cell cultures or tissue with high spatial and temporal resolution. This may help to obtain a better understanding of electrophysiological mechanisms in the application of cryogenic technology such as catheter cryoablation. However, a prerequisite to investigate hypothermia-induced effects in-vitro is the presence of an appropriate measuring system. Therefore, a system based on MEA technology was developed, which allows cooling of myocardial cell cultures with simultaneous signal registration. Another issue is the fact that randomly grown cultures of cardiomyocytes often compromise randomly distributed pacemaker centres which complicates the determination of directional parameters. We propose a new algorithm capable of computing the spatial and temporal distribution of these pacemakers. A combination of both approaches enables the measurement and assessment of propagation-direction-dependent features of myocardial cells during cooling.*

Keywords: Hypothermia, Multi-electrode Array, Myocardial Cells, Pacemaker Centre, Signal Recording

1. Introduction

Cultivating cardiomyocytes in culture dishes with integrated microelectrode arrays (MEA) allows long-term and real-time monitoring of electrophysiological changes from contracting multicellular myocardial cultures, induced by external mechanical, chemical or thermal stress with highly spatial and temporal resolution [1, 2]. This technology offers, therefore, a new opportunity for investigating electrophysiological changes of cooled myocardial cell cultures or tissue. In-vitro investigation of electrical signals of cooled myocardial cells with MEA technology may help to further advance knowledge on electrophysiological mechanisms in the application of cryogenic technology such as catheter cryoablation. This is a minimally invasive surgical method to treat cardiac arrhythmias by ablating arrhythmic cardiac tissue using shock freezing. The MEA data obtained can be used for a spatio-temporal investigation of cellular activity such as the spread of excitation, the conduction velocity or special parameters of registered field potentials for example the field potential rise time. A correlation between field potential and intrinsic action potential (AP) parameters of cardiac muscle cells allows us to draw conclusions on the myocardial action potentials based on the registered signals which are usually measured with standard patchclamp approaches [3]. However, randomly grown primary cultures of cardiomyocytes often compromise randomly distributed pacemaker centres [4], which may change the active centre, more or less frequently resulting in an alteration of spread directions. To analyse propagation-direction-dependent features such as excitation velocity, it is important to have detailed information about the spatial and temporal distribution of active pacemaker centres and, thus, associated changes of direction in wave front propagation.

A prerequisite for the analysis of such characteristics during hypothermia is the availability of a suitable temperature controlled measurement system and a computational approach to estimate the location of active pacemaker centres and their temporal changes.

To study these characteristics, we used a microelectrode array with 60 electrodes and modified an existing measurement system (Multi Channel Systems, Reutlingen, Germany) to register field potentials of isolated embryonic chicken cardiomyocytes at different temperatures. In addition, we developed an algorithm to detect active pacemaker centres in and outside the registration area of the MEA to study the spread dependent characteristics of individual pacemaker centres.

2. Methods

Cell cultivation

Ventricles of 12-day-old chicken embryos were minced and digested with 0.05% trypsine. One drop of the cell suspension was plated onto the electrode grid of fibronectin-coated MEA in the centre of a petri-dish. The petri-dish was carefully filled with culture medium to a volume of 1.5 ml. 1 ml of which was periodically renewed after 24 hours. After 3 to 4 days, the cells formed a continuous spontaneous beating monolayer covering the whole MEA area. The cells attached firmly onto the electrodes without significant dislocation during contraction.

Cooling System

The cooling system developed provides an adjustable heating module to register signals under physiological conditions (T = 37°C) by default. To enable measurements under hypo-thermal conditions, the heating module was replaced by an in-house developed adjustable heating and cooling device.

This device consists of an adapted water cooling system (see Fig. 1), in which the water temperature is adjusted by a Peltier element (Global Component Sourcing) based on the principle of a thermo-electric converter. A special Peltier-element-controller (PR-59, Supercool) is used for controlling the temperature of the system continuously in the range between T = 10°C and T = 40°C. The Petri dish with an integrated MEA in the centre (60 electrodes arranged in a 8x8 grid) is placed directly on the copper plate of the module and is composed of a glass-bottom with the electrode array and a plastic ring that forms the final culture chamber (see Fig. 2b).

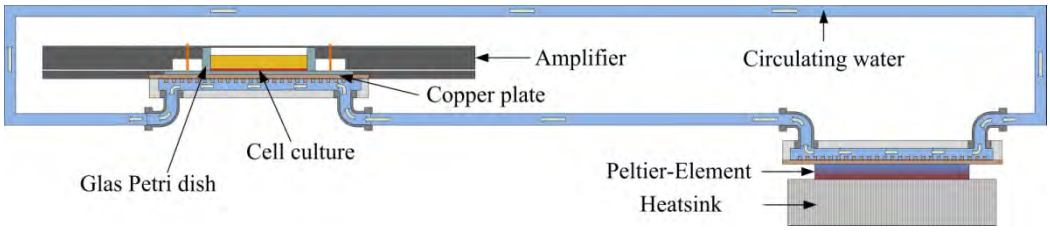

Fig 1. Schematic illustration of the amplifier with inserted culture dish and cooling-heating element based on an adapted water cooling system.

The temperature of the heating and cooling module is determined by a sensor integrated into the copper plate (see Fig. 1). The temperature gradient is greatly influenced by water capacity, the power of the Peltier element and thermal isolation of the system. To register data at

different temperatures, it is necessary to estimate the temperature of the cell layer. In order to eliminate a possible influence on the measurement through a temperature sensor which is directly attached to the cell layer (e.g. noise or damage of electrodes), a computer model based on the finite element method (FEM) was developed to simulate the temperature distribution of the module and attached Petri dish. This model was experimentally evaluated by measuring the surface temperature of the Petri dish filled with nutrient solution using a high resolution infrared camera. The experimentally registered thermal data was further compared with computer simulations for validation.

Detection of the pacemaker centres

For estimating the origin of electrical activation of a single wavefront, the algorithm developed uses information obtained from calculating the negative two dimensional spatial gradient of the wave front's arrival time within the electrode array as recently described in [5]. This approach relies on the fact that the negative gradient of the wave front arrival time in each point of a circular wave points towards the origin of this wave. This implies that the intersection point of two approximated lines in the direction of two arbitrary selected gradients marks the starting point of the circular wave.

Algorithm 1. Pseudo code for excitation source detection of a single wavefront

---

Require: Detected spikes of all field potentials for a single wavefront moving across the array
Start
  Get time stamps of each spike
  Calculate gradient of the wavefront's arrival time for each electrode
  for $i=1 \rightarrow$ Number of Electrodes **do**
    for $j=1 \rightarrow$ Number of Electrodes **do**
      $il \leftarrow$ Line equation (gradient, electrode i)
      $jl \leftarrow$ Line equation (gradient, electrode j)
      $P_{ij} \leftarrow il \cap jl$
    end for
  end for
  Eliminate all intersection points outside the Petri dish
  Eliminate all intersection points which are not located in the direction of the excitation source
  Divide area into bins b_i
  Count P_{ij} (intersection points) for each $b_i \rightarrow w_i$
  Calculate weighted arithmetic mean for the x and y coordinates of intersection points P_{ij} where w_i of the corresponding b_i are used as weight.
  return Source $\leftarrow$ mean(x), mean(y)
end

An excitation front in a cardiac cell layer across the MEA can be interpreted as a part of a circular wave. Based on inhomogeneities in the structure of the cardiac cell layer, however, the wavefront yields distorted formation. As a consequence of this deformation, not all intersection points from each of two arbitrary approximated lines in the direction of two gradients meet in a single point, but rather result in a point cloud from which the centre needs to be estimated. To increase the detection accuracy of the algorithm, a weighted average approach is used. Algorithm 1 shows a pseudo code description of the algorithm for estimating the spatial origin of the pacemaker centre from registered experimental data. To identify local clusters of active pacemaker centres inside the cell culture, the computed local

coordinates of the spatial excitation source of each single wavefront propagation was used to perform a cluster analysis using a density-based cluster detection algorithm called DBSCAN [6]. DBSCAN detects clusters based on a local density measure (number of minimal objects in a defined neighbourhood) while objects not fulfilling this criterion are defined as "noisy" objects. The centroid of each detected cluster denotes the most likely position of an active pacemaker centre in a cell layer. Additionally, the degree of activity and the temporal activation pattern of each single pacemaker can be determined.

3. Results

Cooling System

The computer model permits the estimation of the temperatures of the cell layer based on the measured temperature of the integrated sensor of the heating-cooling module. This is relevant in order to eliminate possible disturbances by a sensor located close to the cell culture and the MEA. Fig. 2a displays a simulated temperature profile whereby the temperature of the heating-cooling module was adjusted from 37°C to 27°C. Fig. 2c shows the time course of the cooling process of a Petri dish containing 1.5 ml culture medium. In this case, the cell layer reaches the temperature of 27°C, after about 190 seconds.

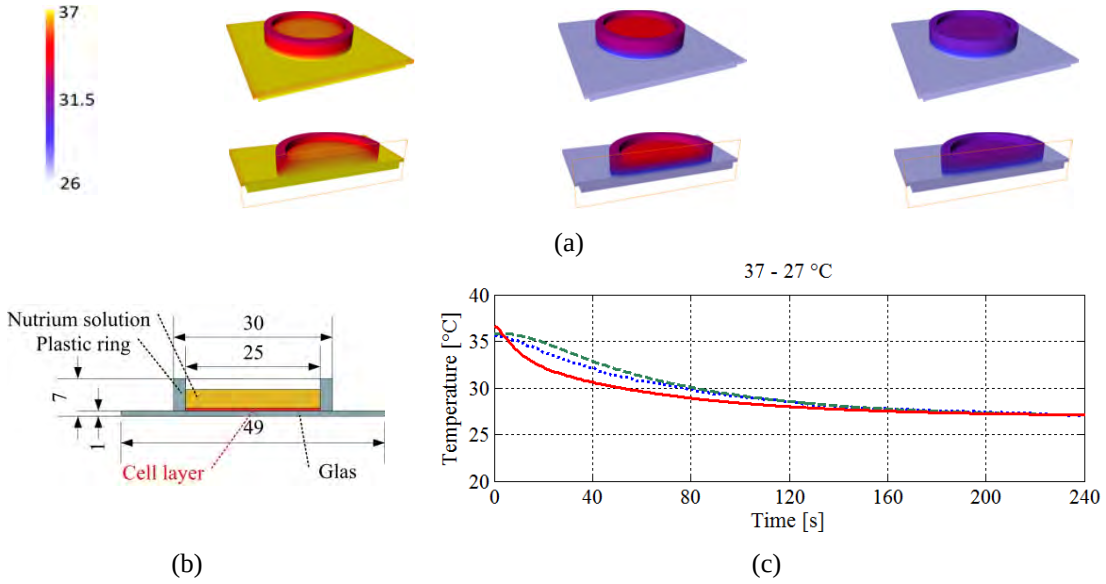

Fig 2. (a) Simulation results of the temperature distribution within the measuring setup. Computed temperature distributions of the cooled Petri dish at the beginning (left), after 30 seconds of cooling (middle), and after 60 seconds of cooling (right) from 37 ° C to 27 ° C (Complete view and cross section of the dish).(b) Cross-section of the Petri dish (all dimensions are in mm). (c) Temperature profiles of the average surface temperature of the medium in the experiment (dotted line), in the simulation (dashed line) and approximately 1 mm above the cell layer determined by the simulation (solid line).

Detection of the pacemaker centres

To demonstrate the feasibility of the algorithm, experimental data with multiple active pacemaker centres during cooling (from 37°C to 29°C) was analysed. The characteristics of an experimental dataset are summarized in Table 1. Fig. 3a shows the estimated spatial distribution of the pacemaker sources after cluster analysis outside and inside the active MEA. This experimental dataset comprises 6 different active pacemaker centres where each point marks the calculated position of the excitation source of a single wavefront. Fig. 3b displays

the degree of activity of the detected pacemakers measured over the entire experiment, dominated by three primary active centers. Fig. 3c shows the temporal activation pattern of each detected pacemaker centre, where temperature-induced changes of the dominant pacemaker centre can be observed in the temperature range 35°C - 33°C, and 31°C - 29°C.

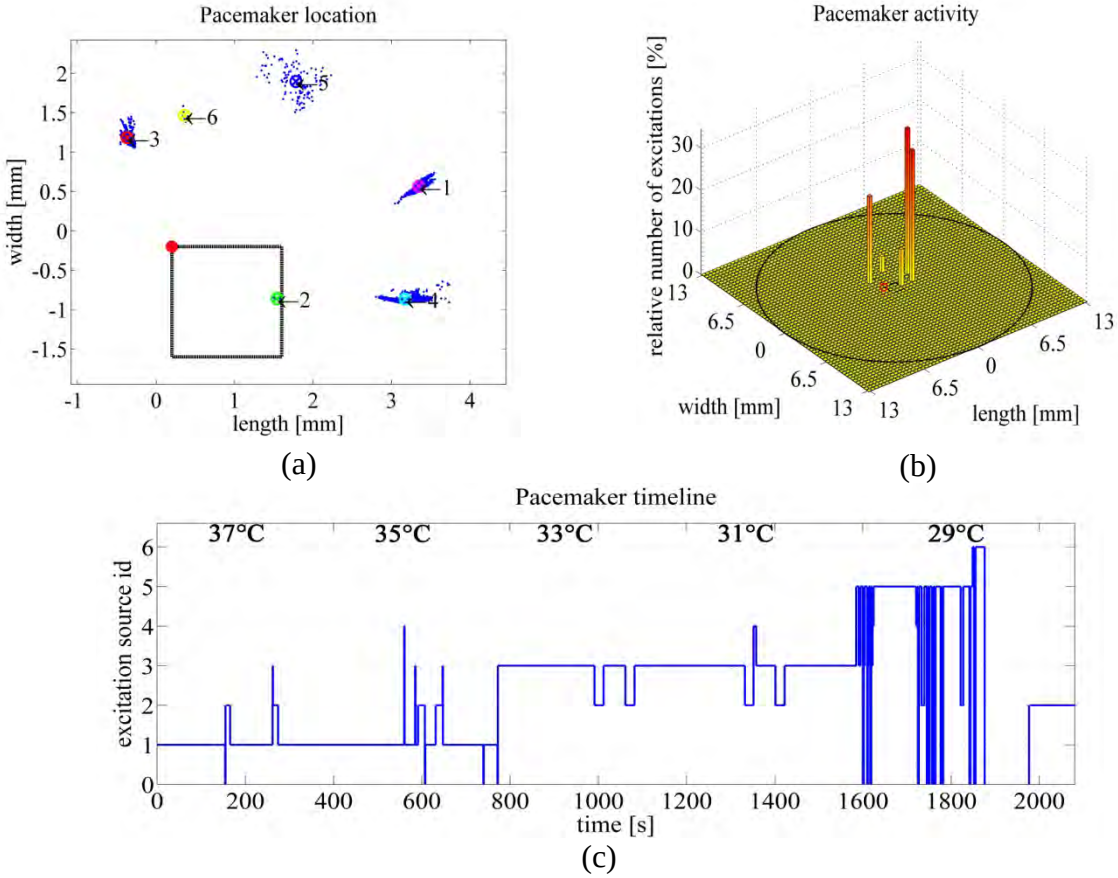

Fig 3. Results of the proposed algorithm to detect multiple active pacemaker centres within a randomly grown myocardial cell culture. (a) Detected pacemaker centres after cluster analysis. Number 1 and numbers 3 to 6 are biological pacemaker centres and number 2 indicates an artificial stimulus. The dashed line marks the active MEA registration area. (b) Degree of activity of detected multiple pacemaker centres. The black circle symbolizes the Petri dish. (c) Temporal activation patterns of the detected pacemaker centres during cooling (at 37°C, 35°C, 33°C, 31°C and 29°C). Id 1 and id 3 to 6 are biological pacemaker centres and number 2 indicates an artificial stimulus. Number 0 indicates wavefront propagation centres which could not be assigned to a cluster.

Table. 5 Dataset characteristics

Property	Value
Time of cultivation	4d
Active pacemaker centres	n = 5
Artificial stimulus centres	n = 1
Recording time	t = 2080s
Recording temperature, number of excitations	T = 37°C, n = 549
	T = 35°C, n = 279
	T = 33°C, n = 166
	T = 31°C, n = 157
	T = 29°C, n = 254

4. Discussion and Conclusion

Our adapted MEA system enables a reproducible in-vitro registration of thermally induced effects in field potentials of cardiomyocytes in-vitro. The proposed algorithm is capable of computing the spatial and temporal distribution of the excitation sources within a randomly grown cell culture of primary cardiomyocytes in and outside the MEA registration area. This information may be used to investigate thermal effects of propagation direction dependent features such as the excitation velocity [7] or field potential rise time [1].

The aim of our ongoing work is to derive an especially focused understanding on cardiac muscle cell death during hypothermia. Thereby the relation of extracellular potentials to intracellular action potentials allows us to draw conclusions on the myocardial action potential during cooling based on the data gained by the developed system [3]. These results are now used to develop a temperature-dependent ion-current model to simulate hypothermia effects on cardiac action potentials.

Acknowledgements

This work was funded by the K-Regio-Project of the Standortagentur Tirol, Innsbruck, Austria and by the European Regional Development Fund (ERDF).

References

[1] Egert U, Banach K, Meyer T. Analysis of cardiac myocyte activity dynamics with micro-Electrode arrays, in Advances in Network Electrophysiology. M Taketani, M Baudry. Springer, US, 2006, 274-290.

[2] Stett A, Egert U, Guenther E, Hofmann F, Meyer T, Nisch W et al. Biological application of microelectrode arrays in drug discovery and basic research. *Anal Bioanal Chem* 2003; 377 (3): 486–95.

[3] Halbach M, Egert U, Hescheler J, Banach K. Estimation of action potential changes from field potential recordings in multicellular mouse cardiac myocyte cultures. *Cell. Physiol. Biochem.* 2003; 13 (5): 271–84.

[4] Igelmund P, Fleischmann BK, Fischer IR, Soest J, Gryshchenko O, Böhm-Pinger MM et al. Action potential propagation failures in long-term recordings from embryonic stem cell-derived cardiomyocytes in tissue culture. *Pflugers Arch.* 1999; 437 (5): 669–79.

[5] Kienast R, Stöger M, Handler M, Fischer G, Hanser F, Baumgartner C. Detection of multiply pacemaker centers in cardiomyocyte cell layers for estimating wavefront propagation patterns. to appear in Biomedical Engineering / Biomedizinische Technik; 2013.

[6] Ester M., Kriegel H., Sander J., Xu X. A density-based algorithm for discovering clusters in large spatial databases with noise. In Proceedings of the Second International Conference on Knowledge Discovery and Data Mining (KDD-96), 1996, 226–231.

[7] Chung C, Bien H, Entcheva E. The role of cardiac tissue alignment in modulating electrical function. *J. Cardiovasc. Electrophysiol.* 2007; 18 (12): 1323–9.

ATRIAL ACTIVATION AS DISPLAYED IN AUTOCORRELATION MAPS OF YOUNG ADULT CONTROLS - A PRELIMINARY STUDY

K. Kozlíková

Institute of Medical Physics, Biophysics, Informatics and Telemedicine,
Faculty of Medicine, Comenius University in Bratislava, Bratislava, Slovak Republic
Email: katarina.kozlikova@fmed.uniba.sk

Abstract. *Atrial activation can be analyzed using autocorrelation maps (ACMs) based on body surface isopotential maps (IPMs). The aim of this work was to study the form of the ACMs in young adults. We constructed IPMs in 92 young controls (49 women) without cardiovascular disease every 5 ms during the P wave. Every IPM was compared with every IPM using Pearson´s correlation coefficient r. We analyzed the ACM regions of high positive correlation $r \geq 0.9$. We identified 4 types of ACMs: the widest high positive correlation at the beginning of the P wave (22 men, 10 women), at the end (8 men, 14 women), in the middle (8 men, 8 women) or uniform width along the main diagonal. Different types and areas of the ACMs probably display atrial activation represented by circular isochrones (slow changes) or preferential paths (quick changes). Further studies are needed to prove this hypothesis.*

Keywords: Body Surface Potential Mapping, Atrial Activation, Autocorrelation Map

1. Introduction

Atrial depolarization can be displayed in the form of body surface isopotential maps that may be analyzed in different ways, as well as in isointegral maps [1]. Autocorrelation maps concerning body surface potential mapping were first introduced in 1976 [2] to express the normal ventricular repolarization in the body surface distribution of T potentials. Later, autocorrelation analysis was used to analyze the effect of intrathoracic heart position on the electrocardiogram [3] or the beat-to-beat repolarization measurements [4]. In all of the studies mentioned, this analysis dealt with the QRST interval. Therefore, the aim of this work was to study the autocorrelation maps in healthy young adults during the P wave and to find out, whether these maps from different subjects have common features.

2. Methods

Subjects

We studied 92 young adults, 49 women, 43 men, of mean age 18.6 ± 0.4 years, range 18 - 20 years. None of the controls had signs of cardiovascular diseases or cardiovascular risk; all had normal blood pressure values, 12-lead standard electrocardiographic and echocardiographic findings.

Body surface potential mapping

Unipolar electrocardiograms for body surface potential mapping were registered using the limited 24-lead system after Barr based on a grid of 10 rows and 15 columns [5] and processed using the mapping system ProCardio [6]. All data were registered in the supine position during normal expiration. Linear baselines were taken through TP segments in each electrocardiogram. The onset and offset of the P wave were established manually from the root mean square signal. The limiting points were set at the end of a sequence of decreasing values when started from the middle of the P wave. We constructed isopotential maps every 5 ms of the duration of the P wave (see Fig. 1).

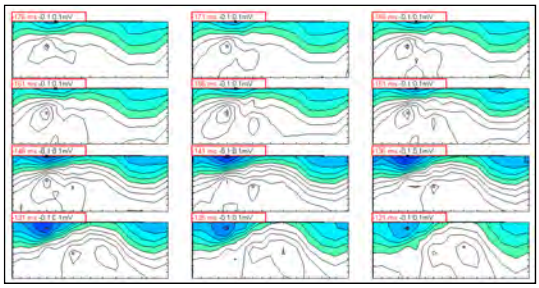

A

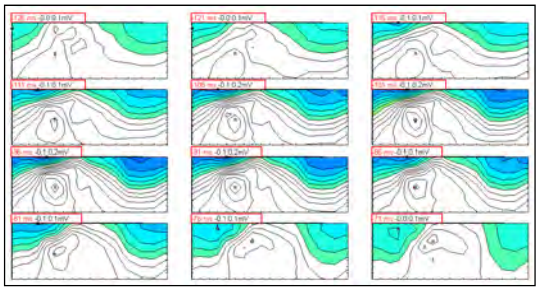

B

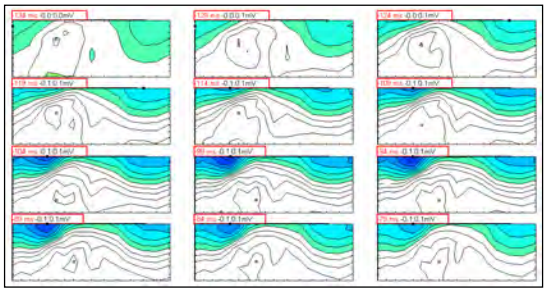

C

D

Fig 1. Examples of isopotential maps of four evaluated subjects. The first map is always displayed 15 ms after the P wave onset; next map follow always after 5 ms. The left half of the rectangle corresponds to the anterior chest, the right half to the back. White areas display positive potentials, grey areas display negative potentials. Step between isopotential lines is 0.02 mV. The letters A, B, C, and D correspond to the types of autocorrelation maps in Fig. 2.

For each subject, every isopotential map (map A) of a single beat was compared with every isopotential map (map B) of the same beat using Pearson´s correlation coefficient r (r_{AB}) [7]

$$r_{AB} = \frac{\sum_{i=1}^{150}(U_{Ai} - \overline{U}_A)\cdot(U_{Bi} - \overline{U}_B)}{\sqrt{\sum_{i=1}^{150}(U_{Ai} - \overline{U}_A)^2}\cdot\sqrt{\sum_{i=1}^{150}(U_{Bi} - \overline{U}_B)^2}}, \qquad (1)$$

where

U_{Ai} (U_{Bi}) the value of electric potential in the i-th point of the map A (B),
$\overline{U}_A$ ($\overline{U}_B$) mean value of electric potential in the map A (B).

Comparisons were presented in the form of autocorrelation maps, squared graphs displaying the correlation coefficients of every possible pair of potential distribution with values $r = 1$ on the main diagonal and symmetrical around it. We analyzed the form of regions with high positive correlation $r \geq 0.9$ where the potential distribution changed slowly.

3. Results

The P wave potentials in the isopotential maps ranged from – 0.18 mV to 0.19 mV (see Fig. 1). The mean P wave duration was 84 ± 11 ms (women: 81 ± 12 ms; men: 88 ± 10 ms; $p < 0.05$ according to the t-test [7]). Therefore, 11 to 22 isopotential maps were constructed per subject and the corresponding autocorrelation maps displayed 121 to 484 values, ranging from $r = -0.70$ to $r = 1.00$.

The mean correlation coefficients of the autocorrelation maps were 0.69 ± 0.09 (range 0.46 - 0.88). A negative correlation coefficient was found in 56 autocorrelation maps, more often in women (73 %) than in men (47 %; $p < 0.05$ according to the proportion test [8]). It occurred at the borders of the autocorrelation maps, i.e. when comparing the isopotential maps at the beginning or at the end of the P wave with the middle parts (see Fig. 2).

We identified four types of autocorrelation maps according the form of regions with high positive correlation (see Fig. 2). In the type A (22 men, 10 women), the widest area appeared at beginning of the P wave; in the type B (8 men, 14 women) at the end of the P wave, in the type C (8 men, 8 women) approximately in the middle of the P wave. This widening was always connected with narrow parts at its borders. In the remaining 22 cases (5 men, 17 women - the type D), the region of $r \geq 0.9$ had approximately uniform width along the main diagonal. Occurrence of these four types of maps differed for men and women ($p < 0.05$ according to the chi-square test [8]).

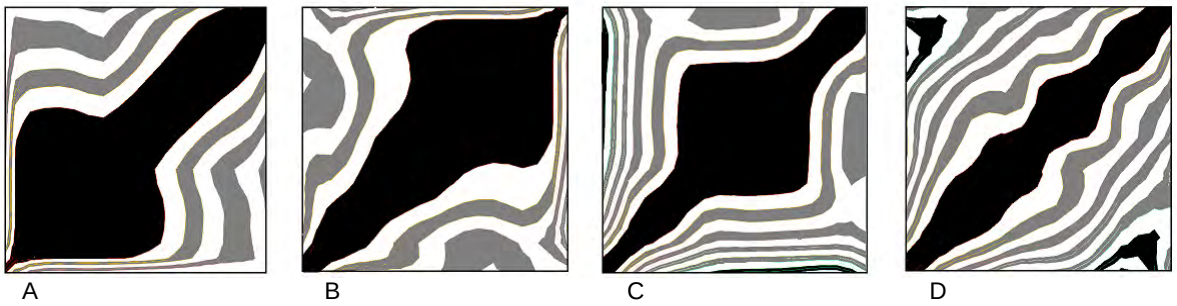

Fig 2. Examples of four different types of autocorrelation maps. The time increases from bottom to top and from left to right with the same step for all maps. Black areas correspond to the areas of high correlation ($r \geq 0.9$ along the main diagonal) and to negative values (maps C and D at the borders). The white and grey areas change with step $r = 0.10$. The letters A, B, C, and D correspond to the types of isopotential maps in Fig. 1.

4. Discussion

According to the experimental study concerning the QT interval [3], the autocorrelation maps reflect only phenomena taking place in the electric source (myocardium), are very little influenced by the geometry of the volume conductor (thorax) that connects it to the lead system, and are very sensitive to variations in the activation sequence. Comparing the P wave autocorrelation map with the corresponding isopotential map sequence we found, that the wider the area of high positive correlation around the main diagonal, the smaller the change in shape of the activation sequence between successive instants (see the "D" maps against remaining three, Figs. 1 and 2).

A great variety of shapes of autocorrelation maps occurred within the group studied. However, we could identify four main types of autocorrelation maps. It is not clear yet, why they occurred with different frequency in men and in women, but it could be due to "flatter" isopotential maps in women than in men (the root mean square signal was 44 ± 12 mV in women versus 57 ± 18 mV in men; $p < 0.05$ according to the t-test [7]).

Different types and areas of the autocorrealation maps probably display atrial activation represented by circular isochrones (slow changes) or preferential paths (quick changes). This hypothesis could be investigated in further studies.

Acknowledgements

This study was partially supported by the grant KEGA 004UK-4/2011 from the Ministry of Education, Science, Research and Sport, Slovak Republic.

References

[1] Kozlíková K. Surface integral maps, their characteristics and methods of quantitative analysis. (in Slovak) *Bratislava Medical Journal* (previously *Brat Lek Listy*), 1990; 91: 815 – 823.

[2] Abildskov JA, Burgess MJ, Lux RL, Wyatt R, Vincent GM. The expression of normal ventricular repolarization in the body surface distribution of T potentials. *Circulation,* 1976; 54: 901 – 906.

[3] Corlan AD, MacLeod RS, DeAmbroggi, L. The effect of intrathoracic heart position on electrocardiogram autocorrelation maps. *Journal of Electrocardiology*, 2005; 38: 87 – 94.

[4] Kozmann G, Haraszti K. Importance of body surface potential field representation fidelity: analysis of beat-to-beat repolarization measurements. *The Anatolian Journal of Cardiology*, 2007; 7(Suppl 1): 5 – 7.

[5] Barr RC, Spach MS, Herman-Giddens GS. Selection of the number and positions of measuring locations for electrocardiography. *IEEE Transactions on Biomedical Engineering*, 1971; 18: 125 – 138.

[6] Rosík V, Tyšler M, Turzová M. Portable device of for ECG mapping. In Proceedings of International Conference of Measurement. Frollo I and Plačková A, Editors. SAV, Bratislava, 1997; 367 – 370.

[7] Kozlíková K, Martinka J. The Essentials of Biomedical Measurement Processing II (in Slovak). Asklepios, Bratislava, 2009.

[8] Altman GG. Practical Statistics for Medical Research. Chapman&Hall/CRC, Boca Raton, 1999, 611.

EFFECTS OF GENDER DIFFERENCES AND AGING ON CARDIAC REPOLARIZATION IN MICE

M. Kuwahara, S. Taniguchi, K. Ito

Department of Comparative Pathophysiology, Graduate School of Agricultural and Life Sciences, The University of Tokyo, Tokyo, Japan
Email: akuwam@mail.ecc.u-tokyo.ac.jp

Abstract. *It is generally thought that sex hormones and aging affect cardiac repolarization. We evaluated the cardiac phenotype with electrocardiogram (ECG) and monophasic action potential (MAP) analysis in both male and female mice. Moreover, expression of KCNH2 and KCNQ1 were elucidated by RT-PCR. The QT intervals gradually increased with aging in female mice and were significantly more prolonged than those in other groups. The same tendency was observed in MAP analysis. Although castration did not alter KCNQ1 and KCNH2 expressions, KCNQ1 was decreased and KCNH2 was significantly increased by ovariectomy. These data indicated that ventricular repolarization was altered by aging and female sex hormones. These results suggest that prolongation of cardiac repolarization in female mice may be of relevance to diminished expression levels of IKr channels.*

Keywords: Age, Gender, Ion Channel, Mouse, QT interval

1. Introduction

It is well recognized that sex hormones and aging affect cardiac repolarization, but the mechanisms underlying gender- and aging-specific differences in cardiac repolarization are still largely unknown. Despite the importance of understanding these differences for the interpretation of the work done on transgenic mice, few attempts have been made to determine whether there are gender- and aging-related specific differences in cardiac repolarization in these mice [1]. Therefore, it is valuable to clarify the characteristics of cardiac repolarization on gender and aging in transgenic mice. We believed that the C57BL/6 strain could be suitable to investigate the role of female sex hormones in the regulation of ventricular repolarization, as the strain was considered to be a low androgen level model mouse [2]. In this study, we postulated that female C57BL/6 mice should exhibit longer ventricular repolarization than their male counterparts. In addition, we tested the hypothesis that ovariectomy would shorten ventricular repolarization in female C57BL/6 mice.

2. Methods

Both male and female C57BL/6 mice were used. Water and food pellets were provided ad libitum. All care and experimental procedures of animals were in accordance with the guidelines for the Care and Use of Laboratory Animals published by the National Institute of Health [3] and subjected to prior approval by the local animal committee in The University of Tokyo. Six week-old male and female mice before reaching puberty underwent bilateral castration and ovariectomy, respectively. Other groups of animals were sham-operated, in which testicles or ovaries were exteriorized but replaced intact.

Standard limb lead ECGs were recorded on mice between 3 to 12 months of age in a prone position on a heated mat under pentobarbital (30 mg/kg intraperitoneally) anaesthesia and analysis was performed. Each ECG in lead II was analyzed by ECG processor (Softron Corp., Japan). MAPs from the epicardial surface of the left ventricle were recorded under urethane anesthesia at 12 months of age and analyzed by ECG processor.

MAP recordings were amplified with a DC-coupled bioelectrical amplifier (NEC Sanei 1253A Tokyo, Japan). Action potential duration (APD) at repolarization levels of 20%, 50%, and 90% (APD20 to APD90) were analyzed.

After MAP recording, the hearts were removed. The left ventricular walls were separated and immediately frozen in liquid nitrogen. Total RNA extraction, complementary deoxyribonucleic acid (cDNA) synthesis, and real-time reverse transcription (RT)-polymerase chain reaction (PCR) analysis were performed.

Statistical differences were analyzed using two-way analysis of variance (ANOVA). A p-value < 0.05 was considered to be statistically significant. All data were expressed as means ± SE.

3. Results

There were no significant effects on castration and ovariectomy in most of the ECG parameters in mice at 3 months of age. Fig. 1 shows typical examples of lead II ECG recordings obtained at both 3 months and 12 months of age in each group of mice. Heart rate (HR), P wave and QRS-complex durations increased with aging in all groups of mice, but PR interval was unchanged. HR gradually increased with aging in male mice. The QT interval was slightly longer in female mice of 3 months of age rather than other groups of mice of the same age. Moreover, the QT interval gradually increased with aging in female mice, although the QT intervals in other groups of mice were constant during the experimental period. The QT interval in female mice of 9 and 12 months of age was significantly prolonged in comparison with ovariectomy mice.

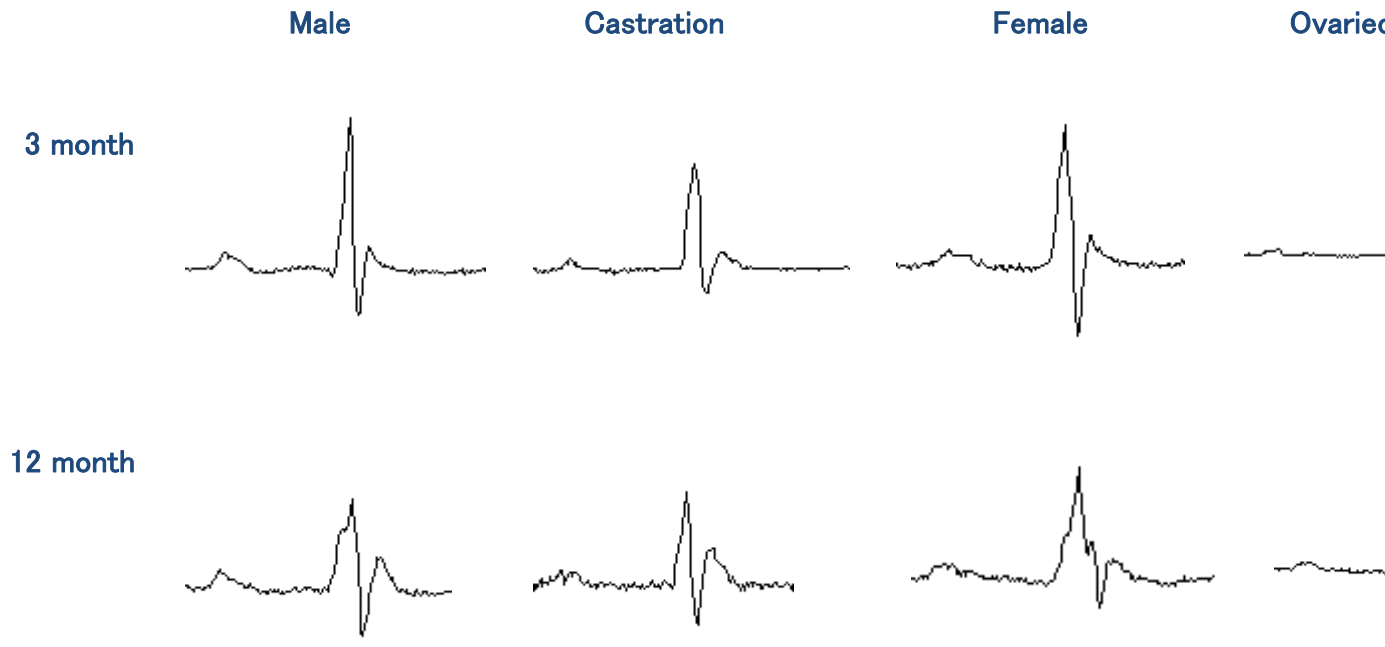

Fig. 1. Representative limb lead II ECGs in mice.

APD50 and APD90 of MAPs were significantly longer in female mice compared with both male and ovariectomy mice. However, there was no significant difference in APD20 among any of the groups. The expression levels of KCNQ1 in female mice were higher than those in male mice. In contrast, expression levels of KCNH2 in female mice were lower than those in male mice. Although castration did not alter these expressions, KCNQ1 was decreased and KCNH2 was significantly increased by ovariectomy.

4. Discussion

The major findings of this study are: (1) female C57BL/6 mice show prolonged cardiac repolarization, and (2) ovariectomy shortened ventricular repolarization associated with higher expression of KCNH2. These results indicate that prolongation of cardiac repolarization in female C57BL/6 mice may be relevance to diminished expression of levels of IKr channels. These results provide convincing evidence that female sex hormones regulate cardiac repolarization in C57BL/6 mice.

According to Xing et al. [4], it is necessary for investigators to choose the appropriate mouse strains to cross to identify the genes that regulate HR, ECG time intervals, and aging-related cardiac conduction changes. C57BL/6 strains background mice have been widely used to develop the transgenic mouse. Therefore, we considered that this strain represented a better model to study the effects of both low levels of testosterone and female sex hormone on the characteristics of cardiac repolarization on aging.

The mechanisms underlying gender-specific differences in cardiac repolarization are still largely unknown. Hormonal regulation of cardiac K+ channel gene expression may affect basal electrical activity. To our knowledge, only a few publications have focused on this issue using an *in vivo* model. Liu et al. [5] first reported that the female rabbit heart had a longer baseline and drug-induced changes in QT interval than the male hears. They also found a small but significant difference for the rapidly activating delayed rectifier K+ current (IKr) and for the inward rectifier K+ current (IK1). Pham et al. [6] found that the IKr blocker dofetilide induced greater APD90 prolongation in females than males whereas the IKs blocker chromanol had no effect on APD. Our data support these earlier observations, since female C57BL/6 mice show prolonged QT interval and APD, and ovariectomy shortened ventricular repolarization associated with higher expression of KCNH2, although K+ currents were not examined. Saba et al. [7] reported that neither ovariectomy nor estrogen administration affected QT interval. These discrepancies may be due to strain differences and experimental conditions. Castration did not induce any significant changes in ventricular repolarization in C57BL/6 mice. Moreover, Brouillette et al. [8] observed that male C57BL/6 mice display similar ventricular repolarization as their female counterparts. Therefore, estrogens are potential regulators of cardiac repolarization in C57BL/6 mice but more studies are required to delineate their functional roles.

References

[1] Trepnier-Boulay V, St-Michel C, Tremblay A, Fiset C. Gender-based differences in cardiac repolarization in mouse ventricle. *Circulation Research*, 2001; 89: 437-444.

[2] Bartke A. Increased sensitivity of seminal vesicles to testosterone in a mouse strain with low level of testosterone. *Journal of Endocrinology*, 1974; 60: 145-148.

[3] Revised Guide for the Care and Use of Laboratory Animals *NIH Guide* 1966;25(28); August.

[4] Xing S, Tsaih S, Yuan R, Svenson KL, Jorgenson LM, So M, Paigen BJ, Korstanje R. Genetic influence on electrocardiogram time intervals and heart rate in aging mice.

American Journal of Physiology Heart and Circulation Physiology, 2009; 296: H1907-H1913.

[5] Liu XK, Katchman A, Drici MD. Gender difference in the cycle length-dependent QT and potassium currents. *Journal of Pharmacological and Experimental Therapeutics*, 1988; 285: 672-679.

[6] Pham TV, Sosunov EA, Gainullin RZ, Danilo P Jr, Rosen MR. Impact of sex and gonadal steroids on prolongation of ventricular repolarization and arrhythmias induced by i(k)-blocking drugs. *Circulation*, 2001 103: 2207-2212.

[7] Saba S, Zhu W, Aronovits MJ, Estes III NAM, Wang PJ, Mendelsohn ME, Karas RH. Effects of estrogen on cardiac electrophysiology in female mice. *Journal of Cardiovascular Electrophysiology*, 2002; 13: 276-280.

[8] Brouillette J, Rivard K, Lizotte E, Fiset C. Sex and strain differences in adult mouse cardiac repolarization: importance of androgens. Cardiovascular Research, 2005; 65: 148-157.

PHYSIOLOGICAL AND PATHOLOGICAL MYOCARDIAL REMODELLING IN PATIENTS WITH SUDDEN OBSTRUCTION OF THE RIGHT CORONARY ARTERY

[1]S. Sclarovsky, [2]K. Nikus, [3]Zhan Zhong-qun, [4]F.J. Femenia

[1]Tel Aviv University, Tel Aviv, Israel
[2]Tampere University Hospital, Tampere, Finland
[3]Renmin Hospital of Wuhan University, Wuhan City, Shiyan Taihe Hospital, Hubei University of Medicine, Shiyan City, China
[4]Hospital Español de Mendoza, Mendoza, Argentina
Email: samuel_s@netvision.net.il

Abstract. *The concept of cardiac remodelling, which was conceived in basic science laboratories, deals with the structural changes occurring in the chronic phase of myocardial infarction in the non-involved muscle in an experimental model. This concept was further expanded to hypertrophic, electrophysiologic and ionic remodelling. Recently, the structural changes in hypertrophic physiological and pathological remodelling in an experimental model were described. The current paper introduces the clinical concept of physiological and pathological remodelling in sudden obstruction of a right coronary artery in the human.*

Keywords: Cardiac Remodelling, Myocardial Infarction, Hypertrophic, Ionic

1. Introduction

The concept of cardiac remodelling, which was conceived in basic science laboratories, deals with the structural changes occurring in the chronic phase of myocardial infarction in the non-involved muscle in an experimental model [1, 2]. This concept was further expanded to hypertrophic, electrophysiologic and ionic remodelling [3, 4].

It has previously been reported that the change in the electrocardiogram (ECG) is able to express the metabolic, ionic, and hemodynamic changes occurring in the myocardium due to a sudden coronary occlusion [5].

Our task was to compare the ECG changes with the coronary angiography findings in the myocardium not involved in the ischemic process during a sudden obstruction of the right coronary artery (RCA).

The term physiological remodelling is applied to the changes occurring in the non-involved myocardium in an isolated sudden obstruction of the RCA. The coronary circulation supplying the non-involved area is normal – the non-culprit artery may be angiographically normal, or there may be non-critical obstruction (<75% diameter obstruction).

Pathological remodelling is defined as the molecular ionic and hemodynamic changes occurring in a myocardial region not being supplied by the culprit artery during total RCA obstruction, and without critical obstruction in the arteries supplying this area.

2. Methods

One of the authors (SS) analyzed all the ECGs submitted from three different university hospitals. The ECGs were recorded during sudden obstruction of the RCA, which was confirmed by angiography. The ECGs were transmitted without any clinical or personal data.

We excluded patients with ECG signs of reperfusion (inverted T waves) or with previous myocardial infarction (Q waves). The ECG findings were matched with the coronary angiographic findings.

Pathological remodelling was defined as: ECG changes of a sudden total obstruction of the RCA (ST segment and T waves in LIII higher than in LII accompanied by ST-segment depression and inverted T waves in AVL), and ECG signs of acute anterior wall ischemia.

We used the following determinations of anterior wall ischemia:

1) Dominant RCA supplying the low lateral, apical and/or low anteroseptal wall (1-vessel disease) expresses the electrical changes occurring on the healthy non-involved myocardium due to the hemodynamic, biological and electrophysiological events occurring as a consequence of a severe depression of the activity of the ischemic area.

2) The anterior wall is supplied by a chronic critical obstruction of the LAD (2-vessel disease with ECG signs of acute regional subendocardial ischemia).

3) The anterior and lateral walls are supplied by critical chronic obstruction of the left main coronary artery or by chronic, critical obstruction of the left anterior descending and (LAD) and circumflex (CX) arteries (ECG signs of circumferential subendocardial ischemia).

Physiologic remodelling was defined as an ECG showing signs of RCA occlusion without signs of anterior wall ischemia.

3. Results

Of 155 ECGs with non-anterior wall ST-elevation myocardial infarction, 80 were classified as sudden obstruction of the RCA. ECG signs of physiologic remodelling with 1-vessel disease was found in 33 out of these 80 cases (predictive value 71%, $p<0.01$).

ECG signs of pathological remodelling with 1-vessel disease (dominant RCA) was found in 16 out of 80 cases (predictive value 77%, $p<0.01$) and of 2-vessel disease (concomitant critical LAD obstruction) in 18 out of 80 cases (predictive value 68%, $p< 0.01$). There were ECGs showing signs of 3-vessel disease in 13 out of 80 cases (predictive value 77%, $p<0.01$).

4. Discussion

The concept of cardiac remodelling has been introduced in the literature during the past 30 years. Vast information has been fundamentally provided by the basic sciences of molecular biology and electrophysiology.

During the past 40 years, clinical research has been dedicated to identifying patients with a sudden obstruction of the RCA, in particular to identify the high-risk patients, aiming to find appropriate medical and invasive treatment [6]. Molecular biology and basic electrophysiology allow us to better understand the different ECG manifestations of physiologic and pathophysiologic mechanisms in the non-involved myocardium.

The increased intracavitary pressure induced by acute myocardial ischemia stimulates the endocardial potassium receptors, resulting in a shortening of the action potential of this layer, but not the epicardial layer; this effect is expressed by ST-segment depression with inverted T waves [7]. In the case of only RCA occlusion, there is segmental remodelling with favorable prognosis. The ECG expression, including the number of leads involved in the process, is determined by a genetic –phenotype interaction and is dependent on the distribution of septal tension receptors [8]. In these cases, the maximal ST-segment depression is always in lead V2. In the case of remodelling with ST-segment depression with inverted T waves maximally

in V4-V5, there is probably severe 3-vessel disease or left main disease. These are urgent cases, which need emergency invasive cardiac evaluation and treatment [9]. One type of pathological remodelling in sudden RCA occlusion is ST-segment depression with a high positive T wave in V2 to V4. This high and peaked T wave suggests a shortening of the epicardial action potential, with the probable protective effect of preventing the entrance of calcium into the sarcomere, thereby reducing the oxygen demand and myocardial injury in this layer [10]. This metabolic -electrophysiological phenomenon is enabled by adenosine, which stimulates the ATP-dependent potassium receptors [11]. The presence of this ECG pattern suggests a critical obstruction of a non-culprit artery supplying the anteroseptal wall, usually the LAD [12].

In conclusion, there is strong association between the ECG patterns and coronary anatomy in patients with sudden total obstruction of the RCA. We have introduced the clinical concept of physiological and pathological remodelling in sudden obstruction of a RCA for the first time.

References

[1] Swynghedauw B. Molecular mechanisms of myocardial remodeling. *Physiol Rev*, 1999; 79: 215-62.

[2] Ruan H, Mitchell S, Vainoriene M, et al. Gi alpha 1-mediated cardiac electrophysiological remodeling and arrhythmia in hypertrophic cardiomyopathy. *Circulation*, 2007; 116: 596-605.

[3] Jeyaraj D, Wilson LD, Zhong J, et al. Mechanoelectrical feedback as novel mechanism of cardiac electrical remodeling. *Circulation*, 2007; 115: 3145-55.

[4] Kong SW, Bodyak N, Yue P, et al. Genetic expression profiles during physiological and pathological cardiac hypertrophy and heart failure in rats. *Physiol Genomics*, 2005; 21: 34-42.

[5] Sclarovsky S. Upgrading the electrocardiogram in the 21st century. *J Electrocardiol*, 2009; 42: 35-8.

[6] Sclarovsky S, Angina at rest and acute myocardial ischaemia, in: Electrocardiography of Acute Myocardial Ischaemic Syndromes. Sclarovsky S , Editor. Martin Dunitz Ltd. London, UK, 1999, 1-29 .

[7] Kelly D, Mackenzie L, Hunter P, et al. Gene expression of stretch-activated channels and mechanoelectric feedback in the heart. *Clin Exp Pharmacol Physiol*, 2006; 33: 642-8.

[8] Stones R, Gilbert SH, Benoist D, et al. Inhomogeneity in the response to mechanical stimulation: Cardiac muscle function and gene expression. *Prog Biophys Mol Biol*, 2008; 97: 268-81.

[9] Assali AR, Sclarovsky S, Herz I, et al. Comparison of patients with inferior wall acute myocardial infarction with versus without ST-segment elevation in leads V5 and V6. *Am J Cardiol*, 1998; 81: 81-3.

[10] Hearse D. Activation of ATP-sensitive potassium channels: A novel pharmacological approach to myocardial protection? *Cardiovasc Res*, 1995; 30: 1-17.

[11] Furukawa T, Kimura S, Furukawa N, et al. Role of cardiac ATP-regulated potassium channels in differential responses of endocardial and epicardial cells to ischemia. *Circ Res*, 1991; 68: 1693-702.

[12] Nikus KC, Sclarovsky S, Huhtala H, et al. Electrocardiographic presentation of global ischemia in acute coronary syndrome predicts poor outcome. *Ann Med*, 2012; 44: 494-502.

ECG MANAGEMENT IN GLASGOW – FROM "PATIENT TO PORTAL"

M.P. Watts, M. Gray, D.L. Murdoch, A. Cowe

NHS Greater Glasgow and Clyde Health Board, Glasgow, United Kingdom
E-mail: markp.watts@nhs.net

Abstract *A GE Healthcare MUSE ECG management system has been implemented in the Greater Glasgow and Clyde Health Board which facilitates ECG records being retrieved from an Orion Health clinical portal as part of a patient's Electronic Patient Record. The main operational challenges involved in implementing this system related to ECG recording issues and demographic input. Multiple repeat ECGs for recording quality improvement have been studied in one clinical area which show that 44% of these do not result in any improved ECG quality. ECG lead quality checks show that, whilst cardiac technician ECG recording quality was, in general, superior to that of nursing staff, the difference on average was less than expected.*

Keywords: ECG Management, Clinical Portal, Data Quality

1. Introduction

The NHS Greater Glasgow and Clyde (GGC) Health Board is one of the largest in the UK and serves a population of 1.2 million and covers an area of 452 square miles. It currently comprises ten major hospitals including two ambulatory care hospitals. Several years ago, prior to the addition of the Clyde hospitals, and as part of an ongoing service development, it was decided that 12 lead ECGs from seven acute and ambulatory care hospitals should be uploaded to a central GE Healthcare MUSE ECG management system. They would then be made available for all clinical staff to view through an Orion Healthcare Glasgow clinical portal along with other clinical data from the patient. The clinical portal currently has over 18,000 active users in GGC [1].

Prior to this development, there was a wide variation in the ECG management practice in the different hospitals. Two hospitals used existing ECG management systems which served the local hospital and the remainder either retained ECG paper records for one year or not at all. A proposal from a baseline review of the current ECG practice identified the following requirements for the new ECG system:

- The availability of diagnostic 12 lead ECGs through a clinical portal for all clinical staff.
- A facility for checking demographic data entered into to the electrocardiograph.
- A multi-vendor approach for the procurement of electrocardiographs.

Following a competitive procurement procedure, a GE Healthcare MUSE 7.1 ECG management system was selected which, as part of the specification, required a demographic checking interface with the Glasgow Scottish Care Information (SCI) Store data repository to be developed.

2. Methods

The overall current ECG functional data flow developed is shown in Fig. 1

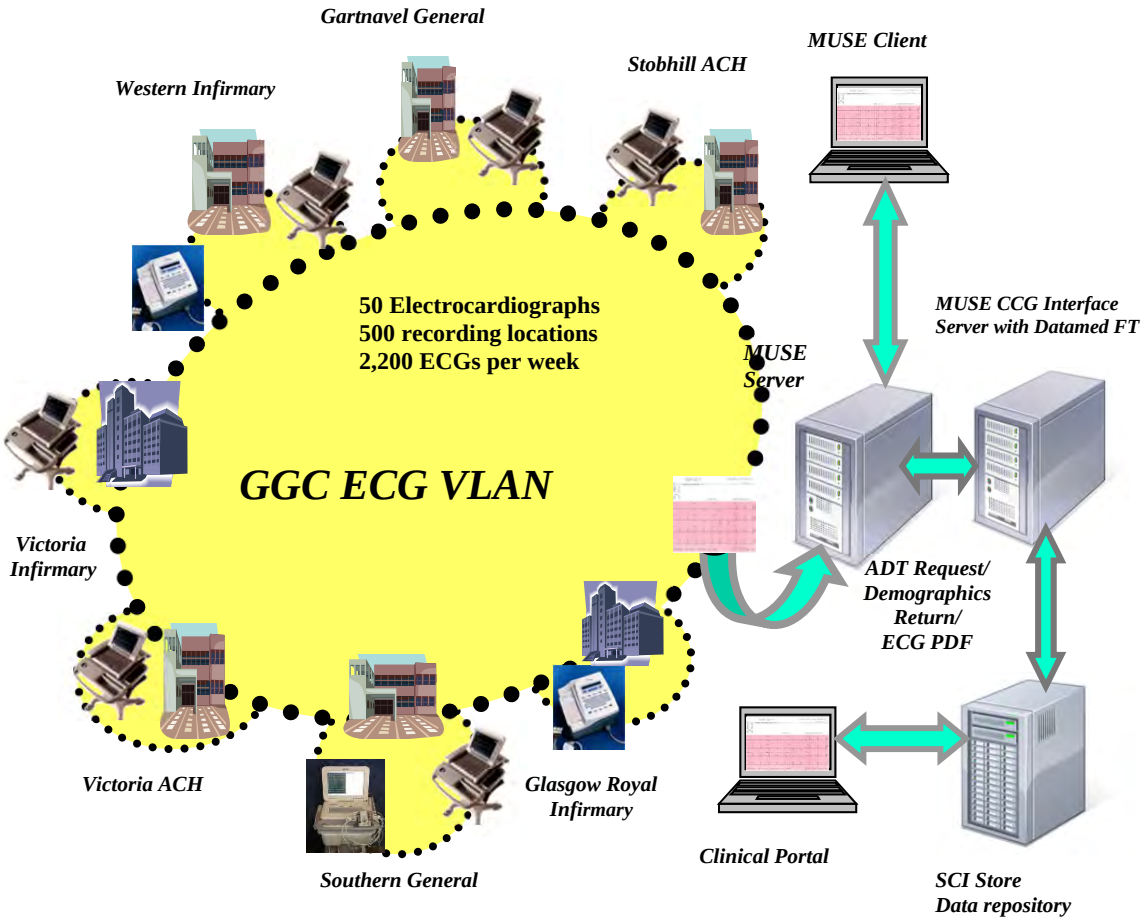

Fig. 1. ECG functional data flow

Fifty electrocardiographs of three different models upload ECGs via the GGC ECG VLAN to the MUSE 7.1 system. The GE Healthcare Mac5500 electrocardiograph transmits ECGs via the serial IP software on the MUSE server and the Burdick Atria 6100 and Philips TC 70 electrocardiographs transmit via a Datamed Format translator running on the MUSE CCG interface server.

When ECGs are received by the MUSE system the demographics are validated against those in SCI Store and any difference in surname or date of birth flags a “Mismatch” which is dealt with manually. ECG records with validated demographics are then sent as a PDF to SCI Store where they can be viewed through the clinical portal.

Approximately 500 ECG requesting/recording locations were identified across the seven hospitals in order that ECGs arriving in MUSE could be source identified.

3. Results

The project pilot commenced in March 2011 and has rolled out to the Cardiology and other high usage ECG areas in the Glasgow hospitals. Currently over 2000 ECGs per week are uploaded to the MUSE system with approximately 150,000 ECGs being currently viewable in the clinical portal.

The decision to opt for a multi-vendor solution, with currently three different electrocardiographs, has proved to be straightforward to implement and to date has presented no significant operational disadvantages [2].

The MUSE system running with detailed ECG source location data across all hospitals has allowed the collection of ECG data which previously would not have been possible or at least would have been highly time consuming. It has also allowed measured analysis of a range of issues.

An increasing number of nursing staff are routinely recording ECGs in Accident and Emergency Departments, Assessment and Admission Units and data collected from MUSE indicates that currently approximately 41% of all ECGs in the Glasgow hospitals are recorded by nursing staff. The transition from paper recording to electronic uploading has meant that a substantial culture change is required by many staff. Three main data quality issues have been identified:

Multiple Repeat ECGs (MREs)

ECGS recorded on the same patient over a 1-2 minute period to improve recording quality. If these are allowed to route to the clinical portal they could slow the retrieval of ECGs as multiple successive ECGs would need to be opened in order to find the optimum ECG recording. Data from MUSE was used to investigate the occurrence of MREs on a sample of ECGs in one large clinical area (Table 1).

Table 1 Analysis of Multiple Repeat ECGs (MREs) in one clinical area

Total ECGs recorded by nursing staff in the month,	1089	%
Total number of MREs	97	9
Total number of MREs which did not improve quality or made it worse (sample of 50)	22	44
Total number of single ECGs (non MREs) with suboptimal ECG quality (sample of 60)	8	13

This indicates that 9% of ECGs were recorded at least twice and in nearly half of these ECGs there was no clear advantage in doing this. It cannot therefore be assumed that the later ECG is of an improved quality.

Patient ID entry

Ten variants of patient ID entry error have been identified which can cause up to 10% of ECGs to fail demographic verification. Some can be rectified with the MUSE mismatch facility but most will be resolved with further training, feedback and the future introduction of bar code readers.

Poor data quality - ECG recordings uploaded to MUSE

In the same clinical area a comparison of ECG lead quality between cardiac technical staff and nursing staff was made using the hook-up advisor on the Mac5500 electrocardiographs (Table 2). This advisor provides an indication of ECG quality based on a number of measurements and classifies them as Green (generally acceptable quality), Yellow (range of noise/artefact) or Red (extreme baseline wander/ lead fail).

Table 2 Comparison of ECG lead quality between cardiac technical and nursing staff from MUSE data

	No. of ECGs by cardiac staff	No. of ECGs by nursing staff	% ECGs by cardiac staff	% ECGs by nursing staff
GREEN	238	637	73.7	65.3
YELLOW	81	311	25.1	31.9
RED	4	27	1.2	2.8

Whilst the cardiac technical staff, as expected, had a higher percentage in the green band and lower in the red band the differences were not as marked as might have been expected.

4. Conclusions and discussion

ECGs are now available to all Health Board clinical staff in the clinical portal as part of the Electronic Patient Record. The major benefit for clinical staff is access to previous ECGs for comparison, especially out of hours, in Accident and Emergency Departments.

The MUSE system has facilitated the collection of a wide range of ECG data across all hospitals which previously would have been extremely difficult to collect.

The most significant operational issues are ECG recording and demographic data input to the electrocardiograph which is common to both cardiac technicians and nursing staff. A study of MREs in one large clinical area showed that 9% were repeat ECGs, to improve recording quality, which were saved and uploaded to the MUSE system along with the original. A sample of these indicated that 44% showed no improvement over the original. These are significant because if routed to the clinical portal, each would need to be opened to find the optimum ECG record.

When ECG lead recording quality from the Mac5500 hookup adviser was analysed in MUSE between cardiac technicians and nursing staff in the same clinical area ,cardiac technicians ,as expected, had a better generally acceptable quality figure ,but only by about 8%.

The results indicate that whilst cardiac technician recording quality requires some minimal further improvement, there is a core of about 10-20% of ECGs recorded by nursing staff which cause issues with the system in terms of MREs and demographic input. Raising the profile of the ECG with more training is indicated as a priority [3].

Future challenges are to roll out the system to all remaining hospitals in the GGC Health Board as currently any ECGs which are not recorded on newer models of electrocardiograph require to be scanned into the clinical portal.

References

[1] Todd R, Focus on: NHS Greater Glasgow and Clyde. *E-Health Insider*, June 2012.

[2] Fornell D, Connecting ECG Management Systems. *Diagnostic and Interventional Cardiology (DAIC)*, March, 2011

[3] Kligfield P, Gettes LS, Bailey JJ et al. Recommendations for the Standardisation and Interpretation of the Electrocardiogram. Part 1. The Electrocardiogram and its Technology. *Journal of the American College of Cardiology*, 2007; 49:1109-27

Acknowledgements

This project was sponsored by the Greater Glasgow and Clyde (GGC) Heart Disease Managed Clinical Network under the previous chair Caroline Morrison. The authors would like to thank Malcolm Gordon and Peter Macfarlane for their input in the early stages of the development.

Many members of GGC staff have contributed to this development. Particular thanks go to the Cardiology Technical Heads of Service across Glasgow and their staff, to Mark Quinn, Chris McBain and Scott Hendry of the GGC IT Department and to Clinical Physics equipment management staff. Thanks also go to Roman Schwartz, Tim Killington and Tim Brass of GE Healthcare for their support of the MUSE system.

THE QT INTERVAL, ARTERIAL STIFFNESS, ENDOTHELIAL FUNCTION, CORONARY PERFUSION AND VASCULAR AGE

[1]I. Mozos, [2]L. Filimon

[1]Victor Babes University of Medicine and Pharmacy, Timisoara, Romania
[2]Military Hospital, Timisoara, Romania
Email: ioanamozos@umft.ro

Abstract. *The prolonged QT interval is a known predictor of sudden cardiac death. Arterial stiffness and endothelial dysfunction are markers of premature cardiovascular disease. The aim of the present study is to assess the relationship between QT interval and arterial stiffness, endothelial function and arterial age, respectively. A total of 32 apparently healthy participants, aged 34±8 years, 69% male, underwent standard 12-lead electrocardiogram (ECG) recording and arteriography. QT intervals were automatically measured and pulse wave velocity (PWV), brachial and aortic augmentation index (Aixbra and Aixao, respectively), arterial age and diastolic coronary perfusion variables were assessed. Linear and multiple regression analysis revealed significant associations between heart rate corrected QT intervals (QTc) and brachial and aortic augmentation indices. QTc was also significantly associated with arterial stiffness, early arterial aging and impaired coronary perfusion. Arterial stiffness, endothelial dysfunction, impaired coronary perfusion and increased arterial age are associated with borderline and prolonged QT intervals.*

Keywords: QT interval, Arteriography, Early Arterial Aging, Pulse Wave Velocity, Augmentation Index

1. Introduction

The prolonged QT interval is a known predictor of sudden cardiac death The QT interval is classified as prolonged if it exceeds 460 ms in women and 450 ms in men [1]. Borderline QT intervals are those of 430-450 ms in men and 450-470 in women [2].

Cardiovascular mortality is linked to atherosclerosis and its complications [3]. Arterial stiffness and endothelial dysfunction are markers of subclinical atherosclerosis.

Vascular aging is the effect of several factors, involving oxidative stress, endothelial dysfunction, formation of advanced glycation endproducts, telomere damage, depletion of vascular progenitor cells, accumulation of senescent endothelial and vascular smooth muscle cells, vascular inflammation, microvascular rarefaction, increased arterial stiffness, and is accelerated in the presence of classical cardiovascular risk factors [4,5]. Arterial age is considered a better predictor of cardiovascular disease compared to the classical risk factors and was associated with longevity [6].

The aim of the present study was to assess the relation between QT interval and arterial stiffness, endothelial function and arterial age, respectively.

2. Methods

A total of 32, apparently healthy participants were recruited from a general practitioners office. They underwent standard 12-lead ECG and arteriography consecutively.

Exclusion criteria and ethical aspects

The most important exclusion criteria were: electrolyte imbalances, atrial fibrillation, history of myocardial infarction, stroke or diabetes mellitus and the use of drugs known to influence the QT interval or arterial stiffness.

The investigations conformed to the principles outlined in the Declaration of Helsinki [7] and were approved by the Ethics Committee of the University. Written informed consent was obtained from each patient.

Standard 12-lead ECG

Standard 12-lead ECG was performed at a paper speed of 25 mm/s and QT intervals were automatically measured.

Arteriography

Arteriography (TensioMed Ltd, Budapest, Hungary) was used to assess pulse wave velocity (PWV) as a marker of arterial stiffness, brachial and aortic augmentation index (Aixbra and Aixao, respectively) as markers of endothelial dysfunction, diastolic reflection area (DRA) and diastolic area index (DAI) as measure of coronary perfusion, arterial age (AA) and the differences between arterial and chronological age, and blood pressure values (SBP, DBP). The methodology was previously described [3]. Early arterial aging (EAA) was considered if the arterial age exceeded the chronological age.

Statistical methods

Categorical data are given as numbers and percentages, and continuous data as means ± standard deviation. Linear and stepwise multiple regression analysis were used as statistical methods.

A power analysis was conducted in order to calculate the minimum required sample size. It was found to be 31 for regression analysis with two predictors, 0.05 probability level and a desired statistical power of 0.8.

3. Results

The characteristics of the study population are included in Table 1. Heart rate corrected QT interval (QTc) according to the Bazett formula [8] was: 422±29 ms, arterial age: 44±14 years, Aixbra: -44±25%, Aixao: 15±2.31%, PWV: 8±1.45 m/s.

Considering the criteria of the European Society of Cardiology [9], blood pressure values were normal and optimal in most of the participants (62%) and high normal in 19%. Hypertension was detected in 19% of the participants.

QTc exceeded 430 ms in 38% of the participants.

Aixbra was optimal, normal and high in 78%, 13% and 9% of the participants, respectively. PWV was high (>9.7m/s) in 19% of the patients.

DAI and DRA were up to 50% and 50, respectively in 22% and 31% of the participants.

Linear regression analysis

QTc was significantly associated with arterial age, brachial and aortic augmentation indices, DAI, DRA and PWV (Table 2). Linear regression analysis also revealed significant associations between borderline and prolonged QTc and elevated PWV, impaired coronary perfusion and early arterial aging, respectively (Table 2).

Stepwise multiple regression

Multiple regression analysis revealed significant associations between heart rate corrected QT interval (QTc) and brachial and aortic augmentation indices.

QTc was also significantly associated with arterial stiffness and increased arterial age. Another regression model associated QTc with impaired DRA and DAI (Table 3).

Table 1. Characteristics of the study population

Variable	Results
Age	34±8 years
Gender	22 (69%) males
BMI	27±6.34 kg/m²
SBP	125±13 mmHg
DBP	74±10 mmHg
HR	73±10 beats/minute
Aixbra	-44±25%
Aixao	15±2.31%
DRA	53±10
DAI	53±5%
PWV	8±1.45m/s
AA	44±14 years
QTmax	377±27 ms
QTc	422±29 ms

4. Discussion

The current study demonstrates significant associations between QTc and endothelial function, arterial stiffness, arterial age and coronary perfusion.

Several previous studies demonstrated correlations between ECG variables and arterial stiffness. Chung et al independently found that arterial stiffness related to ECG left ventricular hypertrophy [10]. An independent association between brachial pulse wave velocity and QTc interval prolongation was reported by Maebuchi et al [11].

QT and QTs correlated with other markers of subclinical atherosclerosis, including intima media thickness in diabetic patients [12] and in healthy subjects in the SAPHIR program (Salzburg Atherosclerosis Prevention Program in Subjects at High Individual Risk) [13]. Takebayashi et al demonstrated that QTc prolongation in type 2 diabetes mellitus is caused primarily by coronary atherosclerosis rather than by cardiac autonomic neuropathy [12].The QT interval was also previously associated with coronary endothelial dysfunction [14].

The present study draws attention to the relation of borderline and prolonged QTc with endothelial dysfunction, arterial stiffness, impaired coronary perfusion and early arterial aging. As far as we know, it is the first study to demonstrate an association between diastolic coronary perfusion variables (DAI and DRA) and borderline and prolonged QT intervals.

Heart rate was not included in the regression models as QTc was already heart rate corrected using the Bazett formula.

The most important limitations of the present study refer to the use of the Bazett formula for heart rate correction of the QT interval, the cross-sectional design and a lack of direct arrhythmia data. The use of the Bazett formula results in an overcorrection of the QT interval at higher heart rates and an undercorrection at lower heart rates. Nevertheless, the Bazett correction formula is frequently used in clinical practice or research, especially measuring physiological heart rates. HR reached 60 beats/minute in two of the patients and exceeded 80 beats/minute in six patients in this study. QT interval and arterial stiffness have many sources of variability, including advanced age, drugs, body mass index, diabetes mellitus, dyslipidemia, smoking, heart failure, impaired renal function and hypertension. The number of patients with comorbidities was low in the present study and QT prolonging drugs were excluded. The cross sectional design does not demonstrate causative associations. It is possible to have a cause-effect relation. Left ventricular diastolic dysfunction with an impaired coronary perfusion may be the link between arterial stiffness and borderline and prolonged QT intervals. Subclinical arterial disease and coronary atherosclerosis may also be parallel processes. Surrogate markers of ventricular arrhythmia risk were used and no direct arrhythmia data were provided. Longitudinal studies are needed to confirm the causal relationship between arterial stiffness and ventricular arrhythmias and sudden cardiac death and then to confirm the findings on different populations.

Subclinical atherosclerosis is associated with borderline QT intervals. The QT interval may be used as a marker of subclinical atherosclerosis.

Table 2. Linear regression analysis. Significance F<0.01

Variable	Associated with	Multiple R	R square	Adjusted R
QTc	AA (p< 0.01)	0.949	0.902	0.869
QTc	Aixbra (p< 0.01)	0.870	0.757	0.725
QTc	Aixao (p< 0.01)	0.754	0.568	0.536
QTc	DRA (p< 0.01)	0.983	0.967	0.935
QTc	DAI (p< 0.01)	0.993	0.987	0.954
QTc	PWV (p< 0.01)	0.983	0.966	0.934
QTc > 430 ms	PWV > 9.7 m/s (p=0.00079)	0.555	0.308	0.276
QTc > 430 ms	DRA<50 (p=0.039)	0.365	0.133	0.101
QTc > 430 ms	EAA (p=0.0015)	0.53	0.281	0.248

Table 3. Multiple regression analysis. Variables significantly associated with QTc. Significance F<0.01

Associated with	Multiple R	R square	Adjusted R
Aixbra (p< 0.01)	0.997	0.995	0.961
Aixao (p< 0.01)			
Aixbra < -10%	0.969	0.939	0.904
(p= 0.01)			
EAA (p< 0.01)			
DRA < 50 (p< 0.01)	0.994	0.989	0.955
DAI < 50%			
(p< 0.01)			

5. Conclusions

Arterial stiffness, endothelial dysfunction, impaired coronary perfusion and increased arterial age are associated with borderline and prolonged QT intervals.

Detection of subjects with preclinical atherosclerosis and early arterial aging could represent an effective primary prevention method for sudden cardiac death. Borderline QT intervals could be markers of subclinical atherosclerosis.

In conclusion, further large, follow up studies are needed in order to demonstrate the usefulness of arterial stiffness, endothelial dysfunction and arterial age as predictors of sudden cardiac death.

References

[1] Rautaharju PM, et al. AHA/ACC/HRS recommendations for the standardization and interpretation of the electrocardiogram. Part IV: The ST segment, T and U waves, and the QT interval: A scientific statement from the American Heart association Electrocardiography and Arrhythmias Committee, Council on Clinical Cardiology; the American College of Cardiology Foundation; and the Heart Rhythm Society; Endoresed by the International Society for Computerized Electrocardiology. *Circulation*, 2009; 119: e241-e250.

[2] Goldenberg I, et al. QT interval: How to measure it and what is "normal". *J Cardiovasc Electrophysiol*, 2006; 17: 333-336.

[3] Mozos I, et al. Arterial age and shift work. *International Journal of Collaborative Research on Internal Medicine and Public Health*, 2013; 5(5): 340-47.

[4] Kotsis V, et al. Arterial stiffness and 24 h ambulatory blood pressure monitoring in young healthy volunteers: The early vascular ageing Aristotle University Thessaloniki Study (EVA–ARIS Study). *Atherosclerosis*, 2011; 219: 194-199.

[5] Ungvari Z, et al. Mechanisms of vascular aging: New perspectives. *J Gerontol A Biol Sci Med Sci*, 2010; 65A(10): 1028-1041.

[6] Nandish S, et al. Keeping your arteries young: Vascular health. *J Clin Hypertens*, 2011; 13: 706-7.
[7] World Medical Assocation Declaration of Helsinki. Recommendations guiding physicians in biomedical research involving human subjects. *Cardiovascular Research* 1997; 35: 2-3
[8] Bazett HC. An analysis of the time-relations of electrocardiograms. *Heart*, 1920; 7: 353-70.
[9] Mancia G, et al. 2013 ESH/ESC Guidelines for the management of arterial hypertension. *Eur Heart J*, 2013, doi:10.1093/eurheartj/eht151.
[10] Chung CM, et al. Arterial stiffness is the independent factor of left ventricular hypertrophy determined by electrocardiogram. *Am J Med Sci*, 2012; 344(3): 190-3.
[11] Maebuchi D, et al. Arterial stiffness and QT interval prolongation in a general population: The Hisayama study. *Hypertension Research*, 2008; 31: 1339-45.
[12] Takebayashi K, et al. Association between the corrected QT intervals and combined intimal-medial thickness of the carotid artery in patients with type 2 diabetes. *Metabolism*, 2004; 53(9); 1152-7.
[13] Strohmer B, et al. Relationship of QT interval duration with carotid intima media thickness in a clinically healthy population undergoing cardiovascular risk screening. *J Intern Med*, 2005; 257(3): 238-46.
[14] Kumar G, et al. Electrocardiographic changes in coronary endothelial dysfunction. *Coron Artery Dis*, 2008; 19(6): 395-8.

RELATION OF PREOPERATIVE HEART RATE TURBULENCE PARAMETERS WITH VENTRICULAR ARRHYTHMIAS AFTER CORONARY ARTERY BYPASS GRAFTING

E. Dyuzheva, G. Ryabykina, A. Sobolev, A. Vlasova

Russian Cardiology Research and Production Complex, Moscow, Russia
E-mail: ecg.newtekh@gmail.ru

Abstract. *The aim of this study was to reveal the relationship of preoperative heart rate turbulence (HRT) parameters with ventricular arrhythmias (VA) after coronary artery bypass grafting (CABG). We studied 58 patients with multiple coronary vessel disease: 16 – with depressed left ventricular ejection fraction (LVEF), 42 – with preserved LVEF. 44 (76%) had a history of myocardial infarction. The control group consisted of 17 patients without coronary artery disease (CAD) with normal LVEF. Turbulence onset (TO) and turbulence slope (TS) were calculated from Holter recordings of participants. Holter was repeated in 7-14 days and 4-6 months after CABG. There were significant differences in TO mean and TS mean between CAD and control groups: -1, 1 vs -3, 1, p<0,01 (TO); 4,7 vs 12, p<0,01 (TS). TO max was significantly higher in depressed LVEF subgroup (LVEF s) compared with preserved LVEF s: 11,9 vs 7,2, p<0,05. Preoperative TO max moderately correlated with postoperative ventricular premature complexes (VPCs) (r-0,5, p<0,05). Patients with postoperative unsustained ventricular tachycardia (VT) had significantly higher preoperative TO max than those without; 11 vs 5, 9, p<0,05. Preoperative TS min moderately correlated with postoperative ventricular premature complexes (VPCs) and ventricular pairs (VP) (r = -0,6, p<0,05). If preoperative TS min was less than "– 2", than there were significantly more postoperative VPCs: 1707 vs 99, p<0,01; and VP: 35 vs 0,6, p<0,05. Preoperative and early postoperative TO max and TS min can be prognostic factors of postoperative VA.*

Keywords: Heart Rate Turbulence, Coronary Artery Bypass Grafting, Ventricular Arrhythmia

1. Introduction

Sudden cardiac death (SCD) risk assessment and the selection of candidates eligible for primary prevention of lethal arrhythmia remains an important question for modern cardiology. Heart rate turbulence (HRT) evaluation is one of the main risk assessment methods that are used in patients following myocardial infarction. HRT refers to the baroreflex-mediated fluctuations of RR intervals following spontaneous ventricular premature complexes (sVPC) [1]. The prognostic value of HRT has been confirmed in a number of clinical trials [1-5]. It is important that this method helps to identify the individuals at high risk for SCD who do not present with severe left ventricular dysfunction [3]. A small numbers of studies employing the assessment of HRT in patients undergoing coronary artery bypass grafting (CABG) have been published [3, 4].

The aim of our study was to reveal the relationship of preoperative and early postoperative HRT parameters with VA after CABG.

2. Methods

We studied 58 patients with multiple vessel coronary artery disease (46-men, 12-women) with a.mean age of 63±8 years. There were 16 patients with depressed left ventricular

ejection fraction (LVEF) (mean=32±6%), 42 – with preserved LVEF (mean=56±7%). 44(76%) had a history of myocardial infarction, 14(24%) – diabetes mellitus. The control group consisted of 17 patients without coronary artery disease (CAD) and with normal LVEF. All participants underwent Holter monitoring (HM) (DMS Advanced Technologies equipment). CABG surgery with complete revascularization was performed in 47 CAD patients. HM was repeated in 7-14 days (n=47) and 4-6 month (n=36) after CABG.

PVCs applicable for HRT assessment were selected by the program based on the set criteria of Schmidt et al [5].We determined turbulence onset (TO), turbulence slope (TS) according to these authors. TO is calculated as:

TO={[(RR1+ RR2) – (RR-2 + RR-1)]/(RR-2 + RR-1)} x 100%,

where RR-2 and RR-1 – 2 RR intervals immediately preceding the VPC coupling interval, RR1 and RR2 intervals immediately after compensatory pause.

TS is defined as the maximum positive regression slope assessed over any 5 consecutive sinus rhythm RR intervals within the first 15 sinus RR intervals after a VPC.

As well as assessing mean TO and TS values, we investigated the extreme (maximum and minimum) values of these parameters (Fig.1), thus, focusing on the largest deviation from the norm of the investigated parameters.

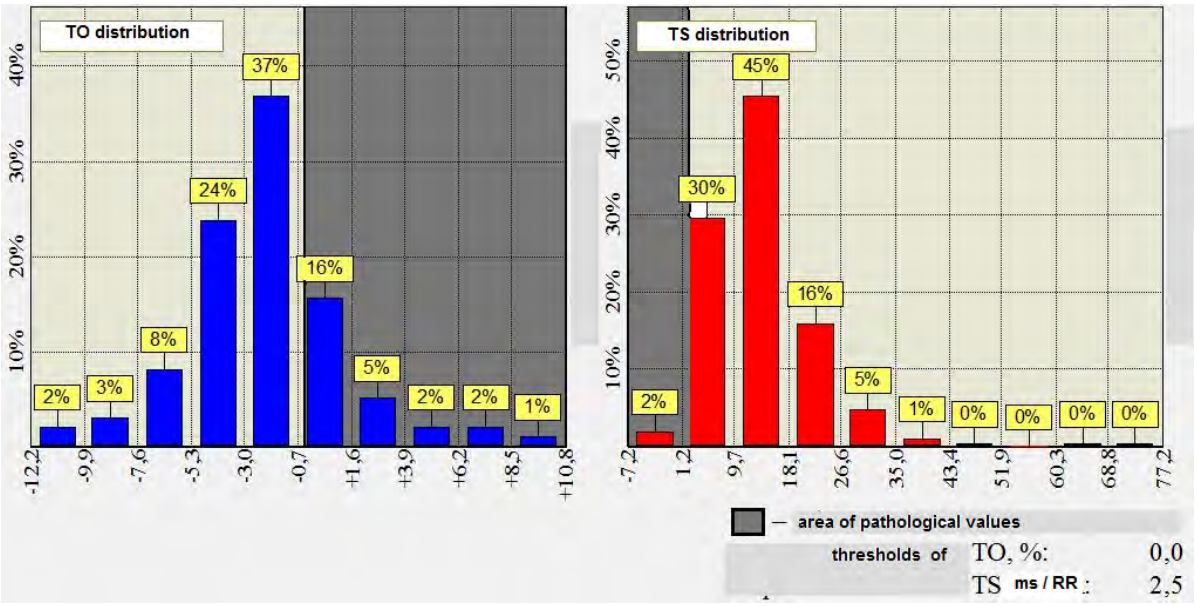

Fig. 1. TO and TS distribution in 24 hour Holter recording

3. Results

There were significant differences in TO mean and TS mean between CAD and control groups (Table 1). TO max was significantly higher in depressed LVEF subgroup (LVEFs) compared with preserved LVEFs: 12 vs 7, 2, p<0,05. Depressed LVEFs patients were more likely to have HRT category 2 and less likely - HRT category 0 compared with preserved LVEFs (Table 2). Preoperative TO max moderately correlated with postoperative ventricular premature complexes (VPCs) (r=0,5, p<0,05). Preoperative TS min moderately correlated with postoperative ventricular premature complexes (Fig 2), ventricular pairs (VPs) (r= -0,5, p<0,05) and nonsustained ventricular tachycardia (nVT) (r= -0,4, p<0,05). Severity of postoperative ventricular arrhythmias depends on the preoperative TS min and TO max values. If preoperative TS min was less than “– 2”, then there were significantly more

postoperative VPCs and VP (Table 3). If preoperative TS min was < -2, then more than 30 PVCs/h were in early postoperative period (sensitivity-90%, specificity- 63%). For Preoperative TO max>10 (sensitivity was-60%, specificity-79%)

TO and TS mean values have shown no significant correlation with ventricular arrhythmias in study group.

Table. 1 .HRT parameters in CAD patients compared with controls

Group	TO mean	TO max	TO min	TS min	TS max	TS min
CAD N=17	-1,2±1	8,7±6	-9,1±5	4,8±4	42±21	-2±5
Control N=17	-3,1±2	8±4	-13±4	10±7	60±18	0,7±3
t-test	P<0,05	NS	NS	p<0,01	P<0,05	NS

Table. 2 HRT categories distribution in CAD subgroups with different LVEF

Mean LVEF %	Single HRT episodes Category 0	Normal TO, TS Category 0	Abnormal TO or TS Category 1	Abnormal TO and TS Category 2
56±6,7 N=42	18(43%)	19(45%)	5(12%)	0 (0%)
32±6 N=16	3 (19%)	6(37,5%)	1(6%)	6 (37,5%)

Table. 3 Relationship between postoperative ventricular arrhythmia severity and preoperative TS min values

Postoperative Ventricular Arrhythmias	TS min ≤ -2 Before CABG	TS min > -2 Before CABG	T-test
PVCs	1707	99	P<0,01
VPs	35	0,6	P<0,05
nVT	1,1	0,2	P=0,06

Early postoperative TS min and TO max differ significantly in patients with more or less than 30 PVCs/h in 4-6 month after CABG: TS min -2,5 vs -1, p<0.05, TO max 15,3 vs 5,6, p<0,05, respectively. Using the proposed threshold levels, we can assume the occurrence of ventricular arrhythmias after CABG: Early postoperative TS min < -2 suggests the occurrence of more than 30 PVCs/h at 4-6 months after CABG (sensitivity-64%, specificity-81 %). TO max >10 - sensitivity-60%, specificity-86%)

4 Discussion

The normal mean TO and TS values (regarding the thresholds proposed by Schmidt et al [5]) were the most common values in the study group of patients. No deaths including sudden cardiac death occurred during the study period. As TO and TS mean values had no significant

correlation with VA in the study group, new approaches were found to be needed to achieve the aim of the study. Cygankiewicz et al [3] suggested the use of other thresholds of mean TO and TS to allow a better risk stratification in the study group of patients before CABG.

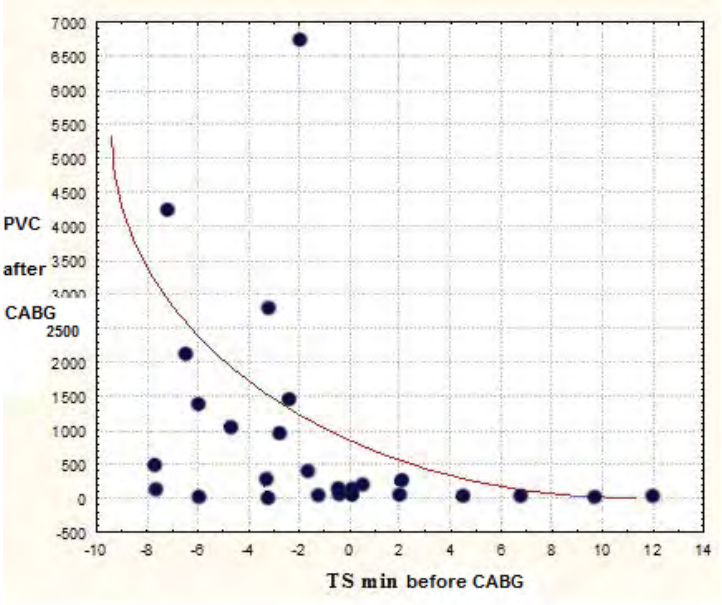

Fig. 2. Relation between preoperative TS min and postoperative ventricular arrhythmias (R= -0,6, p<0,05)

We identified the HRT parameters (namely TO max and TS min) that had significant correlation with VA. Moreover, preoperative TO max and TS min correlated with early postoperative VA, while early postoperative TO max and TS min were significantly worse in patients with more than 30PVCs/hour at 4-6 months after CABG. The results led us to conclude that further investigations are necessary to confirm the value of TO max and TS min.

5. Conclusions

i. HRT parameters reflecting the greatest deviation of the TO and TS values towards abnormal values can be important markers of autonomic dysfunction

ii. Interdependences between preoperative TS min TO max values and postoperative VA were identified. These HRT parameters can be useful prognostic factors of postoperative ventricular arrhythmias.

References

[1] Bauer A, Malik M, Schmidt G et al. Heart rate turbulence: Standards of measurement, physiological interpretation, and clinical use. *International Society for Holter and Noninvasive Electrophysiology consensus/Journal of the American College of Cardiology*, 2008; 52: 1353-1365.

[2] Bauer A, Barthel P, Schneider R et al. Improved stratification of autonomic regulation for risk prediction in post-infarction patients with preserved ventricular function (ISAR-Risk) *European Heart Journal*, 2009; 30: 576-583.

[3] Cygankiewicz I, Wranicz JK, Bolinska H, Zaslonka J, Jaszewski R, Zareba W. Prognostic significance of heart rate turbulence in patients undergoing coronary artery bypass grafting. *American Journal of Cardiology*, 2003; 91: 1471-4.

[4] Cygankiewicz I, Wranicz JK, Bolinska H, Zaslonka J, Jaszewski R, Zareba W. Influence of coronary artery bypass grafting on heart rate turbulence parameters. *American Journal of Cardiology*, 2004; 94; 186-9.

[5] Schmidt G, Malik M, Barthel P et al. Heart rate turbulence after ventricular premature beats as a predictor of mortality after acute myocardial infarction. *Lancet*, 1999; 353: 1390-6.

ECG VS. BLOOD PRESSURE (SYSTOLIC, DIASTOLIC, MEAN AND PULSE): AN EXTENDED APPROACH TO BAROREFLEX SENSITIVITY

A. Singh, B.S. Saini, G.S. Dhaliwal

Department of Electronics and Communication Engineering,
National Institute of Technology, Punjab, India
Email: apsingh.lpu@gmail.com

Abstract. *Cardiac baroreflex is an important short-term mechanism which controls (regulates) blood pressure (BP) by altering heart rate (HR). The vital role of baroreflex sensitivity (BRS) as a prognostic factor for various cardiovascular diseases is well established. All BP measures are strongly and directly related to the risk of cardiovascular problems but their relative role in baroreflex control is yet to be fully understood. To explore the relative importance of all types of BP variabilities on baroreflex control, BRS is estimated using the transfer function method with weighted coherence ≥0.2 by choosing systolic BP (SBP), diastolic BP (DBP), mean arterial pressure (MAP) and pulse pressure (PP) as input variables and RR intervals derived from the electrocardiogram (ECG) as output variables. Correlation between BRS indices obtained using all BP measures is computed. BRS is estimated on 10 healthy subjects recorded using Biopac MP100 system. EuroBaVar data is used for the analysis. It is found that except for SBP based BRS estimation, all other BRS estimates provide a decreased number of BRS responses, especially for patients with impaired baroreflex. Correlation between DBP, MAP and PP based BRS estimation is found with SBP based BRS estimation with coefficients of 0.708, 0.816 and 0.952 respectively in the low frequency (LF) region. It is also found that weighted coherence criterion provides enhanced coherence values as compared to mean coherence which results in an increased number of BRS responses.*

Keywords: Baroreflex Sensitivity, Coherence, Weighted Coherence Transfer Function

1. Introduction

The baroreflex mechanism plays a vital role in cardiovascular regulation by contributing to the sympathetic-vagal imbalance triggered by the baroreceptor reflex, and hence is crucial for predicting the development and progression of many cardiovascular diseases. Blood pressure (BP) is an important predictor of future cardiovascular risk. Blood pressure changes are detected by the baroreflex and a corrective action is initiated by controlling sympathetic and vagal outflow to alter heart rate accordingly. Therefore BP plays an important role in functioning of the baroreflex. Moreover, clinicians have traditionally recognized all the components of blood pressure, viz. systolic BP (SBP), diastolic BP (DBP), mean arterial pressure (MAP) and pulse pressure (PP). SBP has been found to possess an important prognostic value, particularly in older subjects [1]. Framingham Heart Study [2] and other studies [3] have found that SBP increases continuously with age, whereas DBP increases until the age of 60 years and then begins to decrease gradually. BP is also characterized by its pulsatile (estimated by PP) and steady (estimated by MAP) components [4]. Two recent studies [5, 6] have highlighted the importance of PP, defined as SBP-DBP, as a predictor of cardiovascular events or mortality in the elderly. MAP is defined as 1/3rd of systolic BP plus 2/3rd of diastolic BP as a predictor of cardiovascular disease risk. It remains unclear which measures of BP, either itself or in combination; best predict the risk of cardiovascular disease mortality [4]. The Brisighella Heart Study [7] has shown that SBP is a stronger predictor of

cardiovascular events than DBP. MAP is considered to be a function of left ventricular contractility, heart rate and vascular resistance and elasticity averaged over time [8]. It remains unclear whether SBP, DBP, MAP and PP variabilities reveal different or similar aspects of autonomic control. Baroreflex sensitivity (BRS) has been evaluated using a variety of techniques [9] which used SBP and MBP along with RR intervals and pulse intervals (PI). Recent methods use non-invasive means of evaluating BRS and are based on spontaneous beat-to-beat measurement of both blood pressure and heart rate. Sequence method and cross correlation methods are among the most popular time domain methods. Frequency domain methods include parametric and non-parametric spectral estimation to estimate low frequency (LF) and high frequency (HF) gain [10]. Some studies have also taken into account the phase or time-delays between beat-to-beat systolic pressure and RR intervals series to estimate BRS [11]. The measurability of spectral techniques is affected by various limitations which include the presence of ectopic beats and strict algorithmic parameters such as coherence criterion. The use of coherence criterion (>0.5 is mostly used) to assess the strength of the linear association between blood pressure and RR interval oscillations is too strict in the case of pathological conditions where coherence drastically falls. The use of coherence criterion used by Clayton et al [12] has been challenged on the account that reliable BRS measurement is not guaranteed even after checking the coherence. Accordingly, there exists trade-off between accuracy and measurement in BRS estimation. In this paper, we focus on the accuracy of BRS estimation as well as the measurability aspect by using a weighted coherence criterion. In addition, the relative role of SBP, DBP, MAP and PP is analyzed in the estimation of BRS.

2. Methods

A. Sample

21 subjects from the EuroBaVar dataset (4 males and 17 females) aged 20 to 68 years (38±14.7, mean±SD) along with the recorded data of 10 healthy subjects aged between 20 to 27 years (23±2.2, mean±SD) were obtained for BRS estimation. In the EuroBaVar dataset, there are 4 healthy volunteers, 8 outpatients, 3 hypertension patients, 2 hypercholesterolemic patients, 1 diabetic patient without neuropathy, 1 diabetic patient with neuropathy (BRS failure), 1 heart transplant patient (BRS failure) and 1 pregnant woman.

B. Data Pre-processing

Ectopic beats were manually removed from the EuroBaVar data. Pulse pressure is calculated as the difference between SBP and DBP. RR intervals, SBP, DBP, MAP and PP are mean subtracted. RR intervals, SBP, DBP, MAP, and PP are irregularly sampled as heart rate spectral distortions may be present. Therefore, to avoid these problems, all variables are interpolated and resampled at 4 Hz.

C. Weighted Coherence

Coherence is calculated by performing cross spectral analysis which gives the linear association between each observed rhythm in one variable on the same rhythm in the second variable. Spectral analysis is performed using the Welch method with 50% overlap using the Hann window [13]. Magnitude squared coherence is defined as the square of the correlation between two signals as a function of frequency and is given by the following equation:

$$Coh^2(f) = \frac{|S_{XY}(f)|^2}{S_X(f).S_Y(f)} \quad (1)$$

Weighted coherence provides an exact measurement of the proportion of variance on a series that is shared between two processes [14]. The two variables may have similar spectra during the states in which the two processes are related. Therefore, to quantify the relation between two signals in a particular frequency band, a new measure C_W termed weighted coherence is proposed and is defined by the following equation:

$$C_W = \frac{\sum_{f_1}^{f_2} Coh^2(f).\ S_X(f)}{\sum_{f_1}^{f_2} S_X(f)} \tag{2}$$

D. BRS estimation using transfer function method

BRS index over the LF and HF band is calculated by considering the power values in the LF and HF band to obtain LF-BRS and HF-BRS as per following equations:

$$\alpha_{LF} = \sqrt{\frac{P_{LF\text{ - }RR}}{P_{LF\text{ - }X}}} \tag{3}$$

$$\alpha_{HF} = \sqrt{\frac{P_{HF\text{ - }RR}}{P_{HF\text{ - }X}}} \tag{4}$$

Where, X is taken as SBP, DBP, MAP and PP power for calculation of BRS index using all component BP variabilities respectively.

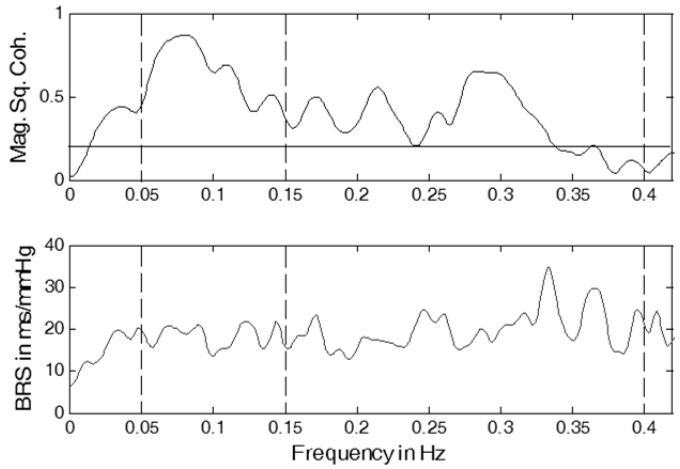

Fig. 1. Coherence function between RR intervals SBP values (top), BRS transfer (gain) function (bottom) dotted lines indicate bifurcation of LF and HF band, solid line indicates the weighted coherence of threshold of 0.2

Magnitude squared coherence is calculated using equation (1) from all the frequencies in the autonomic range (0-0.5Hz) and the corresponding BRS gain is computed as shown in Fig. 1.

Table 1 shows the demographic data of the subjects of the EuroBaVar dataset along with that of the 10 recorded healthy subjects. Both mean and weighted coherence is calculated, followed by BRS estimation. BRS is evaluated using RR interval series with all the four blood pressure variabilities viz. SBP, DBP, MAP and PP. A threshold value of 0.2 for both mean and weighted coherence is used to evaluate BRS estimates. BRS is evaluated for all of the 31 subjects under consideration.

Table 1. Demographic data of the 31 subjects (values are in mean±SE)

Parameters	Mean±SE
Age, yr	38.4±3.3
Height, m	1.65±0.02
Weight, kg	64.1±2.4
Body mass index, kg/m^2	23.3±0.8
HR supine, beats/min	70.7±3.0
SBP supine, mmHg	121. ±4.0
DBP supine, mmHg	61.8±2.6
MAP supine, mmHg	89±3.5
PP supine, mmHg	59.2±1.5
HR standing, beats/min	83.0±3.3
SBP standing, mmHg	121.2±4.7
DBP standing, mmHg	67.9±2.5
MAP standing, mmHg	93.2±2.1
PP standing, mmHg	53.3±2.3

3. Results and Discussion

Table 2 shows the percentage responses of BRS estimation from all of the 31 subjects under consideration with the coherence and weighted coherence threshold>0.2. It has been observed that weighted coherence provides a greater number of BRS estimates than mean coherence. This is true in both healthy as well as pathological cases. Moreover, larger numbers of responses are found both in standing and in supine position when BRS is estimated using SBP rather than DBP, MAP and PP. Weighted coherence is found to be a more sensitive measure than that of mean coherence in BRS estimation using the transfer function method. This is evident from the enhanced values of weighted coherence in the cases where coherence is just below the threshold value of 0.2. Correlation between DBP, MAP and PP based BRS estimation is found with SBP based BRS estimation with coefficients of 0.708, 0.816 and 0.952 respectively and is shown in Figs. 2(a), 2(b) and 2(c). This shows that BRS can be estimated using all four variability components of blood pressure and hence provides greater prognostic information.

Table. 2 Percentage responses using weighted coherence compared with mean coherence

BRS parameters	**Thresholds**	**%age responses (out of 31 subjects)**			
		Supine-LF	**Standing-LF**	**Supine-HF**	**Standing-HF**
SBP, R-R int.	C_W>0.2	95.6	95.6	100	100
DBP, R-R int.	C_W>0.2	91.3	95.6	100	91.3
MAP, R-R int.	C_W>0.2	91.3	100	91.3	82.6
PP, R-R int.	C_W>0.2	100	95.6	95.6	100
SBP, R-R int.	Coh>0.2	91.3	95.6	95.6	100
DBP, R-R int.	Coh>0.2	100	91.3	100	91.3
MAP, R-R int.	Coh>0.2	91.3	95.6	91.3	82.6
PP, R-R int.	Coh>0.2	82.6	91.3	91.3	95.6

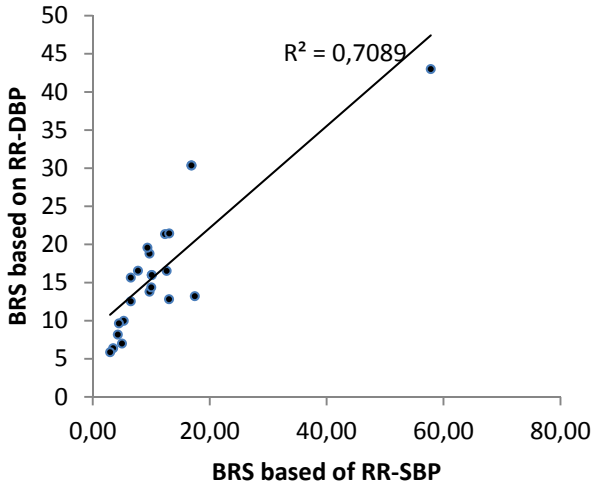

Fig. 2(a). Correlation between BRS obtained using RR-SBP and RR-DBP

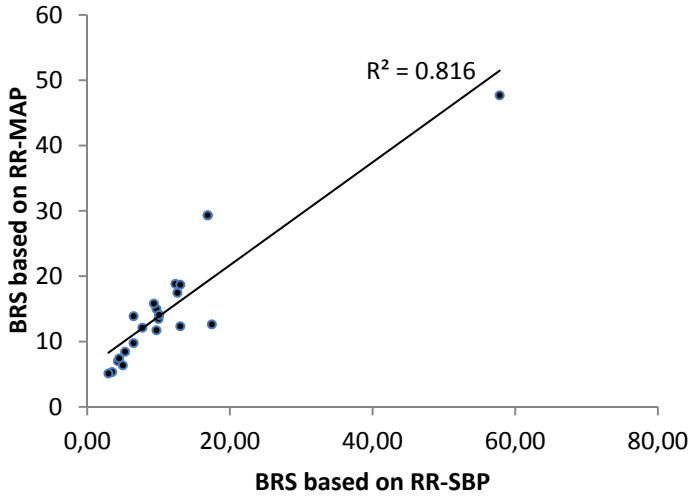

Fig. 2(b). Correlation between BRS obtained using RR-SBP and RR-MAP

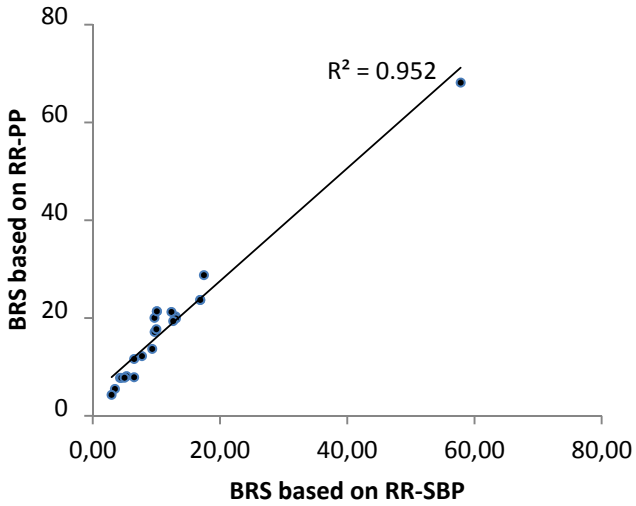

Fig. 2(c). Correlation between BRS obtained using RR-SBP and RR-PP

4. Conclusions

Weighted coherence is a more sensitive measure than mean coherence and is a novel index to quantify coherence between two related time series such as RR interval and blood pressure. Thus, weighted coherence criterion provides enhanced coherence values as compared to mean coherence which results in increased number of BRS responses. It is found that with the exception of SBP based BRS estimation, all other BRS estimates provide a decreased number of BRS responses, particularly for patients with impaired baroreflex.

References

[1] Benetos A, Thomas F, Bean K, Gautier S, Smulyan H, Guize L. Prognostic value of systolic and diastolic blood pressure in treated hypertensive men. *Arch Intern Med*, 2002; 162: 506–508.

[2] Darne B, Girerd X, Safar M, Cambien F, Guize L. Pulsatile versus steady component of blood pressure: a cross-sectional analysis and a prospective analysis on cardiovascular mortality. *Hypertension*, 1989; 13: 392–400.

[3] Lee ML, Rosner BA, Vokonas PS, Weiss ST. Longitudinal analysis of adult male blood pressure: the Normative Aging Study, 1963–1992. *J Epidemiol Biostat*, 1996; 1: 79–87.

[4] Howard D. Sesso, Meir J. Stampfer, Bernard Rosner, Charles H. Hennekens, J. Michael Gaziano, JoAnn E. Manson, Robert J. Glynn, Systolic and Diastolic Blood Pressure, Pulse Pressure, and Mean Arterial Pressure as Predictors of Cardiovascular Disease Risk in Men. *Hypertension*, 2000; 36: 801-807.

[5] Safar ME, Pulse pressure in essential hypertension: clinical and therapeutical implications. *J Hypertens*, 1989; 7: 769–776.

[6] Darne B, Girerd X, Safar M, Cambien F, Guize L. Pulsatile versus steady component of blood pressure: a cross-sectional analysis and a prospective analysis on cardiovascular mortality. *Hypertension*, 1989; 13: 392–400.

[7] Borghi C, Dormi A, L'Italien G, Lapuerta P, Franklin SS, Collatina S, Gaddi A. The relationship between systolic blood pressure and cardiovascular risk-results of the Brisighella Heart Study. *J Clin Hypertens (Greenwich)*, 2003; Jan-Feb; 5(1): 47-52.

[8] Gabor S, Bedros RJ, Medvegy M. The short term effect of sibutramine treatment on mean arterial pressure and pulse pressure during weight loss. *The Journal of Clinical Hypertension*, 2008; 10: 5SA: 258.

[9] Laude D, Elghozi J, Girard A, et al.. Comparison of various techniques used to estimate spontaneous baroreflex sensitivity (the EuroBaVar study). *Am. J. Physiol, Regulatory, Integrative and Comparative Physiology*, 2004; 286: R226-R231.

[10] Task Force of the European Society of Cardiology and the North American Society of Pacing and Electrophysiology, Heart rate variability-standards of measurement, physiological interpretation and clinical use. *European Heart Journal*, 1996; 17: 354-38.

[11] Khan S, Bandyopadhyay S, Ganguly AR, Saigal S, Erickson DJ, Protopopescu V, Ostrouchov G. Relative performance of mutual information estimation methods for quantifying the dependence among short and noisy data. *Physical Review E*, 2007; 76:1-15.

[12] Clayton RH, Bowman AJ, Ford GA Murray A. Measurement of baroreflex gain from heart rate and blood pressure spectra: A comparison of spectral estimation techniques. *Physiological Measurement*, 1995; 16.

[13] Singh D, Vinod K, Saxena SC, Deepak KK. Effects of RR segment duration on HRV spectrum estimation.*Physiol Meas*, 2004; 25(3): 721-35.

[14] Kumar V, Barua A, Sattaraju I, Mallavarapu N. Weighted Coherence: A More Effective Measure than Average Coherence. *Cardiovascular Engineering: An International Journal*, 2003; 3: No. 4.

EFFECT OF PACING RATE ON CARDIAC OUTPUT AND PULSE WAVE VELOCITY AT REST

[1]L. Soukup, [1,2]V. Vondra, [2]I. Viščor, [1,2]P. Jurák, [1,2]J. Halámek

[1]International Clinical Research Center - Center of Biomedical Engineering, St. Anne's University Hospital Brno, Brno, Czech Republic
[2]Institute of Scientific Instruments AS CR, Brno, Czech Republic
Email: ladislav.soukup@fnusa.cz

Abstract. *The aim of this study was to extend knowledge about the effect of pacing rate on the cardiovascular system, primarily on pulse wave velocity (PWV) and cardiac output (CO). We also wanted to test the bioimpedance method for PWV measurement by using the device designed in ISI Brno in clinical research. The biological signals were measured continuously in 24 volunteers with implanted pacemakers. During the experiment, the patients were in the supine position and the pacing rate was increased from 80 to 100 and 120 bpm repetitively. The PWV and the CO were determined by the bioimpedance method. Systolic pressure, diastolic pressure, mean arterial pressure and pulse pressure were also computed. All parameters were normalized to allow a comparison of trends. After normalization it was ascertained that the CO (2.9% decrease), PWV(1.2% decrease) and blood pressure (except for pulse pressure) do not significantly depend on pacing rate at rest.*

Keywords: Stroke Volume, Cardiac Output, Pulse Wave Velocity, Bioimpedance Method, Pacemakers

1. Introduction

Bioimpedance cardiography, also known as impedance cardiography (ICG), is a method that estimates stroke volume (SV) beat-to-beat. It can also be used for pulse wave velocity (PWV) determination. The basis of this method was founded in 1932 and is still the subject of investigation [1]. The great advantages of this technique are that it is non-invasive, and makes low demands on medical personnel and instrumentation.

Cardiac output (CO) and pulse wave velocity (PWV) are important markers for cardiovascular disease. The level of arterial stiffness and atherosclerosis can be expressed by PWV. Many studies have proven the dependence of PWV and CO on heart rate (HR), but the results are not always the same [2-5]. However, this dependence is poorly described in patients with an implanted pacemaker. The aim of this study was to extend knowledge about the effect of pacing rate on the cardiovascular system. The bioimpedance method appears to be suitable for the estimation of CO and PWV (two channel version) in these patients, but the accuracy of the absolute value of CO is limited. Moreover, this method is convenient for patients. The tests involved used the bioimpedance technique for PWV measurement by the device designed in ISI Brno following clinical research.

2. Methods

The present study was performed with 24 volunteers with an implanted pacemaker. The pacemaker was implanted at least one year before measurement. The patients were examined at their regular check-up at the clinic. The subjects were tested while awake in a supine position on the bed.

Each measurement involves eight 6-minute intervals. The sequence is as follows (with HR controlled by the pacemaker): HR=80bpm; HR=120bpm; HR=80bpm; HR=100bpm; HR=80bpm; HR=100bpm; HR=80bpm; HR=120bpm.

The biological signals were measured continuously, namely ECG (6 or 12 leads), blood pressure, phonocardiogram (PCG), and bioimpedance of thorax and calf. The blood pressure was measured by Finapres-2300 (Ohmeda). For data reporting of bioimpedance, our in house device was used. There were two current sources with frequency offset of 2 kHz (i.e. 48 kHz and 50 kHz) used for the separation of channels [6] (see Fig. 1). The ECG was also recorded by our device. One control ECG lead from the patient's monitor was recorded at the same time. The blood pressure, at the beginning and the end of the test was measured manually from the cuff on the left arm.

The analogue signals were sampled at 500 Hz, and converted to digital form (by a 16-bit Analogue-to-Digital Converter). Data was stored in binary files for subsequent analyses.

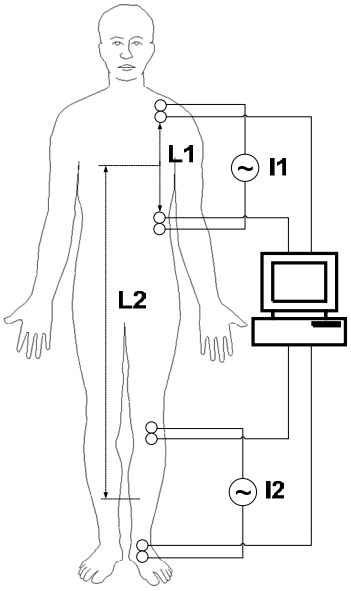

Fig. 1. Setup of bioimpedance device

Estimation of stroke volume

The Sramek-Bernstein formula was applied for evaluation of stroke volume (SV) [1,7,8].
The impedance variables, in addition to the left ventricular ejection time LVET and patient´s height and weight, were input to the following equation:

$$SV = \delta \frac{L^3}{4{,}25} \left(\frac{dZ / dt_{\max}}{Z_0} \right) LVET \qquad (1)$$

where

δ correction factor ($\delta = \sqrt{(BIM \quad / 24)}$)

BMI body mass index

L distance between voltage sensing electrodes on thorax

Z_0 static impedance of tissue

LVET left ventricular ejection time

The left ventricular ejection time (LVET) was calculated from the energy of the PCG by filtering and subsequent detection of heart sounds [9]. It was taken as the time delay between the first and second heart sound (see Fig. 2). The dZ/dt max indicates peak first time-derivative, peak slope, or maximum time-rate of change of the transthoracic cardiogenic impedance pulse variation (Ω/s) [1].

The cardiac output was calculated by multiplying the heart rate by stroke volume (volume of blood ejected per contraction) and serves as an indicator of total blood flow.

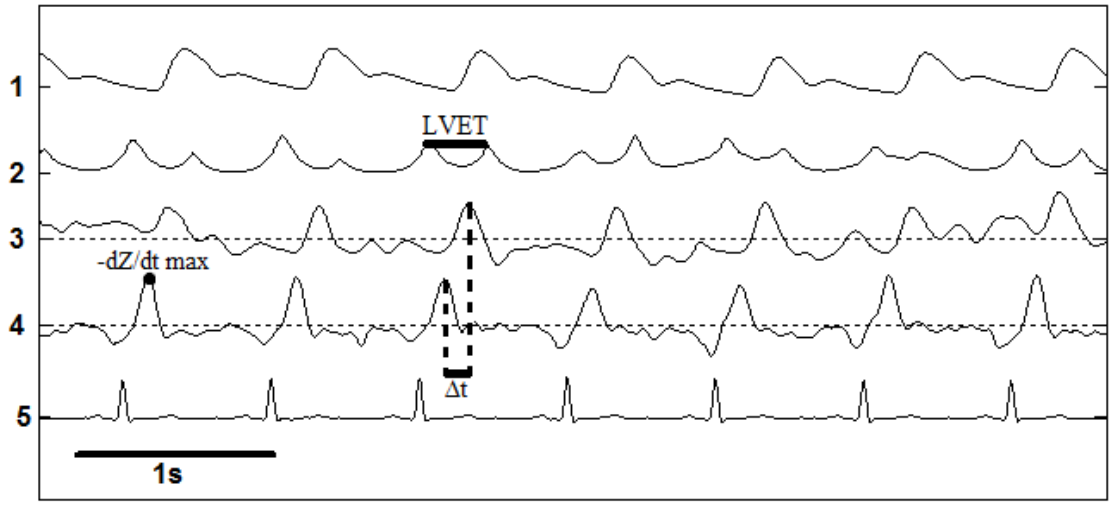

Fig. 2. Example of signals for detection, from top: 1. BP, 2. Energy of PCG, 3. -dZ/dt calf, 4. -dZ/dt thorax, ECG (I lead)

Estimation of pulse wave velocity

The pulse wave velocity (PWV) was determined as the rate of change of position of the pulse wave. Propagation of the pulse wave in the arteries leads to small changes of electrical impedance of the investigated section. It was computed by dividing the length of measured section by the delay between the maximum of derived impedance signals from thorax and calf (see Fig.1 and Fig.2).

$$PWV = \frac{L2}{\Delta t} \tag{2}$$

where

L2 distance between the centres of voltage electrodes on thorax and calf

Δt time delay between maximum of derivative impedance signals from thorax and calf

All processing was done in MATLAB.

3. Results

The statistical group consisted of 20 men and 4 women, average age 74.6±9.4 years. Systolic pressure, diastolic pressure, mean arterial pressure and pulse pressure were also analysed. Only those intervals with all signals without errors and/or artefacts (signal interruption or corruption, extrasystoles etc.) were chosen in order to maximize valid results. All parameters on each HR (80, 100 and 120) were necessary for evaluation. The computed parameters were normalized for comparison trends in the whole group. Parameters for every subject were

normalized individually so that its mean value over all HR (as 100%) was taken and subsequently, the corresponding parameter was normalized to this value. These mean relative changes (± standard deviation) and p-value are displayed in Table 1.

Table 1. Relative change±standard deviation and p-value of computed variables.

HR [bpm]	**80**		**100**		**120**		**Across**
Parameter	change±SD	p-value	change±SD	p-value	change±SD	p-value	p-value
SV	121.7±4,5	<0.001	98.6±4,9	<0.001	81.0±4,2	<0.001	<0.001
LVET	107.6±3,5	<0.001	100.2±2,7	<0.001	92.1±4,1	<0.001	<0.001
CO	100.2±4,1	<0.001	100.5±3,4	<0.001	99.3±4,3	<0.001	0.695
PWV	101.1±3.7	<0.001	100.1±3,7	<0.001	98.2±5,0	<0.001	0.120
SBP	103.3±15.3	<0,001	99.7±3,3	<0.001	97.0±13,8	<0.001	0.260
DBP	98.5±15.3	<0,001	100.0±3,4	<0.001	101.5±14,0	<0.001	0.740
PP	106.8±6.2	<0,001	100.3±4,6	<0.001	93.4±6,3	<0.001	<0.001
MAP	100.3±14.7	<0,001	100.1±2,7	<0.001	99.6±14,0	<0.001	0983

A two-sided sign test was used to determine whether the parameters (on individual HR) come from a continuous distribution with zero median. The p-value <0.05 was detected as significant. P-value across all HR for individual parameters was evaluated by ANOVA. Fig 3. and Fig 4. show the relative changes in box plot, where the dashed line illustrates 100% (mean of absolute value).

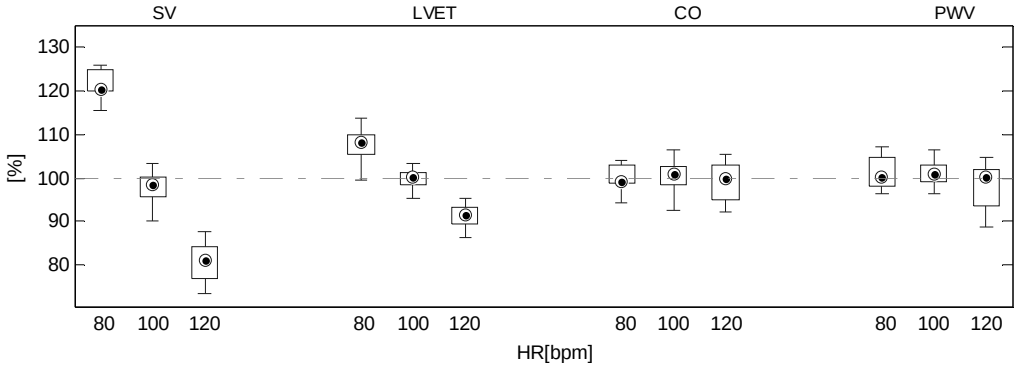

Fig. 3. Graphic representation of relative changes in following hemodynamic parameters (CO, SV, LVET, PWV)

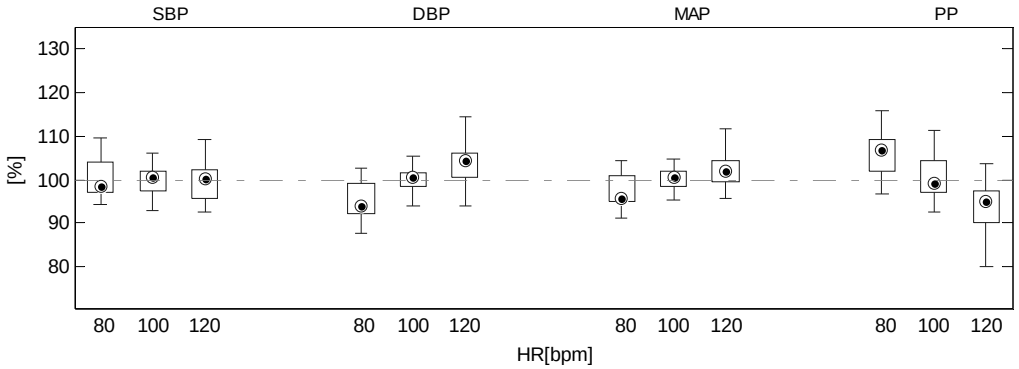

Fig. 4. Graphic representation of relative changes in blood pressures

4. Discussion and Conclusions

The main aim of this study was to explore the dependence of the following hemodynamic parameters, particularly cardiac output and pulse wave velocity, on pacing rate. These two parameters were estimated from the bioimpedance of the thorax and calf. Systolic, diastolic, mean arterial and pulse pressure were also deducted. On the one hand, the estimation of absolute value of cardiac output by the bioimpedance method was not too accurate. On the other hand, after normalisation, it was useful for monitoring the trend. It is an undemanding and comfortable measurement method for patients and medical personnel. In addition, two channels of bioimpedance was easy to apply for the evaluation of pulse wave velocity.

Our results were based on a statistical group which consisted of 20 men and 4 women, average age 74.6±9.4 years. Detection was slightly complicated due to errors and/or artefacts in measured signals (often due to estimation of CO).Those problems were mainly caused by the health state and age of the subjects, e.g. numerous estrasystoles and so on. After normalisation and statistical processing it was found that the cardiac output, pulse wave velocity, systolic pressure, diastolic pressure and mean arterial pressure do not significantly change on increasing the pacing rate at rest. There is 2.9% decrease in PWV and 1.2% decrease in CO across the whole HR interval (80-120 bpm). Independence of cardiac output may be caused by lack of demand for more blood at the rest. There is no sympathetic activity, e.g. vasodilatation and so on. This expectation has been confirmed by blood pressure trends.

It was also found that the bioimpedance method is a feasible and sufficiently robust method for PWV evaluation.

Acknowledgements

Supported by European Regional Development Fund - Project FNUSA-ICRC (No. CZ.1.05/1.1.00/02.0123)

References

[1] Bernstein DP, Lemmens HJM. Stroke volume equation for impedance cardiography, *Med Biol Eng Comput.*, 2005;43: 443-50.

[2] Albaladejo PXC, Boutouyrie P, Laloux BE, Declere AD, Smulyan H, et al. Heart rate, arterial stiffness, and wave reflections in paced patients. *Hypertension*, 2001; 38: 949-52.

[3] Asmar R. Arterial Stiffness and Pulse Wave Velocity :Clinical Applications. Amsterdam, Oxford: Elsevier, 1999.

[4] Koivistoinen T, Koobi T, Jula A, Hutri-Kahonen N, Raitakari OT, Majahalme S, et al. Pulse wave velocity reference values in healthy adults aged 26-75 years. *Clin Physiol Funct I.*, 2007; 27:191-6.

[5] Park BJ, Lee HR, Shim JY, Lee JH, Jung DH, Lee YJ, Association between resting heart rate and arterial stiffness in Korean adults. *Arch Cardiovasc Dis*, 2010; 103: 246-52.

[6] Viscor I, Vondra V, Halamek J, Two-channel high dynamic range bioimpedance monitor for cardiography,. In Proceedings of International Federation of Mechanical and Biological Engineering,2007; 17: 225-8.

[7] Cotter G, Schachner A, Sasson L, Dekel H, Moshkovitz Y. Impedance cardiography revisited, *Physiol Meas*, 2006; 27: 817-27.

[8] Leondes CT, Biomechanical Systems Technology. Hackensack, NJ: World Scientific, 2007.

[9] Wang XP, Li YY, Sun CR, Liu CC, Detection of the First and Second Heart Sound Using Heart Sound Energy. In Proceedings of 2nd International Conference on Biomedical Engineering and Informatics,2009;:478-81.

[10] Alfie J, Waisman GD, Galarza CR, Camera MI. Contribution of stroke volume to the change in pulse pressure pattern with age. *Hypertension*, 1999; 34: 808-12.

[11] Lantelme P, Mestre C, Lievre M, Gressard A, Milon H. Heart rate - An important confounder of pulse wave velocity assessment. *Hypertension*, 2002; 39: 1083-7.

[12] Nitzan M, Khanokh B, Slovik Y, The difference in pulse transit time to the toe and finger measured by photoplethysmography. *Physiol Meas*, 2002; 23: 85-93.

[13] Padilla JM, Berjano EJ, Saiz J, Rodriguez R, Facila L, Pulse wave velocity and digital volume pulse as indirect estimators of blood pressure: pilot study on healthy volunteers. *Cardiovasc Eng*, 2009; 9: 104-12.

[14] Segers P, Rietzschel ER, De Buyzere ML, Vermeersch SJ, De Bacquer D, Van Bortel LM, et al, Noninvasive (input) impedance, pulse wave velocity, and wave reflection in healthy middle-aged men and women. *Hypertension*, 2007; 49: 1248-55.

[15] Sola J, Vetter R, Renevey P, Chetelat O, Sartori C, Rimoldi SF, Parametric estimation of pulse arrival time: a robust approach to pulse wave velocity, *Physiol Meas*, 2009; 30: 603-15.

[16] Sramek BB, Valenta J, Klimes F, Biomechanics of the Cardiovascular System. Prague: Czech Technical University Press; 1995.

[17] Yamashina A, Tomiyama H, Takeda K, Tsuda H, Arai T, Hirose K, et al, Validity, reproducibility, and clinical significance of noninvasive brachial-ankle pulse wave velocity measurement. *Hypertens Res*, 2002; 25: 359-64.